



MDOT RC-1527

**CONDITION ASSESSMENT AND METHODS
OF ABATEMENT OF PRESTRESSED
CONCRETE BOX-BEAM DETERIORATION**

Phase II

**FINAL REPORT
VOLUME I**



MichiganTech

Center for Structural Durability
A Michigan DOT Center of Excellence

Research

Intentionally left blank

Technical Report Documentation Page

1. Report No. Research Report RC-1527		2. Government Accession No.		3. MDOT Project Manager Steve Kahl, P.E.	
4. Title and Subtitle Condition Assessment and Methods of Abatement of Prestressed Concrete Box-Beam Deterioration – Phase II				5. Report Date April 13, 2009	
7. Author(s) WMU: Dr. Haluk Aktan, Dr. Upul Attanayake, and Mr. Evren Ulku MTU: Dr. Theresa Ahlborn and Dr. Yogini Deshpande				6. Performing Organization Code WMU and MTU	
9. Performing Organization Name and Address A joint effort between				8. Performing Org Report No.	
Western Michigan University 1903 W. Michigan Ave, Kalamazoo, MI 49008		Michigan Technological University 1400 Townsend Drive Houghton MI 49931			
12. Sponsoring Agency Name and Address Michigan Department of Transportation Construction and Technology Division PO Box 30049, Lansing MI 48909				Work Unit No.	
				11. Contract Number :	
				11(a). Authorization Number:	
15. Supplementary Notes				13. Type of Report and Period Covered Final Report, 2006-2008	
				14. Sponsoring Agency Code	
16. Abstract Side-by-side box-beam bridge constitutes approximately 17 percent of bridges built or replaced annually on public roads and there is a renewed thrust to use this bridge type for rapid construction under the Highway for LIFE program. Further, failure of a fascia girder of Lakeview Drive bridge in Pennsylvania on December 27, 2005 and with a large number of aging bridges in the U.S., highway agencies are concerned about the safety of similar bridges. This project was developed to evaluate the capacity of distressed box-beam through load testing; investigate the impact of distress types identified during phase I of this project on flexure and shear capacities of a beam in a structural system; identify proper materials and methods for long lasting repairs to improve the structural integrity of distressed box-beam bridges; and by performing simulations of the construction process using finite element (FE) models investigate stresses developed in components during each stage of construction and under operation, develop recommendations for changes or modifications to the design procedures, construction process, material specifications, and to the maintenance and repair techniques of side-by-side box-beam bridge deck. Six tasks were performed in this project ranging from literature review, instrumentation and load testing of a severely deteriorated fascia beam, laboratory investigation of fresh and hardened (durability) properties of shear key grout and repair materials, evaluation of mechanical properties of shear key grout and repair materials, construction process simulation, and evaluation of flexural and shear capacities of distressed beams considering structural system behavior. Recommendations of this project include selection of repair and shear key material, development of comprehensive inspection procedures to assure bridge safety and implementation of the rational design procedure given in the report for improved durability.					
17. Key Words: Box-Beam Bridge, Concrete, Deterioration, Finite Element, Transverse Posttension, Rational Design				18. Distribution Statement No restrictions. This document is available to the public through the Michigan Department of Transportation.	
19. Security Classification (report) Unclassified		20. Security Classification (Page) Unclassified		21. No of Pages 273	22. Price

Intentionally left blank

CONDITION ASSESSMENT AND METHODS OF ABATEMENT OF PRESTRESSED CONCRETE BOX- BEAM DETERIORATION

Phase II

Project Manager: Mr. Steve Kahl, P.E.

Submitted to



Submitted by



Western Michigan University
Department of Civil & Construction Engineering
College of Engineering and Applied Sciences
Kalamazoo, MI 49008
Fax: (269) – 276 – 3211

Dr. Haluk Aktan, P.E.
Professor & Chair
(269) – 276 – 3206
haluk.aktan@wmich.edu

Dr. Upul Attanayake
Assistant Professor
(269) – 276 – 3217
upul.attanayake@wmich.edu

Mr. Evren Ulku
Graduate Research Assistant
(313) – 577 – 3785
evren@eng.wayne.edu

MichiganTech

Michigan Technological University
Dept. of Civil & Environmental Engineering
1400 Townsend Drive
Houghton, MI 49931
Fax: (906) – 487 – 1620

Dr. Theresa M. Ahlborn, P.E.
Associate Professor
(906) – 487 – 2625
tess@mtu.edu

Dr. Yogini Deshpande
Post Doctoral Researcher
(906) – 487 – 1474
yogini@mtu.edu

Intentionally left blank

DISCLAIMER

The content of this report reflects the views of the authors, who are responsible for the facts and accuracy of the information presented herein. This document is disseminated under the sponsorship of the Michigan Department of Transportation in the interest of information exchange. The Michigan Department of Transportation assumes no liability for the content of this report or its use thereof.

Intentionally left blank

ACKNOWLEDGEMENTS

This project is funded by the Michigan Department of Transportation. The authors would like to acknowledge the support and effort of Mr. Steve Kahl for initiating this research. The authors also wish to acknowledge the continuing assistance of the Research Advisory Panel (RAP) members in contributing to the advancement of this study.

Intentionally left blank

EXECUTIVE SUMMARY

INTRODUCTION

Side-by-side box-beam bridge, described as adjacent box-beam bridge, constitutes approximately 17 percent of bridges built or replaced annually on public roads (www.trb.org). The bridge is constructed by placing box-beams adjacent to each other, grouting shear keys, applying transverse posttension, and placing on top either a three inch riding wear surface or a six-inch concrete deck with composite action. The bare top of the box-beam is sometimes used as the riding surface. Adjacent box-beam bridge is the preferred choice for short to medium span bridges, up to 110 feet. Additionally, there is a renewed thrust to use this bridge type for rapid construction under the Highway for LIFE (Longer-lasting highway infrastructure using Innovations to accomplish the Fast construction of Efficient and safe highway and bridges) program (www.fhwa.dot.gov and www.trb.org).

Box-beam design procedure in Michigan and in many other states as well as in many other countries was documented during phase I of this project. In addition, 15 in-service bridges were inspected, distress types and states were documented and the performance was evaluated. Longitudinal deck cracking reflecting from the shear-keys was identified as the leading cause of other distresses. Several distress types were identified as critical to the box-beam capacity. Load rating was performed for various levels of the identified distress types following load factor method described in 2003 Michigan Bridge Analysis Guide.

The objectives for Phase II of this project were identified as follows:

1. Evaluate capacity of a distressed box-beam through load testing,
2. Identify proper materials and methods for long lasting repairs which improve the structural integrity of distressed box-beam bridges,
3. Simulate construction process using finite element (FE) models investigating stresses developed in components during each stage of construction,
4. Investigate impact of distress types identified during phase I of this project on flexure and shear capacities of a beam using 3D full bridge models,
5. Develop changes or modifications to the design procedure, construction process, and to the maintenance and repair techniques of side-by-side box-beam bridge deck.

To satisfy the objectives, this project was organized with six main tasks: (1) literature review; (2) capacity evaluation through load testing; (3) laboratory investigation of fresh and hardened (durability) properties of shear key grout and repair materials; (4) mechanical property evaluation of shear key and repair materials; (5) construction process simulation; and (6) flexural and shear capacity evaluation of distressed beams considering structural system behavior.

LITERATURE REVIEW

A thorough literature review including capacity evaluation and load testing of distressed bridges/components, materials used for shear keys and repair, durability of shear key and repair materials, properties of cementitious materials that have a potential to be used for shear keys, and design parameters for transverse design of box-beam bridge superstructure was performed. Literature regarding the capacity evaluation of box-beams through load testing indicates that fatigue should not be a concern for uncracked beams. It was recommended to avoid frequent loading on bridges that causes bottom fiber stress in excess of $6\sqrt{f_c}$ (psi) or strand stress greater than $0.06f_{pu}$. Transverse connection, established with grout joints (shear key), posttension, and cast-in-place concrete deck governs the load distribution. Diaphragms generate rigid zones in the box-beam bridge superstructure and works as the primary load transfer mechanism. According to the results of a study on the bearing capacity and compressive strength of mortar joints between precast columns, when grout material modulus is lower than the parent material, joint load transfer efficiency increases with reduced joint width. However, uniform thickness of the joint is of paramount importance to maintain uniform stress distribution. Mechanical properties of grout material at the time of posttension govern the stress distribution along the joint and sealing performance. Customized shear key grout mixes can be developed for specified mechanical property requirements achieved at the time of transverse posttensioning.

LOAD TESTING

The second task was to remove a severely deteriorated fascia beam, instrument, and perform load testing for evaluating the capacity of the beam. A 50-year old box-beam with severe longitudinal cracking at the beam soffit was removed from the bridge (S11-38101) that carries Hawkins road over I-94. Beam capacity was calculated using strain data and load rating was performed. Analysis of load test data indicated that the beam capacity was still more than the design

capacity. However, there is a safety concern because beam was designed for smaller load (H-15) than the currently required loads. The remaining prestress was calculated from camber measurements and the strain gauge data; however it was found that using camber overestimates remaining prestress by 40-50 percent. It is essential to implement an inspection procedure that is capable of identifying the concealed corrosion, evaluating condition of transverse posttension strands, characterizing material properties, and quantifying the load transfer.

LABORATORY INVESTIGATION OF SELECTING PROPER REPAIR AND GROUT MATERIALS

The third task included conducting a survey of commonly used repair materials and shear key grouts for prestressed box beam bridges and laboratory evaluation of selected materials. The intended result of the laboratory evaluation was development of required material characteristics from the perspective of dimensional stability and durability of prestressed box beam bridges.

Three shear key grouts were selected for laboratory evaluation. Of these, two were cement based grouts whose mixture proportion was based on MDOT specifications, whereas the third shear key grout was SET 45, a commercially available rapid setting phosphate cement based grout. Laboratory evaluation of shear key grouts consisted of fresh properties including slump and air content and hardened properties including compressive and bond strength testing and free shrinkage. Durability of shear key grouts was evaluated by measuring the resistance to freezing and thawing cycles and sorptivity. It was observed that the cement based grouts had compressive strength of lower than 5000 psi at the end of 28 days whereas all the shear key grouts exhibited lower slant shear bond strength values. All the shear key grouts exhibited good durability properties.

Four commonly used polymer based repair materials were selected to evaluate their performance in terms of dimensional stability and durability. The properties evaluated were slump, air content, rate of gain of compressive strength, bond strength, shrinkage and cracking susceptibility, resistance to freezing and thawing cycles, coefficient of thermal expansion, chloride permeability and sorptivity. It was observed that the repair materials investigated in this study have a wide range of values for all the properties for which the materials were evaluated,

and selection of a repair material for field use must consider prioritization of critical performance properties.

MECHANICAL PROPERTIES OF SHEAR KEY GROUT AND REPAIR MATERIALS

The fourth task was to evaluate mechanical properties of shear key grout and repair materials. Mechanical properties of some of the repair materials and manufactured grout materials (e.g., set gout and set-45) are documented in manufacturers' technical data sheets. Mechanical properties of Type R-2 grout, which is commonly used in Michigan box-beam bridges to form the shear-keys, are not documented in literature. Compressive strength test of grout material was performed. Ultrasonic pulse velocity (UPV) test was performed to determine the dynamic elasticity modulus and the Poisson's ratio of the material. The dynamic modulus is generally greater than the static modulus determined in accordance with ASTM C469. However, for the grout materials, the measured dynamic modulus was lower than the static modulus determined following the ASTM C469 procedure. Further testing to establish the uniaxial stress-strain properties showed a hysteretic strain hardening behavior not typical of concrete. The elastic modulus consequently changes dramatically within the load cycle. The static modulus test (ASTM C469) is not able to capture this behavior and provides a nominal modulus value. Other repair materials also showed a similar behavior and further investigations were suggested. Further, grout materials tested during the project are not capable of satisfying the strength level required by AASHTO Standard or LRFD at the time of posttension.

CONSTRUCTION PROCESS SIMULATION

The fifth task was to simulate construction procedure verifying the design assumptions and identifying the stresses developed within various components. In addition to simulating the construction process stages, box-beam bridge transverse connection design and material parameters were also investigated using sub-assembly models. The parameters investigated are: grout mechanical properties, posttension force magnitude and location, number of diaphragms, and the bridge width. The sub-assembly models with 50 ft long 27×36-in. box beams connected with shear keys and posttension at diaphragm locations were analyzed under concentrated load, dead load, and transverse posttension. Sub-assembly models were developed with three and four box-beams. Analysis results showed that load transfer is primarily

followed through the stiffer sections of the bridge superstructure (i.e., through the diaphragms). AASHTO LRFD (2004) Section 5.14.1.2.8 recommendations regarding transverse normal interface stress distribution are vague. It is not clear whether the minimum stress of 250 psi at joints should be obtained either at shear keys along the entire beam length or diaphragm locations. A comprehensive redesign of diaphragm topology as well as well spacing may be required to obtain uniform stress distribution along the length of shear keys.

Following the latest MDOT design and construction procedures, every step of side-by-side box-beam construction process was simulated. Full bridge models were subjected to loads that may be expected to develop during construction and service life of the bridge. Stresses developed in beams, shear keys, and the deck were documented at each step of simulations. According to the results, barrier loading creates tensile stresses on the 6-in. deck and thermal gradient loading is the primary source generating critical stresses within the deck and certain portions of shear key

A rational analysis and design model (macromechanical model) based on mechanics of materials and macromechanics concepts was presented. Using macromechanical model, changes to construction procedures such as applying posttension in two stages were suggested and evaluated with construction process simulation. It was identified that macromechanical model can predict the posttension requirements to eliminate tensile stresses that occur under gravity loading. With the proposed construction process, applying posttension after deck placement greatly helps reducing tensile stresses in the deck that occur under positive and negative thermal gradient loading. Transverse tensile deck stresses that occur under live load can be completely removed except at some isolated regions close to fascias.

FLEXURAL AND SHEAR CAPACITY OF DISTRESSED BOX-BEAMS

The sixth task was to evaluate flexural and shear capacity of distressed beams considering structural system behavior. Full bridge models used for construction process simulation were also used in the case of capacity evaluation. Three major beam distress types; spall, spall and single broken strand, and spall and two broken strands were incorporated into the models by gradually reducing the elasticity modulus on regions where distress was defined. All the distresses were along the corner of beam bottom flange for calculating flexure and shear critical capacities. Analysis results showed that, for the selected span length of 50 ft., the flexural

capacity was reduced only when the distresses were at the midspan. Spall alone was not a major cause of capacity reduction. Beam capacity reduction was significant if broken tendons were present. In addition to beam distresses, impact of shear key grout loss and broken posttension strands on beam capacity was investigated. Partial loss of grout did not affect the capacity of the beam, however dead and live load demands on the fascia beam changed due to reduced stiffness. It was shown that posttension did not influence the load distribution provided that shear keys were intact. However, it contributed to the beam capacity and provides redundancy to the systems especially when weak bond exists between the grout and beams.

RECOMMENDATIONS

The following key recommendations are based on the findings from the project tasks of literature review, load testing of a salvaged box-beam, testing of grout and repair material properties, and the development of subsequent finite element modeling and simulations:

1. Among the fresh properties of utmost importance is workability in case of polymer based repair materials. Repair materials which do not need excessive force for proper placement and consolidation should be selected.
2. Repair materials with shrinkage values comparable to the substrate concrete should be selected. In this study all the repair materials did not necessarily exhibit the required behavior and, hence, it is essential to select a repair material based on its intended use. It is necessary to evaluate the shrinkage behavior of a selected repair material prior to application on site.
3. To protect exposed steel from corrosion, repair materials evaluated in this study can be adopted for use because all of them exhibited high resistance to chloride ion transport as well as low sorption values.
4. When selecting a shear key grout it is essential to determine the early age compressive strength as well as its early age shrinkage properties based on the load applied to it. A more detailed understanding of shear key grout from a material standpoint as well as the total design of the shear key itself is recommended.

5. Adequate load transfer and achieving a watertight connection along the transverse joint cannot be achieved with the currently specified grout with nonlinear hysteretic behavior. Revisions to grout material specifications are recommended.
6. In-service bridge beam load capacity assessment should be based on material characterization, load transfer evaluation along the shear keys, and estimation or assessment of concealed corrosion.
7. The recommended load analysis procedure and the associated design criteria requiring a two-stage posttension process should be implemented for improved durability performance of side-by-side box-beam bridges.

Intentionally left blank

Contents

ACKNOWLEDGEMENTS	iii
EXECUTIVE SUMMARY	v
TABLE OF TABLES.....	xvii
TABLE OF FIGURES.....	xix
1 Introduction.....	1
1.1 Background.....	1
1.2 Project Objectives and Tasks.....	1
2 State-of-the-Art Literature Review.....	5
2.1 Objective and Approach	5
2.2 Capacity Evaluation of Distressed Girders	5
2.3 Repair Materials.....	7
2.3.1 Characteristic Requirements of Repair Materials for Prestressed Concrete Box-beam Deterioration.....	8
2.3.2 Polymer / Epoxy Based Repair Material	12
2.3.3 Mechanism of Polymerization	13
2.3.4 Fresh Polymer Repair Concrete Properties.....	14
2.3.5 Hardened Polymer Repair Concrete Properties	17
2.3.6 Durability Performance of Polymer Based Repair Concrete.....	19
2.3.7 Gaps in Knowledge.....	20
2.4 Shear Key Materials.....	21
2.4.1 Commercial Grout Materials	21
2.4.2 Other Cementitious Materials	25
2.4.3 The Bond between Girder and Shear Key Materials	29
2.4.4 Load Bearing Capacity of Mortar joints	30
2.5 The influence of diaphragms on Posttension Stress Distribution	32
2.5.1 Assessment of Load Distribution between Adjacent Girders	33
2.5.2 Bridge Width Effect on Posttension Stress Distribution.....	34

2.6	Summary and Conclusions	35
3	Load Testing of Decommisioned Box-Beam	37
3.1	Objective and Approach	37
3.2	Overview	37
3.3	Beam Removal and Load Testing.....	40
3.3.1	Beam Removal Process.....	41
3.3.2	Instrumentation Layout.....	43
3.3.3	Load Configuration.....	45
3.4	Load Testing Data Analysis.....	47
3.4.1	Camber and Remaining Prestress	47
3.4.2	Cracking Moment and Remaining Prestress.....	48
3.4.3	Load Rating – Flexural Strength.....	50
3.4.4	Condition of Prestressing Strands.....	51
3.4.5	Load Capacity of the Beam.....	52
3.5	Summary and Conclusions	52
4	Experimental Procedure for Durability Studies.....	55
4.1	Introduction.....	55
4.2	Materials	57
4.2.1	Repair Materials and Shear Key Grouts	57
4.2.2	Substrate Concrete	58
4.3	Mixture Proportions and Mixing	60
4.4	Test Methods and Requirements.....	63
4.4.1	Slump.....	65
4.4.2	Air Content.....	65
4.4.3	Rate of Strength Gain.....	68
4.4.4	Slant Shear Bond Strength.....	69
4.4.5	Resistance to Freezing and Thawing Cycles	69
4.4.6	Measurement of Free Shrinkage	71
4.4.7	Sorptivity.....	71
4.4.8	Cracking Susceptibility	72

4.4.9	Coefficient of Thermal Expansion.....	74
5	Results and Analysis from Durability Studies	75
5.1	Fresh and Hardened Properties of Repair Materials and Shear Key Grouts.....	75
5.2	Slump.....	75
5.3	Air Content.....	75
5.4	Compressive Strength	82
5.5	Slant Shear Bond Strength.....	85
5.6	Shrinkage Behavior.....	87
5.7	Resistance to Freezing and Thawing	96
5.8	Air Content.....	100
5.9	Coefficient of Thermal Expansion (CTE).....	102
5.10	Sorptivity.....	104
5.11	Chloride Permeability	106
5.12	Summary of Durability Studies	107
6	Material Testing.....	113
6.1	Objective and Approach	113
6.2	Type R-2 Grout	113
6.2.1	Plastic Properties of Type R-2 Grout.....	114
6.2.2	Mechanical Properties of Type R-2 Grout.....	114
6.2.3	Type R-2 Grout Material Behavior under Axial Compression.....	118
6.3	Set 45 Grout Properties	119
6.4	Properties of Repair Material.....	120
6.5	Summary and Conclusions	121

Intentionally left blank

TABLE OF TABLES

Table 2-1. General Requirements of Patch Material for Structural Compatibility (Emberson and Mays 1990)	10
Table 2-2. Grout Material Properties (Issa et al. 2003)	22
Table 2-3. Summary of Grout Material Properties	24
Table 3-1. Beam Sectional Properties and Design Parameters used in 1957	40
Table 3-2. Moment Capacity of the Section	46
Table 3-3. Load at Cracking – Strain Gauge Data.....	49
Table 3-4. Remaining Prestress	50
Table 3-5. Bridge Load Rating (DF = 0.256 per lane; tons).....	51
Table 3-6. Bridge Load Rating – Exterior Beam (DF = 0.5 per lane; tons)	51
Table 3-7. Bridge Load Rating – Interior Beam (DF = 0.5 per lane; tons)	51
Table 3-8. Bridge Posting Requirement in September 1995 (DF = 0.5 per lane; tons).....	51
Table 4-1. Physical Properties of Aggregates used in Substrate Concrete	59
Table 4-2. Mixture Proportions of Commercial Repair Products and Shear Key Materials .	61
Table 4-3. Mixture Proportions for Shear Key Grout (R-2 mortar)	62
Table 4-4. Mixture Proportions for Substrate Concrete.....	62
Table 4-5. List of Tests for Repair Mortar and Shear Key Grout.....	64
Table 4-6. List of Tests for Repair Mortar and Shear Key Grout.....	65
Table 5-1. Test Results for SikaTop123® Plus	76
Table 5-2. Test Results for SikaRepair®SHA	77
Table 5-3. Test Results for HB2 Repair Mortar	78
Table 5-4. Test Results for Conpatch VO.....	79
Table 5-5. Test Results for SET® 45.....	80
Table 5-6. Test Results for Type I Cement Grout	81
Table 5-7. Test Results for Masonry Cement Grout.....	82
Table 5-8. Percent Increase in Compressive Strength over Different Ages	84
Table 5-9. Risk of Cracking of Repair Materials.....	93
Table 5-10. Average Crack Width over Six Days	93

Table 5-11. Void Frequencies and Spacing Factors for Repair Mortars and Shear Key Grouts	102
Table 5-12. Change in Length Observed	104
Table 5-13. Repair Material Test Results Summary	111
Table 5-14. Shear Key Grout Test Results Summary	112
Table 6-1. Grout Mix ID and Description	113
Table 6-2. Slump and Air Content of Grout Mixes	114
Table 6-3. Mechanical Properties of R-2 Grout - Mix BB	114
Table 6-4. Mechanical Properties of R-2 Grout - Mix BBA	115
Table 6-5. Mechanical Properties of R-2 Grout - Mix BBM.....	115
Table 6-6. Mechanical Properties of R-2 Grout - Mix BBN	115
Table 6-7. Mechanical Properties of R-2 Grout - Mix BBS	115
Table 6-8. Mechanical Properties of Set® 45 Grout	120
Table 6-9. Mechanical Properties of SikaRepair® SHA	120
Table 6-10. Mechanical Properties of Conpatch V/O.....	120
Table 6-11. Mechanical Properties of SikaTop® 123 PLUS	121
Table 6-12. Mechanical Properties of HB2® Repair.....	121

TABLE OF FIGURES

Figure 2-1. Instrument for measuring remaining prestress of exposed strands	6
Figure 2-2. Characteristics of an ideal repair material (Parameswaran 2004).....	9
Figure 2-3. Modes of failure in patch repair (Baluch et al. 2002)	11
Figure 2-4. Simplified model of formation of polymer film on cement hydration (ACI 2005)	14
Figure 2-5. Effects of water-cement ratio and polymer-cement ratio on flow of latex modified mortars (Ohama 1995a).....	15
Figure 2-6. Effects of unit water content (water-cement ratio) and polymer-cement ratio on slump of SBR modified concrete (Ohama 1995a).....	16
Figure 2-7. Compressive strength (in MPa) of mortar cubes at different ages (Ghrici et al. 2007)	25
Figure 2-8. Chloride permeability of concrete at (a) 28 days and (b) 90 days (Ghrici et al. 2007)	26
Figure 2-9. Variation of compressive and flexural strength of mortar against time (Arandigoyen and Alvarez 2007)	26
Figure 2-10. Changing mortar compressive strength (MPa) against deformation (mm) (Arandigoyen and Alvarez 2007)	27
Figure 2-11. Variation of uniaxial compressive strength against relative weight loss of mortar (Yurtdas et al. 2005).....	28
Figure 2-12. Variation of elasticity modulus against relative weight loss of mortar (Yurtdas et al. 2005)	28
Figure 2-13. Composite direct tension test (Gulyas et al. 1995)	29
Figure 2-14. Stresses developed at the joints and in the precast elements (Barboza et al. 2006)	30
Figure 2-15. Variation of joint efficiency (α) against the ratio of minor joint width and joint thickness	31
Figure 2-16. Test configuration used by Barboza et al. (2006)	32
Figure 2-17. Deflection of a box-beam bridge (El-Remaily et al. 1996).....	34

Figure 2-18. Posttension force variation with bridge width and beam height (El-Remaily et al. 1996)	35
Figure 3-1. Typical box-beam section used in the 1950s	39
Figure 3-2. H-15-44 and H-20-44 vehicle configuration.....	39
Figure 5-3. Instrumentation layout	44
Figure 3-4. Load configuration developed by the contractor	46
Figure 3-5. Variation of beam camber against length.....	47
Figure 5-6. Moment due to applied load at cracking	49
Figure 4-1. Characteristic material properties required for durable concrete repair.....	56
Figure 4-2. Gradation of coarse aggregates	59
Figure 4-3. Gradation of fine aggregates	60
Figure 4-4. Hobart mixer used for mixing repair materials	60
Figure 4-5. Laboratory pan mixer	62
Figure 4-6. Cross-section of slant shear bond strength test set-up	69
Figure 4-7. Set-up used for splitting of the substrate concrete specimen for freeze-thaw testing.....	70
Figure 4-8. Surface preparation of the substrate concrete specimen	71
Figure 4-9. Diagrammatic sketch of sample location for sorptivity test.....	72
Figure 4-10. Environmental control chamber with ring specimen	73
Figure 4-11. Data logger used for data collection from ring specimens.....	73
Figure 5-1. Compressive strength at various ages for repair materials.....	83
Figure 5-2. Development of compressive strength of shear key grouts	85
Figure 5-3. Development of slant shear bond strength at various ages for repair materials..	85
Figure 5-4. Failures of slant shear bond test specimens	86
Figure 5-5. Voids in HB2 repair mortar specimen for slant shear bond strength test	86
Figure 5-6. Development of slant shear bond strength at various ages for shear key grouts	87
Figure 5-7. Free shrinkage strains in repair materials for samples at 100% RH and 73°F....	88
Figure 5-8. Shrinkage strains in repair materials for samples at 50% RH and 73°F	89
Figure 5-9. Cracking susceptibility of Sika Top [®] 123 PLUS	90
Figure 5-10. Cracking susceptibility of Sika Repair SHA.....	91
Figure 5-11. Cracking susceptibility of Conpatch VO	92

Figure 5-12. Pictorial presentation of crack width and effect on serviceability	94
Figure 5-13. Free shrinkage strains in shear key grouts for samples at 100% RH	95
Figure 5-14. Free shrinkage strains in shear key grouts for samples at 50% RH and 73°F ..	96
Figure 5-15. Relative dynamic modulus of repair materials over 300 cycles of freezing and thawing	97
Figure 5-16. Change of repair materials over 300 cycles of freezing and thawing	97
Figure 5-17. Change in relative dynamic modulus of shear key grouts over 300 cycles of freezing and thawing.....	99
Figure 5-18. Change in length of shear key grouts over 300 cycles of freezing and thawing	99
Figure 5-19. Change in relative dynamic modulus of composite specimens of substrate concrete and repair material over 300 cycles of freezing and thawing	100
Figure 5-20. Air content in hardened repair mortar and shear key grouts	101
Figure 5-21. Specific surface area of repair mortars and shear key grouts.....	102
Figure 5-22. Average coefficient of thermal expansion of repair mortars and shear key grouts	103
Figure 5-23. Comparison of rate of initial absorption of repair mortars and shear key grouts	105
Figure 5-24. Comparison of rate of secondary absorption of repair mortars and shear key grouts	105
Figure 5-25. Comparison of chloride permeability for repair materials	107
Figure 6-1. Compressive strength of grout material during early age	116
Figure 6-2. Dynamic modulus of grout material during early age	117
Figure 6-3. Poisson's ratio of grout material during early age	117
Figure 6-4. Stress-strain behavior of grout (mix BBS) under axial compression.....	118
Figure 6-5. Stress-strain behavior of grout (mix BBS) under axial compression.....	119

Intentionally left blank

1 INTRODUCTION

1.1 BACKGROUND

The side-by-side box-beam bridge, described as an adjacent box-beam bridge, constitutes approximately 17 percent of bridges built or replaced annually on public roads (www.trb.org). The bridge is constructed by placing box-beams adjacent to each other, grouting shear keys, applying transverse posttension, and placing on top either a three-inch riding wear surface or a six-inch concrete deck with composite action. The bare top of the box-beam is sometimes used as the riding surface. The adjacent box-beam bridge is the preferred choice for short to medium span bridges, up to 110 feet. The favorable aspects are: ease of construction, favorable span-to-depth ratios, aesthetic appeal, and high torsional stiffness of the box-beams (El-Remaily et al. 1996; Lall et al. 1998; Miller et al. 1999). Additionally, there is a renewed thrust to use this bridge type for rapid construction under the Highway for LIFE (Longer-lasting highway infrastructure using Innovations to accomplish the Fast construction of Efficient and safe highway and bridges) program (www.fhwa.dot.gov and www.trb.org).

There is a large stock of existing side-by-side box-beam bridges in the U.S.; for example, in Michigan, the numbers exceed 2000. Evolving box-beam design procedures in Michigan and in many other states as well as in many other countries was documented during phase I of this project. In addition, 15 in-service bridges were inspected, distress types and states were documented, and bridge performance was evaluated. From the phase I study, longitudinal deck cracking reflecting from the shear-keys was identified as the leading cause of other distresses. Also, several distress types were identified as critical to the box-beam capacity. Load rating was performed for various levels of the identified distress types following the load factor method described in the 2003 Michigan Bridge Analysis Guide (Aktan et al. 2005).

1.2 PROJECT OBJECTIVES AND TASKS

The overall project objectives are to:

- Evaluate the experimental capacity of a distressed box-beam through load testing of a salvaged beam;
- Identify proper materials and methods for repairs, to improve the structural integrity of distressed box-beam bridges;

- Investigate stresses developed in components during each stage of construction and under operation by performing simulations of the construction process using finite element (FE) models;
- Investigate the impact of distress types identified during phase I of this project on flexure and shear capacities of a beam considering structural system behavior;
- Develop recommendations for changes or modifications to the design procedures, construction process, load ratings, and maintenance and repair techniques of side-by-side box-beam bridges.

The project tasks are as follows: (1) literature review on capacity evaluation and load testing of distressed bridges/girders, materials used for shear keys and repair, durability of shear key and repair materials, properties of cementitious materials that have a potential to be used for shear keys, and design parameters for transverse design of box-beam bridge superstructure; (2) capacity evaluation of a distressed box-beam removed from an in-service bridge through load testing; (3) laboratory investigation of fresh and hardened (durability) properties of shear key grout and repair materials; (4) mechanical property evaluation of shear key and repair materials; (5) construction process simulation; and (6) flexural and shear capacity evaluation of distressed beams considering structural system behavior.

Research findings are documented in two volumes with 12 chapters. The contents of the two volumes of the report are described below:

Volume I:

A Literature review is presented in chapter 2 comprising capacity evaluation and load testing of distressed bridges/girders, materials used for shear keys and repair, durability of shear key and repair materials, properties of cementitious materials that have a potential to be used for shear keys, and design parameters for transverse design of box-beam bridge superstructure.

Chapter 3 includes the condition description of the decommissioned box-beam, beam removal process, instrumentation and load configuration, capacity evaluation using load test data, and load rating of the beam using load factor method.

The experimental procedure for durability studies is presented in chapter 4.

Experimental test results of durability studies and analysis of data are presented in chapter 5.

Mechanical properties of shear key grout and beam repair materials are documented in chapter 6.

Volume II:

Side-by-side box-beam transverse design parameters are investigated using sub-assembly models of box-beams. Model parameters and analysis results are presented in chapter 7.

Chapter 8 contains the model parameters, simulation steps, and the results of construction process simulation. Based on MDOT design and construction procedures, every step of the side-by-side box-beam construction process is simulated using advanced pre/post processing capabilities of HyperMesh and FE analysis capabilities of ABAQUS. Stresses developed in beams, shear keys, and the deck are obtained and documented in this chapter.

Phase I of this project showed that in Michigan and elsewhere the transverse connection design of a side-by-side box-beam bridge is based on empirical procedures. This is due to the lack of rational analysis models that allow the load demand calculation at the longitudinal joints between precast box-beams. Chapter 9 presents a rational analysis and design model for transverse connection design and a proposed construction procedure. Further, the stresses developed in beams, shear keys, and the deck during the recommended construction procedure are investigated, in chapter 9, using advanced FE modeling and analysis techniques.

Chapter 10 presents modeling and analysis of a box-beam superstructure with distressed beams evaluating the influences of distresses on beam capacity and the bridge capacity when the beam is part of the structural system.

Chapter 11 presents the comprehensive results and recommendations.

Chapter 12 discusses the recommendations for further work on this topic towards the implementation of the project findings.

Intentionally left blank

2 STATE-OF-THE-ART LITERATURE REVIEW

2.1 OBJECTIVE AND APPROACH

The objective of the literature review is to identify, review, and synthesize information related to capacity evaluation and load testing of distressed bridges/beams, materials used for shear keys and repair, and properties of cementitious materials that have a potential to be used for shear keys. In addition, a few articles that are relevant to the finite element analysis performed during the second phase of the project are reviewed and summarized in this chapter. The literature review complements the comprehensive literature review related to side-by-side box-beam bridge design and performance conducted during phase I of this project.

2.2 CAPACITY EVALUATION OF DISTRESSED GIRDERS

Failure of a fascia girder on the Lakeview Drive bridge in Pennsylvania on December 27, 2005 prompted the capacity evaluation of the remaining girders to understand the impact of various damage scenarios on the girder capacity. Harries (2006) performed visual inspection, load testing, and analytical and numerical investigations evaluating the load capacity of girders removed from the Lake View Drive bridge. This study shows the importance of quantifying the extent of strand corrosion and other distress. When visual inspection is the only source of information, it is recommended to consider 50% additional strand corrosion than what is observed. Further, it is recommended to measure the camber and estimate the remaining prestress. Unless there is adequate information to verify the functional shear keys and transverse tie rods in existing bridges, the load rating should be performed assuming no load distribution (Harries 2006). When strands are broken, a conservative recommendation is to neglect the entire strand for capacity evaluation or use engineering judgment since redevelopment of strands is uncertain.

Civjan et al. (1998) developed a mechanism to estimate the remaining prestress of exposed strands (Figure 2-1). His estimates are useful for evaluating the remaining prestress of existing bridges for accurate estimation of load carrying capacity.

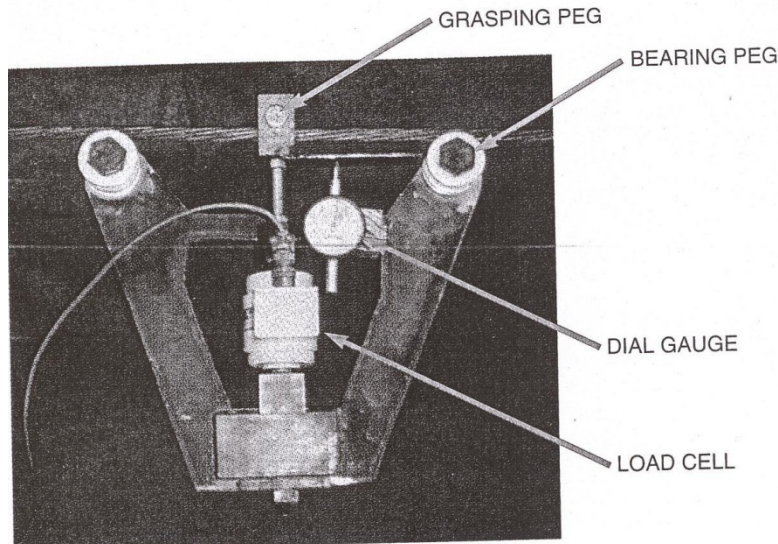


Figure 2-1. Instrument for measuring remaining prestress of exposed strands

Rao and Frantz (1996) performed fatigue tests on 27-years old prestressed concrete box-beams. The beams were 27×36-in. sections. Their span length was 56 ft. One of the beams had two one-foot long cracks at the strand levels while the other beam showed only a few rust stain patches. It was concluded that fatigue should not be a concern for uncracked beams. Cracked beams with nominal bottom fiber stress of $6(f_c')^{1/2}$ were subjected to more than 1,500,000 cycles of loading without any evidence of fatigue problems. When the load was increased to generate bottom fiber stress of $9(f_c')^{1/2}$, strands ruptured after 145,000 cycles. It is recommended that fatigue would be a concern for beams under frequent loading that causes bottom fiber stress in excess of $6(f_c')^{1/2}$ or strand stress greater than $0.06f_{pu}$.

Miller and Parekh (1994) performed a destructive test on a 12-year old 36-in. wide and 33-in. deep prestressed concrete beam. The beam was designed in 1980 and was removed from the bridge in 1992. Beam contained 18 strands but inspection revealed only 15 effective strands. The beam was in good condition with only concrete spall along one edge. The beam was designed for 5500 psi concrete, and at the time of load testing, the compressive strength of the concrete was established to be 8000 psi. Capacity was also evaluated by analytical methods incorporating loss of concrete and strands. Test results were in agreement with the analytical results. It was concluded that the asymmetry of the cross-section due to loss of strands and concrete at the corner influenced the post-cracking and failure behavior.

2.3 REPAIR MATERIALS

Repair of reinforced concrete structures or prestressed concrete structures is not a “band-aid” process; but in actuality is a complex engineering task. It is a process presenting unique challenges which are different from those associated with new concrete construction. A repair system must successfully integrate new materials with old materials, forming a composite system capable of enduring exposure to service loads, exterior and interior environments of the structure and time (Vaysburd 2006).

This Phase II project has been constituted to evaluate in detail the repair materials commonly adopted for repair of adjacent prestressed concrete box beam bridges in Michigan. Investigation results of the MDOT Box-Beam Phase-I project identified several levels of deterioration in fifteen side-by-side prestressed concrete box-beam bridges currently in service (Ahlborn et al. December 2005). The detailed field inspection of the fifteen bridges of various ages indicated a general trend of deterioration in terms of longitudinal and transverse cracking on the decks, substantial of cracking along beam lengths and presence of moisture in beams. A large number of beams in many bridges exhibited concrete spalling and extensive corrosion of steel strands likely due to the presence of moisture and ingress of de-icing chlorides from deck cracks. The field investigations indicated that the shear keys in all bridges built after 1985 were cracked along the length in many cases. Many bridges also exhibited large amount of spalling of the grout in the shear keys.

For a successful repair of a structure, it is essential that the root cause of the deterioration be studied in detail and a solution be developed to stop further damage to the structure. The summary of inspections related to the bridge deck in the Phase-I report identifies extensive longitudinal and transverse cracks in deck concrete. The cracks could have developed due to drying shrinkage, untimely saw cutting of construction joints, improper curing, presence of cold joints and cracks in expansion joints. To ensure long-term performance of the bridge, it is essential to carry out the mitigation of deck deterioration as per proven methods. MDOT has other research projects (completed and ongoing) that address deck deterioration. This Phase II study focused on repair of the beam elements, including shear keys, and assumed that deck deterioration has been mitigated. Additional information on deck repair can be found in the literature (Deshpande 2006; Young and Kreider 2006).

2.3.1 Characteristic Requirements of Repair Materials for Prestressed Concrete Box-beam Deterioration

The selection of repair materials is a predictive effort in order to maximize future performance of the structure by ensuring long-term durability. Typically, the selection of patch repair materials is based on availability, workability requirements, and economical criteria. According to Kosednar and Mailvaganam (2005) selection of a repair material must be based on the knowledge of the physical and chemical properties, function imposed on it and environmental conditions. Every repair job is unique and, especially in the case of this study, the loadings, structural concrete being repaired, environmental conditions and extent of damage vary considerably. Concrete repairs usually fail because of inappropriate selection of the repair material (Vaysburd 2006). There are many commercially available repair materials and there are considerable variations in their chemical composition, mechanical and durability characteristics (Deshpande 2006; Parameswaran 2004). The main factors which cause premature failure of repairs include freezing and thawing, aggressive chemical exposure, mechanical abrasion, loss of bond between existing concrete and repair material, and dimensional incompatibilities between repair material and the existing concrete. While some of the problems associated with premature deterioration of repairs are because of structural failures, most of the problems are related to durability. When a repair material is chosen, care should be taken such that the properties of the repair material match those of the existing concrete to achieve long-term performance of the repair system.

The characteristics of a repair material for long-term performance of repaired concrete under service conditions are illustrated in Figure 2-2.

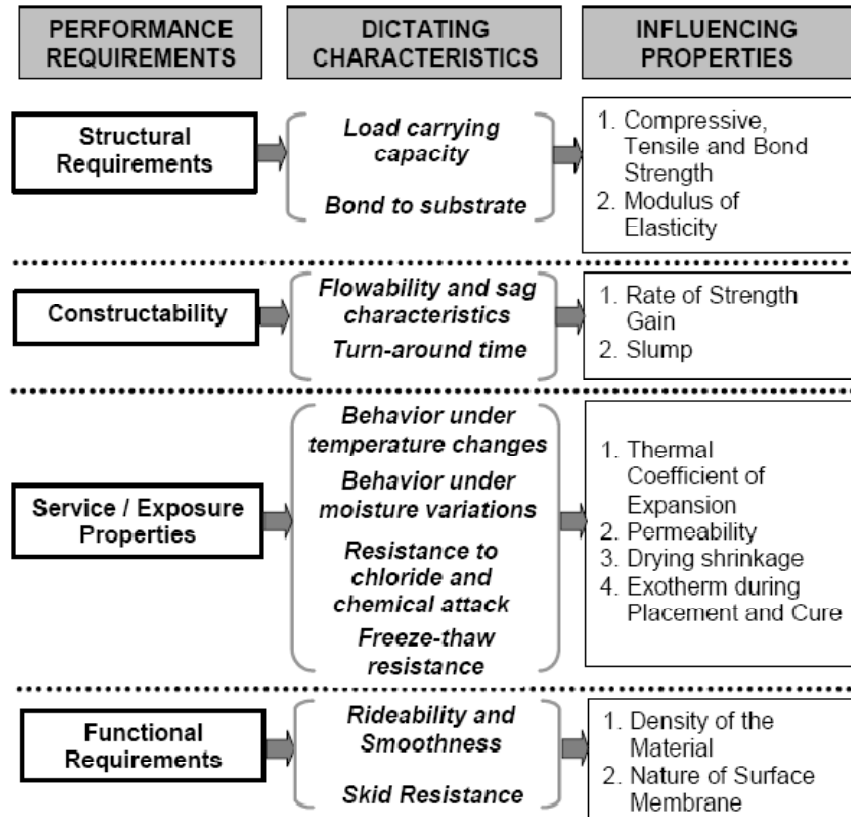


Figure 2-2. Characteristics of an ideal repair material (Parameswaran 2004)

In general the repair material should have the following properties:

1. The repair mortar should have adequate workability so that it can be easily placed, consolidated and finished.
2. The repair mortar must be able to meet the structural requirements of the intended existing structure so as to have sufficient or comparable compressive, tensile and bond strengths. It is also essential that the repair material have a similar stiffness i.e. elastic modulus, than the substrate concrete.
3. The long term durability of the repaired concrete is of great importance for increase in the service life of the repaired structure. The performance of the repair concrete under temperature and moisture changes, freeze-thaw cycles and exposure to deicing salts is very critical. These aspects predominantly affect the bond characteristics and the bond strength between the repair mortar (RM) and concrete substrate (RC).

Emberson and Mays (1990) have provided the summary of the properties required of a patching material for structural compatibility with the existing concrete (refer to Table 2-1).

Table 2-1. General Requirements of Patch Material for Structural Compatibility (Emberson and Mays 1990)

Property	Relationship of repair mortar (R) to concrete substrate (C)
Strength in compression, tension and flexure	$RM \geq RC$
Modulus in compression, tension and flexure	$RM \approx RC$
Poisson's ratio	Dependent on modulus and type of repair
Coefficient of thermal expansion	$RM \approx RC$
Adhesion in tension and shear	$RM \geq RC$
Curing and long-term shrinkage	$RM \leq RC$
Strain capacity	$RM \geq RC$
Creep	Dependent on whether creep causes desirable or undesirable effects
Fatigue performance	$RM \geq RC$

In terms of design requirements, strengths (compressive, tension and flexure) of repair mortar/concrete should be greater than or similar to that of the parent concrete. Higher strength values are necessary especially for tensile and flexural strength due to service loads. Mangat and Flaherty (2000) through an extensive field investigation showed that repairs applied with relatively stiff materials, $E_R > E_C$, display efficient structural interaction with the structure. It was observed that high stiffness repairs were effective: i) in redistributing shrinkage strain to the substrate thereby reducing restrained shrinkage tension and ii) strain transfer to the repair patch in the long term due to external load transfer from the substrate structure. The investigation of low stiffness repair materials ($E_R < E_C$) indicated that they are much more likely to undergo tensile cracking due to restrained shrinkage and displayed no long term structural interaction. In addition, low stiffness repairs were ineffective in redistributing strain.

Loading conditions also affect the stability of the structure when materials of different elastic moduli are expected to carry the load. When load is perpendicular to the bond line the difference in load conditions does not cause problems, whereas if the load is parallel to the bond line the material with lower elastic modulus deforms and transfers a larger part of the load to the material with higher elastic modulus leading to fracture of this material (Kosednar and Mailvaganam, 2005).

Any concrete in general has a tendency to shrink on drying. If the concrete is allowed to dry freely, no cracking is observed whereas if the concrete is restrained from changing its dimension owing to shrinkage then cracking occurs as a result of development of high shrinkage stresses. Similarly, repair mortar/concrete is applied concrete substrate has a tendency to crack on drying. The substrate concrete acts as a restraint at the base or the periphery in case of repair concrete leading to potential damage to the dimensional stability of the total repaired element. The restraint provided by the substrate concrete results in development of different types of stress components and the interaction of which leads to failure in the repaired concrete. The potential failure modes include vertical cracking due to direct tension, horizontal cracking due to transverse or peeling tensile stresses, and delamination due to interface shear stresses as shown in Figure 2-2 (Baluch et al. 2002). Thus, the material properties to be considered to ensure reduced cracking of repaired concrete are tensile strength, shrinkage, relaxation and elastic modulus.

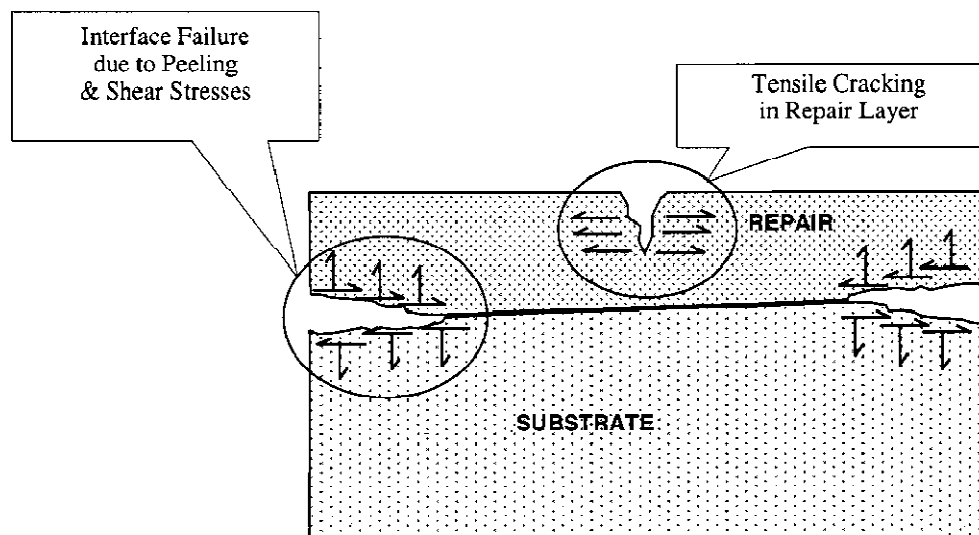


Figure 2-3. Modes of failure in patch repair (Baluch et al. 2002)

Another important property that can potentially increase cracking is coefficient of thermal expansion (CTE). It is important to closely match the CTE of the repair mortar/concrete with the substrate concrete. A composite system of two materials with different CTEs can cause volumetric instability when subjected to temperature changes. Typically, variation in CTE results in debonding of the repair concrete at the interface.

Structural and volumetric stability of repaired concrete is a crucial factor for long-term durability and serviceability of repaired concrete. Surface failure, resulting in cracking or peeling, increases the probability of substrate concrete being damaged by harmful salts and water.

2.3.2 Polymer / Epoxy Based Repair Material

A survey of the repair materials for overhead and vertical repairs was conducted and included manufacturers such as BASF, Sika and Dayton Superior. The survey and communication with the manufacturers indicated that most repair materials used for overhead applications are typically latex based polymer modified mortars.

Polymer modified cement repair materials are typically adopted for overhead and vertical repairs due to need for stiff mortars which do not require longer curing times unlike cement based repair material. Polymer based repair materials are formulated to provide properties tailored to the requirement of a specific application and take in account wet-state properties, surface penetration and hardened properties such as strength and permeability. According to ACI 548 (2005) the improvements from adding polymer modifiers to concrete include increased bond strength, freezing-and thawing resistance, abrasion resistance, flexural and tensile strengths, and reduced permeability. Polymer addition also increases resistance to penetration by water and dissolved salts, and reduced need for sustained moist curing.

The concept of polymer-hydraulic cement system is almost a century old and was first patented in 1923 (Ohama 1995b). There are various types of polymers that are used with hydraulic cements (ACI 2005). Among these, the most popularly used in the construction industry are elastomeric, thermoplastic and thermosetting types. Addition of each type of latex polymer imparts different properties when used as an additive or modifier. The most commonly used polymers for modification of cementitious mixtures are copolymers (S-A), styrene-butadiene copolymers (S-B), vinyl acetate copolymers (VAC), and vinyl acetate homopolymers (PVA) (ACI 2005; Ohama 1995a). According to the review done for ACI 548 (2005), “the selection of a particular polymer for a PMC depends on the specific properties required for the application. The optimum polymer is the least-expensive one that gives the required properties. Although the prices of polymers vary widely, in general, the cost of polymers depends on the price of their monomers and polymer prices from highest to lowest are PAE > S-A > S-B > VAE > PVA.”

2.3.3 Mechanism of Polymerization

The most common method of combining concrete with a polymer is to add polymer latex during mixing. The combination is called latex-modified concrete. Latex is an emulsion, a stabilized suspension of colloidal polymer beads. Polymers are usually used as admixtures; they are supplied as milky white dispersions in water. When a polymer is added to a cementitious mixture the polymerization is underpinned by two major mechanisms: cement hydration and polymer coalescence. In a polymer based cementitious system, typically cement hydration occurs first followed by setting and hardening of the mixture similar to non polymer based cementitious mixture. In case of polymer modified mixtures, the polymer particles start to concentrate in the void spaced created as the mixture starts to set. With continuous water removal by cement hydration, evaporation, or both, the polymer particles coalesce into a polymer film that is interwoven in the hydrated cement resulting in a mixture that coats the aggregate particles and lines the interstitial voids (refer to Figure 2-4). Flocculation of polymer particles takes place as water is removed by evaporation.

Typically, latex particles are greater than 100 nm in diameter and hence cannot penetrate the small capillaries in the cement paste that may be as small as 1 nm. Therefore, it is in the larger capillaries and voids that the latex can be most effective.

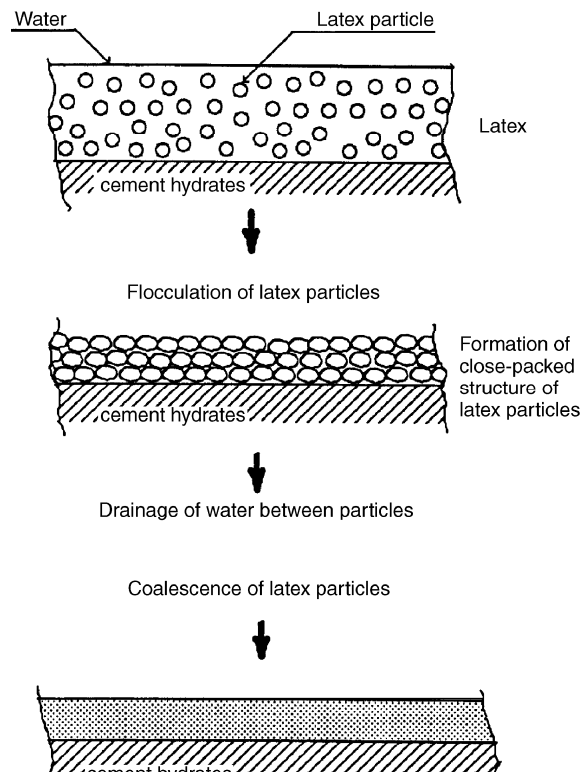


Figure 2-4. Simplified model of formation of polymer film on cement hydration (ACI 2005)

2.3.4 Fresh Polymer Repair Concrete Properties

Each type of polymer imparts different fresh and hardened properties to the polymer modified concrete. The properties of the fresh and hardened mortar and concrete are affected by a multiplicity of factors such as polymer type, polymer-cement ratio, water-cement ratio, air content, and curing conditions.

Figure 2-5 and Figure 2-6 show the effect of unit water content and polymer cement ratio on the consistency of latex modified mortars and concretes respectively (Ohama 1995a). The flow of the latex modified mortars increase as both, the water cement ratio and the polymer cement ratio increase.

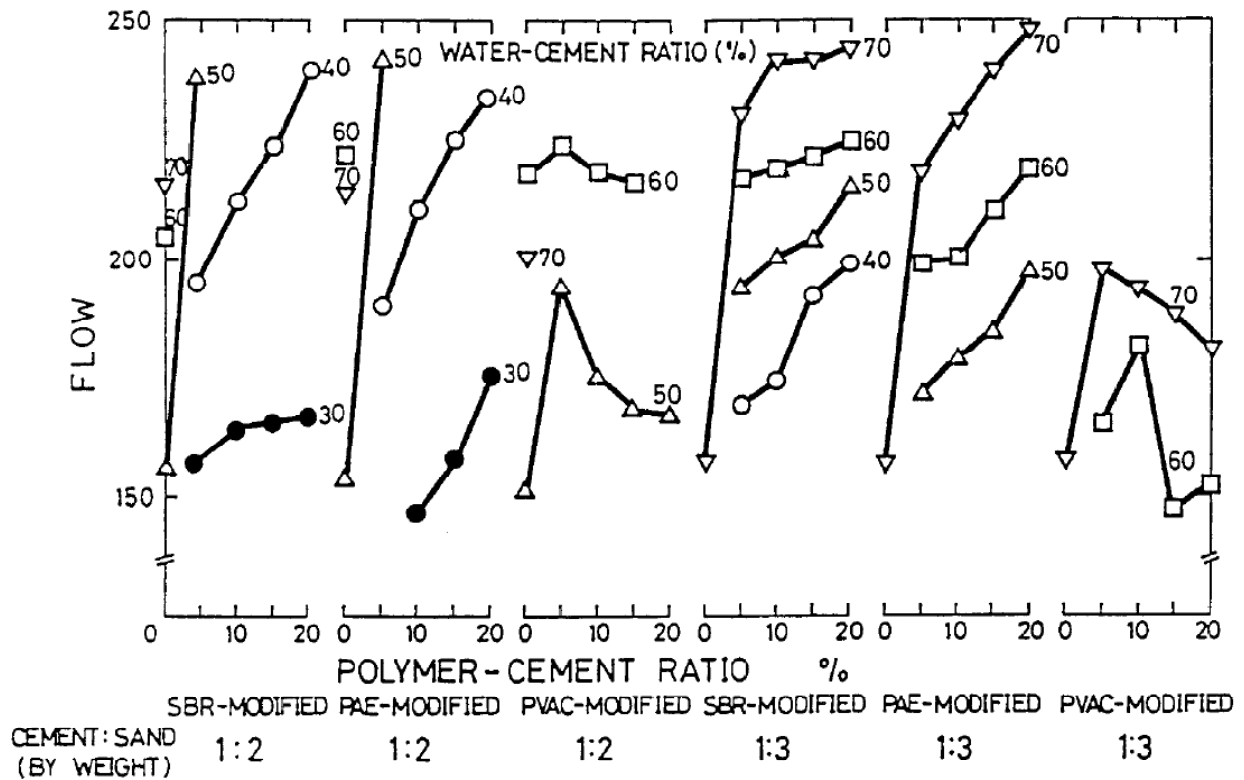


Figure 2-5. Effects of water-cement ratio and polymer-cement ratio on flow of latex modified mortars (Ohama 1995a)

The slump of the latex-modified concretes tends to increase with rising unit water content (or water-cement ratio) and polymer-cement ratio, and at each unit water content, a rise in the polymer-cement ratio causes an increase in the slump. This tendency is more significant at smaller sand-aggregate ratios and at large unit cement contents (Ohama 1995a).

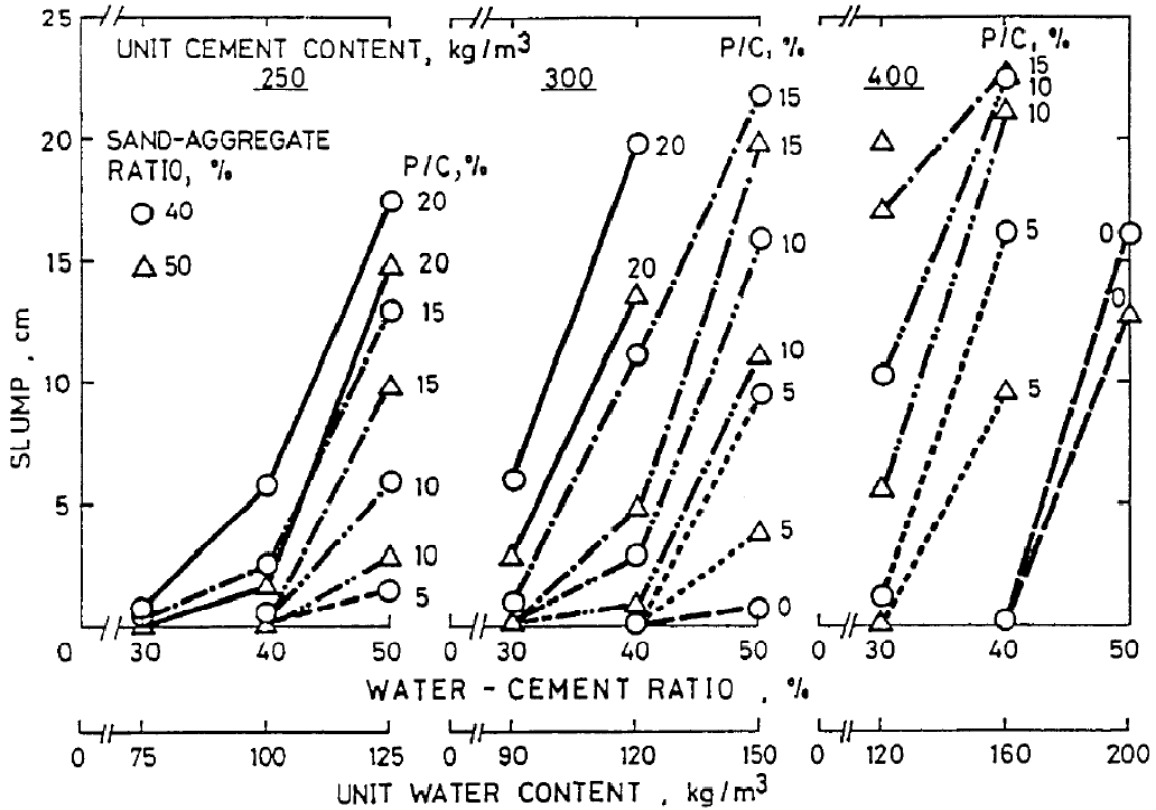


Figure 2-6. Effects of unit water content (water-cement ratio) and polymer-cement ratio on slump of SBR modified concrete (Ohama 1995a)

In most latex-modified mortars and concretes, a large quantity of air is entrained compared to that in ordinary cement mortar and concrete because of an action of the surfactants contained as emulsifiers and stabilizers in polymer latexes. An excessive amount of entrained air causes a reduction in strength and must be controlled by using proper antifoaming agents. Recent commercial latexes for cement modifiers usually contain proper antifoaming agents, and the air entrainment is considerably decreased. Consequently, the air content of most latex-modified mortars is in the range of 5 to 20%, and that of most latex-modified concretes is less than 2%, much the same as ordinary cement concrete. Such decreased air content of the latex-modified concretes over the latex-modified mortars is probably explained by the fact that air is hard to entrain in the concretes because of the larger size of aggregates used (Ohama 1995b).

Latex-modified mortar and concrete have markedly improved water retention over ordinary cement mortar and concrete. The water retention is dependent on the polymer-cement ratio. The reasons for this can probably be explained in terms of the hydrophilic colloidal properties of

latexes themselves and the inhibited water evaporation due to the filling and sealing effects of impermeable polymer films formed. Accordingly, a sufficient amount of water required for cement hydration is held in the mortar and concrete and, for most latex-modified systems, dry cure is preferable to wet or water cure (ACI 2005; Ohama 1995a).

In contrast to ordinary cement mortar and concrete, which are apt to cause bleeding and segregation, the resistance of latex-modified mortar and concrete to bleeding and segregation is excellent in spite of their larger flowability characteristics. This is due to the hydrophilic colloidal properties of latexes themselves and the air-entraining and water-reducing effects of the surfactants contained in the latexes. Accordingly, in the latex modified systems, some disadvantages such as reductions in strengths and water loss caused by bleeding and segregation do not exist. Al-Zaharani et. al. (2003) assessed various types of commercial polymer based repair materials. In their study, they have noted that those polymer mortars which exhibited low flowability exhibited no bleeding in comparison to plain cementitious mortars which had similar flow characteristics.

2.3.5 Hardened Polymer Repair Concrete Properties

To ensure durability of structures repaired with polymer modified mortars/concretes it is necessary to ensure that the properties of the substrate concrete match with those of the repair material intended for use. In this section, hardened properties of polymer modified mortars are discussed.

In a study comparing four commercial polymer based repair materials with cement based repair materials, Al-Zahrani et al. (2003) report that polymer based repair mortars exhibit an increase in compressive strength between 2700 psi to 8700 psi. The polymer based repair mortars did not exhibit any higher strength gains in comparison to the cement and water based mortars. Studies also indicate that the strength gain is clearly dependent upon many factors such as type of polymer and polymer cement ratio adopted in the repair mortar, curing methods and testing methods (Mirza et al. 2002). The strength properties of the latex modified mortars and concretes are influenced by these factors and they tend to interact with each other. In their study of 25 polymer modified mortars, Mirza et al. (2002) have shown that the compressive strength of acrylic based polymer modified mortars increases as the polymer-cement ratio increases,

however the type of curing has a moderate effect on the compressive strength and is slightly reduced when the samples are wet cured.

In general, latex-modified mortar and concrete show a noticeable increase in tensile and flexural strengths but no improvement in the compressive strength as compared to ordinary cement and mortar concrete. The increase in tensile strength is related to the high tensile strength of the polymer in itself and improved cement aggregate bond (Ohama 1995b). Researchers report tensile strengths in the range of $1/10^{\text{th}}$ of the compressive strength for polymer modified mortars using styrene butadiene or acrylic polymers whereas mortars prepared using epoxy based polymers exhibit tensile strengths in the range of $1/5^{\text{th}}$ of compressive strength (Hassan et al. 2000; Mirza et al. 2002).

The bond strength characteristics are vastly improved by using polymer modified cement based repair mortars (Lavelle 1988; Mirza et al. 2002; Ohama 1995b). Studies have shown that mortars containing styrene butadiene rubber based polymer modified cementitious systems exhibit approximately 20 % higher bond strengths in comparison to the bond strengths of mortars modified by acrylic based polymers (Lavelle 1988; Mirza et al. 2002). The type of curing does not affect the bond strength of polymer modified repair mortars. It has been reported that the bond strength of mortars containing styrene butadiene rubber polymer modifiers decreases over time when subjected to freezing and thawing cycles but stabilizes over a period of five years. Surface preparation and adhesion play an important role in the long-term bond strength of polymer based mortars to concrete substrate.

Elastic modulus plays an important role in maintaining the dimensional stability of the repaired structure. Polymer modified mortar and concretes contain polymers with considerably smaller modulus of elasticity compared to cement hydrates. Consequently the deformation of polymer modified mortars and their ductility can differ greatly than ordinary cement mortars and concretes. Generally, the maximum compressive strain at failure increases with increasing polymer-cement ratio though the elastic modulus in compression remains somewhat constant. Researchers have shown that the type of polymer modifier used has a significant effect on the elastic modulus of the repair mortar (Hassan et al. 2000; Lavelle 1988; Mirza et al. 2002).

Polymer properties are sensitive to relatively small temperature changes and they are significantly time dependent. Hence, it is imperative that information on the coefficient of thermal expansion (CTE) for a selected polymer modified mortar be assessed before using it in field. According to Ohama (1995a), the CTE of latex-modified mortar and concrete is directly influenced by that of the aggregates used, as in ordinary cement mortar and concrete. Latex modified mortars and concretes usually have coefficients of thermal expansion equal to or slightly higher than that of ordinary cement mortar or concretes.

Another important aspect of dimensional stability is the shrinkage properties of the individual repair material as well as of the complete structural system as a whole. The drying shrinkage of polymer modified mortars may be either large or small and is dependent upon polymer type and polymer-cement ratio. Researchers have shown that the drying shrinkage at 28 days for commercially available polymer modified repair mortars is typically between 150 μ to 1200 μ . The shrinkage strain development also depends on the ambient relative humidity and the restraint provided by the substrate. A polymer modified mortar exhibiting smaller drying shrinkage strains may not necessarily remain uncracked on the field. It is essential to understand the variation in development of tensile creep, tensile modulus of elasticity and drying shrinkage combined to predict the cracking tendency of polymer modified repair mortars (Pinelle 1995).

2.3.6 Durability Performance of Polymer Based Repair Concrete

The structure of latex modified concretes is such that the micropores and voids normally occurring in hardened portland-cement concrete are partially filled with the polymer film that forms during curing as explained in the section on polymerization (Section 2.3.1). This film is the reason for the mixture's reduced permeability and water absorption. These properties have been measured by several tests, including water-vapor transmission, water absorption, carbonation resistance, and chloride permeability. There are indications that the permeability of latex modified mortars decreases significantly with age beyond 28 days (Kuhlmann and Foor 1984). The same study also indicated that amount of air (i.e. air content present in polymer based mortars) does not affect the chloride permeability. It was found that even at high amounts of air contents the air voids are small and well distributed and permeability does not increase. Researchers have conducted tests to ascertain affects of curing regime on chloride permeability

by ponding specimens for 90 days in plain water and salt solution. It was observed that resistance to chloride ion penetration increased with increasing polymer content.

As reported in ACI 546 the resistance of LMC to damage from freezing and thawing has been demonstrated both in the laboratory (Ohama 1995a; Smutzer and Hockett 1981) and in the field (Bishara 1979). The frost resistance of SBR, PVA and EVA modified mortars is improved markedly at polymer cement ratios of 5% or more. It has been observed that as the degree of expansion by frost (calculated from the residual expansion of specimens from freezing and thawing) increases, the relative dynamic modulus of polymer modified mortars is reduced (Ohama 1995b). Increasing the polymer cement ratio does not necessarily cause an improvement in the frost resistance, and good frost resistance can be achieved by the composite effects of polymer modification and stable air content.

2.3.7 Gaps in Knowledge

During the literature review conducted for this study, it was noted that not many publications are available that deal with the fresh and hardened properties of commercially available proprietary materials. This gap in knowledge can be attributed to the fact that there are numerous types of polymer modified repair mortars and manufacturers develop products based on the needs of the region where it is being sold. Given this diversity in material components, two references that have been cited extensively in the earlier sections (ACI 2005; Ohama 1995b) appear to have a comprehensive collection of information on polymer modified mortars including different types polymers and its effects on properties. In order to approve a particular material for use in repair it is essential to evaluate its fresh and hardened properties. The durability of the repair material itself and the composite system consisting of the repaired concrete and the substrate concrete is an important parameter contributing to the long-term performance of the repaired structure. It is essential to adopt a holistic approach in repairing structures so that concurrent interaction of many factors such as shrinkage, permeability and absorptivity are considered.

2.4 SHEAR KEY MATERIALS

Section 5.14.4.3.2 of AASHTO Standard Specifications (2002) requires that the shear-key depth between the beams shall not be less than 7 inches. Longitudinal shear transfer joints are permitted to be modeled as hinges for analysis. The strength of the non-shrink grout material for the shear-key is required to be a minimum of 5 ksi at 24 hours. Section 5.14.1.2.8 of AASHTO LRFD (2004) specifies that the depth of shear key shall not be less than 5-in. and filled with non-shrink mortar attaining a compressive strength of 4 ksi within 24 hours. Section 708.3 of MDOT Standard Specifications for Construction (2003b) specifies Type R-2 grout to fill the longitudinal joints between beams. The transverse posttension is applied following 48 hours of curing of the grout. The mechanical properties of the Type R-2 grout will be given in Chapter 6.

2.4.1 Commercial Grout Materials

According to Gulyas et al. (1995), non-shrink grout (Set Grout) materials are not able to develop the specified minimum compressive strength within 24 hours. Comparative test results by Gulyas et al. (1995) showed that the magnesium ammonium phosphate ($\text{Mg-NH}_4\text{-PO}_4$) or so-called Set 45 grout samples develop a significantly higher strength than the non-shrink grout specimens. Issa et al. (2003) performed a total of 36 experiments for vertical shear, direct tension, and flexural capacity using four different grout materials. Polymer concrete was found to be the best material for transverse joints in terms of strength, bond, and mode of failure. However, the use of Set Grout was recommended for the transverse joints due to its ease of use and satisfactory performance. It was also recommended that polymer concrete may be used in critically stressed joints and for rapid replacement of bridge decks due to its rapid hardening properties (4500 psi in one hour) (Table 2-2).

Table 2-2. Grout Material Properties (Issa et al. 2003)

Age of Testing	Type of Test	Strength of Grout Materials, psi		
		Set 45 (Mg-NH ₄ -PO ₄)	Set Grout (Non-shrink grout)	Polymer Concrete
3 hours	Compressive	-	-	9752
6 hours	Compressive	3718	-	10,169
1 day	Compressive	3775	2841	10,357
3 days	Compressive	4294	5109	10,460
	Tensile	574	548	988
7 days	Compressive	5516	6312	10,550
	Tensile	587	598	1130
28 days	Compressive	6122	10,031	10,756
	Tensile	605	703	1153

Compatibility of properties between parent material (box-beam material) and the joint material (shear key material) is an important parameter of structural and durability performance of box-beam bridge superstructure. The joint material is expected to transfer moment and shear while retaining the water tightness of the joints. Hence, the grout compressive, tensile, and bond strength, elasticity modulus, shrinkage, thermal expansion coefficient, permeability, and potential of joint sealing properties are of interest in this study. Further, cementitious materials/mixes that are used as grout are studied. Table 2-3 summarizes mechanical and durability properties of materials that are used or have a potential to be used for forming the joints between precast components. Data presented in Gulyas et al. (1995), Issa et al. (2003), Scholz et al. (2007), and Manufacturers' data sheets are the sources of information for developing Table 2-3. Scholz et al. (2007) performed the tests in accordance with the ASTM standards (ASTM C39, ASTM C 496, ASTM C 882, ASTM C 157, and ASTM C 1202). A ponding test was performed evaluating the potential for leakage at the shear key.

AASHTO Standard (2002) Section 5.14.4.3.2 requires 5000 psi grout compressive strength in 24 hours, while LRFD (2004) Section 5.14.1.2.8 requires 4000 psi. According to the data presented in Table 2-3, only a few materials are capable of satisfying the AASHTO strength requirements. According to Michigan practice, posttension is applied 48 hours (2 days) after grouting the shear keys (MDOT 2003b). This two-day lag time will help grout materials develop adequate strength before posttension applications. AASHTO LRFD (2004) requires that transverse posttensioning generates a stress level 250 psi at the shear key. All the materials listed in Table 2-3 show sufficient strength such that 250 psi compressive stress can be applied with a factor of safety of at least three.

In addition to facilitating load transfer through the joints between precast beams, grout materials are expected to prevent moisture intrusion into the joint. The data presented in Table 2-3 contradicts the common perception. It is expected that grout materials with good bond strength and lower shrinkage prevent moisture intrusion through the grouted joints. According to the data presented in Table 2-3, water leaks through the interface when grout material has lower shrinkage but higher bond strength. This indicates that a focus should be placed on not only shrinkage and bond properties, but also many other grout properties such as thermal expansion coefficient, mechanical properties, and compatibility between grout and beam material properties. Scholz et al. (2007) evaluated the joint sealing performance using a ponding test. In the test, the interface was not subjected to any clamping force; whereas, in precast systems, the joint is expected to be under compressive stress of some uniformity. Posttension force magnitude, force application sequence, and number of posttension locations are functions of the material used for shear keys to achieve uniform stress distribution throughout the shear keys.

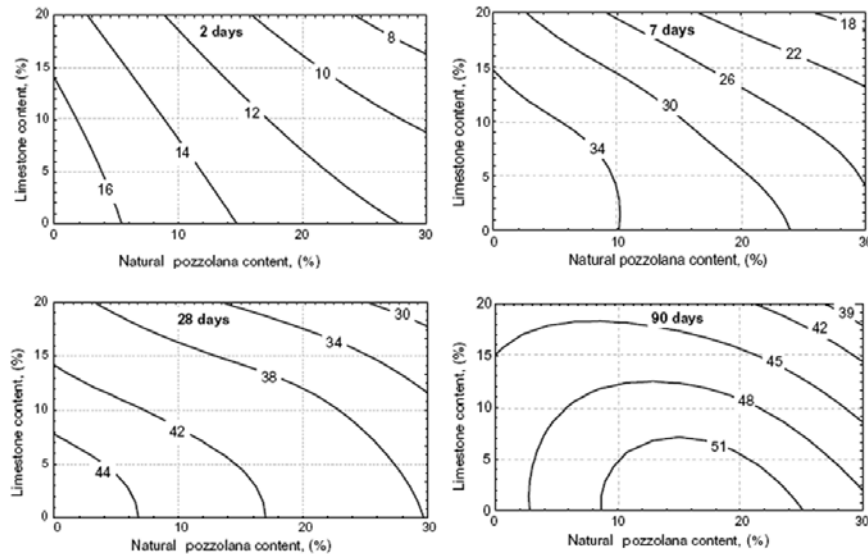
Table 2-3. Summary of Grout Material Properties

Grout Type	Compressive Strength (psi)		Tensile Strength (psi)	Bond Strength (psi)	Shrinkage (in.)	Leakage		Thermal Expansion Coefficient (10 ⁻⁶ /F)	Permeability (coulomb)	Elasticity Modulus (10 ⁶ psi)
	1-Day	7-Day	7-Day		28-Day	1 month	6 months		28-Day	
ThoRoc®10-60	5210	6380	540	540	0.0076	No	No			
SikaQuick®2500	3540	4710	340	1400	0.0080	No	No			4.6
Five Star®Patch	5080	5820	530	1810	0.0029	No	Yes			
Set®45 HW	4930	4930	410	470	0.0034	No	Yes	7.15		5.25
ThoRoc®extended	3150	5040	510	1730	0.0064	No	No			
SikaQuick®extended	1900	2550	335	850	0.0089	No	No			
Five Star®extended	4490	5440	555	1680	0.0036	No	Yes			
Set®45 extended	2650	4180	415	950	0.0018	No	Yes	7.15		5.25
Set®45	3375	5516	587	>252				7.15	606	4.55
Set Grout	2841	6312	598	85					2544	
Polymer concrete	10357	10550	1130						22	

Source: Gulyas et al., 1995, Issa et al., 2003, Scholz et al., 2007, and Manufacturers' data sheet

2.4.2 Other Cementitious Materials

Other cementitious materials that may have a potential of being used as grout materials are reviewed. Ghrici et al. (2007) studied the mechanical properties and durability of mortar and concrete containing natural pozzolana and limestone blended cement. Figure 2-7 shows the variation of compressive strength of mortar cubes made of different proportions of limestone filler (LF) and natural pozzolana (NP). Early age strength can be controlled by varying limestone filler (LF) content from 0 - 14% and natural pozzolana (NP) content from 0-5% (Figure 2-7). This demonstrates the potential for developing customized mixes based on the strength requirements at a specific time upon placement.



Note: 0.0069 MPa = 1 Psi

Figure 2-7. Compressive strength (in MPa) of mortar cubes at different ages (Ghrici et al. 2007)

Further, this study demonstrates that small percentage of natural pozzolana enhances the durability properties of concrete or mortar. The same ratio of blended mortar or concrete (OPC + 20% NP + 10% FL) mixture with a water/binder (w/b) ratio of 0.4 reduced the capillary sorption by 25%. The C-S-H is formed by the pozzolanic reaction in concrete and is instrumental in reducing the capillary sorption of concrete. Also, paste-aggregate interface quality is enhanced by this reaction.

The chloride penetration measured in terms of charge that passes through the specimens in unit time, in coulombs, is obtained at the age of 28 and 90 days. For 0.4 w/b ratio, concrete containing (OPC + 30% NP) exhibits greater resistance to chloride ion permeability (Figure 2-8).

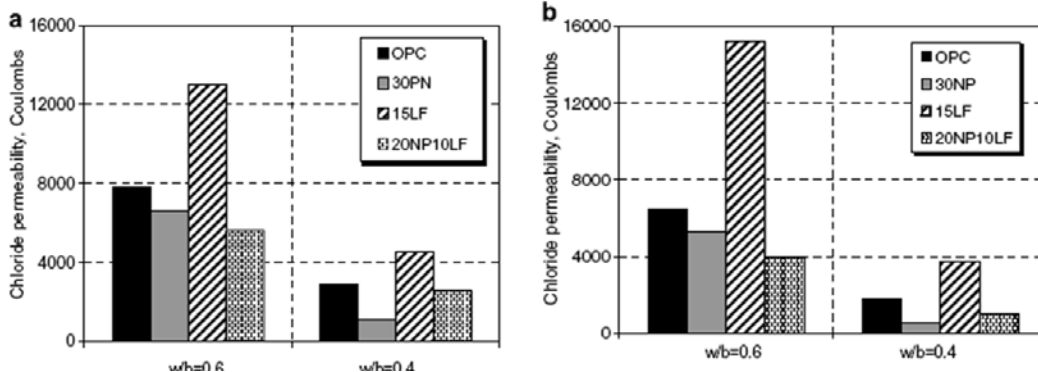
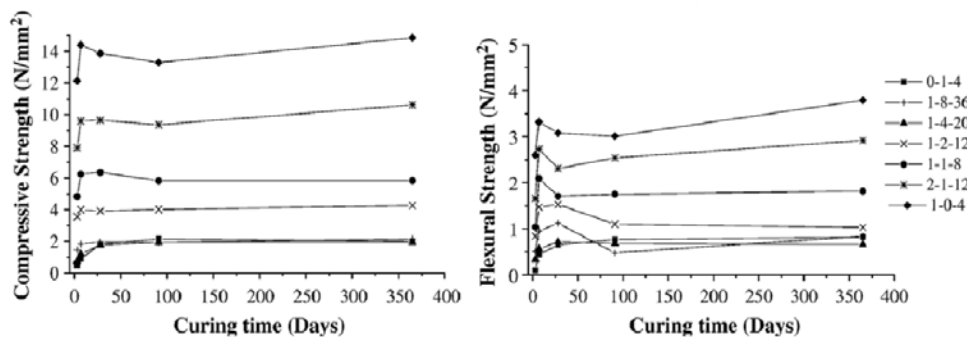


Figure 2-8. Chloride permeability of concrete at (a) 28 days and (b) 90 days (Ghrici et al. 2007)

Arandigoyen and Alvarez (2007) studied pore structure and mechanical properties of cement-lime mortar. According to experiments that were conducted on seven different proportions of cement-lime-calcite aggregate with three different binder/aggregate (B/Ag) ratios (by volume) such as 1:2, 1:3, and 1:4; it was observed that porosity is independent of the lime-cement ratio but depend on B/Ag ratio.

The study on influence of binder composition on mechanical strength of mortar showed that 0 to 40% of an increase in cement-in-lime rich mortar increases mechanical strength slightly. This is in contrast to a 25% increase in lime-in-cement rich mortar, in which mechanical strength diminishes considerably (Figure 2-9).

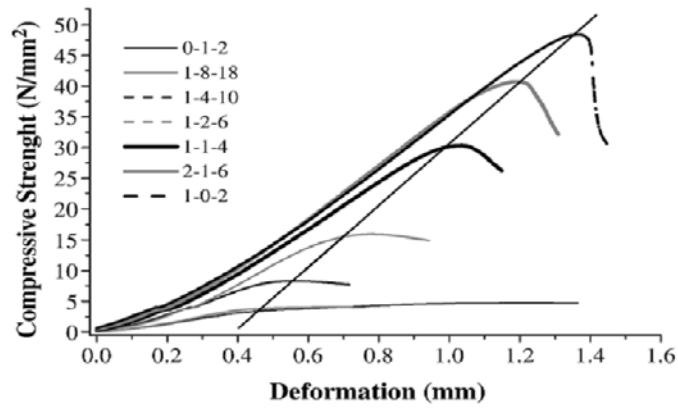


Note: 0-1-4 to 1-0-4 are the cement/lime/aggregate ratios by volume

Figure 2-9. Variation of compressive and flexural strength of mortar against time (Arandigoyen and Alvarez 2007)

Modulus of elasticity increases with the increase in cement percentage in the binder and with the increase in the B/Ag ratio. It was concluded that cement-rich mortar with high modulus may develop cracks and breakage after going through a phase of elastic deformation. On the other hand, lime-rich mortars (0-1-2 and 1-8-18) are able to absorb a high degree of deformation

before the breakage. The presence of plastic zone for the lime – rich mortar is large along with higher flexibility.



Note: From 0-1-2 to 1-0-2 are the cement/lime/aggregate ratios (by volume)

Figure 2-10. Changing mortar compressive strength (MPa) against deformation (mm) (Arandigoyen and Alvarez 2007)

Yurtdas et al. (2005) studied the influence of water/cement (w/c) ratio on mechanical properties of mortars that are submitted to drying. Mortar with two different w/c ratios of 0.5 and 0.8 were labeled as mortar05 and mortar08. Figure 2-11 describes the effect of drying on the uniaxial compressive strength of the Mortar05 and Mortar08. It is observed that the compressive strength of both the mortar samples remains almost constant with the increase in relative weight loss (RWL) which is defined in Eq. 2-1. For the mortar08 the strength increases by 32% at RWL value of 30%, and it decreases by same amount at 100% RWL. The strength of the mortar05 increases by 21% at 30% RWL and then remains constant.

$$RWL(t) = 100 \times \frac{(W_{(t)} - W_0)}{(W_{dry} - W_0)} \quad (2-1)$$

where;

W_{dry} = dry weight of the sample

W_0 = initial sample weight

W_t = weight at time t

Two reasons are defined for the increase in the compressive strength:

1. Isotropic effect of capillary pressure, and
2. Confining of the sample core induced by moisture gradient.

It can also be concluded from Figure 2-11 that the mortar05 has higher compressive strength than the mortar08.

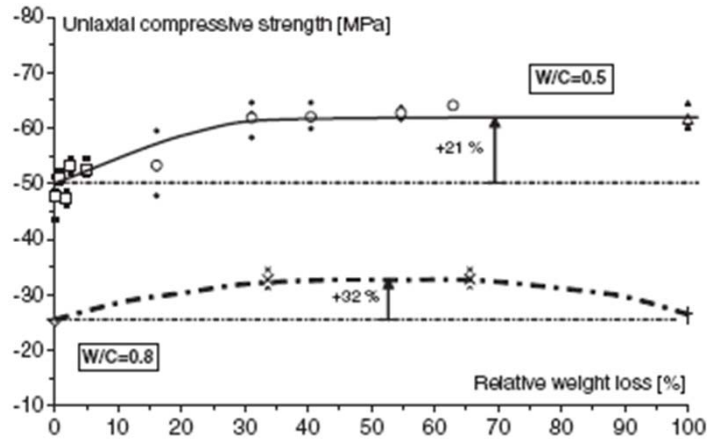


Figure 2-11. Variation of uniaxial compressive strength against relative weight loss of mortar (Yurtdas et al. 2005)

According to the data presented in Figure 2-12, Young's modulus for both samples remains constant up to an extent of relative weight loss (RWL), and then the modulus drops by 15% and 18% for mortar05 and mortar08, respectively. During the curing process capillary suction plays a dominant role due to higher content of water in the sample. This increases the apparent stiffness of the sample and reduces the effect of microcracking on the sample while maintaining the modulus of elasticity. After certain RWL the effect of capillary suction diminishes, and the effect of microcracking becomes dominant; hence, the reduction in the modulus of elasticity is observed.

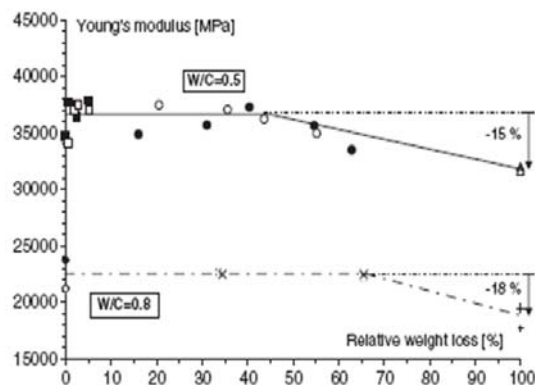


Figure 2-12. Variation of elasticity modulus against relative weight loss of mortar (Yurtdas et al. 2005)

2.4.3 The Bond between Girder and Shear Key Materials

Miller et al., (1999) studied the performance of shear-keys at locations along the girder depth considering non-shrink grout and epoxy as grout material. According to research findings, when epoxy is used substrate concrete cracks rather than the shear-key. This failure mode was defined as undesirable. Gulyas et al. (1995) showed that the failure mode for the non-shrink grout specimens tend to be at the bond line while the failure mode for the Mg-NH₄-PO₄ grout (Set 45) was usually at least partially through the substrate. In the study conducted by Issa et al. (2003), polymer concrete showed failure through the substrate. According to Gulyas et al. (1995) and ACI 503.1 Appendix Testing (1992), preliminary consideration should be given to grout materials that have inherent bond strength high enough to fail in the substrate material.

The composite direct tension test performed by Gulyas et al. (1995) showed that the bond failure occurs at a tensile load of 1940 lbs corresponding to a stress value of about 85 psi for non-shrink grout. The tensile strength of the non-shrink grout was 390 psi. Considering this tensile strength and the three-day tensile strength given by Issa et al. (2003) shown in Table 2-2, the bond between shear key grout and the beam fails before shear key grout tensile strength is reached.

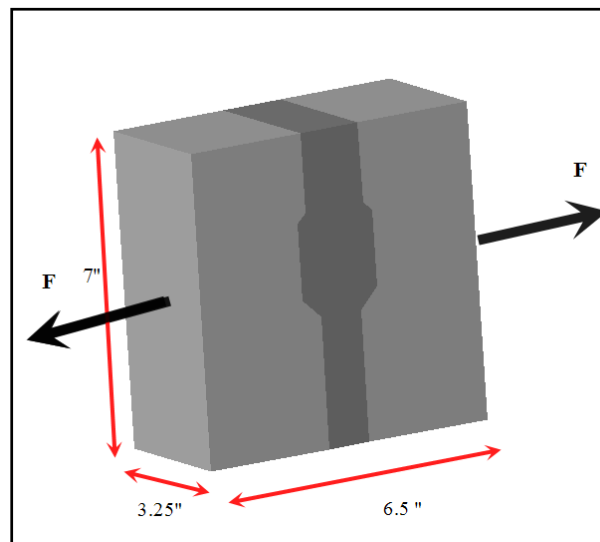


Figure 2-13. Composite direct tension test (Gulyas et al. 1995)

The literature on the side-by-side box beam modeling and analyses with transverse post-tensioning is limited. El-Remaily et al. (1996) modeled the assemblage as a grillage allowing the joint to transfer shear, bending, and torsion. Dong (2002) assumed a perfect bond between the

grout and the beam surface throughout his analysis. Issa et al. (2003) simulated direct shear testing of a specimen modeling concrete crushing and cracking. Hawkins and Fuentes (2003) incorporated the link elements based on a beam-on-elastic foundation concept to define joint flexibility. According to this concept, connectivity stiffness controlling the relative vertical displacements of two adjacent beams is assumed proportional to shear force transmitted through the joint between the beams. The joint stiffness upon cracking and shear key fracture is then modeled by reducing the degree of shear force transferred between girders. It was concluded that cracking of the longitudinal joint had little effect on the stiffness of the bridge provided that the transverse tie rods were snug.

2.4.4 Load Bearing Capacity of Mortar joints

Barboza et al. (2006) studied the bearing capacity and compressive strength of mortar joints between precast elements. The bearing capacity is typically governed by the splitting stress of precast elements. Splitting stresses are developed due to flow of compressed grout to the border that develops frictional forces and “pulls” the precast element apart or the redistribution of stresses at the joint. The hypotheses for these behaviors are illustrated in Figure 2-14.

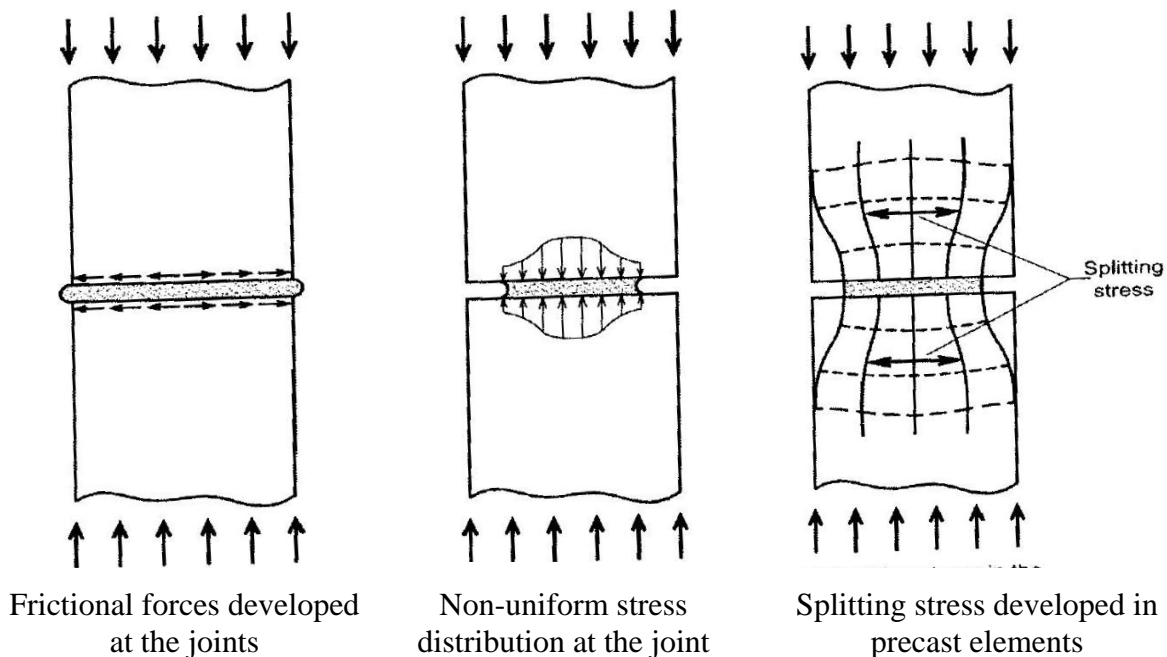


Figure 2-14. Stresses developed at the joints and in the precast elements (Barboza et al. 2006)

Summarizing the work presented by Dragosavic (1978), Barboza et al. (2006) stated that the load-bearing capacity of a mortar grouted joint between precast elements under compressive loads can be determined based on the following conditions:

1. If the mortar compressive strength is greater than that of precast elements, the load-bearing capacity of the connection is equal to the compressive strength of the precast element.
2. If the compressive strengths of the mortar and precast elements are the same, the capacity of the connection will be equal to the compressive strength of the mortar, which equals the compressive strength of the precast elements.
3. If the compressive strength of the mortar is less than the compressive strength of the precast element, and the ratio of minor joint width and the joint thickness is small, the joint load-bearing capacity (f_j) can be calculated using the following equation:

$$f_j = \alpha f'_c \quad (2- 2)$$

where, f'_c is the compressive strength of concrete used in precast elements, and the factor α is determined from Figure 2-15. The factor α defines the joint efficiency.

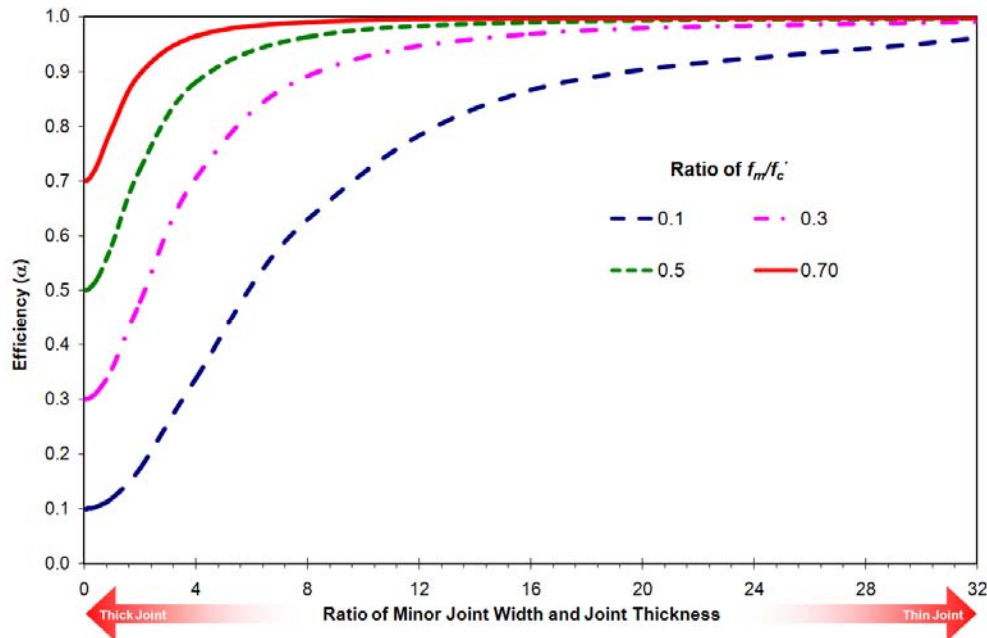


Figure 2-15. Variation of joint efficiency (α) against the ratio of minor joint width and joint thickness

In Figure 2-15, the ratio of minor joint width and the joint thickness is plotted along the x-axis and efficiency (α) along the y-axis. The family of curves, corresponding to the ratio of the compressive strength of the mortar (f_m) and precast element (f'_c), is plotted against α .

Barboza et al. (2006) presented an equation proposed by Vambersky (1990) as an updated version of the original equation proposed by Dragosavic (1978) that incorporates the type of grout.

$$f_i = \eta \alpha f'_c \quad (2-3)$$

where, η

= 0.9 for fluid mortar placed in joint after assembly

= 0.7 for dry mortar placed in joint after assembly

= 0.3 for elements placed on mortar beds

Barboza et al. (2006) also conducted experiments to verify these equations by varying the joint thickness and the compressive strength of grout. The test configuration consisted of two axially loaded square columns with a 7 in. \times 7 in. (175 mm \times 175 mm) cross-section (Figure 2-16).

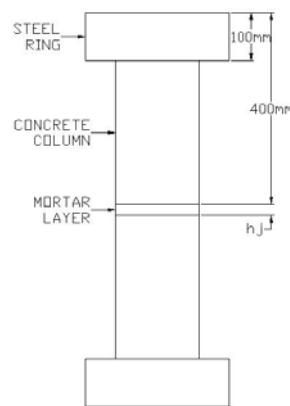


Figure 2-16. Test configuration used by Barboza et al. (2006)

The Barboza et al. (2006) study shows that the use of thin joints increases the joint load-bearing capacity when the grout material strength is lower than that of the precast elements. However, maintaining a uniform thickness of grout in thin joints is difficult but essential to generate uniform stress distribution.

2.5 THE INFLUENCE OF DIAPHRAGMS ON POSTTENSION STRESS DISTRIBUTION

The AASHTO LRFD (2004) Section 5.13.2.2 states that “diaphragms shall be provided at abutments, piers, and hinge joints to resist lateral forces and transmit loads to points of supports unless otherwise specified. Intermediate diaphragms may be used between beams in curved

systems or where necessary to provide torsional resistance and to support the deck at points of discontinuity or at angle points in girders.”

In side-by-side box beam bridges, the diaphragm function is more than what is specified in the AASHTO, such as in the transfer of post tensioning forces, distribution of clamping stress to keep shear keys under compression as well as forming a couple with the shear key for moment transfer between the girders. The AASHTO LRFD (2004) did not provide specific provisions for the side-by-side box beam bridge diaphragms. Several State Highway Departments have developed a criterion for the number of diaphragms and posttension locations and force magnitudes based on the depth of the girder and span length.

El-Remaily et al. (1996) proposed a design procedure for calculating posttension force magnitude from grillage analysis. According to the grillage procedure, the joints between the beams can transfer shear, bending, and torsion. The transverse connection between adjacent box-beams is through the diaphragms, so the shear key along the full length of the beam is not essential for the structural performance of the bridge. Thus, posttensioned diaphragms serve as the primary wheel load transfer mechanism between adjacent boxes. The number of diaphragms was calculated based on a parametric study that was carried out to limit differential displacements between the girders to 0.02 inches. According to the parametric study results, the posttension force magnitude is a function of beam depth and bridge width. The PCI Design Manual (2003), based on El-Remaily’s analyses, recommends the use of three diaphragms for spans up to 60 ft (one @ each end, one @ mid-span) and five diaphragms for spans over 60 ft (1 @ each quarter point, 1 @ center of beam, and 1 @ each beam end).

2.5.1 Assessment of Load Distribution between Adjacent Girders

Posttensioned diaphragms serve as the primary wheel load transfer mechanism between adjacent boxes according to El-Remaily et al. (1996). Without posttensioned diaphragms each beam would have to carry the full wheel line load (Figure 2-17). El-Remaily’s analysis was to assess the posttensioning effect on limiting differential displacement of the girders to 0.02 inches.

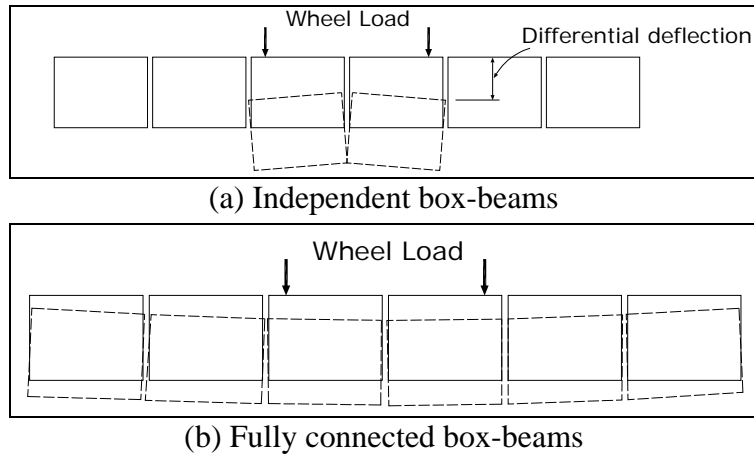


Figure 2-17. Deflection of a box-beam bridge (El-Remaily et al. 1996)

2.5.2 Bridge Width Effect on Posttension Stress Distribution

Section 5.14.1.2.8 of the AASHTO LRFD (2004) requires that transverse posttension stress, after all losses, shall not be less than 0.25 ksi along the shear key. However, the contact area between girders and the procedure for calculating transverse posttension force magnitude are not defined in the AASHTO LRFD (2004). This contact area can be regarded as the shear-key area, or the diaphragm-to-diaphragm contact area, or the entire side surface of the box-girder. El-Remaily et al. (1996) recommends considering the diaphragm-to-diaphragm contact area for the design.

The required posttension force also depends on bridge width (Figure 2-18). According to El-Remaily et al. (1996), the grillage analysis can be performed for calculating the force demand at the diaphragm locations.

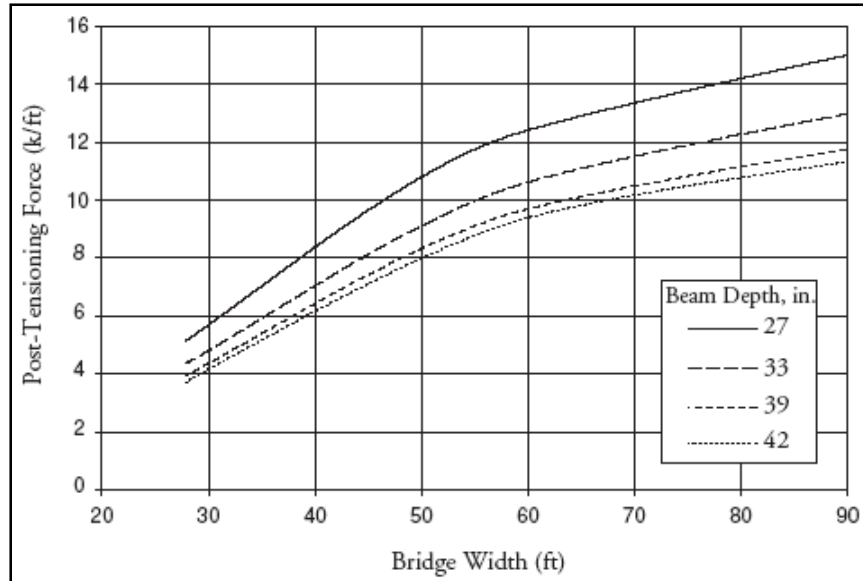


Figure 2-18. Posttension force variation with bridge width and beam height (El-Remaily et al. 1996)

2.6 SUMMARY AND CONCLUSIONS

This chapter summarized research related to capacity evaluation and load testing of distressed bridges/girders, materials used for shear keys, properties of cementitious materials and development of customized materials. The following list of conclusions is reemphasized in order of importance:

1. Fatigue is not an issue for uncracked beams. Fatigue may be an issue under frequent loading on bridges that creates bottom fiber stress in excess of $6(f_c')^{1/2}$ psi or strand stress greater than $0.06f_{pu}$.
2. Distressed beam capacity can be accurately evaluated by analytical models.
3. Customized shear key grout mixes can be developed for specified strength requirements at a particular age of material.
4. Load transfer efficiency of the shear key joint increases as the thickness decreases. However, uniform thickness of the joint is vital to maintain uniform stress distribution.
5. Diaphragms generate rigid zones in the box-beam bridge superstructure and work as the primary load transfer mechanism.
6. The transverse posttension magnitude needs to be specified as a function of bridge width.

Intentionally left blank

3 LOAD TESTING OF DECOMMISSIONED BOX-BEAM

3.1 OBJECTIVE AND APPROACH

The failure of a fascia girder of Lakeview Drive bridge in Pennsylvania on December 27, 2005 prompted the capacity evaluation of box beams with similar deterioration. The objective of the work discussed in this chapter is to remove a severely deteriorated fascia beam, instrument it, and perform load testing for evaluating the capacity of the beam. The remaining prestress was calculated from camber measurements and the strain gauge data. Beam capacity is calculated using strain data, and load rating is performed.

3.2 OVERVIEW

The four span side-by-side box beam bridge is located in Jackson County and carries traffic in north-south directions of Hawkins Road over the I-94 freeway (Photo 3-1). This bridge was built in 1957 and contains 11 double-cell box-beams on each span. The width of each beam is 36-inches. Spans two and three contain 21-inch deep beams over the I-94 freeway. The other two spans have nine 17-inch deep interior beams and two 21-inch deep fascia beams. The width of the bridge is 33' – 7½". The total length of the bridge is 164 ft. Each span over the freeway is 48'-6" long.



Photo 3-1. Bridge on Hawkins Road over I-94 (S11-38101)

Inspections revealed that the west fascia beam over westbound I-94 had a full-length crack with heavy leaching on the beam soffit (Photo 3-2).



Photo 3-2. West fascia beam with full-length crack

The bridge wearing surface showed multiple longitudinal cracks (Photo 3-3) reflecting from the girders. The transverse connection between the beams is provided by a shallow grouted shear key and a one-inch diameter tie-rod at 1/3rd locations along the second and third spans and at the center of the first and fourth spans (Photo 3-4).



Photo 3-3. Wearing surface with multiple longitudinal cracks

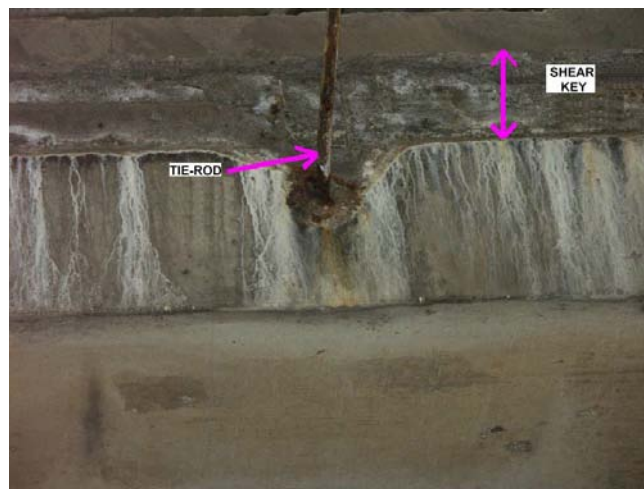


Photo 3-4. Shallow grouted shear key and tie-rod

The box-beams used in the 1950s were fabricated with open stirrups as shown in (Figure 3-1). The development of longitudinal full-length cracks and rust leaching out from the cracks raised safety concerns.

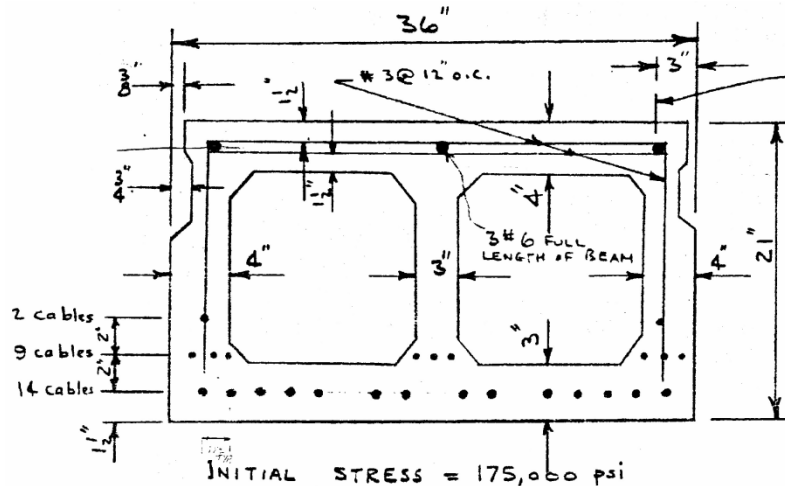


Figure 3-1. Typical box-beam section used in the 1950s

The beam was designed for the H-15-44 live load (Figure 3-2). Cross-section properties and the design parameters of the beam are given in Table 3-1. Concrete design strength was not specified on the plans. Michigan State Highway Department (MSHD) Specifications for Highway Bridges (1958) required 5000 psi ultimate concrete cylinder strength at 28 days for prestressed beams.

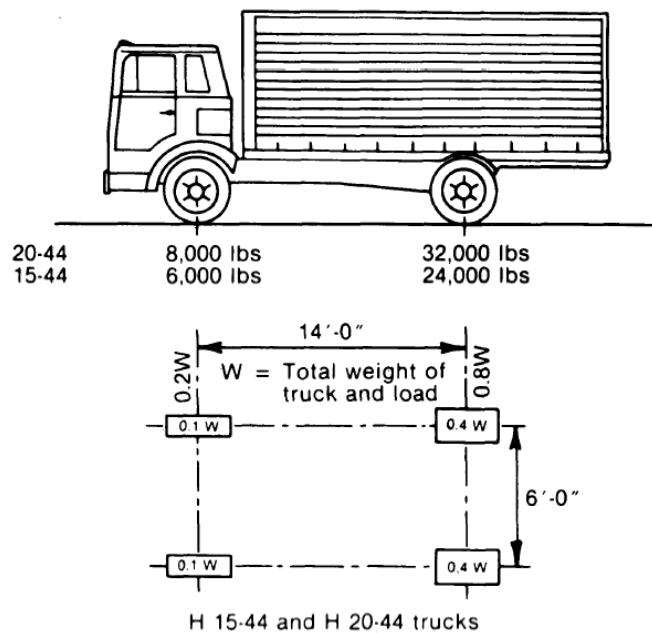


Figure 3-2. H-15-44 and H-20-44 vehicle configuration

Table 3-1. Beam Sectional Properties and Design Parameters used in 1957

Span length (in)	582
Beam length (in)	581.25
Beam span (distance between position dowels) (in)	568.25
Cross-sectional area, A (in ²)	407
Moment of inertia, I _c (in ⁴)	22,000
Weight of the beam (lb/ft)	424
Distance to top fiber, y _t (in)	10.21
Distance to bottom fiber, y _b (in)	10.79
Impact factor	0.291
Distribution factor	0.6×(wheel load)
Dead load moment M _{DL} (in-kip)	1,405
Live load moment M _{LL+I} (in-kip) (including impact factor and distribution factor)	1,450
Moment due to wearing surface M _{WS} (in-kips)	795
Total initial prestressing force P _i (kips)	350
Ultimate prestressing force, P _u (kips)	80% × (P _i)
Prestressing strand diameter (in)	3/8
Cross-sectional area of a strand, (in ²)	0.08
Center of gravity of strands, e (in)	8.15
Strand positions from bottom flange fiber (in)	14 @ 1.5 9 @ 3.5 2 @ 5.5

3.3 BEAM REMOVAL AND LOAD TESTING

On Monday September 25, 2006, I-94 west bound was closed at 9 p.m. for beam removal. E.C. Korneffel Co., of Trenton, Michigan was the contractor for beam removal and load testing. The Western Michigan University research team (at that time the research team was affiliated with Wayne State University) developed the load configuration and instrumentation layout. MDOT technicians installed the strain gauges, displacement transducers (DCDT), and cable actuated position sensors (CAPS) and also recorded the load test data.

3.3.1 Beam Removal Process

The contractor removed the bridge barriers of the fascia beam and saw cut the joint between the fascia and the interior beam (Photo 3-5). Lifting bracing was attached at the beam ends (Photo 3-6). Two cranes were used to lift the beam from its position. To avoid any possible damage to the beam during lifting, two hydraulic jacks were used to gently push the beam ends from the supports (Photo 3-7). The beam was lifted using two cranes, loaded onto a trailer, and transported to the test site (Photo 3-8 and Photo 3-9).



Photo 3-5. Saw cut at the exterior and interior beam joint

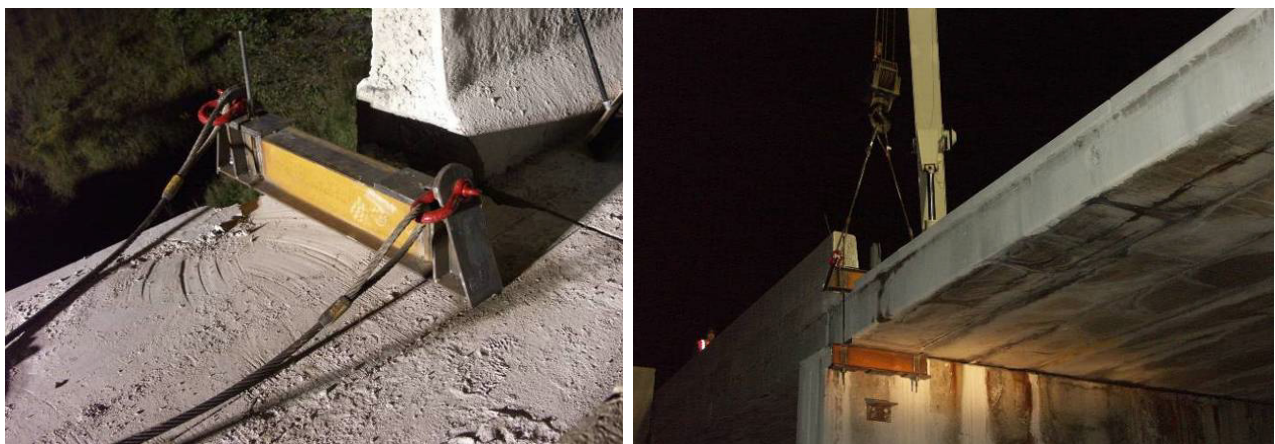


Photo 3-6. Lifting devices attached at the beam end



Photo 3-7. Force application using hydraulic jacks at both ends of the beam



Photo 3-8. Lifting of the beam using two cranes



Photo 3-9. Beam on the trailer before being transported to the test site

3.3.2 Instrumentation Layout

Shear strains within the end zones, flexural strains at the mid-span, vertical and horizontal deflections at the mid-span, and the support settlements were measured during load testing of the beam. Rosettes near the beam ends, uniaxial strain gauges at the mid-span, cable actuated position sensors at the mid-span, and displacement transducers (DCDT) next to the supports were mounted as shown in Figure 5-3 and Photo 3-10.

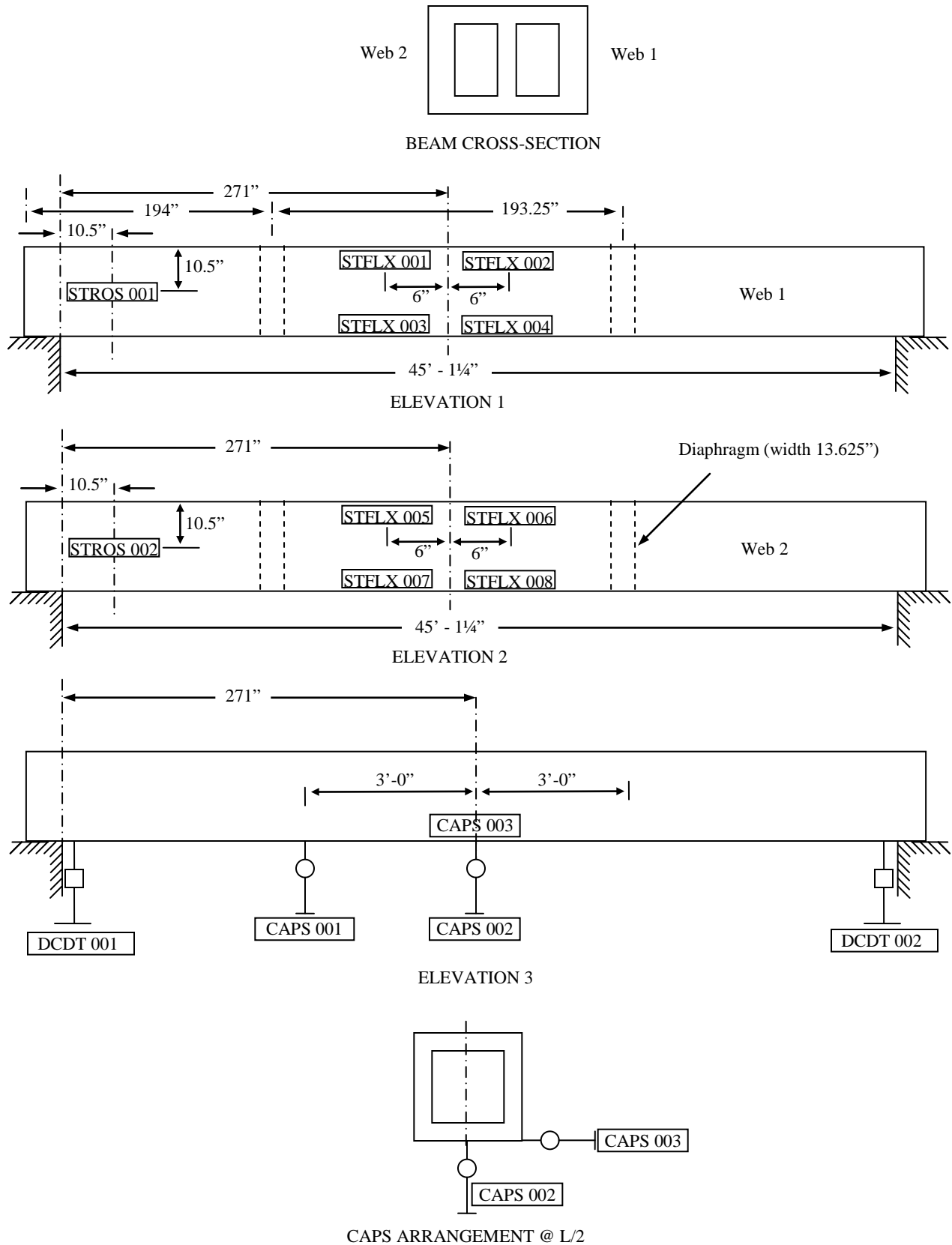


Figure 5-3. Instrumentation layout



Photo 3-10. Strain gauges at (a) beam end and (b) mid-span and cable actuated position sensors at mid-span for (c) vertical and (d) horizontal displacement measurement.

3.3.3 Load Configuration

The cracking moment of the section was calculated as 399 k-ft using the concrete compressive strength of 5000 psi given in the MSHD (1958), and other data given in Table 3-1 and Table 3-2. Following Section 9.18.2 of the AASHTO Standard Specifications (2002) cracking moment was calculated.

A four-point bending test was performed (Figure 3-4). Because of the uncertainties involved in calculating flexural capacity of the distressed beam with unknown prestressing strand conditions and the observed distresses, it was decided to load the beam until flexural cracks initiation while closely monitoring the crack developments and recording loads, displacements, and strains. Once the flexural cracks developed and the moment on the beam exceeded the cracking moment

capacity, the beam was loaded to failure without close monitoring. The load configuration was developed with the assumption that the flexural capacity of the beam should be 80% of the ultimate moment of the section. Section 9.17 of the AASHTO Standard Specifications (2002) was used for the ultimate moment capacity calculations.

Table 3-2. Moment Capacity of the Section

Concrete strength, (f'_c), psi	5000
Modulus of rupture, ($f_r=7.5 \times (f'_c)^{1/2}$), psi	536
Section modulus, ($S_c = I/y_b$), in ³	2041
Effective prestress (i.e., 80% of initial prestress), ksi	140
Compressive stress of concrete due to effective prestress forces, (f_{pe}), psi	1810
Cracking moment, (M_{cr}), k-ft	399
Ultimate moment (M_u), k-ft	663

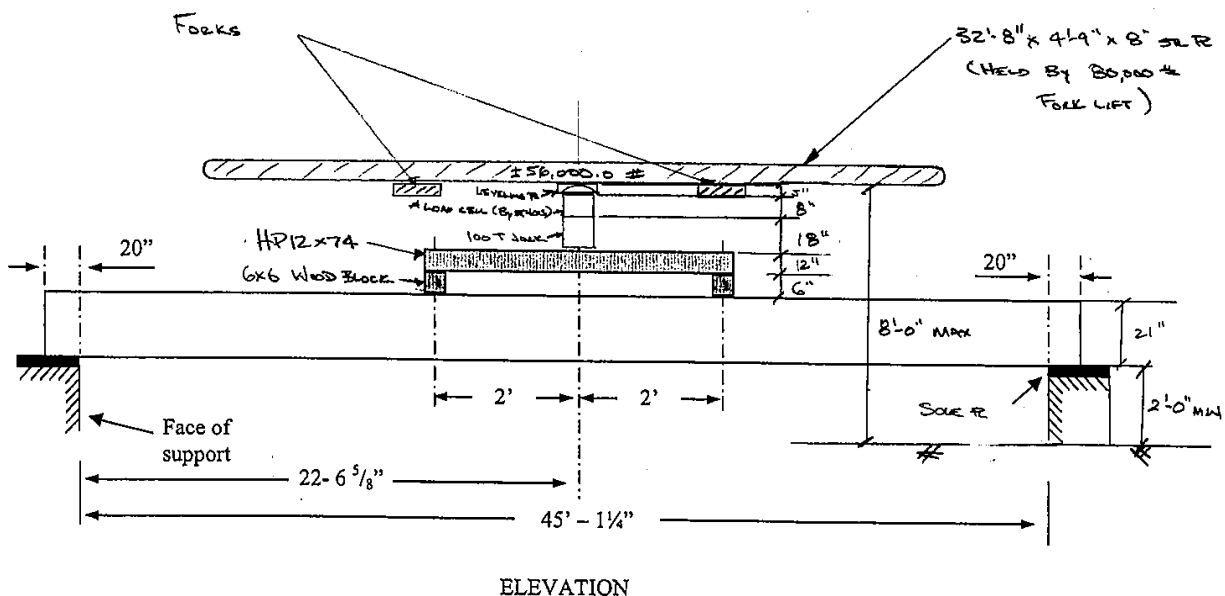


Figure 3-4. Load configuration developed by the contractor

Load testing was performed on November 13, 2006. Prior to conducting the load test, the beam camber was measured using a total station. During load testing the load was applied in 2 kips increments up to 20 kips; 1 kips increments from 20 to 30 kips; and 0.5 kips increments from 30 to 41 kips. After that the load was monotonically increased expecting to crush the beam. Due to

limitations of the load application system, the maximum load applied to the beam was 51 kips. At 51 kips load, the resulting moment on the beam was about 80 percent of its ultimate capacity. Once the loads were removed, the beam deformations recovered. No signs of yielding in terms of permanent set were observed.

3.4 LOAD TESTING DATA ANALYSIS

3.4.1 Camber and Remaining Prestress

Camber measurement was performed using a total station, and the measurements are shown in Figure 3-5. Photo 3-11 shows the camber of the beam when it was placed at the test site.

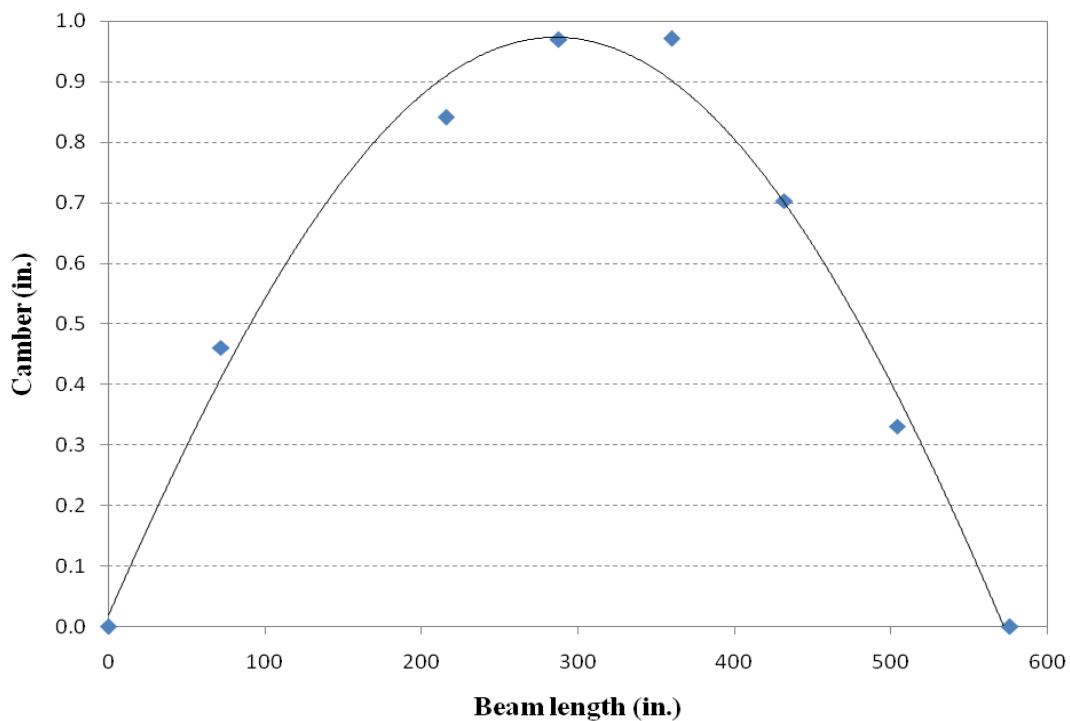


Figure 3-5. Variation of beam camber against length



Photo 3-11. Box-beam camber

Concrete material property tests were not performed. MSHD (1958) specifies the required concrete design strength as 5000 psi. According to Aktan et al. (2003), greater compressive strengths than 5000 psi were common in 1950s. Neglecting concrete material degradation, but not the strength development, a range of strength values was used for the calculations. The remaining prestress in the tendons are calculated as follows:

Concrete strength	= 5000 – 7000 psi
Concrete modulus of elasticity	= $57\sqrt{f_c'}$ ksi = 4030 – 4769 ksi
Beam camber (Δ_c)	= 0.97 in.
Beam self weight deflection (Δ_d)	= 0.64 – 0.54 in. (for $f_c' = 5000$ psi and 7000 psi)
Remaining prestress force	= $[(\Delta_c + \Delta_d) 8EI/eL^2]$ = 413.7 – 459.3 kips (for $f_c' = 5000$ psi & 7000 psi)
Remaining stress	= 206.8 – 229.7 ksi (25 strands -2.0 in ² .)
Initial prestress	= 175 ksi
Prestress loss	= 118 – 131 %

3.4.2 Cracking Moment and Remaining Prestress

As shown in Photo 3-12, two flexural strain gauges were attached to the bottom flange on each face of the beam at the mid-span. During load testing flexural cracks were documented as formed and marked on the beam faces near the mid-span bottom flange of the beam (Photo 3-12). Even though cracking sounds were heard during load application, the first flexural crack could not be noticed until the applied load reached 33 kips.



Photo 3-12. Flexural cracking at mid-span

Analysis of the data recorded by the strain gauges mounted near the bottom flange indicated that the first crack formed when the load was about 26.5 kips (Table 3-3). Based on the strain gauge data, the moment at mid-span due to applied load is 283 k-ft (Figure 3-6). The mid-span moment due to self weight of the beam was 125 k-ft. Thus the experimental cracking moment is calculated as 408 k-ft. As shown on Table 3-2, the analytical cracking moment of the section is 399 k-ft and correlates very well with the experimental data. The remaining prestress is calculated using Section 9.18.2 of AASHTO Standard Specifications (2002) as shown in Table 3-4. The remaining prestress for 5000 psi concrete corresponds to 82.6% of initial prestress.

Table 3-3. Load at Cracking – Strain Gauge Data

Strain Gauge	Load at Cracking (kips)
STFLX 003	26.5
STFLX 004	32.6
STFLX 007	30.9
STFLX 008	32.1

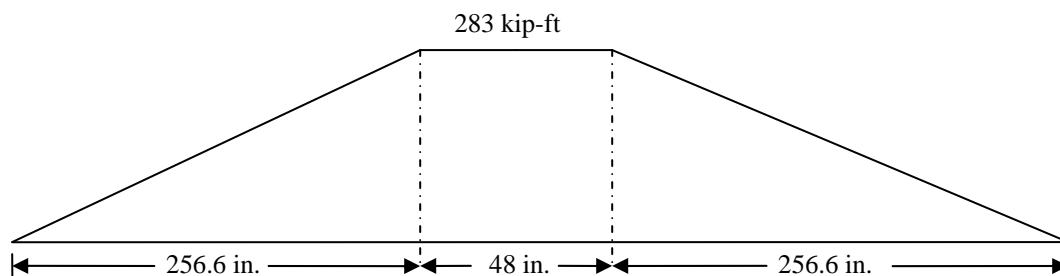


Figure 3-6. Moment due to applied load at cracking

Table 3-4. Remaining Prestress

Cracking Moment ft-kips	Effective Prestress Force P_{se} , kips		Remaining Prestress ksi	
	$f'_c = 5000$ psi	$f'_c = 7000$ psi	$f'_c = 5000$ psi	$f'_c = 7000$ psi
408	289	274	144.5 (82.6%)	137 (78.2 %)

The remaining prestress calculated using camber measurements ranges from 118 – 131 percent of initial prestress while the strain gauge readings yielded 78 – 83 percent. Prestress losses calculated using strain gauge data are in the order of 20 percent of initial prestress, which complies with the design assumptions. The use of camber measurements overestimates the remaining prestress by 40 – 50 percent.

3.4.3 Load Rating – Flexural Strength

Load rating was performed according to the MDOT Bridge Analysis Guide (2003). A concrete compressive strength of 5000 psi was used for the calculations. A live load distribution factor of 0.512 per wheel line load was calculated based on the AASHTO Standard (2002). It was also assumed that shear keys are functional and the tie rods are snug. Additional load rating was also performed assuming non-functional shear keys thus no load distribution between the beams (i.e., distribution factor = 1 per wheel line). Further, load rating was performed considering interior and exterior positions of the beam, assuming no load transfer. AASHTO Standard (2002) load distribution factors for interior and exterior beams are the same.

Table 3-5 summarizes the rating factors for interior/exterior beam with adequate load transfer as envisioned at the design stage. Table 3-6 and Table 3-7 summarize the rating results for an exterior and interior beam with no load distribution. When there is no load transfer, posting is required. The posting loads become considerably low when barrier loads are directly acting on the exterior beam with no load distribution. Table 3-8 summarizes the posting loads, recommended by MDOT in 1995, that were obtained from the bridge files.

Table 3-5. Bridge Load Rating (DF = 0.256 per lane; tons)

	Inventory Rating	Operating Rating			
		Federal Level	Michigan Legal Level		
			1 Unit	2 Unit	3 Unit
Flexural Strength	33.8	56.2	60	85	97

Table 3-6. Bridge Load Rating – Exterior Beam (DF = 0.5 per lane; tons)

	Inventory Rating	Operating Rating			
		Federal Level	Michigan Legal Level – Bridge should be Posted		
			1 Unit	2 Unit	3 Unit
Flexural Strength	10.6	17.6	15	16	22

Table 3-7. Bridge Load Rating – Interior Beam (DF = 0.5 per lane; tons)

	Inventory Rating	Operating Rating			
		Federal Level	Michigan Legal Level – Bridge should be Posted		
			1 Unit	2 Unit	3 Unit
Flexural Strength	18.4	30.5	25	28	38

Table 3-8. Bridge Posting Requirement in September 1995 (DF = 0.5 per lane; tons)

Michigan Legal Level – Bridge should be Posted		
1 Unit	2 Unit	3 Unit
33	42	47

3.4.4 Condition of Prestressing Strands

Corrosion stains were visible in the vicinity of the cracks at the bottom flange as seen in Photo 3-13a. Upon the completion of the load testing, the concrete was chipped away within the vicinity of cracks. There were no severed strands due to corrosion (Photo 3-13b).

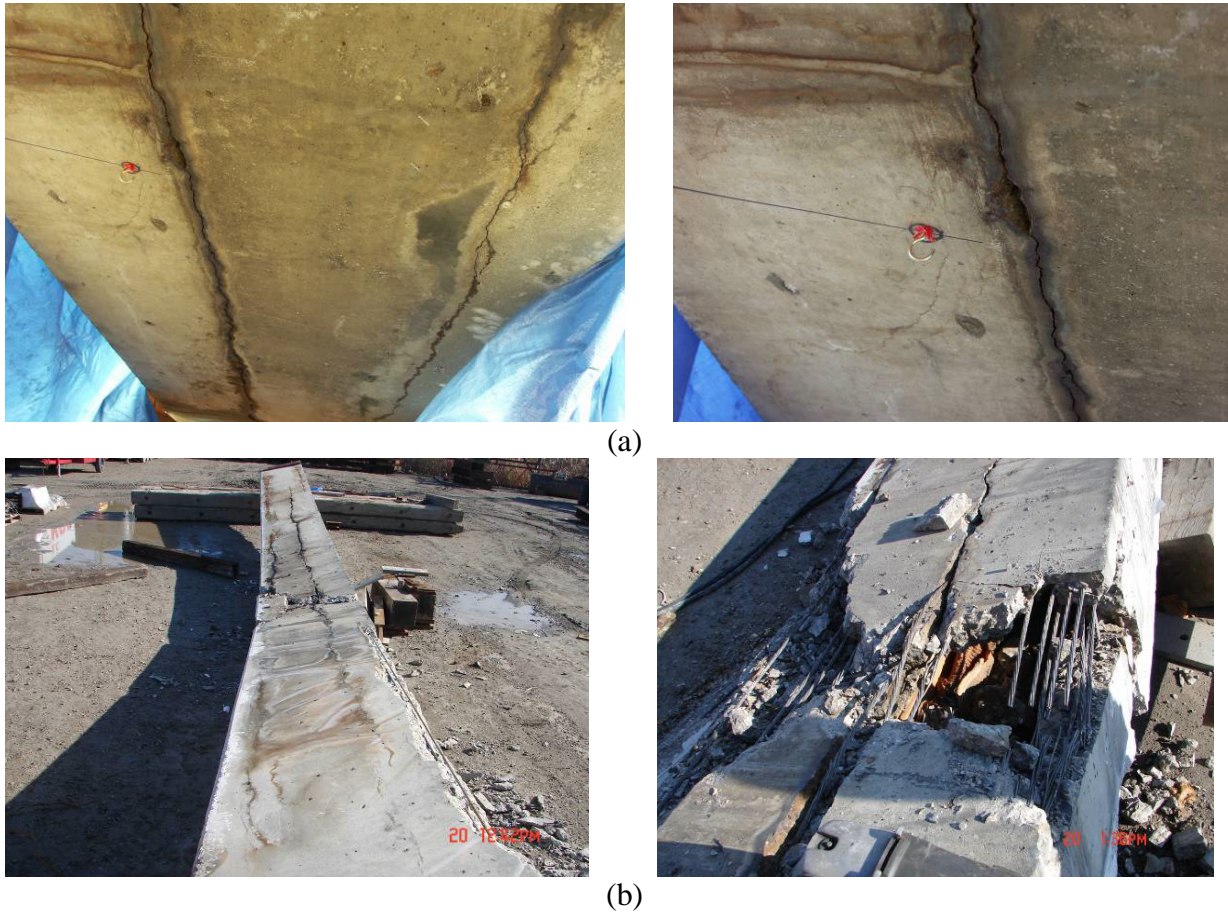


Photo 3-13. Beam bottom flange condition (a) before and (b) after the testing was performed

3.4.5 Load Capacity of the Beam

Analysis results of the test data showed the longitudinal cracks on the bottom flange did not affect the flexural capacity of the beam. The beam was designed for H-15 loading following the guidelines given in MSHD (1958). The primary reason for rating and posting the bridge with similar beams would be due to non-functional shear keys. However, accurate assessment of load distribution is required to assure the safety of these bridges.

3.5 SUMMARY AND CONCLUSIONS

A 50-year old box-beam was removed from the bridge that carries Hawkins Road over I-94. This beam had severe longitudinal cracking at the beam soffit. After the Pennsylvania bridge beam collapsed in December 2005, there were concerns about the safety of similar

bridges/beams. The beam was carefully removed, and load testing was performed. The following conclusions are drawn from the analysis results:

1. The bridge beam's experimental capacity was still in excess of its designed capacity. The beam, however, was designed for an H-15 which is lower than the current loads.
2. The use of camber measurements overestimates the remaining prestress by 40 – 50 percent.
3. A methodology needs to be developed for assessing load distribution of existing side-by-side box-beam bridges.
4. Concealed tendon corrosion evaluation and material characterization using nondestructive methods are essential for accurate safety assessment of distressed girders.

Intentionally left blank

4 EXPERIMENTAL PROCEDURE FOR DURABILITY STUDIES

4.1 INTRODUCTION

Task 4 of this study as outlined in Chapter 1 consists of experimental studies to determine the mechanical and durability properties of repair materials. Durability is a concern for design of new concrete structures as well as for repaired concrete structures. In order to design concrete repair for durability, different material parameters of the repair material as well as that of the concrete substrate need to be considered.

Vaysburd and Emmons (Beushausen and Alexander 2007) have stressed the importance of developing an integrated systems approach for concrete repair projects, including important design parameters such as environmental conditions, repair locations in the existing structure, its geometry, restraint, and nonuniformity, in connection with the specification of relevant material properties. Vaysburd (2006) also stresses the need for holistic approach to concrete repair since the repair process must successfully integrate new materials with old materials, forming a composite system capable of enduring exposure to service loads, exterior and interior (inside the structure) environments and time.

Figure 4-1 provides an overview of repair material characterization (based on Beushausen and Alexander 2007) required for ensuring long term performance of repaired structures. From a long term performance standpoint, a concrete repair must have adequate strength, resistance to freezing and thawing cycles, adequate transport properties and low susceptibility to cracking. It is important to relate individual material characteristics with the composite system as explained in Chapter 2.

A similar approach can be applied to shear key grout behavior. The literature review of Phase I of this project indicated that typically shear key grouts exhibit cracking at a very early age. It is essential to have a shear key grout that exhibits similar properties as those of the box beam to ensure a structurally stable composite element.

The overall goal of this task of this project was to analyze in detail commonly used polymer based repair materials commonly used for repair as well as evaluate shear key grouts used in construction of prestressed box beam bridges. The scope can be summarized as below:

- 1) Characterize individual material properties of common repair materials.
- 2) Establish key performance requirements for repair materials used for repair of prestressed concrete box beam bridges.
- 3) Determine the behavior of repair mortar in the fresh state
- 4) Determine the mechanical properties such as compressive strength and bond strength at various ages
- 5) Evaluate dimensional stability of repair mortars and shear key grouts by determining the shrinkage properties and cracking susceptibility of repair mortars and fatigue behavior of repair mortar and shear key grouts
- 6) Evaluation of long term durability of repair mortar and shear key grouts in terms of resistance to damage under freezing and thawing cycles, resistance to chloride ion penetration and rate of absorption of water
- 7) Evaluation of behavior of repair concrete under freezing and thawing cycles and fatigue by applying a ‘systems approach’.

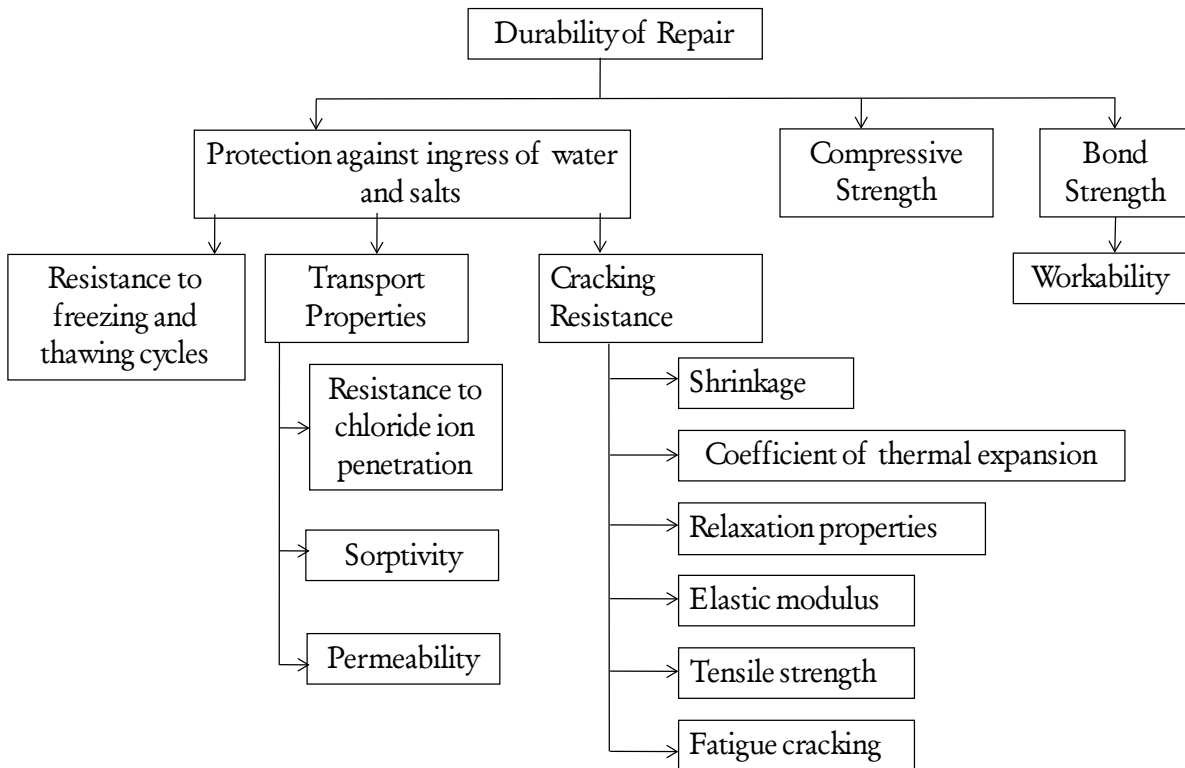


Figure 4-1. Characteristic material properties required for durable concrete repair

This chapter explains in detail the research plan adopted to study the durability and dimensional stability of selected repair materials and shear key grouts. Section 3.2 discusses the criteria adopted for the selection of available repair materials and shear key grouts. Information on the materials used in production of parent concrete is also provided in this section. Section 3.3 outlines the mixture proportions for the repair materials and the parent concrete whereas Section 3.4 provides information on test procedures adopted for this study. The testing regime included assessment of various fresh and hardened concrete properties such as slump or slump flow, setting time, rate of compressive strength development at various ages, drying shrinkage, cracking potential, freeze-thaw resistance and slant shear bond strength. The procedures adopted for preparation of combined specimens (repair material/parent concrete) are outlined in detail in Section 3.4.

4.2 MATERIALS

In this section, the materials used in the research program are described. Properties of the ingredients used in preparation of repair mortars, shear key grouts and the substrate concrete are specified below in Section 3.2.1 and 3.2.2, respectively.

4.2.1 Repair Materials and Shear Key Grouts

Based on the discussions held during the project progress meeting on May 4, 2007, four repair materials and three cements for shear key grouts were selected. There are many types of products and innumerable manufacturers of repair materials. Data sheets of various polymer based repair materials from different manufacturers were collected. An in-depth analysis of information provided by the manufacturer on the characteristics of the repair material was performed. To ensure a good sample size, the materials were chosen based on selection criteria involving:

- product approved by MDOT
- acceptable performance as indicated by a literature survey
- variability in manufacturer and chemical composition
- variability in elastic modulus of hardened repair concrete

The repair materials selected based on the above criteria include:

- 1) SikaRepair[®] SHA – According to the manufacturer, Sika[®], SikaRepair[®] SHA is a fast-setting, one-component, cementitious based ready to use repair mortar. The repair material can be modified in to a polymer based repair mortar by addition of SikaLatex R instead of water. For this research, SikaLatex R will be used. SikaRepair[®] SHA is supplied in 50 lbs bags and the SikaLatex R is provided in 1 gallon plastic jug and provides a yield of 0.55 cu.ft/bag.
- 2) Sika Top[®]123PLUS - According to the manufacturer, Sika[®], SikaTop[®]123PLUS, is a two-component, polymer-modified, portland cement-based fast-setting, non-sag mortar. The cementitious component in addition to cement and small size aggregate also contains a penetrating corrosion inhibitor. The repair material is available in 44 lb bags while the liquid component is provided in a 1 gallon plastic jug; the two combined have a yield of 0.39 cu.ft/bag.
- 3) HB2 Repair Mortar – is a repair product manufactured by BASF. It is a two component polymer-modified high-build, lightweight repair mortar.
- 4) Conpatch V/O - Conpatch V/O is a single component, cement based, polymer modified repair mortar manufactured by Dayton Superior.

Material data sheets for the repair materials are included in Appendix A. Currently all shear keys are grouted using Type I Portland cement. The cements selected for characterization of shear key materials were Type I Portland cement conforming to ASTM C 150, masonry cement Type M conforming to ASTM C 91 and SET 45. Type I cement is normally used by MDOT for shear key grouts in prestressed box beam bridges. Masonry cement and SET 45 were selected for evaluation so that these cements can be used as an alternative to Type I cement mortar currently used for shear key construction. SET 45 is magnesium phosphate based rapid-setting cement manufactured by BASF. The cement is supplied by the manufacturer in 50 lbs bags and is premixed with single size (~ 2mm diameter) siliceous aggregates.

4.2.2 Substrate Concrete

The substrate concrete necessary for preparing composite specimens was manufactured as per MDOT specifications. Information regarding materials and mixture proportion of concrete used for manufacturing box beam bridge components was obtained from local manufacturer of prefabricated prestressed box-beam elements. Type III Portland cement manufactured by

Lafarge Industries was used as the cementitious component of the mixture. The coarse and fine aggregate used in this study were conforming to MDOT 6A and 2NS, respectively. The physical properties of the aggregates are given in Table 3-1 whereas the gradation curve for coarse aggregate is shown in Figure 4-2 and for fine aggregate in Figure 4-3.

Table 4-1. Physical Properties of Aggregates used in Substrate Concrete

Physical Property	Coarse Aggregate	Fine Aggregate
Bulk Specific Gravity (Oven Dry)	2.69	2.62
Bulk Specific Gravity (Surface Saturated Dry (SSD))	2.69	2.63
Percent Absorption	1.2	1.8
Percent Moisture Content	1.8	1.9
Fineness Modulus	5.75	2.6



Figure 4-2. Gradation of coarse aggregates



Figure 4-3. Gradation of fine aggregates

4.3 MIXTURE PROPORTIONS AND MIXING

The mixture proportions for the repair materials and one shear key grout material selected as suggested by the manufacturer are given in Table 4-2. Mixing of the proportioned materials was carried out in a Hobart mixer as shown in Figure 4-4. The mixing process for this study was performed at the Benedict Laboratory of Michigan Technological University.



Figure 4-4. Hobart mixer used for mixing repair materials

Table 4-2. Mixture Proportions of Commercial Repair Products and Shear Key Materials

Product	Cementitious Component (A)	Liquid Component (B)	Quantity of (A) lb	Quantity of (B) Gallons
Sika Repair SHA	Sika Repair SHA	Sika Latex R	50	1
Sika Top 123 PLUS	Component A	Component B	44	1
HB 2 Mortar	HB 2 Mortar	Liquid	45	1
Conpatch V/O	Conpatch V/O	water	50	0.85
SET 45	SET 45	water	50	0.52

Repair mortar mixtures were prepared for evaluation in the laboratory without making any changes to the proportions suggested by the respective manufacturers. The amount of repair material mixed was governed by two factors - the mortar volume required to prepare specimens of a test as well as the time required for placing and consolidating the mortar in the molds. The time required for preparing the specimens was an important consideration because the selected repair materials have a very small window of time before the repair mortar starts to harden. Appendix B provides data on volume of material required for each test. Typically batch volumes of no more than 0.1 cu. ft was mixed at one time to ensure proper placing and consolidation before the repair mortar starts to harden. As a consequence the suggestion of all manufacturers about using one bag of repair material for mixing even if required volume is lower than the yield was not adopted in this study.

Three-fourths of the liquid was poured in the mixing container followed by the repair material. The mixture was then mixed continuously for three minutes with the mixer speed maintained at two. To ensure uniform consistency of mixing, the remaining liquid was added after two minutes of mixing.

The mixture proportion developed for shear key grout assessment using Type I cement and masonry cement is given in Table 4-3. The mixture proportions developed are as per MDOT R-2 mortar criteria (MDOT 2003). The fine aggregate used for these mixtures conform to the MDOT gradation specified for Type 2 NS.

Table 4-3. Mixture Proportions for Shear Key Grout (R-2 mortar)

Ingredients	Specific gravity	Quantity (lb/cu.yd)
Cement (Type I/Masonry Cement)	3.15	930
Fine aggregate	2.63	1942
water	1.00	416
Air entraining admixture		1

Mixing was performed in a laboratory pan mixer as shown in Figure 4-5. Fine aggregate and air entraining agent were added initially to the mixer container and mixed for a minute. Cement and water were added next and mixed for five minutes.



Figure 4-5. Laboratory pan mixer

The mixture proportions for the substrate concrete to be used in testing the repair material's resistance to freezing and thawing cycles and fatigue specimens using Type III cement is outlined in Table 4-4. The mix design is representative of the mixture proportions approved by MDOT for construction of prestressed concrete box-beam girders.

Table 4-4. Mixture Proportions for Substrate Concrete

Ingredients	Specific gravity	Quantity (lb/cu.yd)
Cement (Type III)	3.15	600
Fine aggregate	2.63	1725
Coarse aggregate	2.69	1306
Water	1.00	230
Air entraining admixture		0.1
High-range water reducer		5.00

4.4 TEST METHODS AND REQUIREMENTS

Based on the literature review and evaluation of the data sheets of the selected repair materials, the following properties were selected as the key properties of the repair material that influence the long term performance of repair concrete:

1. Slump,
2. Air content,
3. Rate of strength gain,
4. Freeze-thaw durability,
5. Drying shrinkage,
6. Cracking potential,
7. Bond strength,
8. Chloride permeability,
9. Sorptivity, and
10. Coefficient of thermal expansion

Table 4-5 and Table 4-6 list the tests conducted to evaluate the above select material properties. The relevant standards adopted for conducting the test are also mentioned. In reviewing the data sheets of the selected repair materials (Appendix A) it was observed that none of them provided information on a performance criteria for material properties. All data sheets reviewed provide information on the test method and the performance of the material in a particular test. For this study, ASTM C 928 was adopted for comparing the performance of the repair materials for different properties.

Table 4-5. List of Tests for Repair Mortar and Shear Key Grout

Material Property	Type of Material	Test Method	Material Condition	# Specimens	# of Materials
Slump	RM	ASTM C 928	Fresh	1	4
	SK		Fresh	1	3
	Parent	ASTM C 143	Fresh	1	1
Air content	RM	ASTM C 928	Fresh	1	4
	SK		Fresh	1	3
	Parent	ASTM C 173	Fresh	1	1
Compressive Strength at the age of 24 h, 7 days and 28 days	RM	ASTM C 109	24 h, 7 days and 28 days	6	4
	SK		24 h and 28 days		3
	Parent		28 days		1
Slant Shear Bond Strength at 1 and 7 days	RM / Parent	ASTM C 882 and in-house	1 day/ 28 days	3	4
			7 days/ 28 days		
	SK / Parent		1 day/ 28 days		3
			7 days/28 days		
Resistance to freezing and thawing	RM	ASTM C 666 Procedure B	14 days	3	4
	RM / Parent		14/ 28 days		
	SK		14 days		3

Table 4-6. List of Tests for Repair Mortar and Shear Key Grout

Material Property	Type of Material	Test Method	Material Condition	# Specs.	# of Materials	% Complete
Free Shrinkage/Length Change	RM	ASTM C 157	----	3	4	100
	SK				3	100
Chloride Permeability 28 days	RM	ASTM C 1202	28 days	2	4	50
Sorptivity⁴	RM	ASTM C 1585	28 days	2	4	100
Hardened concrete air content	RM	ASTM C 457	28 days	1	4	100
Restrained Ring Shrinkage Test	RM	AASHTO PP 34	----	3	4	50
Coefficient of thermal expansion	RM	AASHTO TP 60	7 days	2	4	50
	SK					50
	Parent					100
RM = repair material, SK = shear key grout, Parent = substrate concrete						

In this section the test procedures for measuring fresh and hardened concrete properties, deviation from approved test procedures if any, changes in curing regimes in comparison to those listed in relevant standards, requirements established for different tests, are specified in detail for the research program.

4.4.1 Slump

The workability of all repair materials and shear key grouts was measured in terms of slump of the concrete and the test was conducted as per ASTM C 143. The concrete/grout was poured in the slump cone in three layers. The material was rodded 25 times after each layer was poured.

4.4.2 Air Content

The air content of fresh concrete was measured as per ASTM C 231 for concrete/grout mixtures. Air content of hardened concrete was carried out as per ASTM C 457. One sample each was tested at the age of 28 days. Hardened concrete samples were sawed and polished before conducting the test. The procedure used here for the automatic characterization of the air-void system of hardened concrete works on the same principle of contrast enhancement and digital

analysis first described in 1977 by Chatterji and Gudmundsson. The procedure used here can be broken into four basic steps:

- A. Preparation of polished slabs
 - B. Black and white contrast enhancement procedure
 - C. Image collection
 - D. Automated ASTM C457
- A) Each slab is trimmed to a width of 76 mm and a height of 100 mm to accommodate the dimensions of the retaining rings of the automated lapping equipment; a LapMaster with a 305 mm diameter grooved cast iron rotating lap with guide yokes. The slabs were ground flat using hand pressure on a water-cooled rotating wheel topped with a 60 grit metal-bonded diamond platen, followed by 24 minutes with an 800 grit SiC water slurry on the LapMaster. The flatness of the lap was monitored and maintained within ± 2.5 m. The surfaces were cleaned between steps with gentle pressurized water spray and a short ultrasonic water bath. The slabs were dried in a 50°C oven followed by the application of a 5:1 by volume solution of acetone and clear fingernail hardener, (New York Color brand 207A) (Roberts and Scali, 1984). The solution was brushed onto the lapped surfaces in two coats. After the hardener had set, the slabs were briefly polished using hand pressure on the water-cooled rotating iron wheel topped with 600 grit adhesive backed SiC paper, and cleaned as described previously.
- B) Contrast enhancement was achieved by drawing slightly overlapping parallel lines with a wide tipped black permanent marker (Avery brand Marks-A-Lot). This was done in three coats, changing the orientation 90 between coats. After the ink dried, a few tablespoons of 2 m median size white powder (NYCO Minerals Inc. NYAD 1250 wollastonite) were worked into the samples using the flat face of a glass slide. A razor blade was used to scrape away excess powder, leaving behind powder pressed into voids. Residual powder was removed by wiping with a clean and lightly oiled fingertip. A fine tipped black marker (Sharpie brand) was used to darken voids in aggregates.
- C) Each slab was scanned individually, and placed as near to the center of each flatbed scanners glass plate as possible. 8-bit grayscale, 3,175 dpi, (125 dpm, 8 x 8 m pixel) images were collected. A flat steel plate with applied black and white vinyl electrical tape was included at

the top of each scan. The intensity distribution (histogram) of a population of 4 million pixels covering equal areas of the black and white tape was recorded for each scan in order to monitor variation in the gain of each scanners charged coupled device (CCD) array using Adobe Photoshop CS2 software enhanced with Reindeer Games Inc, Image Processing Toolkit 4.0 Plug In functions. To compensate for minor differences in gain between scans, a linear stretch was performed on the entirety of each scanned image.

D) A Visual Basic script developed at Michigan Technological University was used to compute paste volumes based on mix design information provided with the concrete samples according to the simple formula:

$$P=(100-A)[(Pm/Aggm)/(1-Pm/Aggm)] \quad (3-1)$$

where:

P = Vol. % paste in sample.

A = Vol. % air determined from automated procedure.

Pm = Paste volume computed from mix design.

Aggm = Aggregate volume computed from mix design.

Alternatively, the Visual Basic script also allows for paste content to be input directly for each sample. A third option available in the script allows for a manual point count to be performed on an image scanned from the polished sample before the black and white treatment. The script divides up the image into frames, and the operator answers either yes or no as to whether the cross-hairs fell on an aggregate particle or not. The paste volume is then computed according to the simple formula:

$$P = 100 - Agg - A \quad (3-2)$$

where:

Agg = Vol. % aggregate computed from point count data.

The script utilizes Adobe Photoshop CS2 to select the areas on the images to be analyzed, to extract the traverse lines, and to apply the threshold levels. The script also utilizes Microsoft Excel and Word to perform air-void calculations and to generate reports. The script has the option of whether or not to report an air-void chord length distribution.

4.4.3 Rate of Strength Gain

The compressive strength test for repair materials and shear key grouts was performed as per ASTM C 109 by casting samples in 2 x 2 in cubes. A total of 18 samples were cast for each repair material and shear key grout. The samples were prepared in two layers. The mortar was tamped in each cube compartment 32 times in about 10 s in 4 rounds, each round to be at right angles to the other and consisting of eight adjoining strokes over the surface of the specimen. Immediately after casting, the specimens were covered with a plastic sheet on the top to disallow moisture loss due to evaporation. The specimens were then demolded after 24 h after first addition of mixing liquid to the repair material. Six specimens were tested at age of 24 h. The other 12 specimens were placed in the moist room in Dillman Hall for curing. The specimens were removed from the moist room about 15 minutes prior to testing at ages 7 and 28 days. Specimens of SET 45 were not placed in the moist curing room since it is specified by the manufacturer that the material should not be moist cured.

The samples were subjected to compressive loading using the Tinius Olsen equipment located in Dillman Hall. The loading rate applied was between 250 to 300 lbs/s. The maximum failure load was recorded and the subsequently compressive strengths for the repair materials and shear key grouts were obtained.

The compressive strength test for substrate concrete was conducted as per ASTM C 39. Three 4 x 8 in. cylindrical specimens were cast in three layers of 2.5 in. each. The concrete was consolidated by tamping 25 times after placement of each layer. The specimens were covered with a lid on top after consolidation to avoid any water loss due to evaporation. The samples were demolded after 24 h after the first addition of water to the ingredients and placed in the moist cure room for curing purposes. The compressive strength test was performed at the age of 28 days.

The compressive strength test was performed on the Baldwin compressive strength testing equipment in Benedict Laboratory. The rate of loading for testing the substrate concrete specimen was 35 psi/s.

4.4.4 Slant Shear Bond Strength

The slant shear bond strength was performed as per ASTM C 882. The test set-up consists of repair mortar applied to substrate mortar to establish a 3 x 6" cylinder as shown in Figure 4-6.

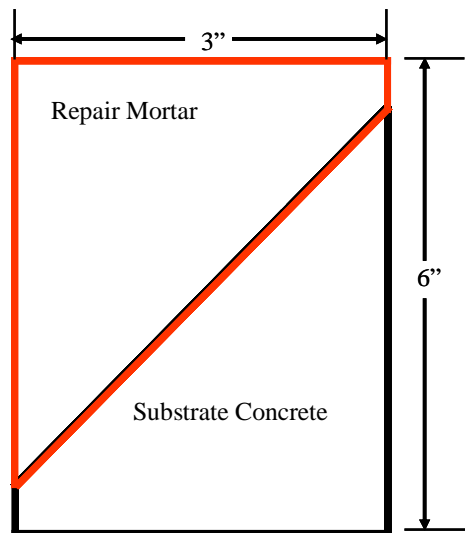


Figure 4-6. Cross-section of slant shear bond strength test set-up

To prepare the substrate concrete samples, initially a dummy sample was required. For this purpose an aluminum cylindrical rod was cut as per the dimension specified in ASTM C 882. The cut specimen was then placed in a 3 x 6" cylinder and this set-up was used as a mold to prepare the dummy samples. Five dummy samples were prepared using epoxy. Substrate concrete samples using Type III cement and mixture proportions as per ASTM C 882 were prepared by using the dummy samples in place of the repair mortar. The substrate concrete samples were cured for 28 days. The substrate concrete sample was then placed in a 3 x 6" cylinder and the repair concrete was cast against the substrate concrete. The combined specimen was demolded after 24 h.

The slant shear bond strength test was performed using the Tinius Olsen testing equipment. The rate of loading applied to the specimen was 200 lbs/s.

4.4.5 Resistance to Freezing and Thawing Cycles

The samples for evaluating the resistance of the selected repair materials and shear key grouts to freezing and thawing cycles was performed as per the ASTM C 666 *Procedure B*. Two types of samples of repair materials were prepared to ascertain the behavior of the selected materials.

One type of sample consisted of the repair material or the shear key grout only. The samples were cast in 3 x 3 x 16 in. molds in three layers and tamped 25 times after each layer was placed. The samples were demolded 24 h after the first addition of water and placed in moist curing room for 14 days. After 14 days the samples were removed from the moist curing room and the dynamic modulus was measured before placing each sample in the freeze thaw chamber. The samples were placed in the freeze-thaw machine for 300 cycles. Subsequently the samples were removed every 30 cycles to measure the dynamic modulus. Three samples of every repair material and shear key grout were tested under this regime.

The second type of sample was prepared as a combined specimen, one half of which was made of substrate concrete whereas the other half was made of the repair material. For the measurement of resistance to freezing and thawing of repair materials when cast on substrate concrete, initially specimens of the substrate concrete were prepared and cured for 14 days at temperature of 105-120°F to accelerate curing. The samples were split in the middle by applying a 3-point bending load as shown in Figure 4-7. The exposed surface of the sample was further prepared by using a chisel and hammer as shown in Figure 4-8 to simulate a roughened surface similar to that found in the field. The substrate sample was then placed in the mold and the repair concrete was placed in the remaining space. The final samples were demolded at 24 h after first addition of water to the repair material and cured for 14 days before being placed in the freeze-thaw chamber. Two samples of every repair material were tested under this regime.



Figure 4-7. Set-up used for splitting of the substrate concrete specimen for freeze-thaw testing



Figure 4-8. Surface preparation of the substrate concrete specimen

The dynamic modulus was measured in the same way as explained earlier. The samples were removed after every 30 cycles to measure the change in modulus.

4.4.6 Measurement of Free Shrinkage

The free shrinkage of repair materials was evaluated as per ASTM C 157. Six samples of each repair mortar and shear key grout of size 1 x 1 x 12 in. were cast. The samples were demolded 24 h after addition of water to the mortar. Two types of conditioning methods were adopted in this test. Three samples were cured in a humidity chamber having 100% humidity at 73°F whereas the other three samples were cured in an environmental chamber with 50% relative humidity (RH) at 73°F. The first measurement was taken 24 h after preparation of samples after which the samples were moved to different curing conditions as described earlier. Thereafter, measurements were taken every 24 h for 28 days from time of first addition of water.

4.4.7 Sorptivity

The measurement of rate absorption (sorptivity) of water by repair mortar and shear key grouts was conducted as per ASTM C 1585 by measuring the increase in the mass of a specimen resulting from absorption of water as a function time when only one surface of the specimen is exposed to water.

Cylinders of size 4 x 8 in. were cast as per ASTM C 192 and cured in moist curing room for 28 days. The cylinders were then removed from the curing room and cut using a water saw. The middle 2 in. of the cylinder was taken for the test as shown in Figure 4-9.

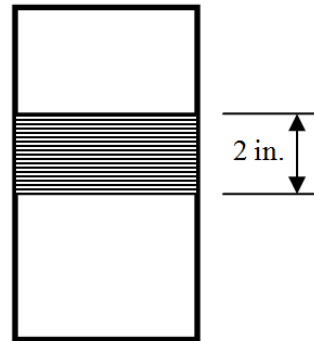


Figure 4-9. Diagrammatic sketch of sample location for sorptivity test

The two samples of size 2 x 4 in. were then placed in desiccators at a temperature of 122°F and RH of $80 \pm 3\%$ for three days. The desired relative humidity was achieved by placing a petri dish with potassium bromide solution in the bottom of the desiccator. The solution was maintained at a saturation point as stated in ASTM C 1585. The samples were removed from the desiccator after 3 days and placed in a sealable container. The containers were stored at 73°F for 15 days before performing the test. The samples were removed from the containers and the cylindrical part was coated with epoxy. The diameter of the surface exposed to water was measured and the sample then placed in a tub on two small supports so as to maintain the level of water 1 to 3 mm above the top of the support device. Change in mass of the specimen was observed for 9 days as per the standard.

4.4.8 Cracking Susceptibility

The cracking susceptibility of repair materials was evaluated as per AASHTO PP 34. The test set-up for measurement of cracking susceptibility through restrained shrinkage ring testing is elaborated in this section. A special environmental controlled chamber (50% RH and 73°F) was built for testing of the specimens. Steel rings as per AASHTO PP 34 were prepared and strain gages were mounted on the inside of the ring to monitor strains developed in the repair mortar. The strain gages with $120.0 \pm 0.3\%$ resistance and 2.08 nom gage factor were manufactured by Vishay Measurements Group. Figure 4-10 shows the test set up developed in the environmental controlled chamber.



Figure 4-10. Environmental control chamber with ring specimen

The Michigan Tech laboratory has a data logger MEGADAC 3451 AC manufactured by Optim Electronics as shown in Figure 4-11. The data is collected by the data acquisition system through TCS software which is supplied by Optim Electronics. The data logger had been procured about 10 years ago and had not previously set up for data collection for measuring the cracking susceptibility.



Figure 4-11. Data logger used for data collection from ring specimens

The rings were cast using six batches of repair mortar. Because the repair mortar tends to start setting quickly, tamping and consolidation was performed using a putty knife and pressing by hand. The rings were connected to the data logger within 20 minutes of mixing and placing. The outer mold ring was removed after 24 h. The ring was covered with plastic sheathing to avoid drying due to evaporation.

4.4.9 Coefficient of Thermal Expansion

Two 4 x 8 in. cylindrical samples of size of repair materials were cast and cured for 5 days. The coefficient of thermal expansion was measured as per AASHTO TP 60-00 (2004) using the PINE equipment in Benedict Laboratory. The top half-inch and bottom half- inch was then sawed using a kerosene saw to get the required test size of 4 x 7 in. The samples were then placed in water for 24 h so as to achieve constant weight.

The sample was then placed in the water bath of the equipment. One test cycle (one heating segment and one cooling segment) lasted approximately 24 hours. However, several specimens required longer to test to meet the AASHTO specification for successive CTE values (difference of no more than 0.5 micro strain/°F (0.3 micros strain/°C) between successive CTE values). Those samples which required longer testing time are listed in the chapter detailing the results and analysis of different tests

5 RESULTS AND ANALYSIS FROM DURABILITY STUDIES

5.1 FRESH AND HARDENED PROPERTIES OF REPAIR MATERIALS AND SHEAR KEY GROUTS

The fresh and hardened concrete properties evaluated for the different materials are listed in Table 5-1 through Table 5-7. The measured average value obtained in the lab for various material properties evaluated is compared with those listed in the data sheet of the relevant manufacturer if available. Coefficient of variation (COV) for test data is shown in brackets wherever applicable. Discussion of the different material properties is compiled in the sections below.

5.2 SLUMP

The slump of the repair materials was zero due to extremely stiff mixtures and low workability. Among all repair materials, HB2 Repair Mortar was extremely stiff right after completion of mixing. The slump of the shear key grouts was between 7-8 in. and is provided in Table 5-5 through Table 5-7. No reference value was provided by the manufacturer of SET 45 and MDOT also does not have a minimum slump value for shear key grouts. The slump values of 8, 7 and 8 in. for SET 45, Type I cement grout and masonry cement grout, respectively, indicate that the grouts had sufficient workability and would lead to dense hardened mortar when properly consolidated.

5.3 AIR CONTENT

As explained in the note provided at the end of Table 5-7, the air content for repair materials and SET 45 was not measured due to its tendency to set rapidly (Refer Appendix A for manufacturer's data sheet for setting time values). It was observed that all commercial repair materials and shear key grouts used in this study lost workability and became stiff in about 10 minutes after the addition of water. The air content in the fresh state for Type I cement grout and masonry cement are within the MDOT requirements specified of 14+4.

Table 5-1. Test Results for SikaTop123® Plus

Test	Measured Value			Manufacturer's Data Sheet		
Slump (in.)	0			N/A		
Air content (% , fresh state)	N/A ¹			N/A		
Compressive Strength at the age of 1, 7 and 28 days (psi)	1 day	7 days	28 days	1 day	7 days	28 days
	3500 (7.71)	5381 (7.91)	6712 (2.81)	3500	6000	7000
Slant Shear Bond Strength at 1 and 7 days (psi)	1 day		7 days	28 days		
	1005 (1.98)		1298 (1.85)	2200		
Freeze/thaw Resistance @ 300 cycles (% , RDM)	96.5 %			98 %		
Free Shrinkage (micro strains) @ 90 days	100 % RH	50 % RH		N/A		
	450	1440				
Chloride permeability 28 days	504 Coulombs (100-1,000 very low)			500 Coulombs		
Sorptivity	Initial Absorption	Secondary Absorption		N/A		
	5.5×10^{-6}	8.0×10^{-7}				
Hardened concrete air content at 28 days	10.7 %			N/A		
Restrained Ring Shrinkage Test	First test specimen cracked in 8.7 days and second in 6.7 days			N/A		
Coefficient of thermal expansion (mm/mm/°C) ³	18.88×10^{-6}			N/A		

Table 5-2. Test Results for SikaRepair®SHA

Test	Measured Value			Manufacturer's Data Sheet		
Slump (in.)	0 ¹			N/A		
Air content (% , fresh state)	N/A ¹			N/A		
Compressive Strength at the age of 1, 7 and 28 days (psi)	1 day	7 days	28 days	1 day	7 days	28 days
	2530 (6.06)	4090 (8.37)	6205 (6.88)	2500	3500	5000
Slant Shear Bond Strength at 1 and 7 days (psi)	1 day		7 days	28 days		
	876 (3.75)		1166 (2.7)	1800		
Freeze/thaw Resistance @ 300 cycles (% , RDM)	86 %			N/A		
Free Shrinkage (micro strains) @ 90 days	100 % RH	50 % RH		N/A		
	86	1200				
Chloride permeability 28 days	800 Coulombs (100-1,000 very low)			N/A		
Sorptivity (mm/√s)	Initial Absorption	Secondary Absorption		N/A		
	3×10^{-6}	5.0×10^{-7}				
Hardened concrete air content at 28 days	12.43 %			N/A		
Restrained Ring Shrinkage Test	First specimen did not crack within 28 days			N/A		
Coefficient of thermal expansion (mm/mm/°C) ³	14.80 x10 ⁻⁵ (5.13)			N/A		

Table 5-3. Test Results for HB2 Repair Mortar

Test	Measured Value			Manufacturer's Data Sheet		
Slump (in.)	0 ¹			N/A		
Air content (% , fresh state)	N/A ¹			N/A		
Compressive Strength at the age of 1, 7 and 28 days (psi)	1 day	7 days	28 days	1 day	7 days	28 days
	2535 (10.43)	4766 (3.32)	6538 (3.65)	2300	4500	5800
Slant Shear Bond Strength at 1 and 7 days (psi)	1 day		7 days	7 days		28 days
	336 (7.98)		1146 (6.67)	2100		2700
Freeze/thaw Resistance @ 300 cycles (% RDM)	See Note ⁴			N/A		
Free Shrinkage (micro strains) @ 90 days	100 % RH		50 % RH	350 (does not specify RH)		
	1420		1360			
Chloride permeability 28 days (Coulombs)	1012 (100-1,000 very low)			N/A		
Sorptivity (mm/ \sqrt{s})	Initial Absorption		Secondary Absorption	N/A		
	6.0×10^{-7}		8.0×10^{-7}			
Hardened concrete air content at 28 days	33.5%			N/A		
Restrained Ring Shrinkage Test	See Note ⁴			N/A		
Coefficient of thermal expansion (mm/mm/ $^{\circ}C$) ³	10.88×10^{-6} (11.71)			8.1×10^{-6}		

Table 5-4. Test Results for Conpatch VO

Test	Measured Value			Manufacturer's Data Sheet		
Slump (in.)	0 ¹			N/A		
Air content (% , fresh state)	N/A ¹			N/A		
Compressive Strength at the age of 1, 7 and 28 days (psi)	1 day	7 days	28 days	1 day	7 days	28 days
	4805 (9.21)	6145 (1.99)	9688 (5.25)	4500	7000	8000
Slant Shear Bond Strength at 1 and 7 days (psi)	1 day		7 days	NA		
	1067 (0.31)		1356 (0.92)			
Freeze/thaw Resistance @ 300 cycles (% RDM)	98.7			96		
Free Shrinkage (micro strains) @ 90 days	100 % RH		50 % RH	N/A		
	290		713			
Chloride permeability 28 days (Coulombs)	970 (100-1,000 very low)			430		
Sorptivity (mm/√s)	Initial Absorption		Secondary Absorption	N/A		
	7.5 x 10 ⁻⁶		3.0 x 10 ⁻⁶			
Hardened concrete air content at 28 days	7.6 %			N/A		
Restrained Ring Shrinkage Test	Rings cracked after 1.6 and 2.3 days of casting			N/A		
Coefficient of thermal expansion (mm/mm/°C) ³	13.66 x 10 ⁻⁶ (0.79)			4.4 x 10 ⁻⁶		

Table 5-5. Test Results for SET® 45

Test	Measured Value			Manufacturer's Data Sheet		
Slump (in.)	8			N/A		
Air content (% , fresh state)	N/A ¹			N/A		
Compressive Strength at the age of 1, 7 and 28 days (psi)	1 day	7 days	28 days	1 day	7 days	28 days
	4330 (7.85)	5382 (7.91)	6688 (4.62)	6000	7000	8500
Slant Shear Bond Strength at 1 and 7 days (psi)	7 days		28 days	NA		
	1513 (2.63)		1900 (0.73)			
Freeze/thaw Resistance @ 300 cycles (% RDM)	82			80		
Free Shrinkage (micro strains) @ 90 days	100 % RH	50 % RH		N/A		
	750	128				
Sorptivity (mm/√s)	Initial Absorption	Secondary Absorption		N/A		
	3.0×10^{-5}	3.0×10^{-6}				
Hardened concrete air content	11.13 %			N/A		
Coefficient of thermal expansion (mm/mm/°C) ³	12.48×10^{-6} (1.14)			4.4×10^{-6}		

Table 5-6. Test Results for Type I Cement Grout

Test	Measured Value			MDOT		
Slump (in.)	7			N/A		
Air content (% , fresh state)	13.5			14 ± 4		
Compressive Strength at the age of 1, 7 and 28 days (psi)	1 day	7 days	28 days	1 day	7 days	28 days
	4017 (5.44)	4269 (8.53)	4905 (2.59)	N/A	N/A	N/A
Slant Shear Bond Strength at 1 and 7 days (psi)	7 day		28 days	NA		
	1043 (4.85)		1402 (1.18)			
Freeze/thaw Resistance @ 300 cycles (% RDM)	99 %			NA		
Free Shrinkage (micro strains) @ 90 days	100 % RH	50 % RH		N/A		
	150	720				
Sorptivity (mm/√s)	Initial Absorption	Secondary Absorption		N/A		
	2.5 x 10 ⁻⁵	8.0 x 10 ⁻⁶				
Hardened concrete air content	11.25 %			N/A		
Coefficient of thermal expansion (mm/mm/°C) ³	10.32 x 10 ⁻⁶ (6.23)			N/A		

Table 5-7. Test Results for Masonry Cement Grout

Test	Measured Value			MDOT		
Slump (in.)	8			N/A		
Air content (% , fresh state)	10.5			14 ± 4		
Compressive Strength at the age of 1, 7 and 28 days (psi)	1 day	7 days	28 days	1 day	7 days	28 days
	2441 (12.86)	3450 (1.87)	4500 (0.89)	NA	NA	NA
Slant Shear Bond Strength at 1 and 7 days (psi)	7 day		28 days	NA		
	924 (2.30)		1146 (2.09)			
Freeze/thaw Resistance @ 300 cycles (% RDM)	98 %			N/A		
Free Shrinkage (micro strains) @ 90 days	100 % RH	50 % RH		N/A		
	350	610				
Sorptivity (mm/√s)	Initial Absorption	Secondary Absorption		N/A		
	3.0 x 10 ⁻⁵	3.0 x 10 ⁻⁶				
Hardened concrete air content	8.432			N/A		
Coefficient of thermal expansion (mm/mm/°C) ³	9.57 x 10 ⁻⁶ (2.38)			N/A		

Notes:

1. The measurement of air content in the fresh state was not performed for repair mortars due to its rapid hardening characteristic which hindered the testing process.
2. Test values for two samples tested at 7 and 9 days are provided. Detailed explanation provided in Section 4.8.
3. HB2 Repair Mortar samples were not cast for this test.

5.4 COMPRESSIVE STRENGTH

The rate of compressive strength gain was measured for repair materials as well as shear key grouts at the ages of 1, 7 and 28 days. Six samples were tested for each age for each repair material and shear key grout. Individual results are supplied in Appendix C, whereas the analysis of mean compressive strengths is provided in this section. The mean compressive strength was calculated as per ASTM C 109 whereas the acceptance criteria adopted was as per ASTM C 109. Figure 5-1 shows a comparison of the compressive strength results at various ages for all repair materials with respect to the manufacturer’s data sheet as well as ASTM C 928 minimum.

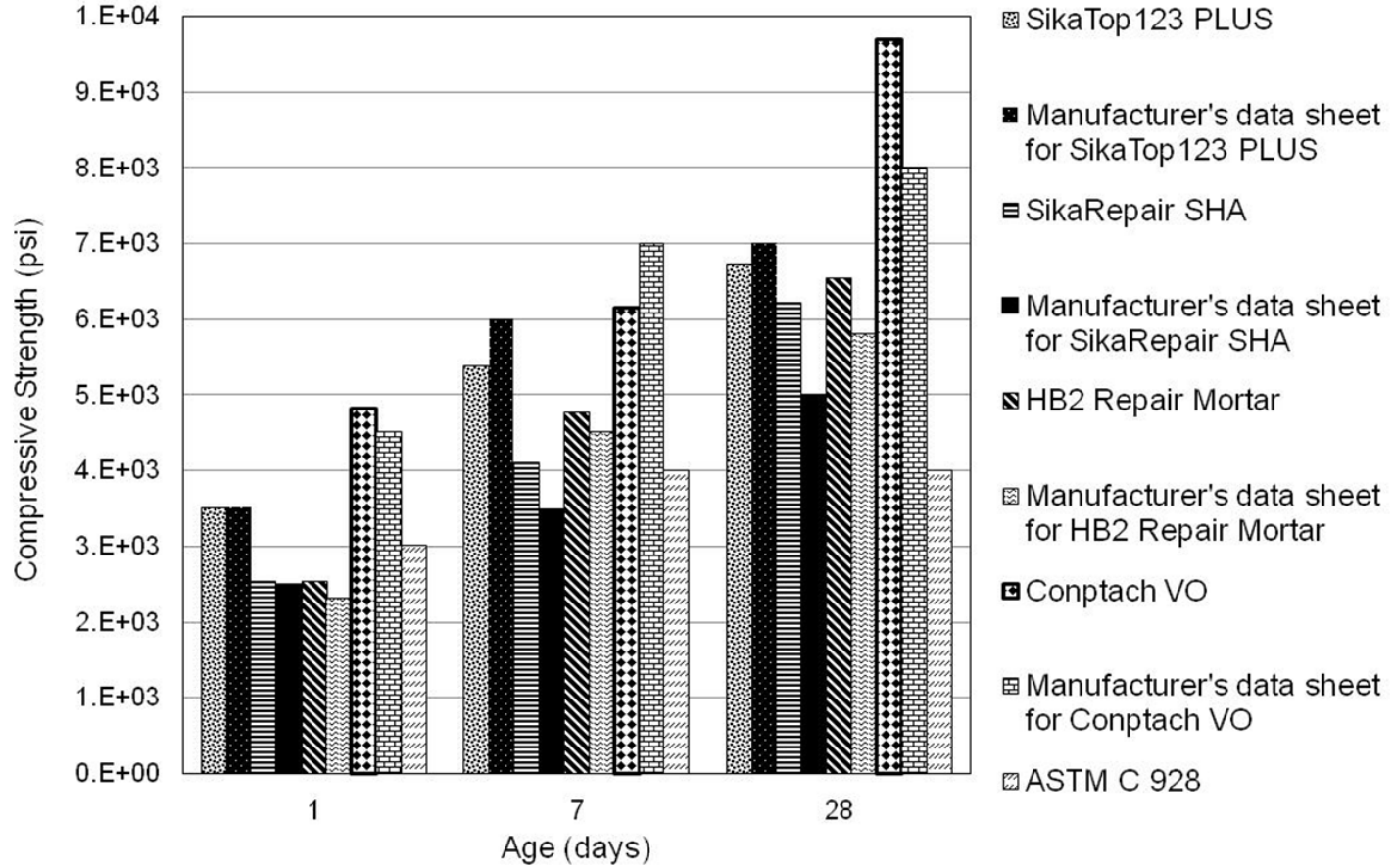


Figure 5-1. Compressive strength at various ages for repair materials

As shown in Figure 5-1, the compressive strength at 1 day was less than that specified by ASTM C 928. The coefficient of variation for all ages was between 6 to 8.5 % for Sika Repair[®] SHA. In case of HB2 Repair Mortar, the 1-day strength was lower than that stipulated by ASTM C 928. The COV for 1-day strength was also high (10.43). Amongst all repair materials evaluated, Conpatch VO exhibited the highest compressive strength results at all ages. The 7 days strength of Conpatch VO as measured in this study was lower than that stipulated in the manufacturer’s data sheet. From Figure 5-1 it can be observed that SikaTop 123[®]PLUS exhibited lower compressive strengths at 7 and 28 days in comparison to that stated by the manufacturer. The coefficient of variation (COV) of strengths at 7 days is higher (7.91) compared to that at 28 days (2.81). Compressive strengths at all ages for SikaTop 123[®]PLUS were above those required as per ASTM C 928. Sika Repair[®] SHA exhibited lowest compressive strength values amongst all the repair materials evaluated in this study.

Table 5-8 provides information on the percent increase of compressive strengths at ages 7 days and 28 day relative to the 1-day strength of the repair material. It can be observed that the highest increase in strength values is observed for HB2 Repair Mortar followed by Sika Repair SHA and Sika Top 123 PLUS. In the literature review it was discussed that the compressive strength of repair concrete/ mortar should be greater than or equal to the compressive strength of the substrate concrete. Based on the analysis in Figure 5-1 and Table 5-8, it can be concluded that for repair purposes of substrate concrete with compressive strength of 6000 psi or more, any of the repair materials evaluated in this study can be used based on the 28 day strength. Early age strengths are an important factor for rehabilitation projects because it is essential to open the bridge to traffic as soon as possible. If downtime is a factor in the decision of using a particular repair material, this study indicates that Sika Repair SHA and HB2 Repair Mortar have lower early age strengths but gain a higher percentage of strength at later ages.

Table 5-8. Percent Increase in Compressive Strength over Different Ages

Material	Percent Increase over 1 –day Compressive Strength	
	7–day (%)	28–day (%)
SikaTop 123 [®] PLUS	35	48
Sika Repair [®] SHA	38	59
Conpatch VO	22	52
HB2 Repair Mortar	47	61

Figure 5-2 shows the graphical presentation of development of compressive strength at various ages for the shear key grouts. Among the three grouts, masonry cement grout exhibited the lowest compressive strength whereas SET 45 exhibited the highest compressive strengths for all ages. It has to be noted that though SET 45 exhibited high strength, the measured strengths are lower than those stipulated by the manufacturer in the data sheet.

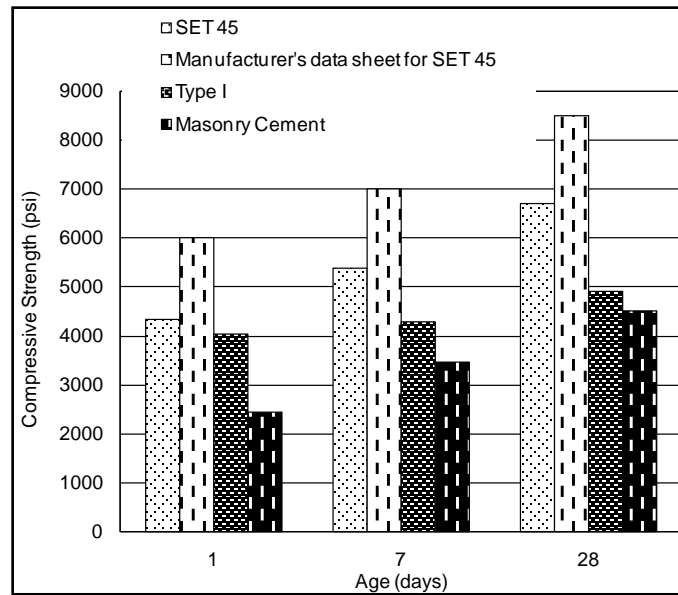


Figure 5-2. Development of compressive strength of shear key grouts

5.5 SLANT SHEAR BOND STRENGTH

In this section the analysis of mean slant shear bond strength at ages 1 and 7 days is discussed. Three samples for each age for each repair material and shear key grout were tested. Figure 5-3 shows the mean slant shear strength at ages 1 and 7 days for the repair materials tested.

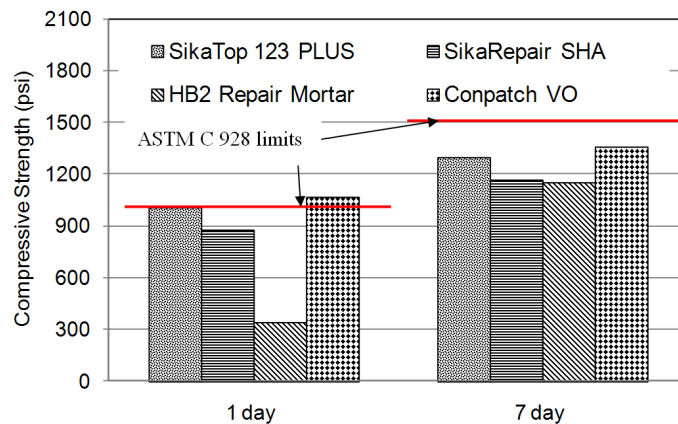


Figure 5-3. Development of slant shear bond strength at various ages for repair materials

ASTM C 928 prescribes performance requirements for slant shear bond strength testing for ages 1 and 7 days as 1000 psi and 1500 psi respectively (shown as bold lines). Figure 5-3 indicates that none of the selected materials exhibited the required strength at the age of 7 days. The slant shear compressive strength is the lowest for HB2 Repair Mortar at all ages. The COV for all of the repair materials is below 5% except for HB2 Repair Mortar (refer to Table 5-1 through Table 5-4). Some of the samples failed along the cylindrical cut surface of the specimen (slant shear) whereas some samples sheared along the middle (compressive failure) as shown in Figure 5-4. Information on sample failure is provided in Appendix D.

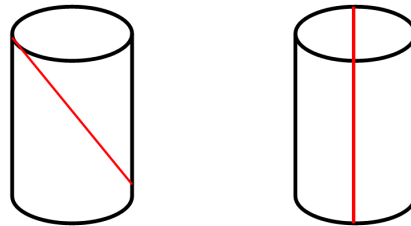


Figure 5-4. Failures of slant shear bond test specimens

One of the reasons for low strengths of HB2 Repair Mortar may be due to the early stiffening of the repair mortar in the fresh state. Due to rapid loss of workability of HB2 Repair Mortar, it was difficult to consolidate the mortar after placing it in the mold. This resulted in the presence of extensive voids in the sample as shown in Figure 5-5. A large part of the curved portion of the sample was not filled with repair mortar (area around the curve shown in Figure 5-5). Samples which exhibited large size voids as shown in Figure 5-5 due to improper consolidation were rejected but among those eventually selected for testing had small size voids (~0.2 in. in width).



Figure 5-5. Voids in HB2 repair mortar specimen for slant shear bond strength test

Figure 5-6 is a graphical presentation of development of slant shear bond strength at 7 and 28 days for shear key grouts. SET 45 exhibited the highest slant shear bond strength among all shear key grouts. Since the shear key grouts were workable and could be consolidated easily in to the molds, the overall appearance of the test samples was smooth. No voids were observed in the specimens but this did not necessarily result in higher bond strengths. This indicates that the slant shear bond strength is dependent upon the material properties as well as the finish of the specimen.

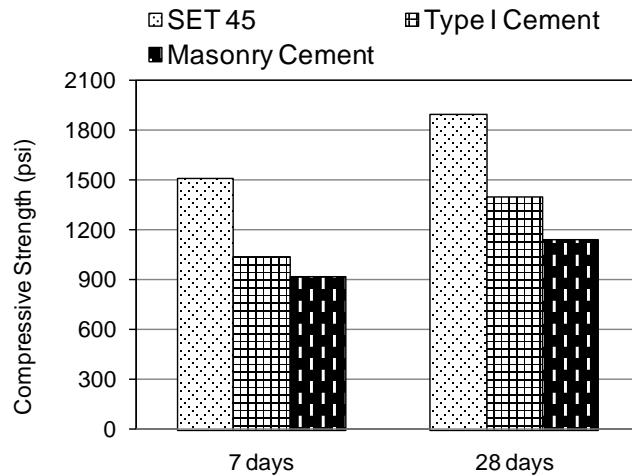


Figure 5-6. Development of slant shear bond strength at various ages for shear key grouts

5.6 SHRINKAGE BEHAVIOR

Similar to concrete, repair mortars too have a tendency to shrink on drying. A repair mortar patch is unable to shrink freely due to the restraint provided by the substrate concrete at the bottom interface of the patch, as well as the periphery in the case of an enclosed patch. If the repair mortar develops high shrinkage strains, the restraint prohibits it from shrinking leading to development of cracks in the patch. Presence of cracks not only reduces the dimensional stability of the repair patch, but also increases the chances of deterioration of the repaired structure due to exposure of internal concrete to penetration of de-icer salts and water through the cracks. In this study, free shrinkage and the cracking susceptibility of repair materials was studied whereas only free shrinkage was evaluated for shear key grouts (Appendix E). For the evaluation of cracking susceptibility, the crack width after appearance of the first crack was measured over a period of six days so as to ascertain the long term serviceability of the repair material.

Figure 5-7 represents the development of average free shrinkage strains in selected repair mortars. The specimens were stored in 100% RH at 73°F for a period of 95 days.

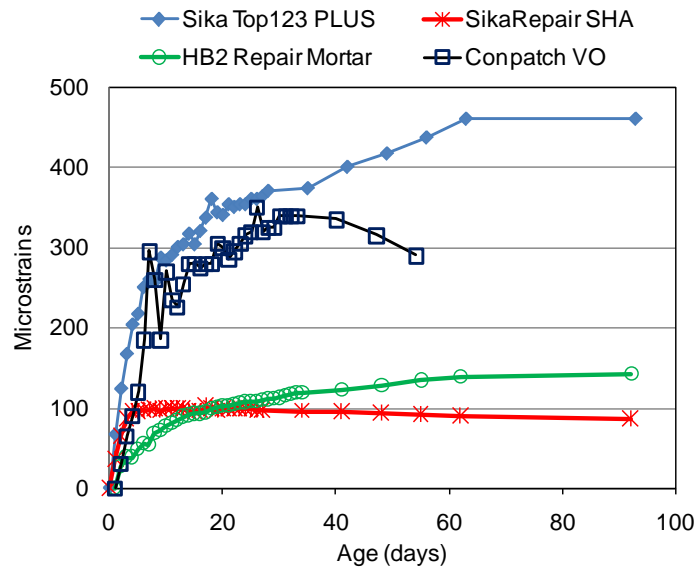


Figure 5-7. Free shrinkage strains in repair materials for samples at 100% RH and 73°F

The free shrinkage strains of specimens stored at 100% RH increased very rapidly at early ages for all the repair mortars. Sika Repair[®] SHA and Conpatch VO exhibited an initial expansion followed by a drop in the shrinkage strain after about 30 days indicating that some amount of relaxation had taken place. Overall, Sika Repair[®] SHA exhibited lowest shrinkage strains among all materials tested whereas Sika Top[®]123 PLUS exhibited the highest shrinkage strain values for specimens stored at 100% RH.

Free shrinkage strains of Sika Top[®]123 PLUS at 100% RH were measured over 150 days (refer to Figure E-1, Appendix E). The shrinkage strains progressively increased over time and exhibited extremely high average value of 483 microstrains. Typically, the shrinkage of repair material should be less than that of the substrate concrete. Such high strains even in 100% RH can be cause of concern but would also strongly depend upon the restraint provided by the substrate concrete.

Free shrinkage strain of Conpatch VO samples in 100% RH does not exhibit a smooth linear progression like other repair mortars (refer to Figure 5-7 and E-7 in Appendix E). This behavior is consistently observed in all the specimens. Due to proprietary nature of repair mortars exact

information about the ingredients are not known making it difficult to analyze the reasons for such behavior.

Figure 5-8 shows the graphical representation of free shrinkage strains developed in repair materials stored at 50% RH and 73°F. The overall behavior of the repair materials under lower humidity conditions is similar but reversed to that when placed in 100% RH, i.e., Sika Top[®] 123 PLUS exhibited highest free shrinkage strains and Sika Repair[®] SHA and HB2 Repair Mortar exhibited lowest free shrinkage strains. Free shrinkage strains developed rapidly in the early ages for Sika Top[®] 123 PLUS and Conpatch VO. Conpatch VO and Sika Repair[®] SHA did not exhibit a drop in free shrinkage strains for specimens stored at lower relative humidity unlike the drop in shrinkage strains over time observed in specimens stored at 100% RH (refer Figure 5-7 and Figure 5-8).

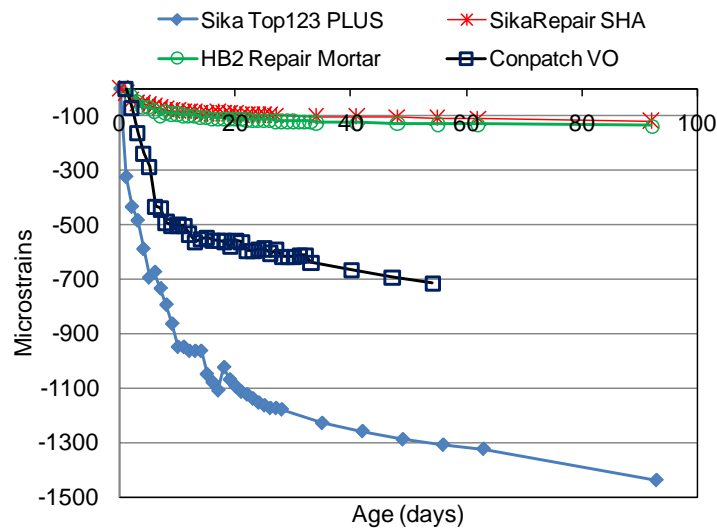


Figure 5-8. Shrinkage strains in repair materials for samples at 50% RH and 73°F

The main phenomena that are believed to contribute to the shrinkage of cement paste are the capillary stress, disjoining pressure, and changes occurring in the calcium silicate hydrate. At lower humidity, the capillary volume reduces leading to a quick rise in stresses. Literature suggests that polymer modification of repair mortar aids in reducing development of shrinkage strains. The reduction in strains is related to the low free water content and a well developed microstructure with fewer capillary pores in a polymer modified mortar. Thus, the development of high shrinkage strains in Conpatch VO can be explained by the lack of polymer modification. At the same time the high strain values in Sika Top[®] 123 PLUS cannot be explained due to lack of information on the ingredients of this repair material or its specific microstructure.

The term ‘‘crack’’ in this report refers to a macrocrack that can be visually detected wherein the smallest measurable crack width would be 0.004 in. and above. Two ring specimens were prepared as per AASHTO PP 34. The average strains reported is the average of strains recorded using four strain gages per ring. Figure 5-9 shows the cracking susceptibility of Sika Top[®]123 PLUS. The ambient conditions were maintained at 50 % RH and 73°F. The induced tensile strain increases rapidly in the first six hours after addition of water to about -40 $\mu\epsilon$ for both specimens. The first ring cracked at 8.75 days beyond the addition of water to the repair mortar, whereas the second ring cracked at 6.20 days. The maximum strain reached by both specimens was comparable with each other at -105 $\mu\epsilon$ for Ring 1 and -95 $\mu\epsilon$ for Ring 2.

The variability in the age of cracking for the two specimens can be related to the batch variation and consolidation of the repair mortar in the specimen mold. Due to the large volume of mortar required, the mold was filled with 7 batches of mortar of 0.1 cu. ft each. The rapid-setting nature of the repair mortar at times made the process of consolidation slightly difficult leading to presence of voids in the specimen.

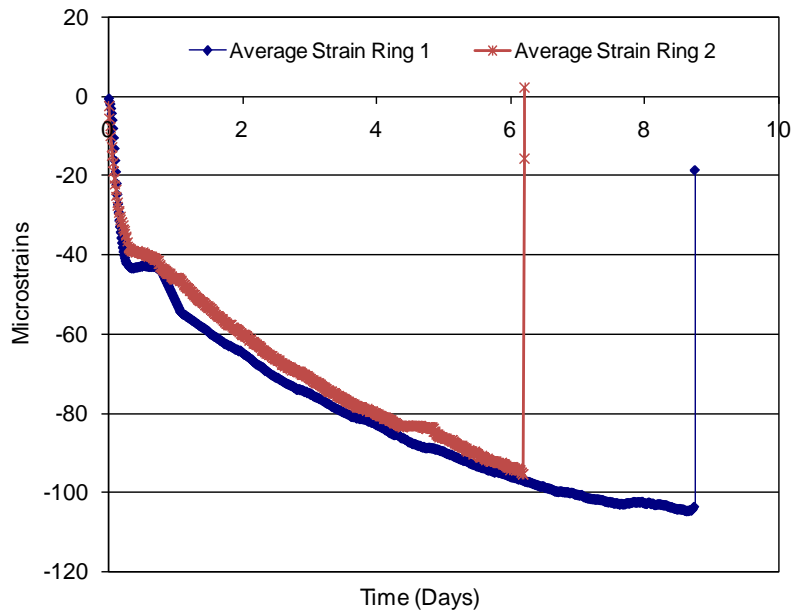


Figure 5-9. Cracking susceptibility of Sika Top[®]123 PLUS

Figure 5-10 shows the cracking susceptibility of Sika Repair SHA. Two specimens were cast to study the cracking susceptibility. The behavior exhibited by both the specimens was vastly different. Ring 1 specimen as seen in Figure 5-10 exhibited an initial expansion within the first few hours after addition of water to the mortar followed by steady rise in tensile strains. The

specimen did not crack within 28 days from the time of addition of water to the mortar. Ring 2 did not exhibit any early expansion and the specimen cracked at the age of 3 days from addition of water to the repair mortar. These vast differences in behavior could be a result of - a) the two specimens were cast at different dates (Ring 1 was prepared on June 23, 2008 whereas Ring 2 was prepared on Aug 8, 2008) and b) a large number of voids were observed in Ring 2 due to insufficient consolidation. As noted in an earlier paragraph, the volume of repair mortar required for one specimen is very large and typically 1.5 bags containing about 45 lbs of repair mortar were used for casting one specimen.

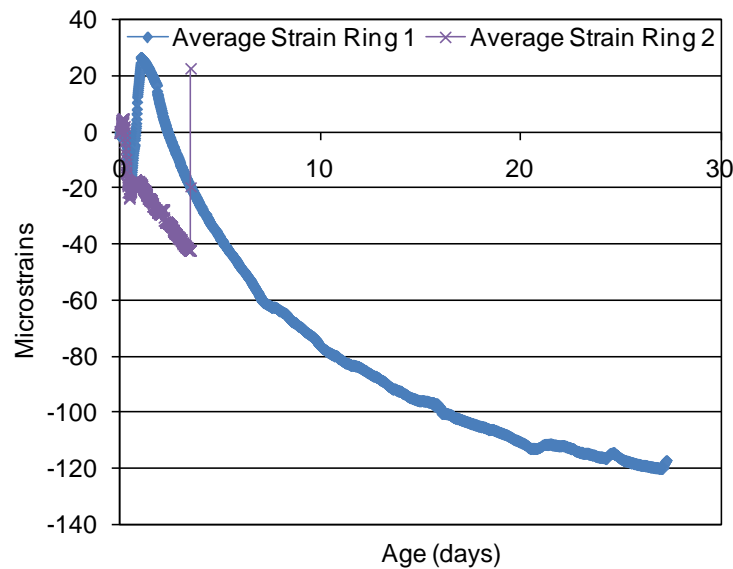


Figure 5-10. Cracking susceptibility of Sika Repair SHA

Figure 5-11 represents the development of tensile strains in ring specimens for Conpatch VO. The first ring developed a crack at the about 1.6 day since the addition of water whereas the second ring cracked at about 2.3 days since addition of water. Both rings exhibited a rapid rise in strains within the first two hours of casting the specimens followed by a drop in strains immediately after a time period of two hours. This behavior was not observed in any of the other repair materials. At the same time it has to be noted that this behavior was also observed at a later age (about 0.3 days) for free shrinkage specimens of Conpatch VO stored at 100 % RH (refer Figure 5-8). As mentioned earlier the mixing liquid used for mixing of Conpatch VO is water unlike the other repair materials. The initial increase in the strain values could be related to the increase in stress in capillary pores which eventually was reduced as the cement hydrated.

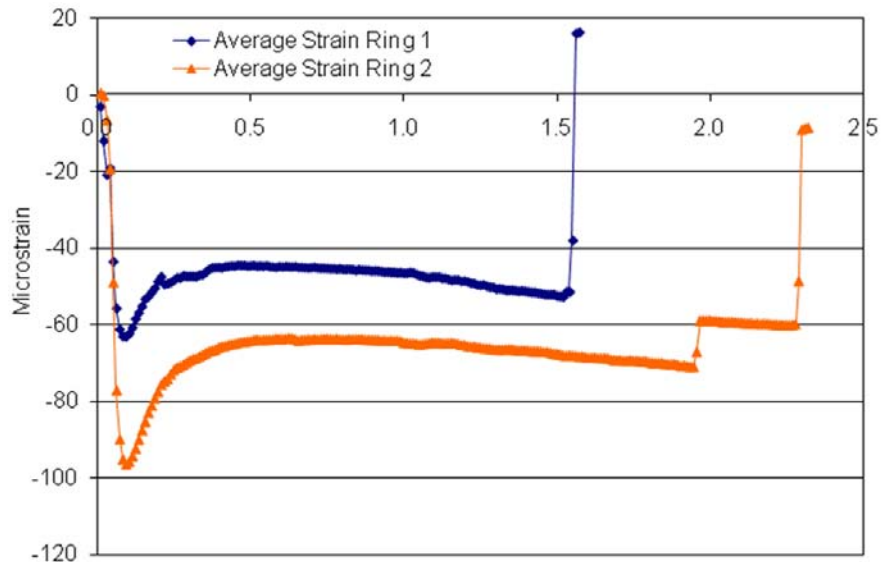


Figure 5-11. Cracking susceptibility of Conpatch VO

The potential of a material to crack under restrained conditions is related to its elastic modulus, tensile strength and relaxation stresses. The ‘risk of cracking’ of a repair material, based on the assumption of a rigid concrete substrate, is defined as $\epsilon_{sh}E/f_t$ where f_t is the tensile strength, E is the modulus of elasticity, and ϵ_{sh} is the drying shrinkage strain (Al-Zahrani et al. 2003). The risk of cracking factor for the repair materials evaluated in this research is presented in Table 5-9. A high number indicates higher risk of cracking. In this analysis, the elastic modulus and flexural strength at 28 days of repair material as published in manufacturer data sheets was used (refer Appendix A). The 28-day mean free shrinkage strain developed in specimens stored in 50% RH and 73°F was used (refer Figure 5-7) was assumed for ϵ_{sh} value. This condition was selected because it is closer to the average humidity conditions in the field.

Based on the analysis of risk of cracking, it was observed that Sika Top[®]123 PLUS and Conpatch VO have the highest values of risk of cracking. These results correspond to the behavior of these materials in the restrained shrinkage test mentioned earlier. Both these materials experienced cracking at very early ages. Thus, the risk of cracking factor provides valuable information on the cracking tendency of repair materials.

Table 5-9. Risk of Cracking of Repair Materials

Repair Material	Elastic Modulus, E (psi)	Flexural Strength, f_t (psi)	Free Shrinkage Strain at 28 days	E/f_t	Risk of Cracking
Sika Top [®] 123 PLUS	3500000	2000	1.18	1.8E+03	20.65
Sika Repair [®] SHA	3200000	1100	0.101	2.9E+03	2.94
HB2 Repair Mortar	2000000	1000	0.118	2.0E+03	2.36
Conpatch VO	3900000	1200	0.616	3.3E+03	20.02

The average crack width developed over six days from the first day when cracking was observed in the ring specimens for the repair mortars is given Table 5-10. The average crack width was measured using a crack comparator at six points across the length of the crack and is reported in Table 5-10 as the average crack width. For Sika Repair[®] SHA, the first ring did not crack at the end of 28 days and hence it is reported such. The crack width for other rings increases over age. The restraint provided by the rings induced high restraint shrinkage strains leading to an increase in crack width.

Table 5-10. Average Crack Width over Six Days

Repair Material	Crack Width in Specimen 1 (in.)						Crack Width in Specimen 2 (in.)					
	1 day	2 day	3 day	4 day	5 day	6 day	1 day	2 day	3 day	4 day	5 day	6 day
Sika Top [®] 123 PLUS	0.007	0.009	0.01	0.013	0.016	0.020	0.007	0.009	0.010	0.020	0.020	0.035
Sika Repair [®] SHA	Specimen did not crack						0.005	0.005	0.007	0.007	0.007	0.010
Conpatch VO	0.005	0.005	0.007	0.013	0.016	0.020	0.013	0.013	0.016	0.016	0.020	0.025

The crack width is an important parameter from the perspective of durability of the repaired concrete. Cracking provides passage for water and harmful salts to penetrate the concrete leading to steel corrosion and loss of service life of the structure. Figure 5-13 is a pictorial presentation of the probable future effects of different crack widths in a structure and the allowable crack width from a serviceability perspective as outlined in ACI 318.

Comparing Table 5-10 and Figure 5-12 it can be seen that for specimens under the restraint provided by the steel rings, the average crack width at the end of six days is typically in the range that can cause controllable leakage. If no stress relaxation occurs during this time, the crack

widths can continue to increase over time leading to a path for corrosion of embedded reinforcement.

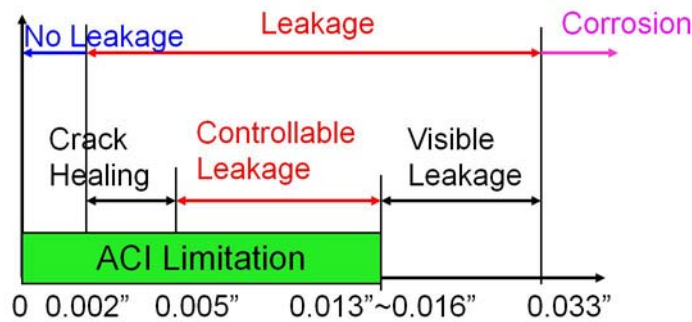


Figure 5-12. Pictorial presentation of crack width and effect on serviceability

It is pertinent to note that these cracks widths are in response to the restraint provided by the steel rings, whereas in the actual structure the restraint provided by the substrate concrete would be of different value. The steel rings provide an equally proportioned restrained stress on the concrete while the substrate concrete can potentially provide unequal restraint. Hence the increase in crack width over age in such cases might differ from this experimental study. In an actual structure, aspects, such as the amount of stress developed at the bottom layers, creep and stress relaxation would also play an important role in the actual shrinkage strains developed in the element. When repair concrete is under stress (tensile or compressive), early age creep serves as a “relief valve” permitting restrained shrinkage to occur with a lower resultant stress.

Figure 5-13 presents the development of free shrinkage strains in three shear key grouts stored in 100% RH. The manufacturer of SET 45 clearly states in the data sheet that SET 45 should not be water cured. In order to maintain an identical environment for all specimens, the SET 45 free shrinkage specimens were also stored at 100% RH. The evidently different behavior of SET 45 under these environmental conditions can be noted in Figure 5-12. Set 45 samples exhibited contraction rather than expansion as observed in the Type I cement grout and Masonry cement grout specimens. Overall, masonry cement grout exhibited minimal expansion at the end of 150 days.

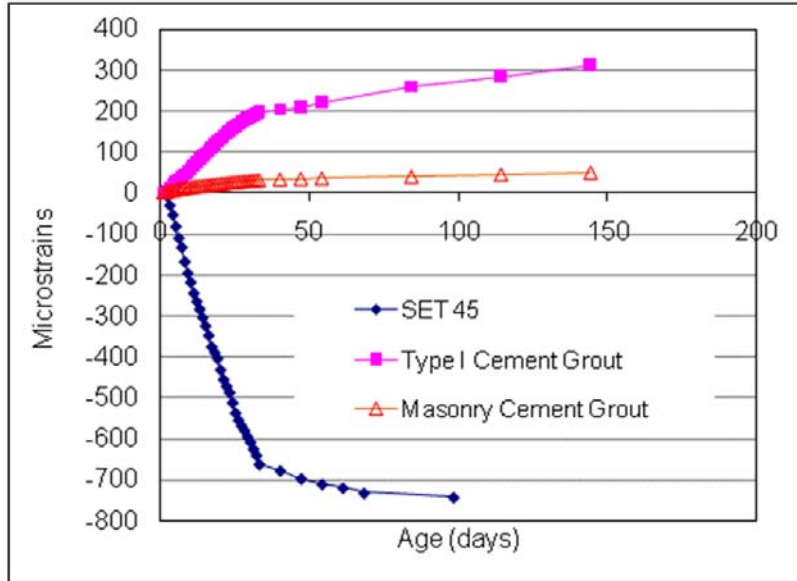


Figure 5-13. Free shrinkage strains in shear key grouts for samples at 100% RH

When free shrinkage specimens were stored in 50% RH it was observed that SET 45 exhibited the least contraction and the lowest development of free shrinkage strains as shown in Figure 5-14. The free shrinkage strains in both grouts are high ($\sim 525\mu\epsilon$ at the end of 150 days). Due to the low humidity and high water to cement ratio of both cement grouts, the rate of diffusion of water from the specimen to the surrounding environment is high, leading to high negative strain value. In cement based system, between the relative humidity of say about 95% to 85%, typically water is lost predominantly from large capillary pores or commonly referred as macropores. As the humidity lowers (between 85% to 50%) water is lost concomitantly from both the mesopores and micropores, i.e. from fine capillary pores as well as from the calcium silicate hydrate. The grout mixtures examined in this study have high water to cement ratios as well as intrinsic high porosity leading to a higher tendency for water loss from the different sized pores, resulting in high strain values.

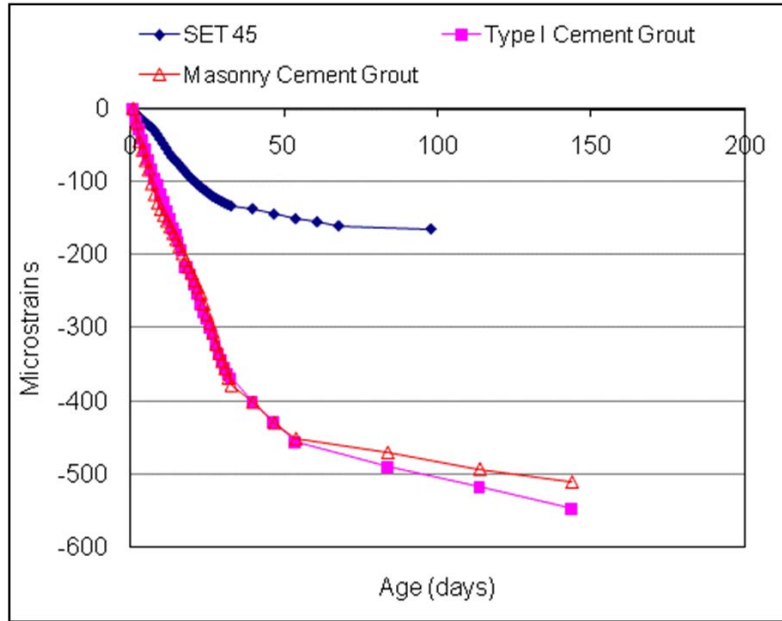


Figure 5-14. Free shrinkage strains in shear key grouts for samples at 50% RH and 73°F

5.7 RESISTANCE TO FREEZING AND THAWING

The long-term durability of repaired concrete is an important aspect in increasing the service life of a structure. In this study, an extensive evaluation of the durability of selected repair materials in freezing and thawing cycles was performed.

Figure 5-15 represents the mean change in relative modulus of different repair materials over 300 cycles of freezing and thawing. The relative dynamic modulus in this test is calculated by measuring the frequency of a wave in the specimen. In this experiment it was observed that the highest frequency was registered for Conpatch VO (~1745 to 1862 Hz at the start of the experiment). Sika Top123 PLUS and Sika Repair SHA had comparable frequencies in the range of 1550 to 1650 Hz at the start of the experiment. The measured frequencies are typically slightly lower than those measured in normal concrete (~1900 to 2100 Hz).

As per ASTM C 666, the relative dynamic modulus at the end of 300 cycles should not be below 60% for a material to be considered to have good resistance to freezing and thawing. All the repair materials evaluated exhibited good resistance to freezing and thawing cycles. Sika Repair® SHA exhibited the highest loss in relative dynamic modulus of 86.5% at 300 cycles. Sika Top123 PLUS and Conpatch VO have excellent resistance to freezing and thawing cycles and exhibit a very low loss in relative dynamic modulus at the end of 300 cycles.

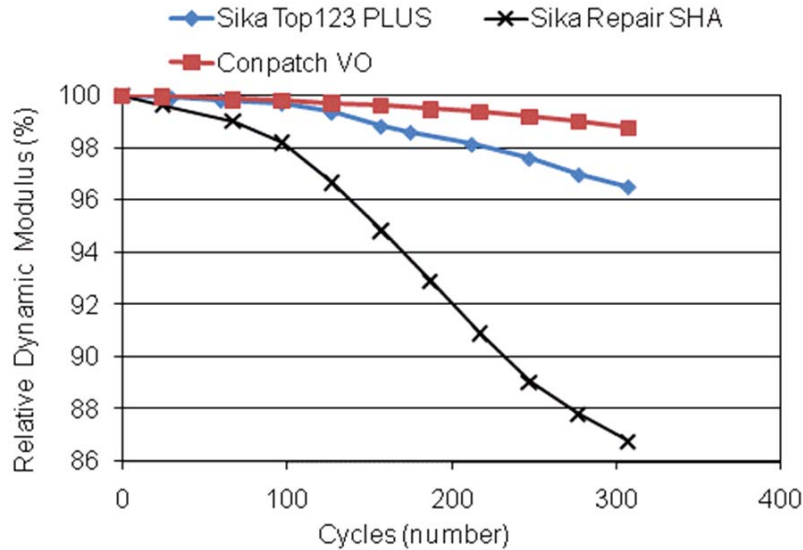


Figure 5-15. Relative dynamic modulus of repair materials over 300 cycles of freezing and thawing

Figure 5-16 shows the average change in length of the specimen for three specimens over 300 cycles of freezing and thawing. A very large change in length was not observed for Sika Top 123 PLUS and Sika Repair SHA specimens whereas Conpatch VO exhibited a high increase in length within the first 30 cycles. Conpatch VO subsequently exhibits a slight drop in its change in length measurements indicating contraction of the specimen. This behavior may be attributed to probable continued hydration of the specimens leading to healing of any cracks that might have formed during the first 30 cycles of the experiment.

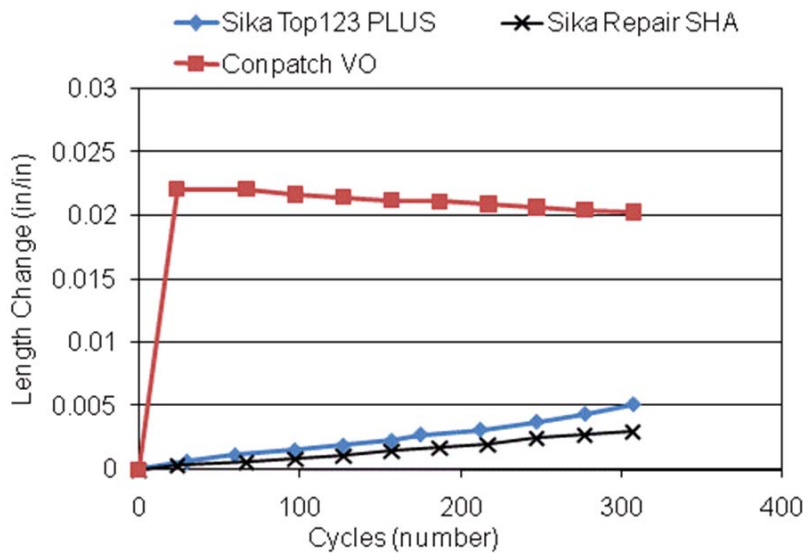


Figure 5-16. Change of repair materials over 300 cycles of freezing and thawing

Appendix F contains graphical presentation of the change in relative dynamic modulus and change in length over 300 cycles of freezing and thawing for all samples tested in this study. Photographs of specimens of repair materials are presented in Appendix F. All repair mortars tested exhibit intact surface on all sides of the specimen at the end of 300 cycles. Specimens of Sika Top123 PLUS and Sika Repair SHA exhibited some circular voids as can be seen in Figures F-13 and F-14 of Appendix F. It should be noted that the occurrence of these voids was very less and overall it did not reduce the relative dynamic modulus of the specimens.

HB2 Repair Mortar samples were not subjected to freezing and thawing cycles because of the presence of large amounts of voids as shown in Figure F-16. Due to the sample size required by ASTM C 666 (3 x 3 x 16 in.) a large volume of the repair mortar is required for preparing the sample. On account of the rapid setting nature of HB2 Repair Mortar, the consolidation of the repair mortar in the molds was very difficult. The mortar was consolidated by vibrating as well as by pressing with fingers and a putty knife in to the mold. Even though different consolidation techniques were adopted, it was observed that a large number of voids (about ½”~1” long) existed in the specimen after the mortar had hardened (refer Figure F-16).

Figure 5-17 is a graphical presentation of the mean change in relative dynamic modulus of shear key grouts subjected to 300 cycles of freezing and thawing. SET 45 had the highest change in relative dynamic modulus in comparison to the traditional cement grouts, but at 82% it is within the requirement of ASTM C 666. Similarly, the change in length of SET 45 samples is also the highest among all the shear key grouts tested (refer Figure 5-18). Type I cement grout, as well as Masonry cement grout, show almost identical changes in relative dynamic modulus and length change over 300 cycles.

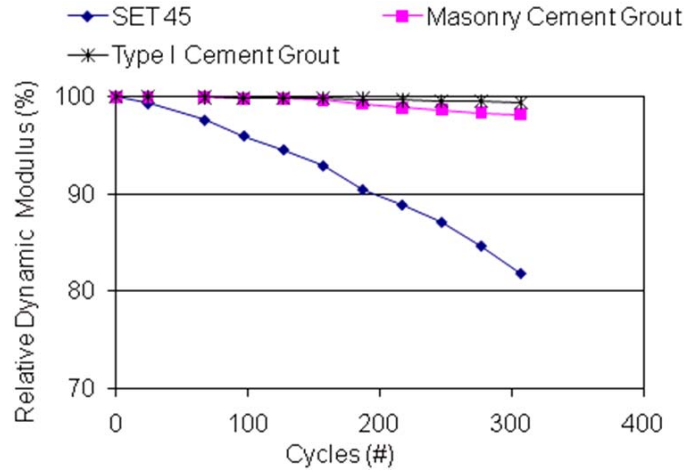


Figure 5-17. Change in relative dynamic modulus of shear key grouts over 300 cycles of freezing and thawing

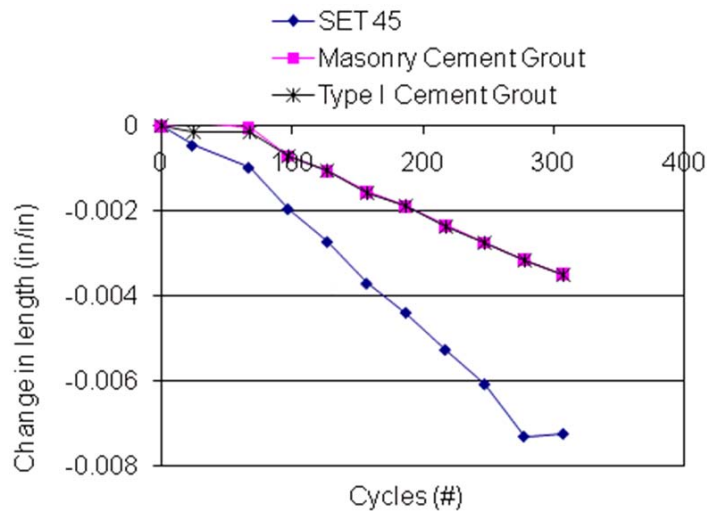


Figure 5-18. Change in length of shear key grouts over 300 cycles of freezing and thawing

Composite specimens of substrate concrete and repair materials were tested for durability of the composite system in freezing and thawing cycles. The composite specimens exhibited excellent resistance to freezing and thawing cycles as shown by the minimal reduction in relative dynamic modulus (see Figure 5-19). As seen in Figure 5.20 Sika Repair[®] SHA showed a slightly larger drop in relative dynamic modulus over 300 cycles in comparison to Sika Top123 PLUS and Conpatch VO. It is necessary to note that Sika Repair[®] SHA exhibits higher durability factor for combined specimens as compared to those specimens of the repair material only (refer to Figure 5-15 and Figure 5-20), whereas the other repair materials exhibited relative dynamic values similar to their composite counterparts.

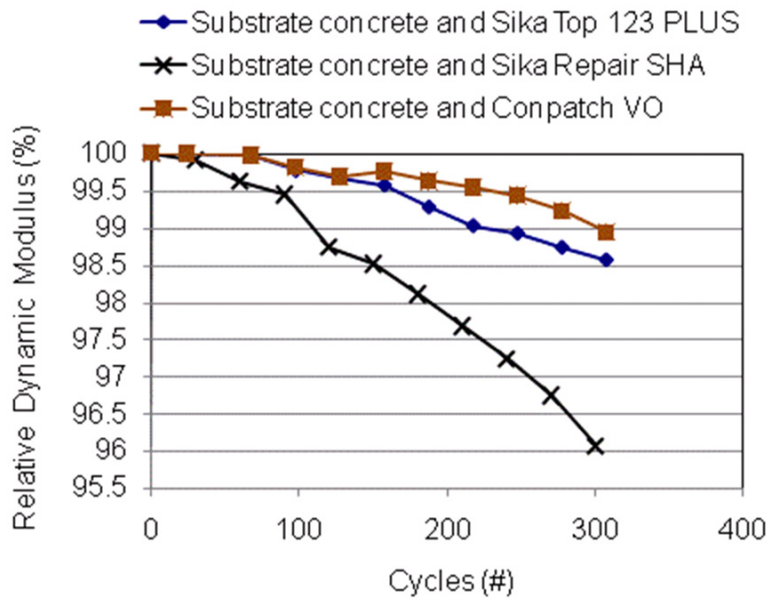


Figure 5-19. Change in relative dynamic modulus of composite specimens of substrate concrete and repair material over 300 cycles of freezing and thawing

5.8 AIR CONTENT

The air void system is critical for the satisfactory performance of the repair mortar and shear key grouts under freezing and thawing conditions. The critical parameters defining a satisfactory air void system are the percentage of air voids, spacing factor, specific area, and bubble frequency. Figure 5-20 shows the amount of air in hardened repair mortar and shear key grouts evaluated in this study. For a durable system, the optimum percentage of air entrainment is about 5 to 6.5%. All the materials evaluated in this study have a higher percentage of entrained air than the prescribed value. HB2 Repair Mortar has the highest amount of air entrainment at 33.5% while the remaining materials ranged from 7.6% to 12.43%.

Figure G-3 in Appendix G shows a stereo image of HB2 Repair Mortar. The image shows the highly porous nature of HB2 Repair Mortar in comparison to other repair mortars (refer Figure G-1 through G-4). Figure G-4 also gives an indication of the high amount of voids formed due to insufficient consolidation given the rapid setting nature of the mortar.

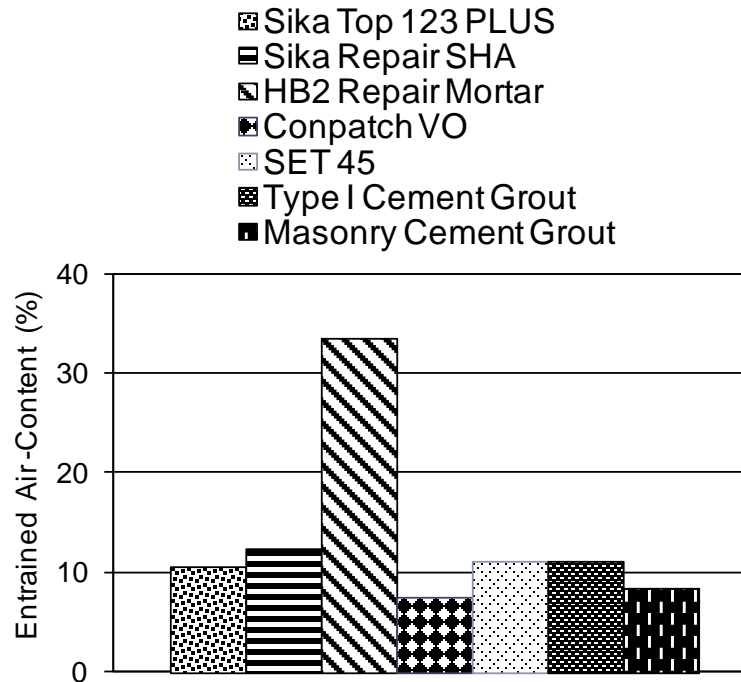


Figure 5-20. Air content in hardened repair mortar and shear key grouts

Specific surface area and void frequency are inter-related and reflect the mean size of the air bubbles. For a protective air void system, the specific surface area should not be less than 25 mm²/mm³. As seen in Figure 5-21, all materials evaluated except for Sika Top[®]123 PLUS have a lower specific surface area than 25 mm. Table 5-11 presents the void frequencies and spacing factors of repair mortars and shear key grouts. For a protective air void system the void frequency should be within 0.3 – 0.6 /mm. Only one repair mortar and two shear key grouts fall within this range. The spacing factor is defined as the average distance between any point in the paste to the edge of the nearest void and typically should not exceed 0.2 mm for adequate resistance to freezing and thawing.

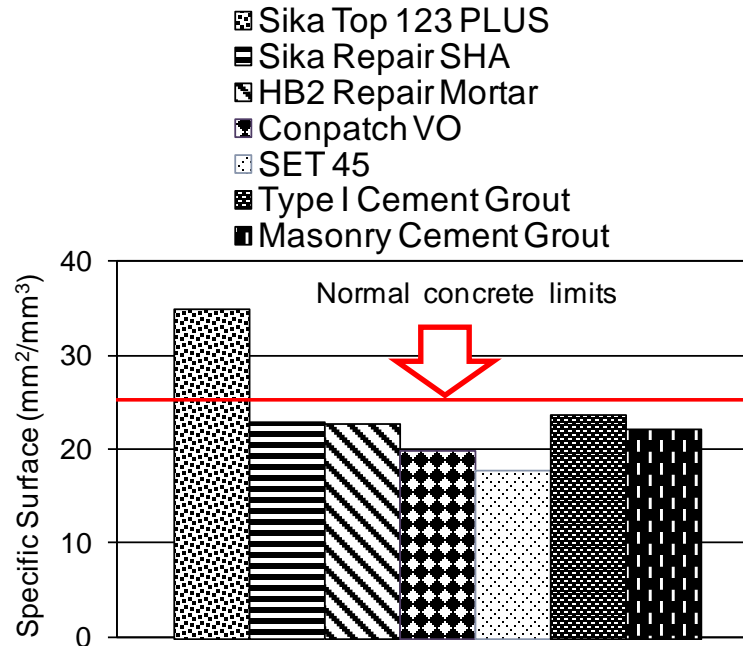


Figure 5-21. Specific surface area of repair mortars and shear key grouts

Table 5-11. Void Frequencies and Spacing Factors for Repair Mortars and Shear Key Grouts

Material	Void Frequency (/mm)	Within Criteria	Spacing Factor (mm)	Within Criteria
Sika Top 123 PLUS	0.939	N	0.144	Y
Sika Repair SHA	0.712	N	0.169	Y
HB2 Repair Mortar	2.039	N	0.055	Y
Conpatch VO	0.381	Y	0.268	N
SET 45	0.496	Y	0.262	N
Type I Cement Grout	0.664	N	0.167	Y
Masonry Cement Grout	0.466	Y	0.218	N

Comparing the air void system data with the results of the freeze-thaw test, it can be observed that although polymer modified repair mortars do not reveal numbers close to the requirement for stable air void system as specified for normal concretes, they do exhibit a desirable performance in the freeze-thaw test.

5.9 COEFFICIENT OF THERMAL EXPANSION (CTE)

Differential thermal strains due to varying CTE values between the substrate concrete and repair mortar can result in an increase in strains in the repaired concrete, leading to cracking and

reduced serviceability. Figure 5-22 shows the average CTE values for repair mortars and shear key grouts. It should be noted that although average values have been used for the graphical presentation, the age difference between any two companion samples varied by up to three days due to equipment scheduling. In Appendix I complete information for each sample is provided.

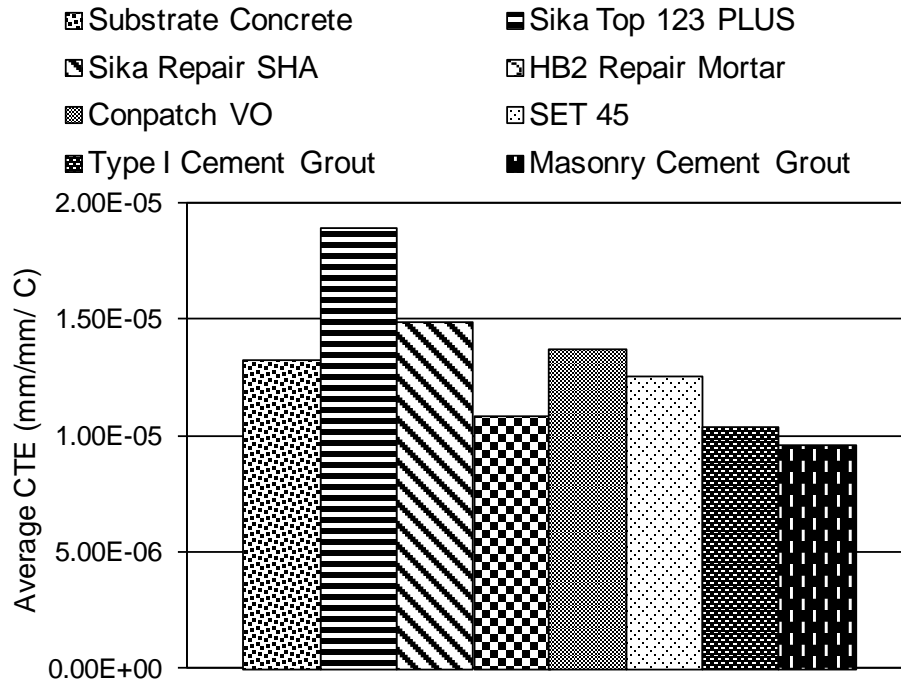


Figure 5-22. Average coefficient of thermal expansion of repair mortars and shear key grouts

In comparison to the substrate concrete, Sika Top 123 PLUS and Sika Repair SHA have higher CTE values whereas cement based grouts have lower CTE values. HB2 Repair Mortar exhibited a high variation in values between the two samples (refer to Appendix H). This variation could be attributed to improper consolidation of the material leading to the presence of voids within the test cylinder. Presence of air in the voids varies the values of change in length with larger difference due to discontinuity in material.

To understand the effects of using repair materials with CTE values different from the substrate concrete, numerical calculations are presented in Table 5-12. If a composite 1 ft long beam is subjected to a temperature variation from 73°F to 113°F, then

$$\text{Change in length } (\Delta l) = \text{length of element } (l) \times \text{CTE } (\alpha) \times \text{change in temperature } (\Delta t)$$

Table 5-12. Change in Length Observed

Material	Change in length (in)	Change in comparison to substrate concrete
Substrate Concrete	0.011	--
Sika Top 123 PLUS	0.016	0.005
Sika Repair SHA	0.013	0.002
HB2 Repair Mortar	0.009	-0.002
Conpatch VO	0.012	0.001
SET 45	0.011	0
Type I Cement Grout	0.009	-0.002
Masonry Cement Grout	0.008	-0.003

A repair mortar having a higher CTE value than the substrate concrete can cause undesirable tensile strain development in the substrate concrete. Sika Top 123 PLUS and Sika Repair SHA exhibit slightly higher length change values in comparison to other repair mortars. Conversely, lower CTE values can cause undesirable compressive strain development.

5.10 SORPTIVITY

The rate of water absorption of repair mortars is an important property because it determines the ability of the material to protect the substrate concrete and reinforcement.

Figure 5-23 and Figure 5-24 compares the values of rate of initial absorption and secondary absorption, respectively, for repair mortars and shear key grouts. ASTM C 1581 states that rate of absorption for a material is accepted only if the regression coefficient for a plot of initial absorption versus time is more than 0.98. It was observed that all repair mortars except Sika Top 123 PLUS has lower regression coefficients (refer Table I-1 in Appendix I).

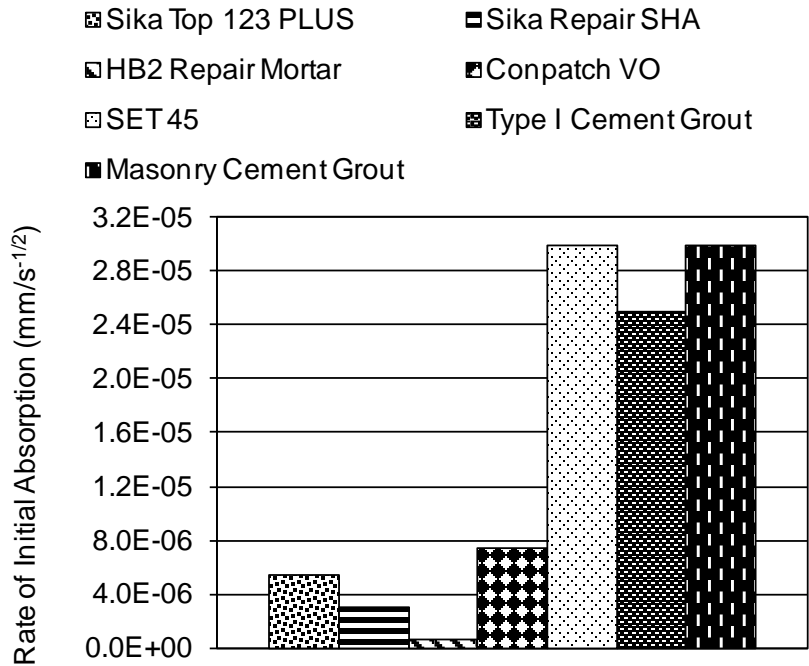


Figure 5-23. Comparison of rate of initial absorption of repair mortars and shear key grouts

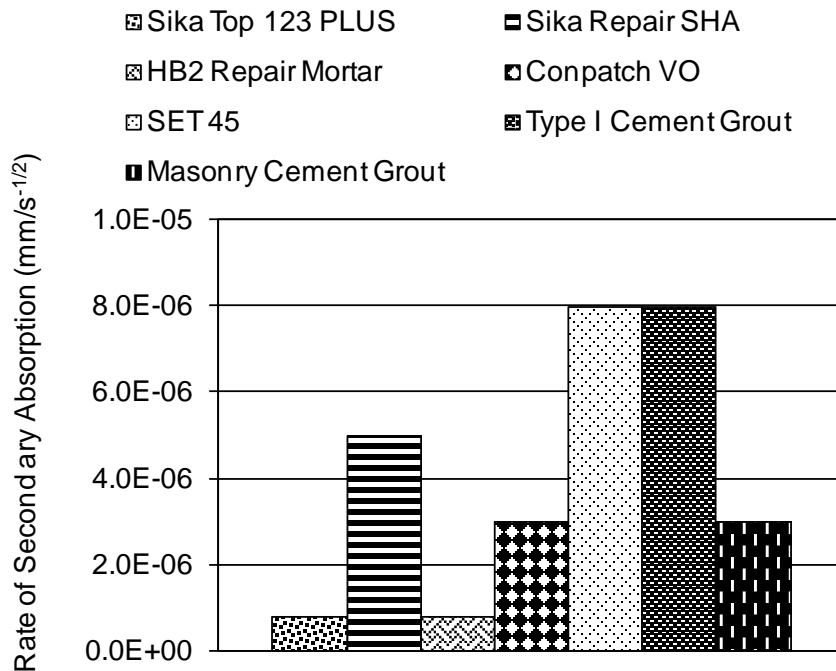


Figure 5-24. Comparison of rate of secondary absorption of repair mortars and shear key grouts

The average data points provided in Figure 5-23 are presented to give a perspective to the absorption behavior of different repair mortars and the values cannot be accepted as absolute values as per ASTM C 1581. The secondary rate of absorption exhibited a more definitive

behavior and all repair mortars had a regression coefficient greater than 0.98. Based on the absorption values, it can be inferred that the repair mortars selected in this study exhibit a lower tendency to absorb water or harmful ions in comparison to the shear key grouts. The absorption values reduce over time thus indicating that as the humidity within the sample increases due to exposure to water, the absorption capacity of the repair mortar is reduced.

In the earlier sections on shrinkage and CTE, the difficulty in measuring a particular property for HB2 Repair mortar has been mentioned. The primary reason for it was related to the difficulty in consolidating HB2 Repair Mortar specimens leading to voids in the hardened mortar. The sorptivity results indicate that the presence of voids inside the specimen did not affect the rate of absorption. In fact, the lowest absorption rate was observed for HB2 Repair Mortar.

5.11 CHLORIDE PERMEABILITY

The ability of repair material to resist chloride ion migration was determined by performing the ASTM C 1202 test. Figure 5-25 shows the average values of charge passed through two test specimens for different repair mortars. Material data sheets of two repair materials (i.e. Sika Top 123 PLUS and Conpatch VO) provide information on chloride permeability. As per ASTM 1202 specifications, a low permeability concrete should pass a charge of 100-1000 Coulombs at the end of the test. Based on this criterion, it was observed that all repair materials evaluated exhibited low permeability. Conpatch VO exhibited higher values than those prescribed as per the manufacturer but the measured value (930 Coulombs) was still in the low permeability range as prescribed by ASTM C 1202.

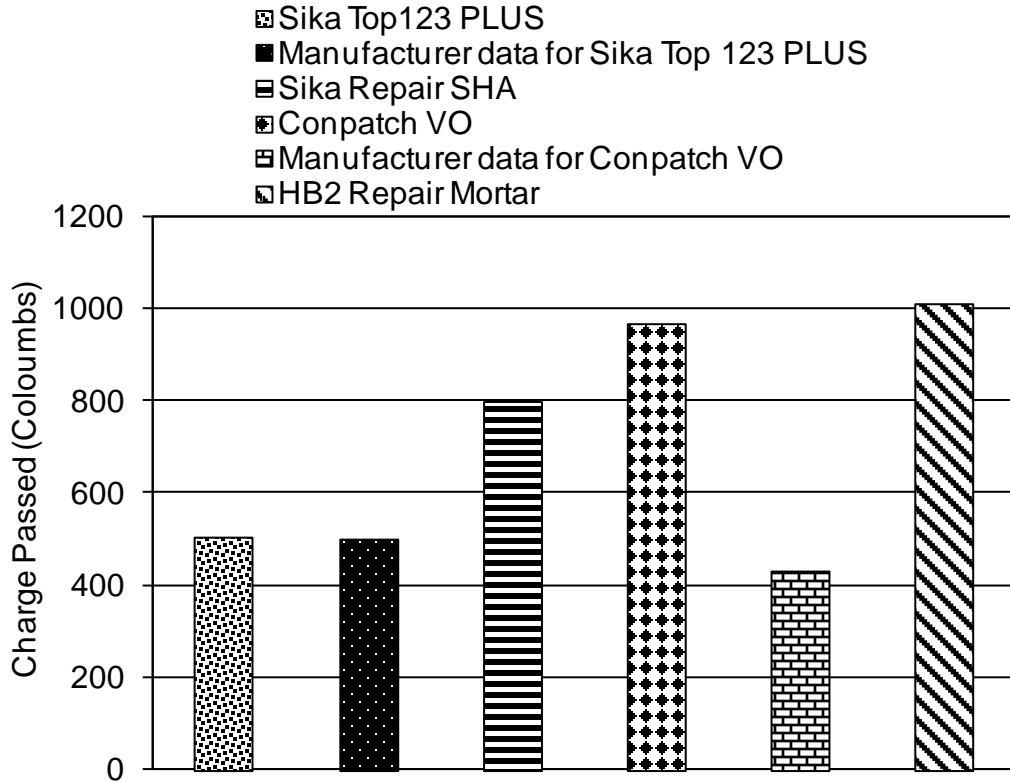


Figure 5-25. Comparison of chloride permeability for repair materials

5.12 SUMMARY OF DURABILITY STUDIES

The basic tenet of this research component was to investigate the durability characteristics of repair materials used for box-beam bridges so as to improve its life expectancy. Phase I of this project identified several levels of deterioration found through inspection of MDOT-owned adjacent box beam bridges. The major concerns observed in Phase I were: 1) the longitudinal reflective cracking and apparent failure of the grouted shear keys between beams, 2) corrosion of concrete especially along the bottom side of the box beams of the bridge. Onset of corrosion is caused due to moisture penetration from existing cracks and application of deicer salts on the bridge deck.

One objective of this project component was to determine the causes of the longitudinal cracking in shear keys by evaluating the mechanical properties of the currently used shear key grouts. Analysis of the design methods and material properties will provide insight in the interaction between the shear keys and the box beams. To evaluate the mechanical properties and its effect on the structural stability of the bridge, three types shear key grouts were selected. Two of these were cement based grouts whose mixture proportion was based on MDOT specifications. The

third shear key grout selected was SET 45, a commercially available rapid setting phosphate cement based grout.

Another objective of the research component was to analyze the dimensional stability and the durability properties of repair materials commonly used by MDOT. Durability is not only the concern for the design of new concrete structures but also needs to be taken into account in concrete repair. Literature review conducted for this study clearly indicated that though repair is performed to increase serviceability and durability of bridges, sufficient research on the repair material parameters governing this behavior has received little attention. One of the main results of the literature review was the development of design parameters from the perspective of durability of repaired structures as shown previously in Figure 4-1. To this end, four commercially available repair materials typically used for bridge repairs were selected to evaluate their performance in terms of dimensional stability and durability. The properties evaluated were slump, air content, rate of gain of compressive strength, bond strength, shrinkage and cracking susceptibility, resistance to freezing and thawing cycles, coefficient of thermal expansion, chloride permeability and sorptivity.

It was observed that the repair materials and shear key grouts investigated in this study have a wide range of values for all the properties for which the materials were evaluated and the results are discussed in the preceding sections of this chapter. A summary of all the test results is provided below:

- 1) All repair materials exhibited zero slump and had very low workability. The most unworkable repair mortar was the HB2 Repair Mortar. The mortar was extremely stiff after mixing and would typically require an excessive amount of consolidation. The shear key grouts, including SET 45, exhibited good workability with slump values in the range of 8 in.
- 2) Compressive strength of commercial polymer modified mortars varies for each material. Amongst all repair materials evaluated in this study Sika Top 123 PLUS exhibited slightly lower strengths in comparison to those listed in the manufacturer's data sheet and Conpatch VO exhibited the highest strength at all ages. All repair materials exhibit strengths in the range of 6000 psi or more at the end of 28 days. Sika Repair SHA and HB2 Repair Mortar exhibited lower early age strengths but gain

- a higher percentage of strength at later ages. The compressive strength of cement based shear key grouts was below 5000 psi whereas SET 45 exhibited slightly higher strength at 28 days.
- 3) Slant shear strength results were compared with the stipulation provided in ASTM C 928. Specimens of polymer repair material tested at the age of 1 day exhibited lower strengths than those stipulated in ASTM C 928 except for Conpatch VO. None of the polymer based repair materials nor the cement based shear key grouts exhibited strengths as per the requirements of ASTM C 928 at 7 days. SET 45 exhibited good bond strength and the average values were above those stipulated by ASTM C 928.
 - 4) The effect of shrinkage on volumetric stability was evaluated by conducting tests to determine the free shrinkage as well as the cracking susceptibility under different curing regimes. It was observed that HB2 Repair Mortar and Sika Repair SHA exhibited low free shrinkage strains under both curing regimes (100% RH and 50% RH). The highest free shrinkage or expansion was observed for Sika Top123 PLUS irrespective of the curing regime. The shear key grouts exhibited opposing behavior when free shrinkage specimens were cured at 100% RH. Cement based shear key grouts exhibited expansion when specimens were stored at 100% RH whereas SET 45 experienced large amount shrinkage ($\sim 700 \mu\epsilon$) under the same environment. Specimens of cement based shear key grouts stored at 50 % RH exhibited high values of free shrinkage strains in comparison to SET 45.
 - 5) Cracking susceptibility was measured for polymer repair materials by performing the restrained ring shrinkage test. Two samples were cast for all materials except HB2 Repair Mortar. It was observed that the cracking susceptibility for the materials varied. All materials cracked within 10 days from the start of the test except for one sample of Sika Repair SHA. The *risk of cracking factor* was determined for the polymer repair materials based free shrinkage strains and elastic modulus. Sika Top 123 PLUS and Conpatch VO exhibited highest risk of cracking factor.
 - 6) Durability of construction materials under freezing and thawing cycles is an important property and was evaluated for both polymer repair materials as well as shear key grouts except for HB2 Repair Mortar. All materials exhibited excellent resistance to freezing and thawing cycles. The resistance to freezing and thawing

cycles is related to the amount and spacing of air content in the mortar. It was observed that though the polymer repair materials exhibit a high air content, the parameters that define stable air content for concretes cannot be directly applied. It was observed that the specific surface area of air bubbles and the void frequency of some of the polymer repair materials were not within the requirements as specified for normal concrete. Cement based shear key grouts also exhibited excellent resistance to freeze thaw cycles. SET 45 though exhibited adequate resistance to freezing and thawing cycles, the value of relative modulus at the end of 300 cycles was 80 % whereas the cement mortar based grouts exhibited had higher relative modulus values of 98% for the same cycles.

- 7) Resistance to freezing and thawing of composite specimens consisting of substrate concrete and polymer repair material was evaluated in this study. Composite specimens of Sika Repair SHA exhibited higher resistance to freezing and thawing cycles in comparison to only repair material samples.
- 8) Thermal coefficient of expansion of polymer repair materials evaluated in this study is approximately equal to the substrate concrete for mortars except for SikaTop 123 PLUS.
- 9) Permeability of chloride ions and water absorption capacity of all the repair mortars evaluated in this study is low. The polymer based repair materials exhibited extremely low values of charge passed through specimen indicating high resistance to chloride ion penetration. Water absorption in terms of sorptivity values for all repair mortars was extremely low in comparison to typical values of sorptivity for substrate concrete.

Table 5-13 and Table 5-14 summarize the results for all repair materials and shear key grouts, respectively. The values are compared with respect to requirements and volumetric stability of the whole system consisting of the substrate concrete and the repair concrete.

Table 5-13. Repair Material Test Results Summary

Property	Ideal Requirement	Repair Materials			
		Sika Top 123 PLUS	Sika Repair SHA	HB2 Repair Mortar	Conpatch VO
Workability	Good	Good	Good	Low	Good
Compressive Strength (psi)					
1 day	≥ 3000	> 3000	< 3000	< 3000	> 3000
7 day	≥ 3000	> 3000	> 3000	> 3000	> 3000
28 day	> substrate compressive strength	~ 6700	~ 6200	~ 5800	~ 9600
Slant Shear Bond Strength (psi)					
1 day	1000	> 1000	< 1000	< 1000	> 1000
7 days	1500	< 1000	< 1000	< 1000	< 1000
Free Shrinkage	low	high	high	low	low
Cracking Susceptibility	low	high	high	NA	low
Resistance to freeze-thaw damage	≥ 60 %	Good	Good	NA	Good
Coefficient of Thermal Expansion	~ substrate concrete	high	equal	equal	equal
Sorptivity	low	low	low	low	low
Chloride Permeability	low	low	low	low	low

Table 5-14. Shear Key Grout Test Results Summary

Property	Ideal Requirement	Shear Key Grouts		
		Type I Cement	Masonry Cement	SET 45
Workability	8 – 10 in.	8	7	8
Air content	14 ± 4	13.5	10.5	--
Compressive Strength (psi)				
1 day	≥ 2000	> 2000	< 2000	< 2000
7 day	≥ 3000	> 3000	> 3000	> 3000
28 day	> substrate compressive strength	~ 4500	~ 4500	~ 5500
Slant Shear Bond Strength (psi)				
7 day	1000	> 1000	< 1000	> 1000
28 days	1500	< 1500	< 1500	> 1500
Free Shrinkage	low	low	low	low
Resistance to freeze-thaw damage	≥ 60 %	Good (80%)	Good	Good
Coefficient of Thermal Expansion	~ substrate concrete	equal	equal	low
Sorptivity	low	low	low	low

6 MATERIAL TESTING

6.1 OBJECTIVE AND APPROACH

One of the project tasks deals with finite element (FE) simulation of box-beam bridge construction stages. Another task deals with developing FE models for load response assessment for the purposes of determining load capacity of the side-by-side box-beam bridges with distressed box-beams. Mechanical properties of materials used in the bridge are required as input parameters to the FE models. Concrete, steel, and prestressing strand properties are well documented in the literature. Mechanical properties of manufactured grout materials (e.g., set grout and set-45) and repair materials and are also documented in manufacturers' technical data sheets. Type R-2 grout is commonly used in Michigan box-beam bridges to form the shear-keys. Mechanical properties of R-2 grout have not been documented in literature.

This chapter summarizes mechanical properties of Type R-2 grout obtained from laboratory testing performed at Western Michigan University. Mechanical properties of repair materials and manufactured shear-key materials that were obtained from manufacturers' technical data sheets and published literature are included in Chapter 2. Mechanical properties of selected manufactured shear key grout materials and repair materials were evaluated for verification purposes and are summarized in this chapter.

6.2 TYPE R-2 GROUT

The mix ID and a brief description of the mixes are given in Table 6-1.

Table 6-1. Grout Mix ID and Description

Mix ID	Description
BB	Grout made of Type 1 Portland cement. Prepared by Consumer's Concrete and used in Oakland over I-94 bridge
BBA	Grout made of Type 1 Portland cement – Laboratory mix
BBM	Grout made of Type M masonry cement – Laboratory mix
BBN	Grout made of Type 1 Portland cement and Type N masonry cement – Laboratory mix
BBS	Grout made of Type 1 Portland cement and Type S hydrated lime – Laboratory mix

6.2.1 Plastic Properties of Type R-2 Grout

Table 6-2 includes slump and percent of air in the grout samples prepared in the laboratory. The mixes were prepared according to the proportions and guidelines given in the Table 702-1 of MDOT Standard Specification for Construction (2003b). Also, Standard Specification Section 708.3 requires approximately 5 in. slump for the grout.

Table 6-2. Slump and Air Content of Grout Mixes

Mix ID	Slump (in) (ASTM C 143)	Air (%) (ASTM C 231)
BBA	7.25	13.5
BBM	9.00	12.75
BBN	21.0*	10.0
BBS	7.75	13.75

*Diameter of the flow

6.2.2 Mechanical Properties of Type R-2 Grout

Ultrasonic pulse velocity (UPV) tests were performed evaluating the dynamic elasticity modulus and Poisson's ratio of the material. The UPV tests were performed in compliance with ASTM C597. In addition, compressive strength of grout was evaluated.

The dynamic modulus is generally greater than the static modulus determined in accordance with ASTM C469. However, for the type R-2 grout materials, the dynamic modulus was measured as lower than the static modulus determined following the procedure given in ASTM C469. The reasons for the disparity was investigated and discussed later in this chapter. Strength, Poisson's ratio, and dynamic modulus of grout materials are presented below:

Table 6-3. Mechanical Properties of R-2 Grout - Mix BB

Age (Days)	Strength (psi)	Poisson's Ratio	Dynamic Modulus (ASTM C597) (ksi)
3	3,730	-	-
7	3,651	0.31	2,985
14	4,385	-	-
28	4,859	0.31	3,163

Table 6-4. Mechanical Properties of R-2 Grout - Mix BBA

Age (Days)	Strength (psi)	Poisson's Ratio	Modulus (ksi)	
			Dynamic (ASTM C597)	Static (ASTM C469)
3	2,693	0.31	2,554	-
7	3,668	0.28	2,718	-
14	4,256	0.30	2,954	-
28	4,309	0.31	3,040	3251

Table 6-5. Mechanical Properties of R-2 Grout - Mix BBM

Age (Days)	Strength (psi)	Poisson's Ratio	Dynamic Modulus (ASTM C597) (ksi)
3	2,125	0.32	2,445
7	2,358	0.32	2,619
14	2,646	0.32	2,737
28	2,677	0.31	2,917

Table 6-6. Mechanical Properties of R-2 Grout - Mix BBN

Age (Days)	Strength (psi)	Poisson's Ratio	Dynamic Modulus (ASTM C597) (ksi)
3	1,916	0.31	2,349
7	2,693	0.32	2,593
14	3,377	0.33	2,734
28	3,680	0.32	2,888

Table 6-7. Mechanical Properties of R-2 Grout - Mix BBS

Age (Days)	Strength (psi)	Poisson's Ratio	Dynamic Modulus (ASTM C597) (ksi)
3	2,470	0.30	2,283
7	2,899	0.31	2,427
14	3,403	0.30	2,349
28	3,626	0.31	2,622

Figure 6-1, Figure 6-2, and Figure 6-3 give the early age changes in the mechanical properties. As seen in Figure 6-1, the compressive strength of grout material varies significantly depending on the cement type used in the mix. Mix BBM made from masonry cement (Type M) gives the

lowest strength. The dynamic modulus and Poisson's ratio of the materials show a more limited difference across the mixes.

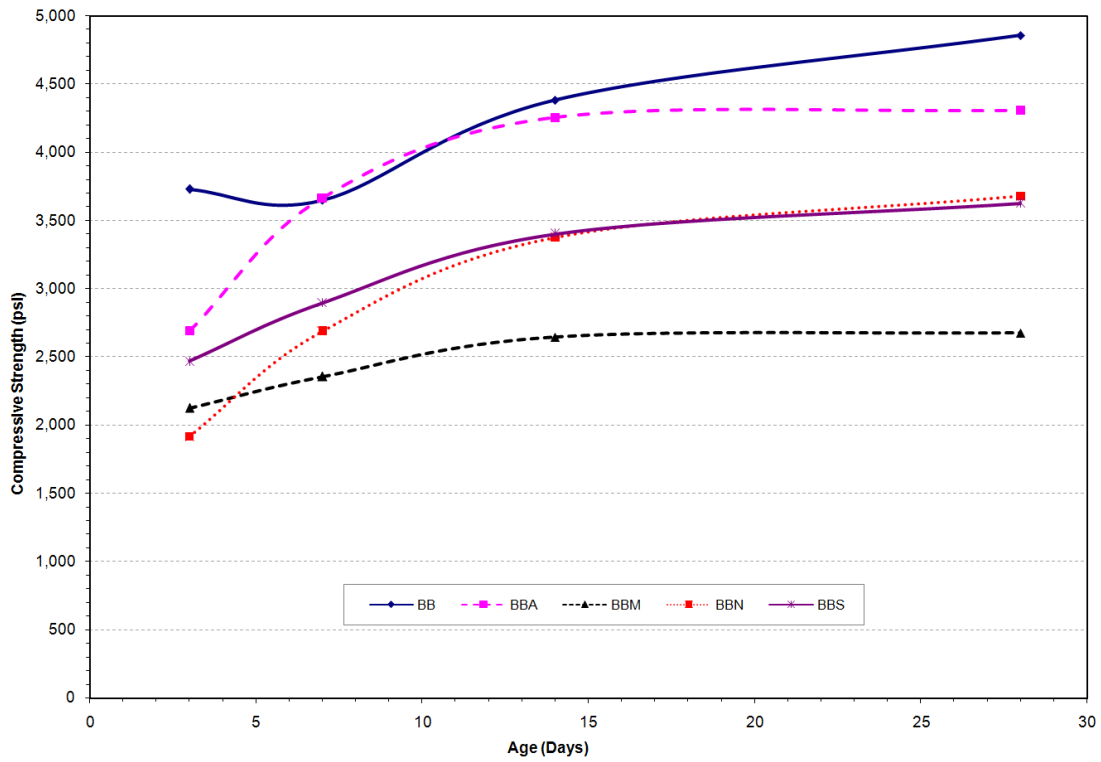


Figure 6-1. Compressive strength of grout material during early age

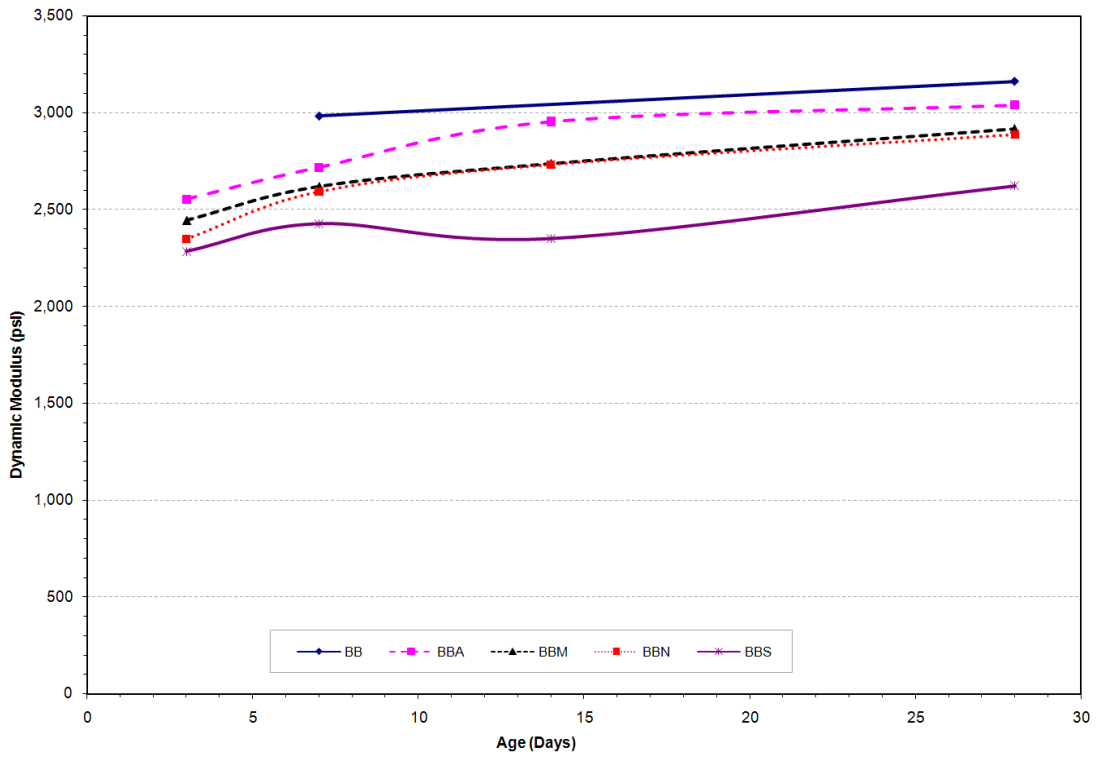


Figure 6-2. Dynamic modulus of grout material during early age

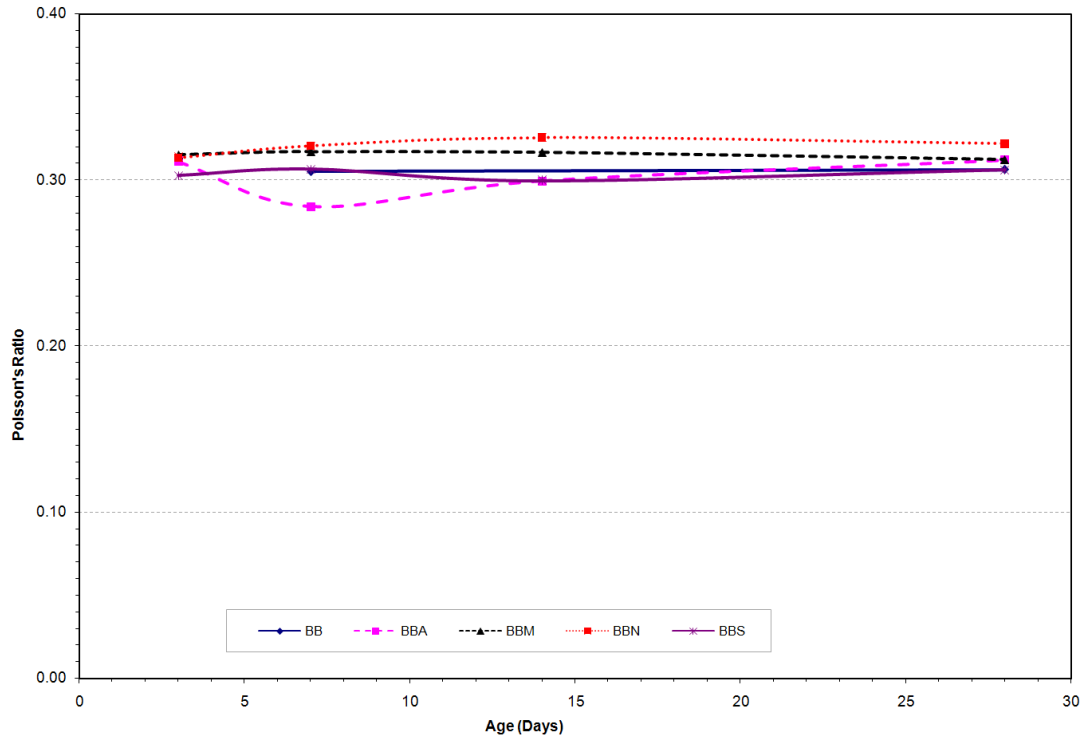


Figure 6-3. Poisson's ratio of grout material during early age

6.2.3 Type R-2 Grout Material Behavior under Axial Compression

The disagreement between the expected values of the static modulus and dynamic modulus of grout material is investigated by establishing the stress-strain relationship of a grout specimen. A cyclic axial compression test on a sample made from the mix BBS was conducted. The applied load reached about 40% of the 14-day compressive strength. The stress - strain plot of the specimen is shown in Figure 6-4. As seen in the figure, the grout specimen exhibits a pinched stress-strain curve with post yielding strain hardening behavior that is not typical of concrete. The second loading cycle falls over the initial loading curve indicating that there is no degradation due to internal cracking at a stress level that reaches only 40% of the compressive strength. Samples prepared using BBS mix contained 13.75% air. The shift in the unloading curve is an indication of energy dissipation due to internal friction. The elastic modulus dramatically changes in proportion to strain within the load cycle. The static modulus test (ASTM C469) is not able to capture this behavior and produces an average modulus value.

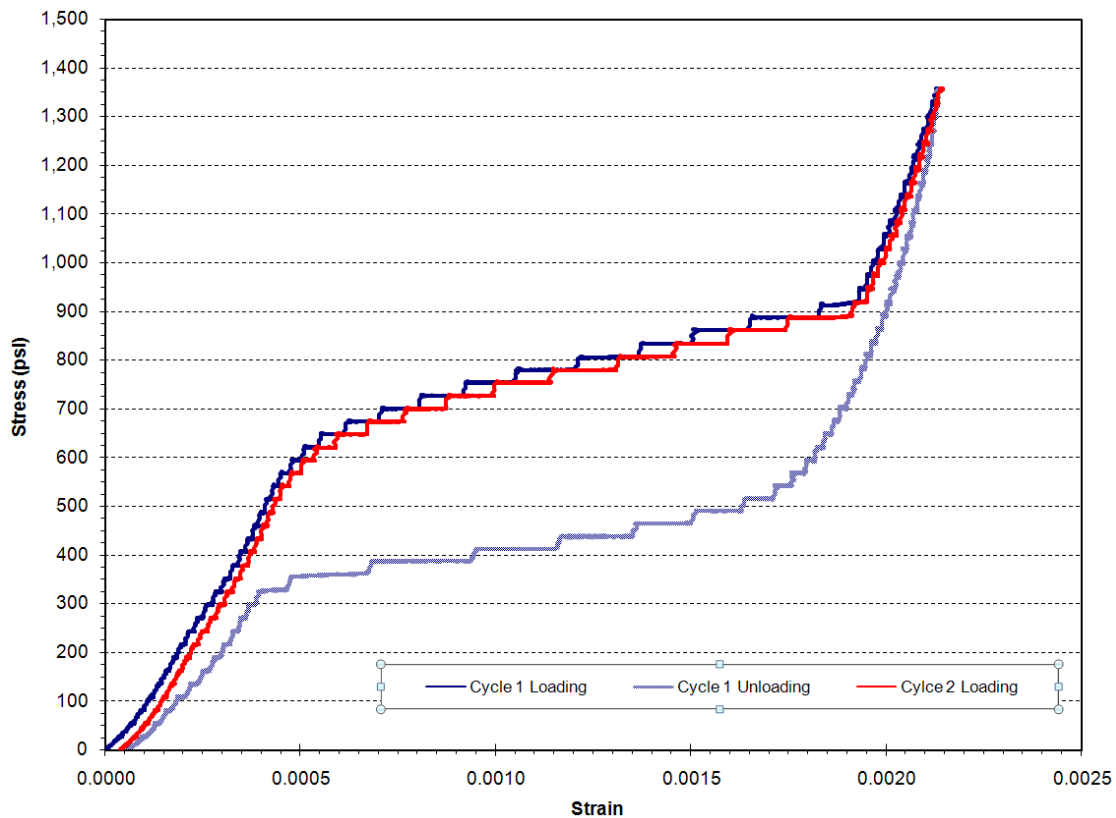


Figure 6-4. Stress-strain behavior of grout (mix BBS) under axial compression

AASHTO LRFD (2004) requires a posttension stress of 250 psi at the shear key. When the stress-strain behavior of the grout BBS is investigated under uniaxial compression, the effective modulus of the material at 250 psi stress level is about 1100 ksi (Figure 6-5). However, using a measured static modulus for this purpose (<3000 ksi), the grout strain would have been much smaller. The effective grout modulus at the time of posttension application is important as it governs the load distribution as well as providing a seal between the beams. Further investigation is required to formulate grout behavior under various load levels since the ASTM C469 procedure is not useful for capturing this elastic nonlinear behavior of the grout material.

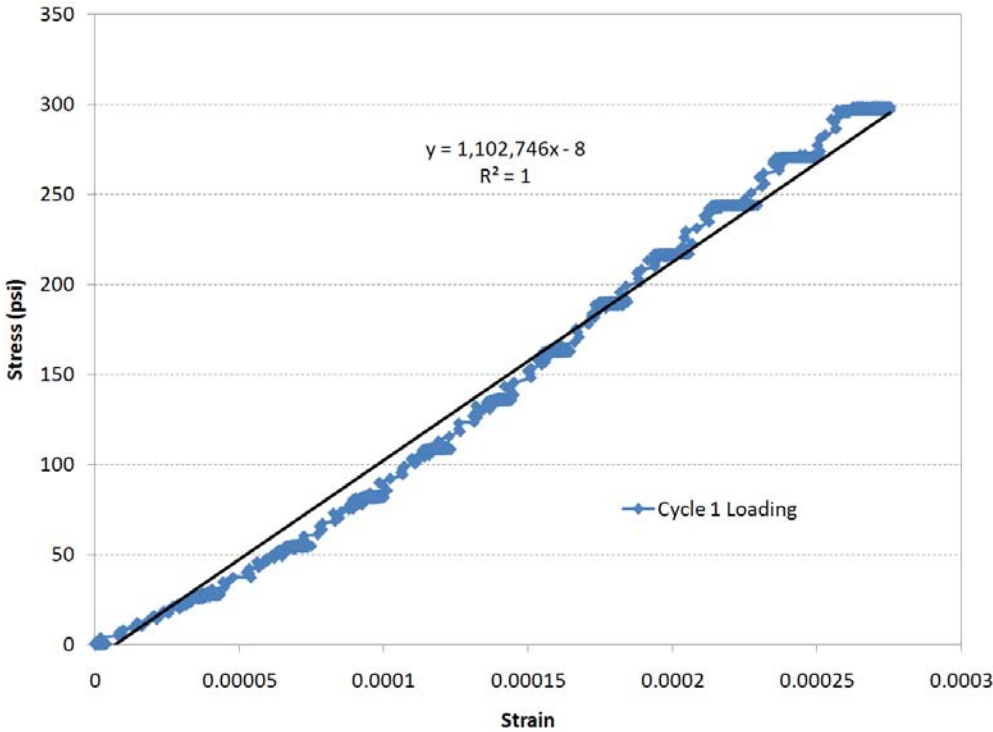


Figure 6-5. Stress-strain behavior of grout (mix BBS) under axial compression

6.3 SET 45 GROUT PROPERTIES

Set® 45 grout properties were tested in accordance with ASTM C109, ASTM C469, and ASTM C597. Strength was measured lower than that the manufacturer spec sheet. The static modulus calculated following ASTM C469 is similar to the dynamic modulus determined as per ASTM C597. As discussed in the previous section, the ASTM C469 procedure is not suitable of capturing the nonlinear elastic behavior of grout material.

Table 6-8. Mechanical Properties of Set® 45 Grout

Set® 45					
Age (days)	Strength (psi)	Poisson's Ratio		Modulus of Elasticity (ksi)	
		Dynamic	Static	Dynamic ASTM C597	Static ASTM C469
1	719	0.29	---	3,265	---
2	774	0.29	---	3,497	---
7	2,104	0.28	0.26	3,377	2,885
14	2,233	0.28	0.24	3,595	3,406
28	4,410	0.29	0.22	3,932	3,844

6.4 PROPERTIES OF REPAIR MATERIAL

Four repair material properties were tested in accordance with ASTM C109, ASTM C469, and ASTM C597. Strength values obtained are lower than those specified by the manufacturers. Similar to R2 grout, the nonlinear elastic behavior of the materials needs to be documented for proper evaluation of the repair application. This is because the repair performance will be a function of the stress or strain level at the location of the repair.

Table 6-9. Mechanical Properties of SikaRepair® SHA

SikaRepair® SHA					
Age (days)	Strength (psi)	Poisson's Ratio		Modulus of Elasticity (ksi)	
		Dynamic	Static	Dynamic ASTM C597	Static ASTM C469
1	1,041	0.31	---	2,623	---
2	1,367	0.31	---	2,738	---
7	3,719	0.31	N/A	2,858	3,032
14	4,132	0.29	0.24	3,126	3,209
28	4,552	0.31	0.22	3,072	3,400

Table 6-10. Mechanical Properties of Conpatch V/O

Conpatch V/O					
Age (days)	Strength (psi)	Poisson's Ratio		Modulus of Elasticity (ksi)	
		Dynamic	Static	Dynamic ASTM C597	Static ASTM C469
1	883	0.32	---	2,829	---
2	1,491	0.31	---	2,902	---
7	2,386	0.31	0.20	3,311	3,242
14	1,868	0.41	0.22	3,244	3,227
28	4,549	0.33	0.24	3,140	3,310

Table 6-11. Mechanical Properties of SikaTop® 123 PLUS

SikaTop® 123 PLUS					
Age (days)	Strength (psi)	Poisson's Ratio		Modulus of Elasticity (ksi)	
		Dynamic	Static	Dynamic ASTM C597	Static ASTM C469
1	3,075	0.31	---	2,357	---
2	3,579	0.31	---	2,480	---
7	4,338	0.30	0.24	2,653	2,281
14	4,484	0.30	0.23	2,706	2,431
28	4,425	0.30	0.24	2,760	2,571

Table 6-12. Mechanical Properties of HB2® Repair

HB2® Repair					
Age (days)	Strength (psi)	Poisson's Ratio		Modulus of Elasticity (ksi)	
		Dynamic	Static	Dynamic ASTM C597	Static ASTM C469
1	1,857	0.30	---	1,565	---
2	1,949	0.31	---	1,609	---
7	1,867	0.31	0.22	1,669	1,640
14	2,320	0.31	0.21	1,689	1,562
28	3,729	0.31	0.23	1,723	1,686

6.5 SUMMARY AND CONCLUSIONS

Mechanical properties of Type R-2 grout specified for Michigan bridges were tested and documented. Additional manufactured shear key grout materials and repair materials were also tested for mechanical properties. The AASHTO Standard (2002) Section 5.14.4.3.2 requires 5000 psi grout compressive strength in 24 hours, while the LRFD (2004) Section 5.14.1.2.8 requires 4000 psi. Grout specimens tested during the project could not satisfy the strength required by the AASHTO Standard or LRFD at the time of posttension. AASHTO LRFD (2004) requires that posttension generates a stress level 250 psi at the shear key. According to Michigan practice, posttension is applied 48 hours after grouting the shear keys (MDOT 2003b). All the grout mixes tested showed sufficient strength such that 250 psi compressive stress can be applied with a factor of safety of at least three.

The static modulus of R-2 grout as well as the commercial grout specimens were measured to be greater than the measured dynamic modulus. This is contrary to the expected properties of

cementitious materials. Further experimental testing showed that grout exhibits nonlinear hysteretic elastic stress-strain relationship. Hardened grout properties given in Chapter 5 are also studied to identify the reasons for the nonlinear hysteretic behavior. Further study is recommended to characterize the grout materials since the elasticity modulus of grout at the time of posttension applications controls the stress distribution and the interface performance between the adjacent beams without separation or cracking in order to develop a watertight fit. The AASHTO LFRD (2004) grout strength requirements should also be investigated.



MDOT RC-1527

**CONDITION ASSESSMENT AND METHODS
OF ABATEMENT OF PRESTRESSED
CONCRETE BOX-BEAM DETERIORATION**

Phase II

**FINAL REPORT
VOLUME II**



MichiganTech

Center for Structural Durability
A Michigan DOT Center of Excellence

Research

Intentionally left blank

CONDITION ASSESSMENT AND METHODS OF ABATEMENT OF PRESTRESSED CONCRETE BOX- BEAM DETERIORATION

Phase II

Project Manager: Mr. Steve Kahl, P.E.

Submitted to



Submitted by



Western Michigan University
Department of Civil & Construction Engineering
College of Engineering and Applied Sciences
Kalamazoo, MI 49008
Fax: (269) – 276 – 3211

Dr. Haluk Aktan, P.E.
Professor & Chair
(269) – 276 – 3206
haluk.aktan@wmich.edu

Dr. Upul Attanayake
Assistant Professor
(269) – 276 – 3217
upul.attanayake@wmich.edu

Mr. Evren Ulku
Graduate Research Assistant
(313) – 577 – 3785
evren@eng.wayne.edu

MichiganTech

Michigan Technological University
Dept. of Civil & Environmental Engineering
1400 Townsend Drive
Houghton, MI 49931
Fax: (906) – 487 – 1620

Dr. Theresa M. Ahlborn, P.E.
Associate Professor
(906) – 487 – 2625
tess@mtu.edu

Dr. Yogini Deshpande
Post Doctoral Researcher
(906) – 487 – 1474
yogini@mtu.edu

Intentionally left blank

Contents

TABLE OF TABLES.....	iv
TABLE OF FIGURES.....	vi
7 Analytical Modeling of Box-Beam Sub-Assemblages	1
7.1 Objective and Approach	1
7.2 Sub-Assemblage Models of Box-Beams	1
7.2.1 The Effect of Shear Key Material Properties and Number of Diaphragms ...	3
7.2.2 Bridge Width Effect on Clamping Stress Distribution	11
7.3 Summary and Conclusions	12
8 Analytical Modeling: Construction Simulation and Service Load Analysis.....	15
8.1 Overview.....	15
8.2 Construction Process Simulation and Analysis Results	19
8.3 Service Load Analysis	23
8.3.1 Load Combination 1: 1.0 DEAD + 1.0 NTG.....	23
8.3.2 Load Combination 2: 1.0 DEAD + 1.0 PTG	25
8.3.3 Load Combination 3: 1.0 DEAD + 1.0 LL	28
8.4 Summary and Conclusions	32
9 Rational Transverse Posttension Design	35
9.1 Overview.....	35
9.2 Construction Monitoring.....	35
9.3 Macromechanical Model	38
9.4 Rational Posttension Design Procedure	42
9.4.1 Overview.....	42
9.4.2 Analysis and Design Procedure	44
9.5 Construction Simulation with Staged Posttension.....	49
9.5.1 Service Load Analysis	55
9.6 Summary and Conclusions	67

10 Capacity Evaluation of a Box-Beam Bridge with Distressed Beams.....	71
10.1 Overview.....	71
10.2 Flexure Critical Distress and Associated Box Beam Capacities	78
10.3 Shear Critical Distress and Box Beam Capacities	85
10.4 Influence of Grout Loss and Broken Posttension Strands	85
10.5 Summary and Conslusions.....	90
11 Summary and Conclusions	95
11.1 Recommendations.....	98
12 Suggestions for Future Research	101
13 References.....	103

Intentionally left blank

TABLE OF TABLES

Table 8-1. Material Properties of Prestressing Strands.....	17
Table 9-1. Averaged Transverse Moment, N-m/m (in-lb/in)	47
Table 9-2. Geometric Parameters of Diaphragms and Transverse Posttension Locations along Beam Height	48
Table 9-3. Posttension Force Requirement for the Sample Bridge	49
Table 10-1. Distress Level Summary in FE Analysis.....	72
Table 10-2. Distress Observed During Field Inspection and Used in FE Models.....	72
Table 10-3. Service Moment Capacities for Box-beams at Various Distress Levels (ft-kips)	79
Table 10-4. Nominal Moment Capacities of Box-beams with Various Distress Levels (ft- kips)	81
Table 10-5. Moment Demands for Distress Levels One through Four at Mid-span	81
Table 10-6. Moment Demands for Distress Levels One through Four at Quarter Point	82
Table 10-7. Rating Factors for Distress Levels One through Four at Mid-span.....	84
Table 10-8. Rating Factors for Distress Levels One through Four at Quarter Points.....	84
Table 10-9. Moments due to Dead and Live Loads, Nominal Moment Capacities, and Rating Factors for Distress at Mid-span.....	87
Table 10-10. Nominal Moment Capacity and Load Demands Based on FE Results (Distress at Mid-span).....	91
Table 10-11. Nominal Moment Capacity and Load Demands Based on the AASHTO LRFD (2004) (Distress at Mid-span).....	91
Table 10-12. Rating Factors for Distress Levels One through Four at Mid-span Obtained from FE Results	92
Table 10-13. Rating Factors for Distress Levels One through Four at Mid-span Obtained Analytically Using AASHTO LRFR Specifications for Lower Bound Dead Load Demand.....	92
Table 10-14. Rating Factors for Distress Levels One through Four at Mid-span Obtained Analytically Using AASHTO LRFR Specifications for Upper Bound Dead Load Demand.....	93

Intentionally left blank

TABLE OF FIGURES

Figure 7-1. Front view of the sub-assembly with three box-beams	2
Figure 7-2. Isometric view of the box-beam sub-assembly	2
Figure 7-3. Clamping stress along the length of shear key for different grout materials (Note: stresses are taken at mid-depth of the beam)	3
Figure 7-4. Stresses YY along shear key length for different number of diaphragms (Note: stresses are taken at mid-depth of the beam)	4
Figure 7-5. Deflection profile of the mid-span transverse section bottom fiber under concentrated load. (Note: solid – with posttension and dash – without posttension)	5
Figure 7-6. Deformed shape at mid-span transverse section under concentrated load: (a) with and (b) without posttension	6
Figure 7-7. Mid-span transverse section vertical deflection at the bottom fiber of the sub-assembly made with grout material of 1000 ksi modulus under concentrated load and posttension	6
Figure 7-8. Mid-span transverse section vertical deflection at the bottom fiber under dead load with and without posttension	7
Figure 7-9. Deformed shape of mid-span transverse section under dead load: (a) with posttension and (b) without posttension	7
Figure 7-10. Deflection plot of the bottom fiber under concentrated load at mid-span transverse section for three diaphragm configuration	8
Figure 7-11. Clamping stress distribution at the mid-span transverse section under concentrated load: (a) without and (b) with posttension	9
Figure 7-12. Clamping stress distribution along the bottom fiber under concentrated load at mid-span transverse section with and without posttension.....	9
Figure 7-13. Clamping stress distribution along the bottom extreme fiber at mid-span transverse section under concentrated load with posttension	10
Figure 7-14. Clamping stress distribution along the mid-span transverse section bottom extreme fiber under concentrated load with posttension for different diaphragm configurations	11

Figure 7-15. Isometric view of sub-assembly model with four beams	11
Figure 7-16. Clamping stress variation along the length of shear keys	12
Figure 8-1. Transverse section of box-beam assemblage model	16
Figure 8-2. Isoparametric view of the box-beam assemblage model	16
Figure 8-3. 27 × 36 box beam geometry	17
Figure 8-4. Axle and lane load positions for two-lane-loaded configuration	18
Figure 8-5. Positive and negative temperature gradient loads	18
Figure 8-6. Stress development under prestressing and self-weight of beams (note: only beam and strand components are active)	19
Figure 8-7. Deformed shape under prestressing and beam self-weight	20
Figure 8-8. Clamping stress distribution in grout layers after posttension application (note: deck is still free from stresses)	20
Figure 8-9. (a) Clamping stress in grout under posttension and deck dead load and (b) clamping stress distribution along the length of the shear key (stresses are extracted using shear key mid-height nodes)	21
Figure 8-10. Cast-in-place concrete deck stresses under barrier loading (a) top and (b) bottom surfaces	22
Figure 8-11. Transverse stress distribution (a) at the top surface of the deck and (b) along the width of the deck top surface over mid-span (Section B-B) and end-diaphragm (Section A-A) under Service I load combination 1	24
Figure 8-12. Transverse stress distribution (a) at the bottom surface of the 6-in thick deck and (b) along the width of the deck bottom surface over mid-span (Section B-B) and end-diaphragm (Section A-A) under Service I load combination 1	25
Figure 8-13. Transverse stress distribution (a) at the top surface of the deck and (b) along the width of the deck top surface over mid-span (Section B-B) and end-diaphragm (Section A-A) under Service I load combination 2	26
Figure 8-14. Transverse stress distribution (a) at the bottom surface of the deck and (b) along the width of the deck bottom surface over mid-span (Section B-B) and end- diaphragm (Section A-A) under Service I load combination 2	27
Figure 8-15. (a) Clamping stress distribution of grout layers under positive thermal gradient loading and (b) clamping stress distribution along the length of grout layers with	

and without the effect of positive gradient loading (stress plots are extracted using shear key top fiber nodes)	28
Figure 8-16. Transverse stress distribution (a) at the deck top surface and (b) along the width of the deck top surface over mid-span (Section B-B) and end-diaphragm centerline (Section A-A) under Service I load combination 3 with live load on a single lane	29
Figure 8-17. Transverse stress distribution (a) at the deck bottom surface and (b) along the width of the deck bottom surface over mid-span (Section B-B) and end-diaphragm centerline (Section A-A) under Service I load combination 3 with live load on a single lane	30
Figure 8-18. Transverse stress distribution (a) at the deck top surface and (b) along the width of the deck top surface over mid-span (Section B-B) and end-diaphragm (Section A-A) under Service I load combination 3 with live load on both lanes	31
Figure 8-19. Transverse stress distribution (a) at the deck bottom surface and (b) along the width of the deck bottom surface over mid-span (Section B-B) and end-diaphragm (Section A-A) under Service I load combination 3 with live load on both lanes	32
Figure 9-1. Location of the new bridge	36
Figure 9-2. (a) Shear-key between beams 11 and 12 and (b) discontinued top posttension strands	37
Figure 9-3. Shear-key interface cracking observed on May 14 th (a) before and (b) after posttension	37
Figure 9-4. Shear-key interface cracks observed on June 4 th	38
Figure 9-5. Deck cracking observed on June 22 nd	38
Figure 9-6. Concept of macromechanical model development procedure	40
Figure 9-7. Notations – forces and moments acting on a plate element	41
Figure 9-8. Side-by-side box-beam configuration	43
Figure 9-9. Cross-section of the RVE (a) without and (b) with deck.	43
Figure 9-10. Diaphragm and shear key locations.	45
Figure 9-11. New Jersey Type 4 barrier (Note: 1 in. = 25.4 mm)	46
Figure 9-12. Position of a single HS-20 truck	46

Figure 9-13. Transverse posttension locations along the beam height	49
Figure 9-14. Clamping stress (a) contours at shear key after the first stage posttension and (b) distribution along the length of the shear key with or without staged posttension (stresses are extracted using shear key mid-height nodes)	50
Figure 9-15. Clamping stress distribution along the shear key between fascia and the first interior beams under (a) posttension and (b) posttension and deck dead load	51
Figure 9-16. Clamping stress distribution along the length of the shear key with or without staged posttension (stresses are extracted using shear key mid-height nodes; compression-negative, tension-positive)	52
Figure 9-17. Transverse stress distribution (a) at the deck top surface and (b) along the width of the deck top surface over mid-span (Section B-B) and end-diaphragm (Section A-A) after second stage posttension	53
Figure 9-18. Transverse stress distribution (a) at the deck bottom surface and (b) along the width of the deck bottom surface over mid-span (Section B-B) and end- diaphragm (Section A-A) after second stage posttension.....	54
Figure 9-19. Transverse stress distribution at the cast-in-place concrete deck top surface (a) before and (b) after the barriers are placed	55
Figure 9-20. Transverse stress distribution (a) at the top surface of the deck and (b) along the width of the deck top surface over mid-span (Section B-B) and end-diaphragm (Section A-A) under service I load combination 1	57
Figure 9-21. Transverse stress distribution (a) at the bottom surface of the 6-in thick deck and (b) along the width of the deck bottom surface over mid-span (Section B-B) and end-diaphragm (Section A-A) under service I load combination 1	58
Figure 9-22. Transverse stress distribution (a) at the top surface of the deck and (b) along the width of the deck top surface over mid-span (Section B-B) and end-diaphragm (Section A-A) under service I load combination 2	60
Figure 9-23. Transverse stress distribution (a) at the bottom surface of the cast-in-place deck and (b) along the width of the deck bottom surface over mid-span (Section B-B) and end-diaphragm (Section A-A) under service I load combination 2	61
Figure 9-24. Clamping stress (a) profile on grout layers under positive thermal gradient loading and (b) distribution along the length of grout layers with and without	

positive gradient loading (stress plots are extracted using shear key top fiber nodes; compression-negative, tension-positive).....	62
Figure 9-25. Transverse stress distribution (a) at the deck top surface and (b) along the width of the deck top surface over mid-span (Section B-B) and end-diaphragm centerline (Section A-A) under service I load combination 3 with a single lane live load	63
Figure 9-26. Transverse stress distribution (a) at the 6-in. deck bottom surface and (b) along the width of the deck bottom surface over mid-span (Section B-B) and end-diaphragm centerline (Section A-A) under service I load combination 3 with a single lane live load	64
Figure 9-27. Transverse stress distribution (a) at the deck top surface and (b) along the width of the deck top surface over mid-span (Section B-B) and end-diaphragm (Section A-A) under service I load combination 3 with live load on two lanes	65
Figure 9-28. Transverse stress distribution (a) at the 6-in. deck bottom surface and (b) along the width of the deck bottom surface over mid-span (Section B-B) and end-diaphragm (Section A-A) under service I load combination 3 with live load on two lanes	66
Figure 9-29. Transverse stress distribution along the width of the 6-in cast-in-place concrete deck bottom surface with and without staged posttension under service I load combination 2	68
Figure 9-30. Transverse stress distribution along the width of the deck top surface with and without staged posttension under service I load combination 1	68
Figure 9-31. Transverse stress distribution along the width of the deck top surface with and without staged posttension under service I load combination 3 with a single lane live load	69
Figure 9-32. Clamping stress distribution along the length of the shear key top surface with and without staged posttension under positive gradient loading	69
Figure 10-1. Finite element model of distress levels 2 and 3: (a) enlarged view of half of the distressed zone along length and (b) section view of the distressed zone (note: broken strands are not visible).....	73

Figure 10-2. Finite element model of distress level 4: (a) enlarged view of half of the distressed zone along length and (b) section view of the distressed zone (note: broken strands are not visible).....	73
Figure 10-3. LRFR decision making flow chart (AASHTO LRFR 2003)	74
Figure 10-4. Axle load configuration of HL-93 generating maximum moment at mid-span (Note: Lane load that generates additional 200 ft-kips moment at mid-span is not shown).....	75
Figure 10-5. Axle load configuration of HL-93 generating maximum moment at quarter point (Note: Lane load that generates additional 150 ft-kips moment at quarter point is not shown).....	75
Figure 10-6. Axle load configuration of HL-93 generating maximum shear 1 ft away from the support (Note: Lane load that generates additional 15.36 kips shear 1 ft away from the support is not shown)	76
Figure 10-7. Axle load configuration of Truck 21 generating maximum moment at mid-span and quarter point	76
Figure 10-8. Axle load configuration of Truck 21 generating maximum shear 1 ft away from the support	77
Figure 10-9. 3D view of the model showing distress on fascia beam and design lanes	78
Figure 10-10. a) A portion of shear key grout remain intact with the beam and (b) beam surface after shear key grout cleanly fall off	86
Figure 10-11. Shear key grout loss	86
Figure 10-12. Shear key grout loss definition.....	86
Figure 10-13. Distress at shear key between a fascia and the first interior beam at mid-span	87
Figure 10-14. Normal stress distribution through the depth of deck-beam composite cross-section under dead load + prestress (tensile +; compression -)	89
Figure 10-15. Normal stress distribution through the depth of deck-beam composite cross-section under service loads that develop 424 psi extreme fiber tensile stress (Tensile +, Compressive -)	89
Figure 10-16. Normal stress distribution through the depth of deck-beam composite cross-section only under 100 percent live load (Tensile +, Compressive -)	90

Intentionally left blank

7 ANALYTICAL MODELING OF BOX-BEAM SUB-ASSEMBLAGES

7.1 OBJECTIVE AND APPROACH

The objective of finite element modeling and dead and live loads analysis is to evaluate the impact of transverse connection design and material parameters on the performance behavior of side-by-side precast prestressed concrete box-beam bridges. The transverse connection design and material parameters used for this purpose are: shear key grout mechanical properties, posttension force magnitude and location, number of diaphragms, and the bridge width.

Box-beam sub-assembly models are developed with three and four beams to study the effect of changing bridge width on posttension distribution (Figure 7-1). The shear key grout material modulus and number of diaphragms are varied to identify their influence on the load response of the bridge. The results presented from the FE analyses include the transverse normal stress (clamping stress) distribution at the shear key location along the beam (i. e., stress YY – refer to Figure 7-2 for the definition of the coordinate system used in the analysis) and the vertical displacement profile of the mid-span cross-section (i.e., at $x=25$ ft). Clamping stress distributions are compared between three and four-beam widths to demonstrate bridge width influence.

7.2 SUB-ASSEMBLAGE MODELS OF BOX-BEAMS

The bridge FE models are based on a 27×36-in. box-beam section. This box section is the most common beam specified in Michigan bridges (Aktan et al. 2005). The FE models are developed in compliance with Section 6.65.13 of the MDOT Bridge Design Guide (2005) provisions. The models consist of three 50 ft long 27×36-in. box beams connected with full-depth shear keys. According to the MDOT Bridge Design Guide (2005), a 50 ft span is the limiting span for four transverse posttension locations. Spans that are greater than 50 ft require five posttension locations. In this analysis, for this 50 ft. limiting span, five posttension locations (1 @ each beam end, 1 @ each quarter point, and 1 @ center of beam) are used in order to evaluate the clamping stress distribution along the shear keys. The posttension force calculated for the HS-25 design load is applied to all five posttensioning locations at the mid-depth of beam (i.e., 104.5 kips). End posttension locations are 1.5 ft away from each beam end. Intermediate diaphragm

thickness is 14 inches. Posttension anchor plates (7.5×7.5×1.5-in.) are also modeled at every posttension location (Figure 7-1 and Figure 7-2).

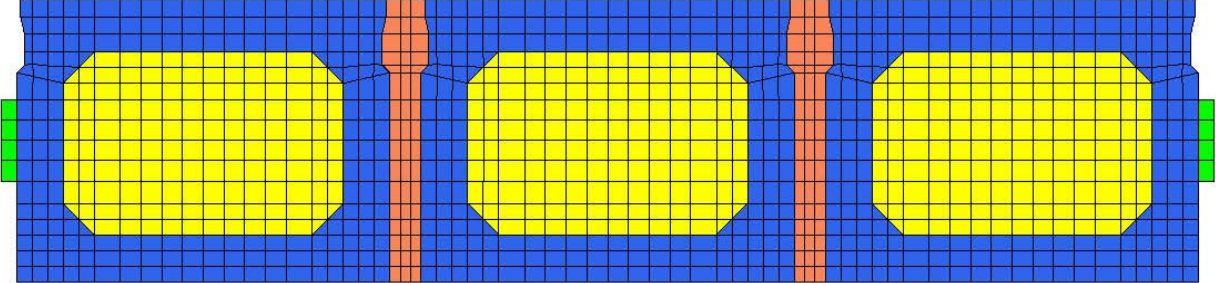


Figure 7-1. Front view of the sub-assembly with three box-beams

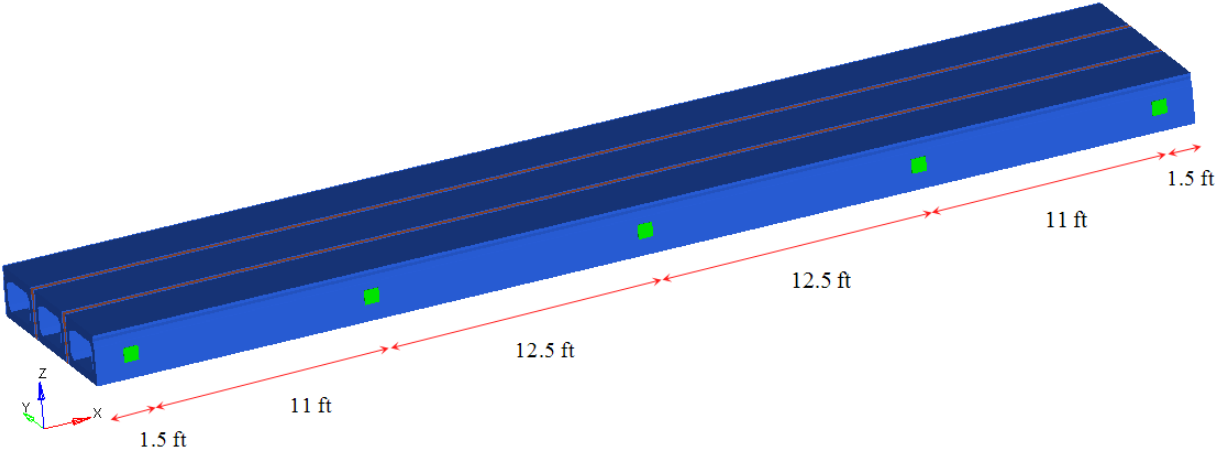


Figure 7-2. Isometric view of the box-beam sub-assembly

In the benchmark model, modulus of elasticity (E) of 5000 ksi and Poisson’s ratio of 0.2 are specified as the mechanical properties of concrete for the beam and shear key grout. The grout modulus of elasticity is high compared to that of R-2 grout used in Michigan bridges (Chapter 6). Grout properties are one of the parameters in analyzing the effects of the variation of shear key material properties on posttension stress (clamping stress) distribution and will be varied parametrically in other analyses. In the analysis, posttension is modeled unbonded and incorporated as a concentrated force of 104.5 kips applied to the anchor plates at each diaphragm location. The steel modulus of 29,000 ksi and Poisson’s ratio of 0.3 defined the material properties of the anchor plates. Live load is applied as a nodal vertical concentrated load of 25 kips at the middle beam’s mid-span. For dead load, both concrete and grout density is assumed to be 150 lb/ft³.

In the figures, tensile stresses are shown with positive (+) values, whereas negative (-) denotes compressive stresses. Downward deflections are presented with negative (-) values.

7.2.1 The Effect of Shear Key Material Properties and Number of Diaphragms

7.2.1.1 Posttension stress distribution along the shear-key

The influence of grout material properties on clamping stress distribution is investigated using five different elasticity modulus values ranging from 5000 ksi to 1000 ksi. The clamping stress variation along the length of the shear key at the beam mid-depth is presented in Figure 7-3. Stresses are calculated along a node line at beam mid-depth.

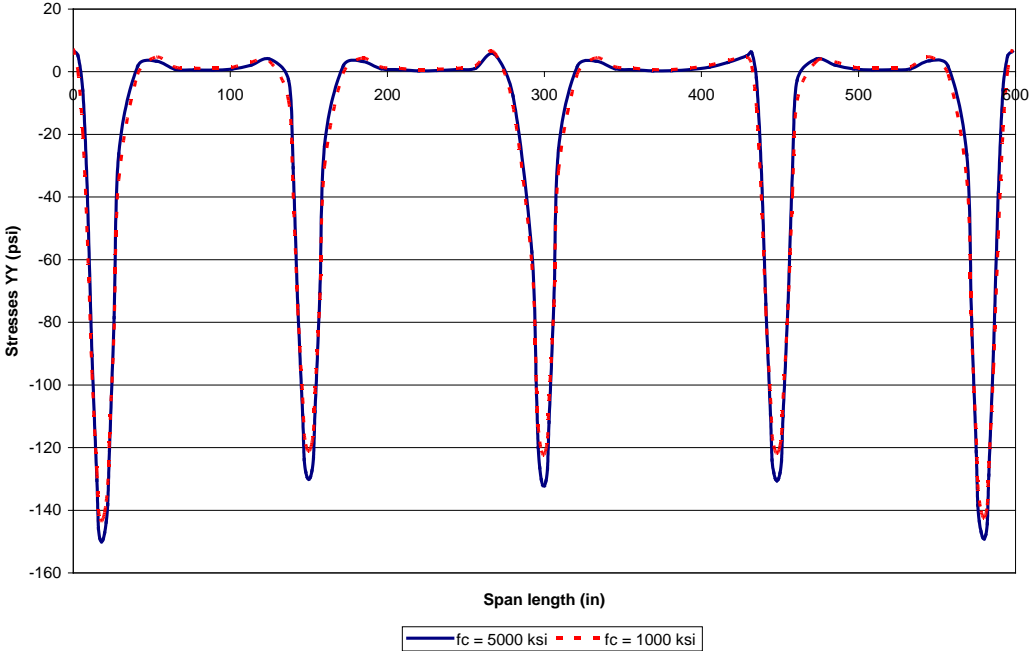


Figure 7-3. Clamping stress along the length of shear key for different grout materials (Note: stresses are taken at mid-depth of the beam)

As seen in the Figure 7-3, the clamping stress generated by the posttension forces is concentrated only within the diaphragm locations, and it is virtually zero or in tension between the diaphragm locations. Conversely, the AASHTO LRFD (2004) Section 5.14.1.2.8 requirement is that nominal transverse posttension stress (clamping stress) along the shear key, after all losses, shall not be less than 0.25 ksi. From Figure 7-3, it is clear that 0.25 ksi stress along the shear key could not be attained even within the diaphragm zone. The change in the elasticity modulus of grout material from 5000 ksi to 1000 ksi did not change the clamping stress variations along the

beam length. At diaphragm locations, the change in clamping stress levels are insignificant, with a 5000 ksi grout modulus generating 7 psi higher stress than that of a 1000 ksi grout modulus.

The impact of the number of diaphragms on the clamping stress distribution is investigated under live and dead loads. For this purpose three and five diaphragm configurations are compared while keeping the grout elasticity modulus constant at 5000 ksi. Clamping stress calculated along the length of the shear key at the beam mid-depth is presented in Figure 7-4.

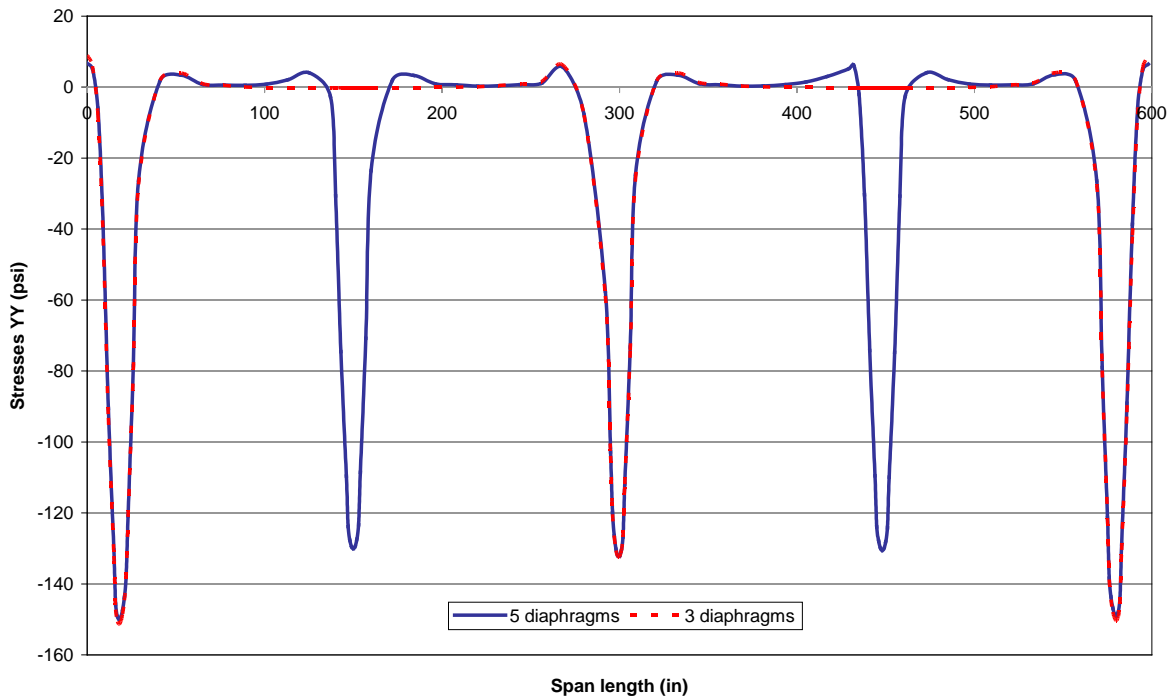


Figure 7-4. Stresses YY along shear key length for different number of diaphragms (Note: stresses are taken at mid-depth of the beam)

As seen in the Figure 7-4, the clamping stress distributions at the diaphragm locations remained identical.

7.2.1.2 Mid-span deflection

Mid-span vertical displacement profiles are calculated from a series of analyses performed to investigate relative displacement of beams with five and three diaphragms. The loading consisted of dead load and a 25 kips concentrated load applied at the center node of the mid-span cross-section. Although the concentrated load does not represent the design live load, it is placed to investigate the influence of the parameters on differential deflection. Both the concrete and grout elasticity modulus are taken as 5000 ksi unless otherwise noted.

Figure 7-5 shows the vertical displacements of a mid-span cross-section when beam sub-assembly with five diaphragms is directly subjected to a concentrated live load with and without transverse posttension. The displacements are extracted along the bottom nodes of the cross-section at mid-span. The shear key positions along the width of the cross-section are shown on Figure 7-5 as dotted lines. It is apparent from the figure that, with shear keys intact, posttension force does not help reduce the vertical displacements.

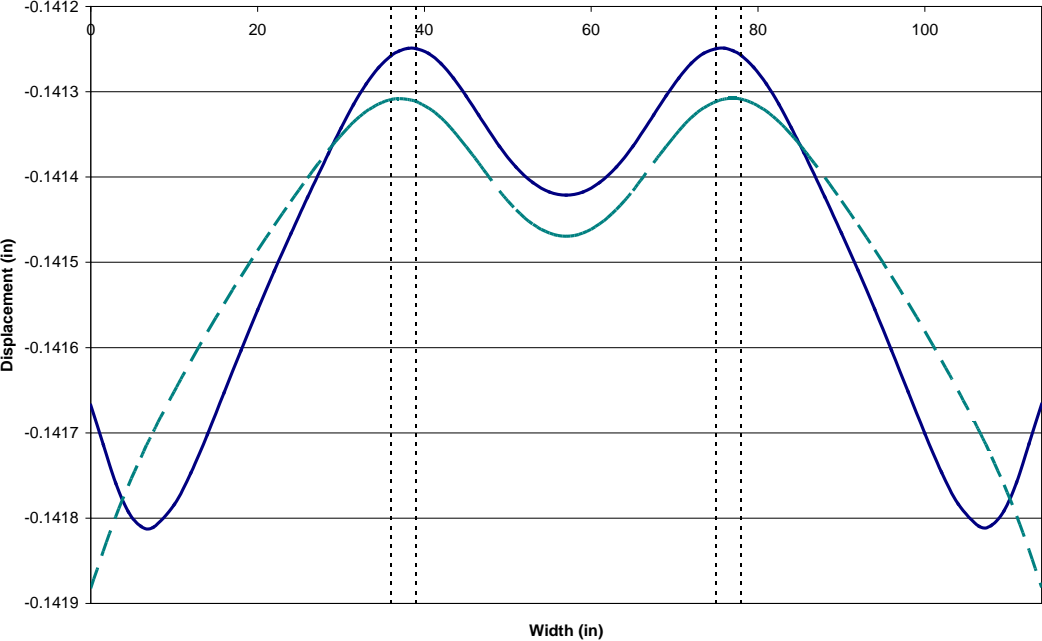


Figure 7-5. Deflection profile of the mid-span transverse section bottom fiber under concentrated load.
 (Note: solid – with posttension and dash – without posttension)

The deformed shapes of the mid-span cross-section with and without posttension are shown in Figure 7-6.

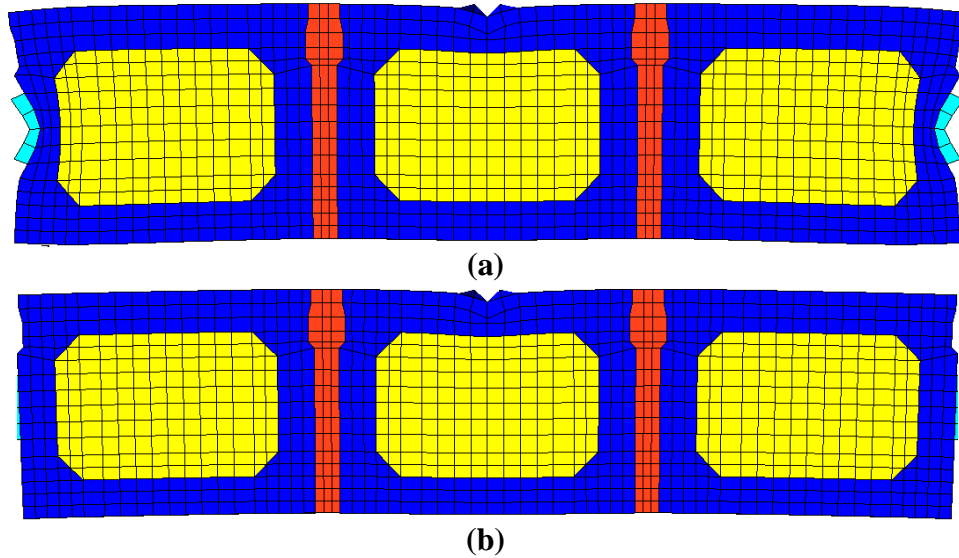


Figure 7-6. Deformed shape at mid-span transverse section under concentrated load: (a) with and (b) without posttension

The vertical displacement profile of the cross-section with five diaphragms and a grout modulus of 1000 ksi (lower bound) is shown in Figure 7-7. Although the deflected shape resembles the profile obtained in the case of 5000 ksi grout, a lower shear key modulus resulted in increased displacements. Sharp variations of vertical displacement within the shear key regions are also documented.

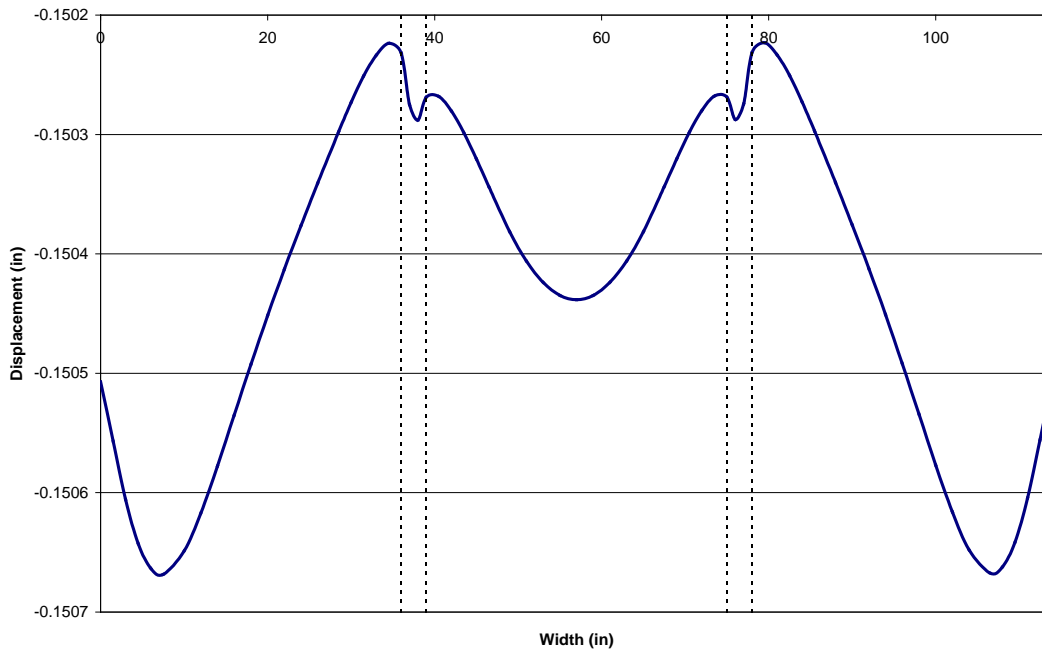


Figure 7-7. Mid-span transverse section vertical deflection at the bottom fiber of the sub-assembly made with grout material of 1000 ksi modulus under concentrated load and posttension

The box-beam sub-assembly with five diaphragms is analyzed under dead load with and without posttension. Figure 7-8 shows the vertical displacement profile of the mid-span cross-section. Figure 7-9 shows the deformed shape of the cross-section under dead load with and without posttension. As seen in Figure 7-9, when shear keys are intact, the application of transverse posttension did not influence the beam displacements.

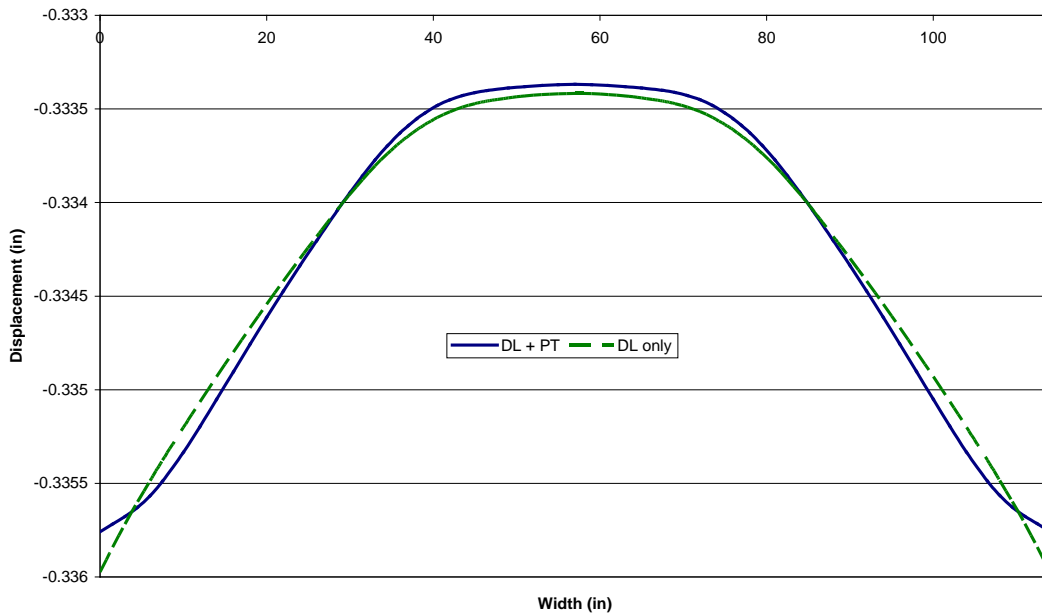


Figure 7-8. Mid-span transverse section vertical deflection at the bottom fiber under dead load with and without posttension

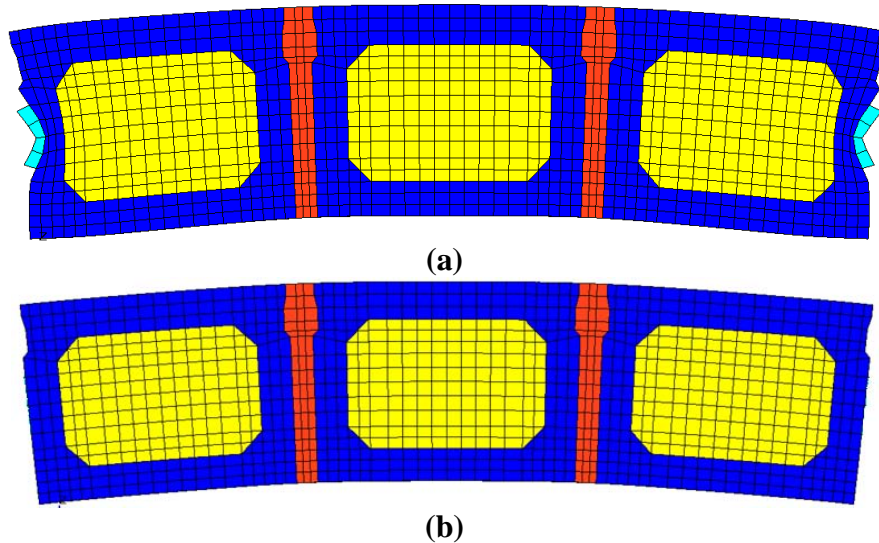


Figure 7-9. Deformed shape of mid-span transverse section under dead load: (a) with posttension and (b) without posttension

In order to evaluate the impact of the number of diaphragms on relative beam displacements, analysis results presented above with five-diaphragm configurations are compared to similar analyses on models with three diaphragms. Figure 7-10 shows the vertical displacement profile of the cross-section under concentrated load and posttension for the three diaphragm configuration. The deflected shape resembles the profile observed in the case of five diaphragms. Displacements are around 0.005-in. greater than those of the five-diaphragm configurations.

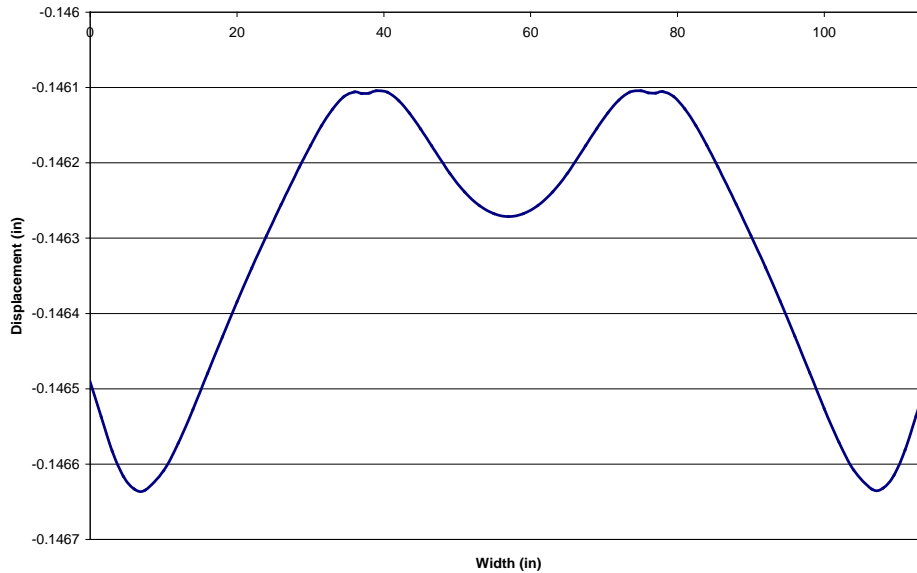


Figure 7-10. Deflection plot of the bottom fiber under concentrated load at mid-span transverse section for three diaphragm configuration

7.2.1.3 Clamping Stress Distribution in Transverse Direction

Figure 7-11 shows the clamping stress distribution within the bridge cross-section with or without posttension under a concentrated load. Figure 7-12 shows the stress profile of Figure 7-11 along the beam bottom fiber. In absence of transverse posttension, tensile stresses are developed at and near the bottom fibers of the cross-section. Application of transverse posttension eliminates most of the tensile stresses except near the boundaries.

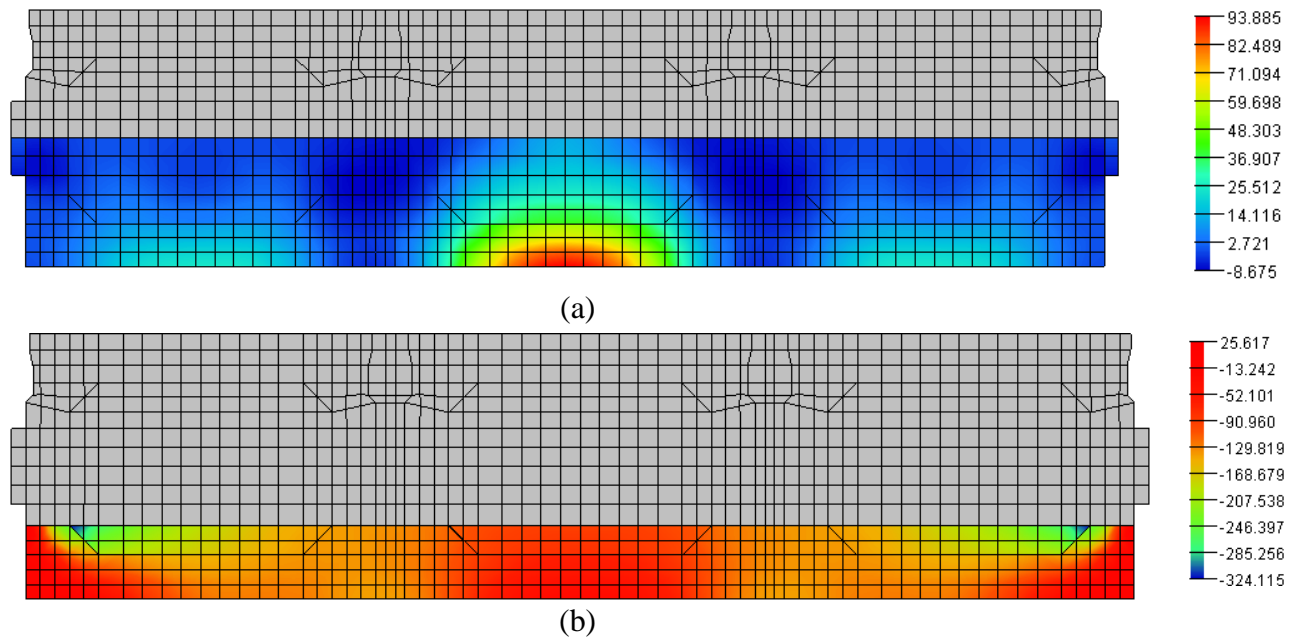


Figure 7-11. Clamping stress distribution at the mid-span transverse section under concentrated load: (a) without and (b) with posttension

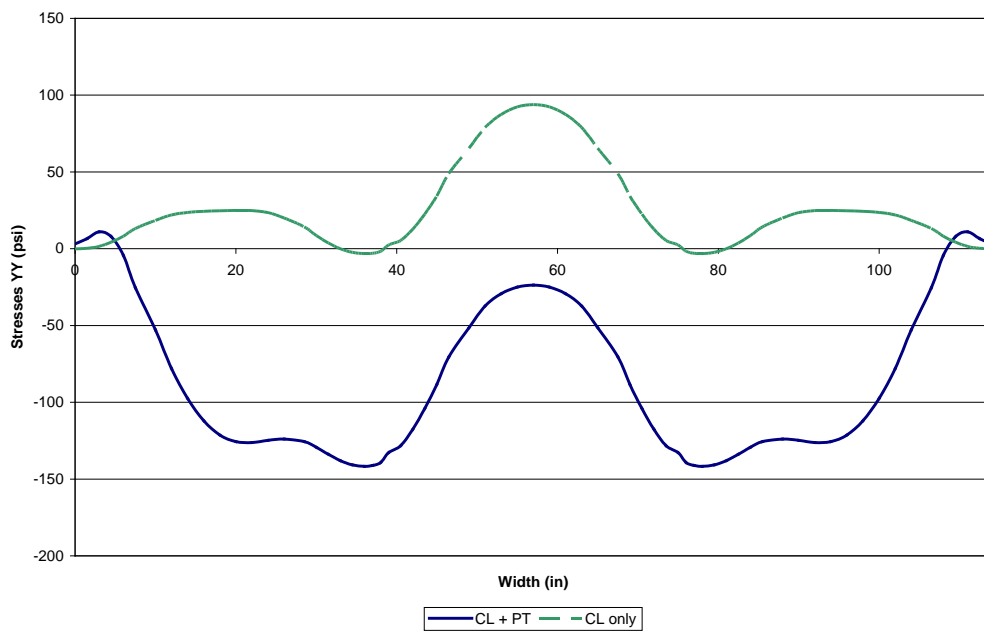


Figure 7-12. Clamping stress distribution along the bottom fiber under concentrated load at mid-span transverse section with and without posttension

Previously, the influence of the decrease in grout elasticity modulus on cross sectional deformations was investigated by comparing the analysis results with a grout modulus of 1000

ksi. The clamping stress profile is compared in Figure 7-13 for both grout modulus values along the beam bottom fiber of the bridge width. Displacements are increased and compressive stress maximum magnitudes near the bottom fiber are reduced with a lower grout modulus. The largest reduction in compressive stress is about 10 psi (i.e., about 7 percent). Results show that the difference between the stress profiles with a reduced grout elasticity modulus is negligible.

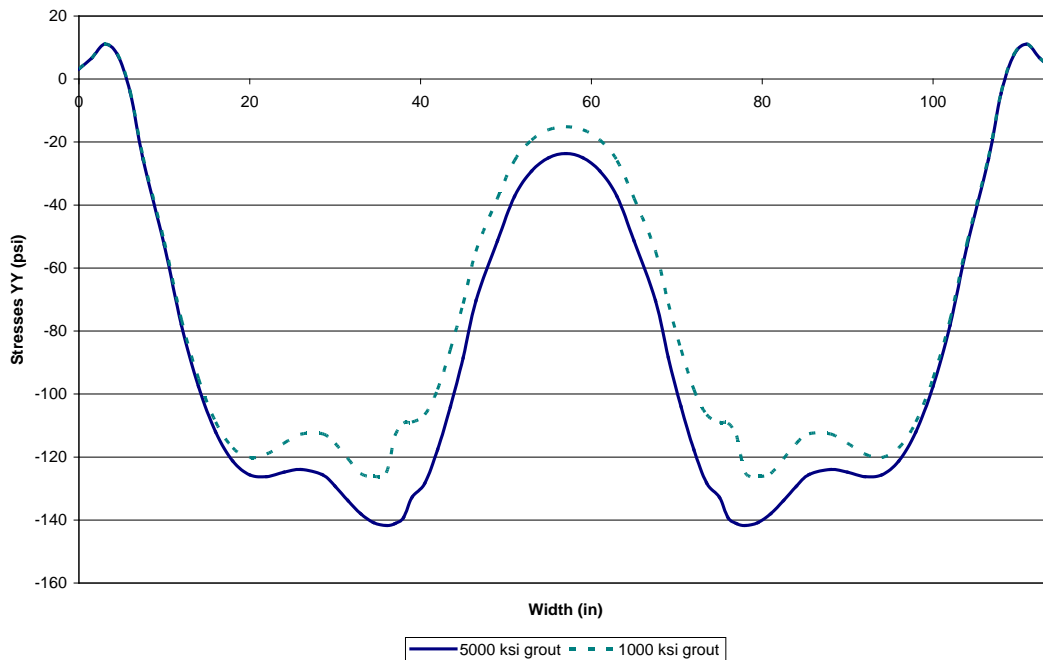


Figure 7-13. Clamping stress distribution along the bottom extreme fiber at mid-span transverse section under concentrated load with posttension

The clamping stress distribution of three and five diaphragm analysis models is compared. In both models there is a diaphragm at the mid-span. Figure 7-14 compares the clamping stress distribution at the mid-span transverse section under concentrated load and posttension along the bottom fibers with three and five diaphragm configurations. The stresses for three and five diaphragm configurations are almost identical.

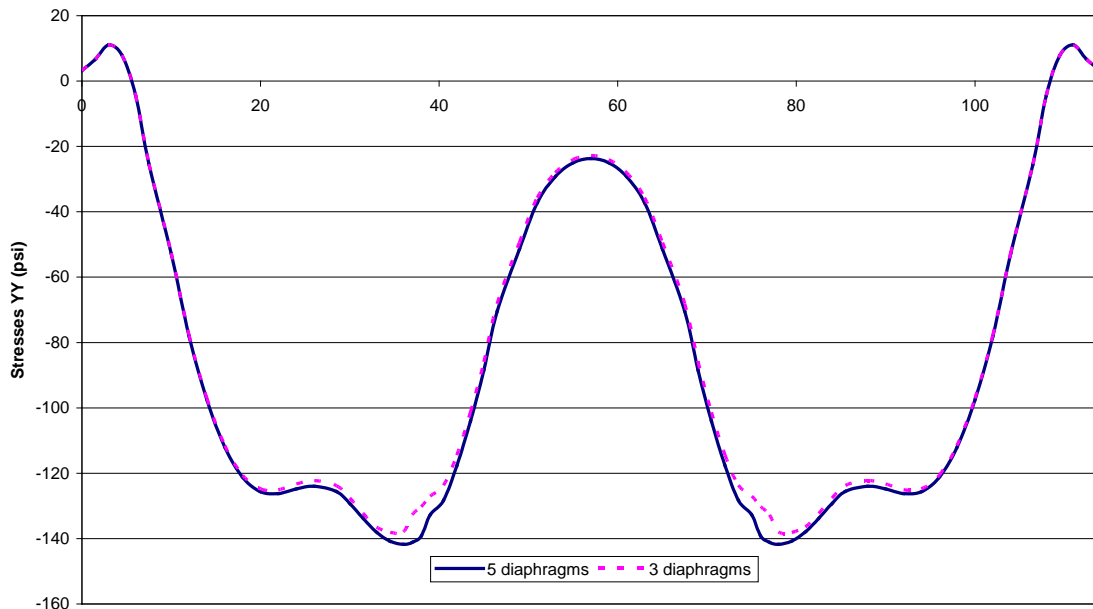


Figure 7-14. Clamping stress distribution along the mid-span transverse section bottom extreme fiber under concentrated load with posttension for different diaphragm configurations

7.2.2 Bridge Width Effect on Clamping Stress Distribution

El-Remaily et al. (1996) showed that the posttension force magnitude is a parameter of bridge width. In order to corroborate the effect of bridge width, a sub-assembly model with four beams is generated (Figure 7-15). Analysis results of four-beam and three-beam models are compared. The comparison of clamping stress along the bridge width shows that stress magnitudes are reduced with increasing bridge width (Figure 7-16). At diaphragm locations, the stress magnitudes at the shear key located at the mid-span transverse section (i.e., the shear key referred to as ‘mid’) are 20 to 40 psi lower than those of the shear key next to the fascia beam (i.e., the shear keys referred as ‘end’).

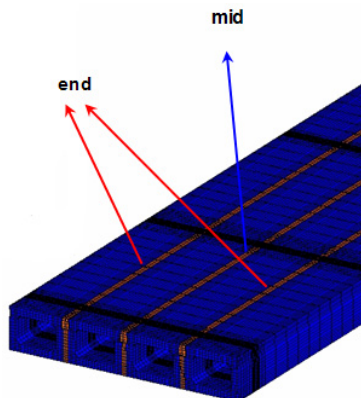


Figure 7-15. Isometric view of sub-assembly model with four beams

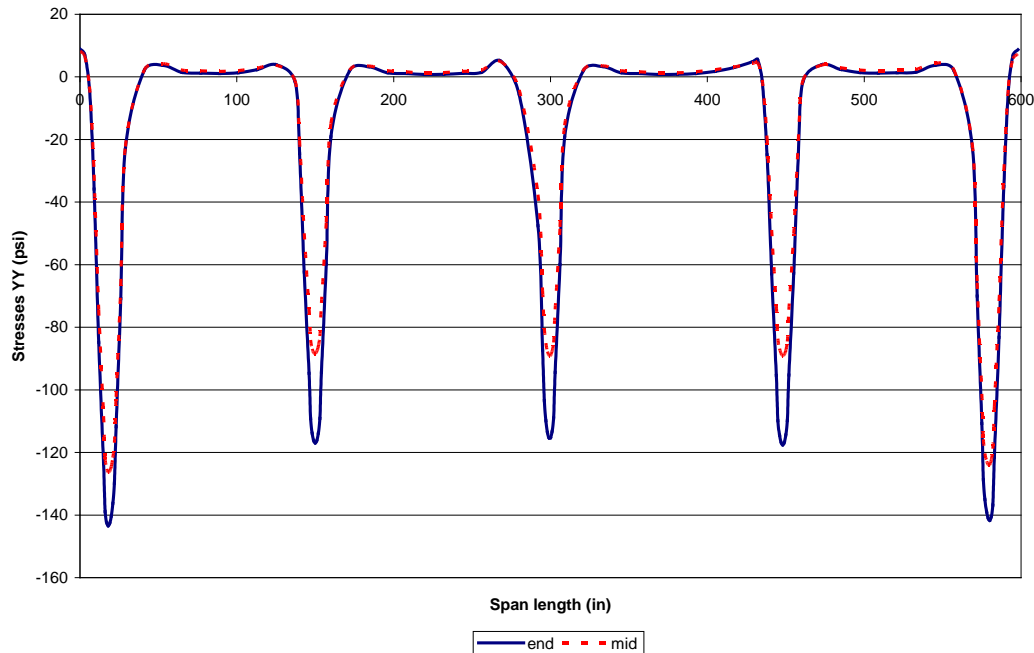


Figure 7-16. Clamping stress variation along the length of shear keys

7.3 SUMMARY AND CONCLUSIONS

FE analyses are carried out investigating the effects of transverse connection design and material parameters: grout modulus, posttension force magnitude, number of diaphragms, and the bridge width. Vertical displacement profiles at the mid-span transverse sections as well as the clamping stress distributions along the shear keys and at the mid-span transverse section are evaluated against the design parameters.

According to the results:

1. Clamping stress transfer is predominantly through the stiffer sections of the bridge superstructure (i.e., through the diaphragms). Shear keys in between the diaphragms are either under tension or zero stress, and are unable to develop a watertight seal without adequate compression.
2. The transverse posttension impact on mid-span deflections is minimal if the shear keys are intact. However, the transverse posttension is required to assure load transfer between girders and to increase the redundancy of the system.

3. AASHTO LRFD (2004) Section 5.14.1.2.8 recommendations regarding clamping stress distribution under transverse posttension are vague. To achieve a minimum stress or even a nominal stress of 250 psi at shear keys along the beam length would require a comprehensive redesign of transverse connection.
4. The transverse posttension force magnitude is a function of bridge geometry, number of diaphragms, shear key material modulus, and shear key width.

Intentionally left blank

8 ANALYTICAL MODELING: CONSTRUCTION SIMULATION AND SERVICE LOAD ANALYSIS

8.1 OVERVIEW

The objective of the refined analysis presented in this chapter is to simulate the construction procedure and sequences for verifying design assumptions and calculating stresses that develop within various components during construction. The analysis results will be used for fine-tuning the design assumptions. The analyses models developed are based on the MDOT Bridge Design Guide (2005) section 6.65.10A and 6.65.13 provisions.

The bridge used for this purpose consists of eight 50 ft long 27×36-in. box beams that are connected with full-depth shear keys, transverse posttension, and a six-inch thick cast-in-place concrete deck. The Bridge has two-lanes with a total width of 25.75 ft. There are five transverse posttension locations (1 @ each beam end, 1 @ each quarter point, and 1 @ center). Posttension force magnitude specified is for HS-25 design loading (i.e., 104.5 kips). Beam end posttension is located 10 in. away from each support centerline. The intermediate diaphragm thickness is 14 inches. The end diaphragm thickness is 26 inches, which satisfies the minimum 2 ft requirement. Posttension anchor plates (7.5×7.5×1.5-in.) are incorporated at each posttension location (Figure 8-1 and Figure 8-2).

Box-beams, diaphragms, shear keys, anchor plates, and deck are modeled with eight-node solid continuum elements (C3D8). These elements have three translational degrees of freedom (dof) at each node with a total of 24 dof. In the longitudinal direction, for the most refined elements, the maximum length is kept at 6 inches for an aspect ratio under six. Prestressing strands are modeled with two-node three dimensional truss elements (T3D2), again with three translational degrees of freedom at each node. Strands are embedded into the solid beam elements and constrained to have equal displacement profiles at coinciding nodes. Prestress is applied as an initial stress in the strand components. The same type of truss elements (T3D2) are used to model posttensioning strands. Also, for accurate representation of the construction sequence, strands are not embedded into the solid elements and are debonded from solid beam, diaphragm, and shear key components.

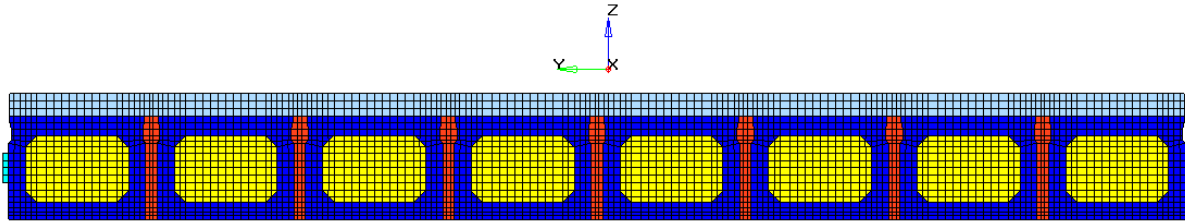


Figure 8-1. Transverse section of box-beam assemblage model

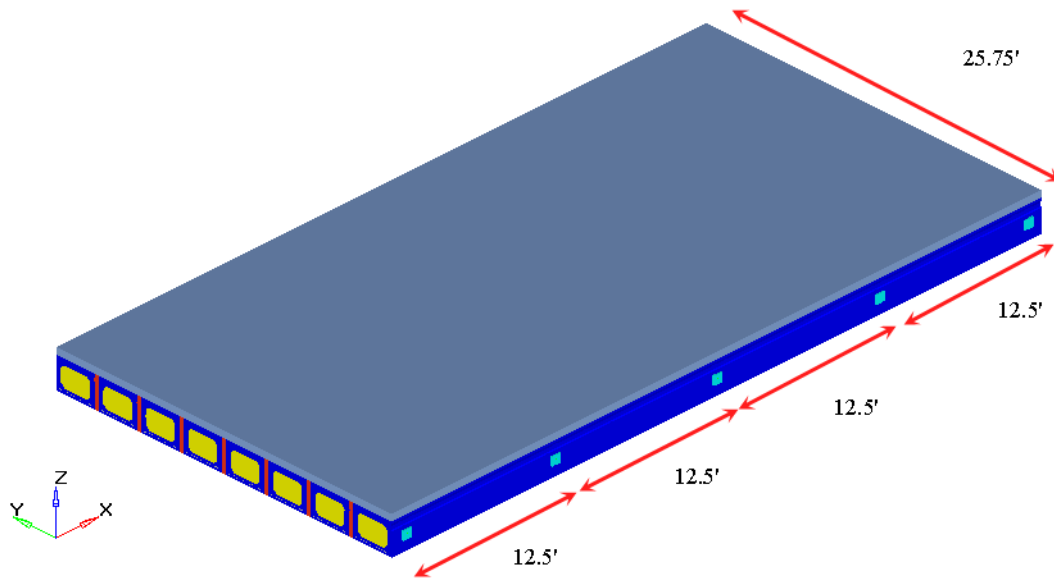


Figure 8-2. Isoparametric view of the box-beam assemblage model

The compressive strength (f'_c) of 5000 psi, modulus of elasticity of 4031 ksi, and Poisson's ratio of 0.2 are specified for both deck and girder concrete. Shear key grout material properties specified are: compressive strength (f'_c) of 4000 psi, modulus of elasticity (E_c) of 3600 ksi, and Poisson's ratio of 0.2. Prestressing strands with a nominal diameter of 1/2-inch and an area of 0.153 in² are embedded in the girders. A total of 10 strands are distributed along the bottom flange of each box girder. Strands are placed with a 2-in. cover as per the MDOT Bridge Design Guide (2005) section 6.65.10 provisions (Figure 8-3). The initial prestress value is 186.3 ksi, calculated after losses due to shrinkage and creep from the initial prestressing stress. The final prestressing after further losses due to relaxation of tendons and elastic shortening is calculated as 163.4 ksi (Table 8-1). UngROUTED posttension ducts are simulated for accurately simulating construction sequence; hence, posttension strands are tied to anchor plates at each diaphragm location. The steel modulus of 29,000 ksi and Poisson's ratio of 0.3 are the material properties of the anchor plates.

Table 8-1. Material Properties of Prestressing Strands

Ultimate stress	270.0 ksi
Yield strength (85% of ultimate)	229.5 ksi
Initial prestressing	186.3 ksi
Final prestressing	163.4 ksi
Modulus of elasticity	28,500 ksi
Poisson's ratio	0.3

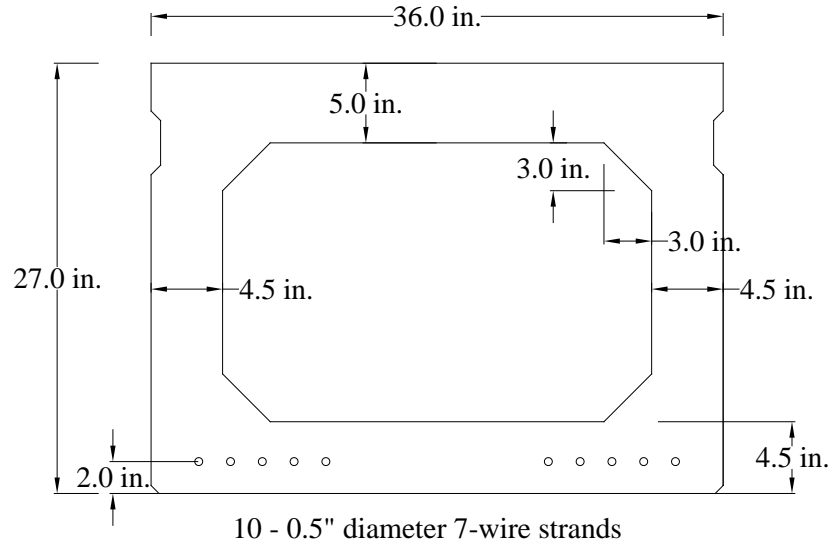


Figure 8-3. 27 × 36 box beam geometry

In the simulation analysis, HL-93 (AASHTO LRFD 2004) loading is placed to create maximum mid-span moment as given in Figure 8-4. The impact factor is taken as 1.75 from Section 3.6.2.1 of the AASHTO LRFD (2004) assuming shear keys act as joints. A lane load of 0.64 k/ft is used in addition to the axle loads, as per Section 3.6.1.3 of the AASHTO LRFD (2004). Multiple presence factors of 1.2 and 1.0 are used for one and two-lane loaded configurations, respectively (AASHTO LRFD Section 3.6.1.1 2004). The wheel load is distributed according to both tire contact area and FE mesh geometry limitations.

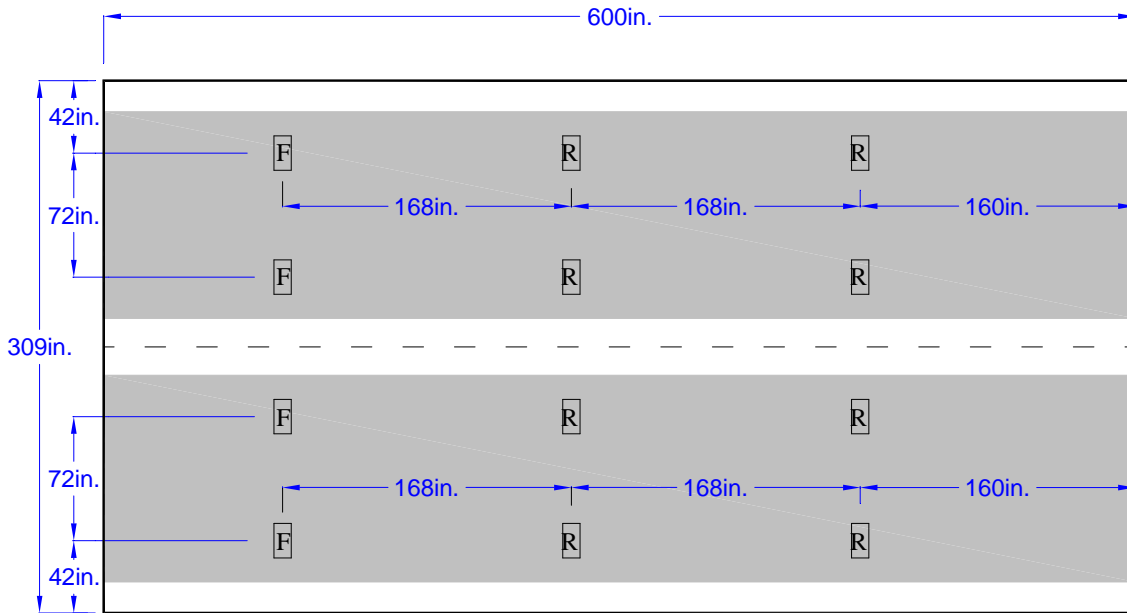


Figure 8-4. Axle and lane load positions for two-lane-loaded configuration

Thermal gradient loads applied in the analysis are for Zone-3 (AASHTO LRFD Section 3.12.3 2004). The negative temperature gradient is calculated in proportion to the positive temperature values by -0.30. Thermal gradient loads are shown in Figure 8-5 with height (h) being the bridge superstructure's full depth including the cast-in-place concrete deck. A uniform thermal expansion coefficient of 6.0×10^{-6} in./in./ $^{\circ}$ F is used for concrete and grout components.

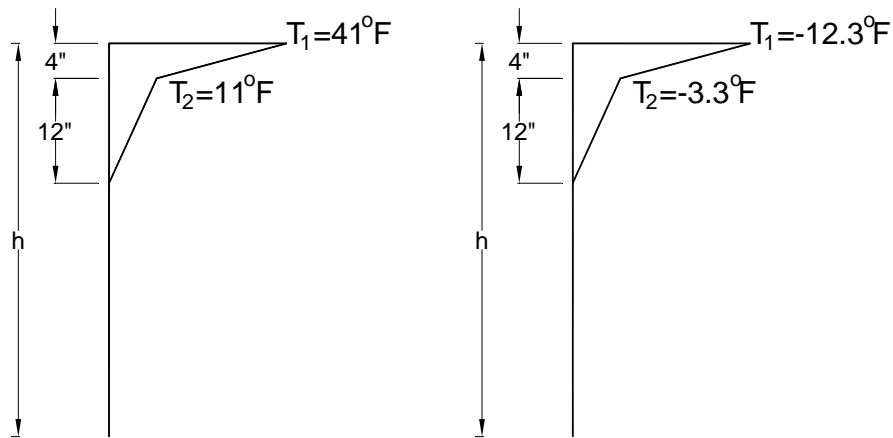


Figure 8-5. Positive and negative temperature gradient loads

The dead load effect is calculated from nominal dimensions and densities. The density of the concrete and grout components (i.e., girder, diaphragm, deck, and shear key) is 150 lb/ft^3 . New

Jersey type IV barrier loads of 475 lb/ft are distributed over 18 in. from the edges of the deck. Analyses do not include volume change loads such as heat of hydration thermal loads and drying shrinkage.

8.2 CONSTRUCTION PROCESS SIMULATION AND ANALYSIS RESULTS

In Michigan, the box-beam bridge superstructure system is constructed in five stages: first, placing precast and prestressed concrete box-beams adjacent to each other; second, grouting 3-in. thick full-depth shear-keys; third, applying transverse posttension; and fourth, casting a six-inch thick concrete deck with a single mat of reinforcement. Last, the barriers are placed and the bridge is opened to traffic. The finite element modeling and analysis sequence that follows the construction sequence is described below:

Step 1: Box-Beams Placement

Precast prestressed beams are erected; beams are subjected to self-weight and prestress only. No other components of the model except beams and prestressing strands are active in the model. Thus, prestressing only affects the beam and diaphragm components as shown in Figure 8-6.

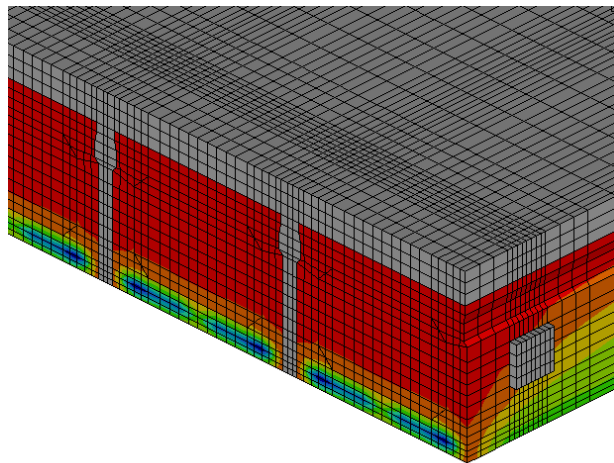


Figure 8-6. Stress development under prestressing and self-weight of beams (note: only beam and strand components are active)

FE analysis results show that beam camber under self-weight is 0.60 inches (Figure 8-7). This matches the analytical solution of 0.625 inches with 96% accuracy.



Figure 8-7. Deformed shape under prestressing and beam self-weight

Step 2: Shear key grout placement

Grout elements are activated. This step is vital. If all beams are modeled as connected to each other through shear keys, then the prestressing effect of each beam would be transferred to shear keys showing shear key stresses before load application. Shear keys should be stress free with proper modeling. Three-inch thick grout elements are activated, and their self-weight is distributed to beams. Beam camber deflection further reduces to 0.55 inches.

Step 3: Posttension application

The posttension application stage is simulated here, compressing/clamping the beam-shear key assemblage. Posttension and anchor plate components are activated. The deck is not placed; hence, deck elements are not activated. The maximum compressive clamping stress magnitude of the shear key elements, at the transverse posttension locations (i.e., at diaphragm locations), is calculated to be 150 psi. The highest shear key compressive clamping stress is observed between the fascia and the first interior beams. The maximum tensile stress of 6.6 psi is calculated at the interface. Clamping stress distribution in shear key grout is shown in Figure 8-8.

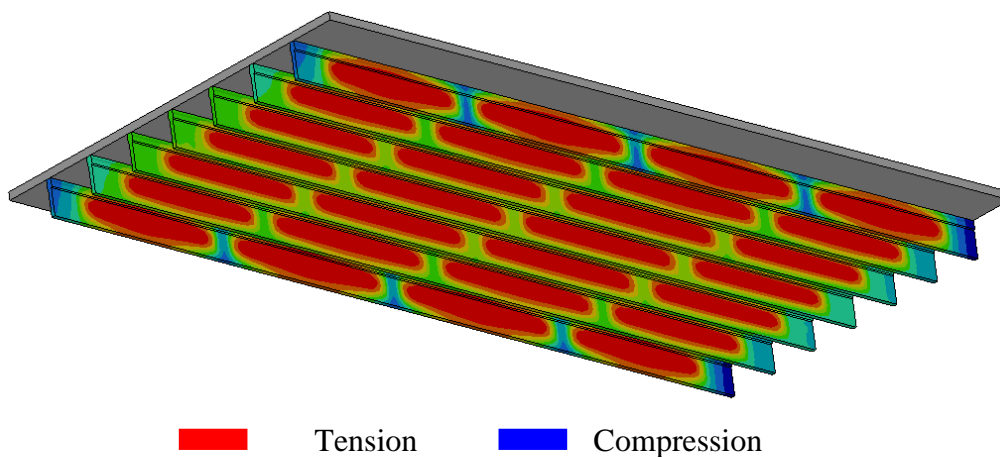


Figure 8-8. Clamping stress distribution in grout layers after posttension application (note: deck is still free from stresses)

Step 4: Deck is placed but not hardened

A dead load of six-inch thick cast-in-place concrete is applied on the assemblage; but deck elements are not active in the model. Upon loading, clamping stress magnitudes decreased in proportion to the distance to shear key from the fascia beam (Figure 8-9 a and b). Applying the deck dead load resulted in minor changes in the clamping stress magnitudes in grout layers. Compressive clamping stress magnitudes are increased to 157 psi from 150 psi; whereas tensile stress magnitudes are decreased to 6.4 psi from 6.6 psi.

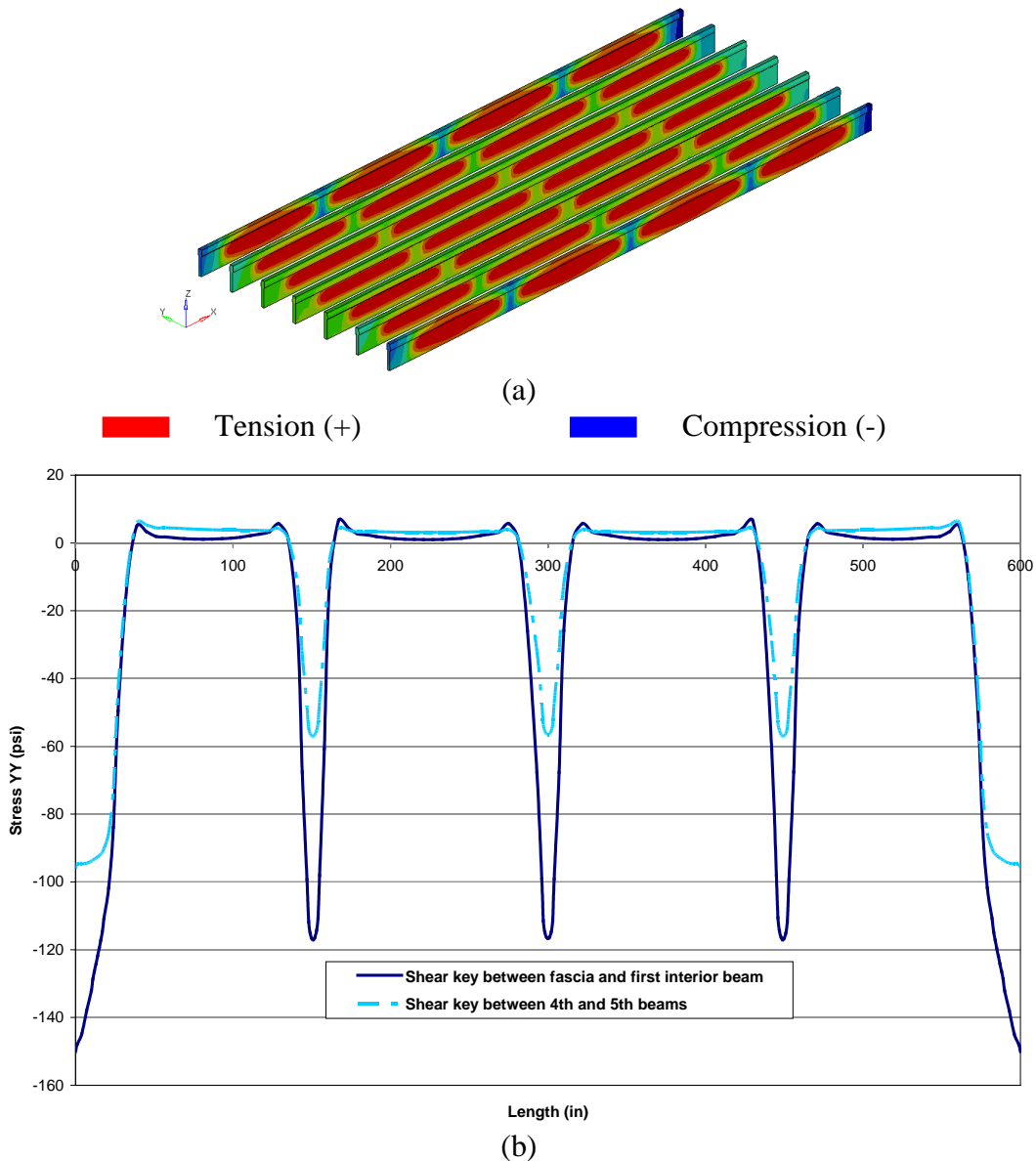


Figure 8-9. (a) Clamping stress in grout under posttension and deck dead load and (b) clamping stress distribution along the length of the shear key (stresses are extracted using shear key mid-height nodes)

Step 5: Deck is hardened and barriers are placed

Deck elements are activated in the model. Deck self-weight was applied in the previous sequence and will not generate deck stresses. Deck stresses are developed once the barrier load is applied. At the end of this step (step 5), all of the dead load components are now acting on the bridge.

Under full dead load, a large portion of the 6-in deck is under transverse tensile stresses, as observed in Figure 8-10. At the top fiber, the magnitude of transverse tensile stress is about 10 psi. The magnitude is reduced to about 5 psi at the bottom fiber. Barrier load effects on shear key grout stress magnitudes are minimal except on the grout layer between the fascia and first interior beam. In the grout layer, the maximum compressive clamping stress is increased to 164 psi from 157 psi; whereas the maximum tensile stress is increased to 6.5 psi from 6.4 psi.

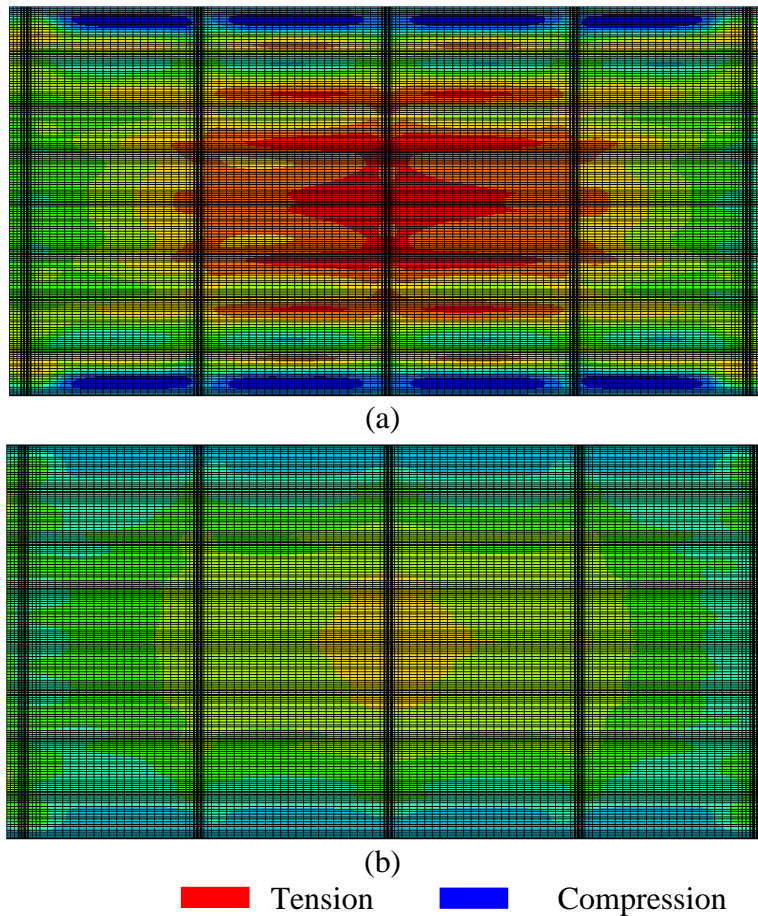


Figure 8-10. Cast-in-place concrete deck stresses under barrier loading (a) top and (b) bottom surfaces

8.3 SERVICE LOAD ANALYSIS

The service I limit state objective is to control cracking (AASHTO LRFD (2004)). As specified in Section 3.4.1 of the AASHTO (2004), γ_{TG} , load factor for temperature gradient may be taken as 1.0 and 0.5 when the live load is excluded or included in the service limit state. Subsequently, three critical load combinations are derived for the analysis. Service I load combination are:

Combo 1: 1.0 DEAD + 1.0 NTG

Combo 2: 1.0 DEAD + 1.0 PTG

Combo 3: 1.0 DEAD + 1.0 LL

where

NTG: Negative thermal gradient loading

PTG: Positive thermal gradient loading

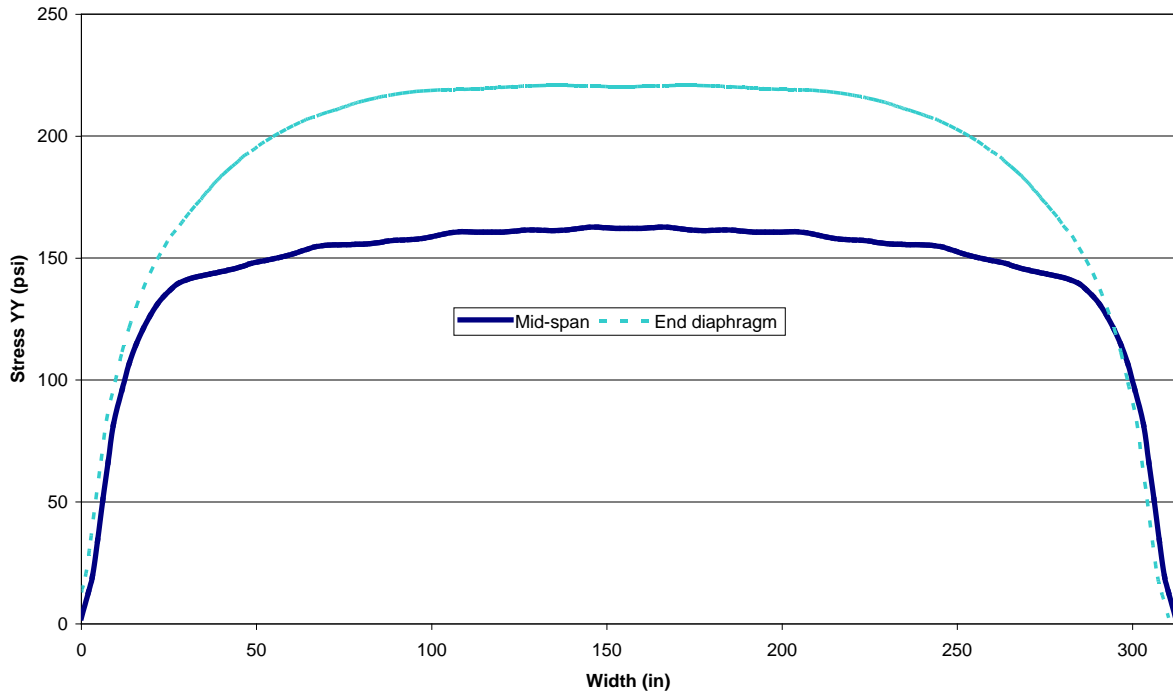
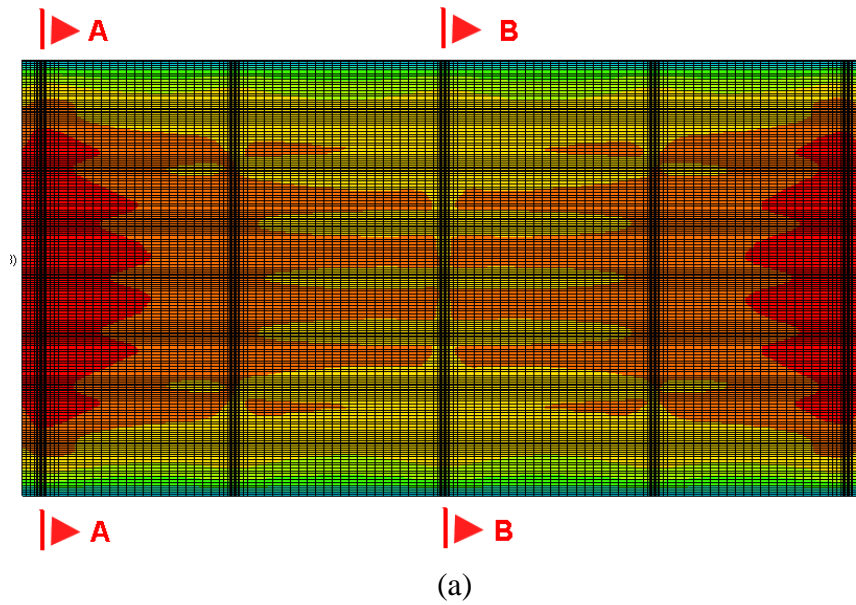
DEAD: Dead load of all components

LL: HL-93 live load with impact and multiple presence factors

Load combinations that include dead, live, and thermal gradient loading are not considered in the analysis. A discussion is presented at the end of the chapter, which explains the reasons for excluding such load combinations.

8.3.1 Load Combination 1: 1.0 DEAD + 1.0 NTG

Load combination consists of the application of negative thermal gradient loading while the stress state developed during construction stages is retained. Under negative thermal gradient loading, deck top fiber tensile stresses are significantly increased (Figure 8-11(a)). Figure 8-11 (b) depicts the stress distribution at the top surface of the deck directly over the end diaphragms (section A-A) and mid span diaphragms (section B-B). A tensile stress of 160 psi develops at mid-span close to the interior girders. Tensile stress further increases towards the supports reaching 230 psi over the end-diaphragms. At the bottom face of the 6-in cast-in-place slab, tensile stresses occur only at locations near the supports (Figure 8-12). Compressive clamping stresses developed in the shear keys are increased to 174 psi from 164 psi and are minimally affected by the negative thermal gradient loading. However, the tensile stress magnitude is increased to 11.6 psi from 6.5 psi along the beam interface, at a location between the fascia and the first interior.



■ Tension (+) ■ Compression (-)

Figure 8-11. Transverse stress distribution (a) at the top surface of the deck and (b) along the width of the deck top surface over mid-span (Section B-B) and end-diaphragm (Section A-A) under Service I load combination 1

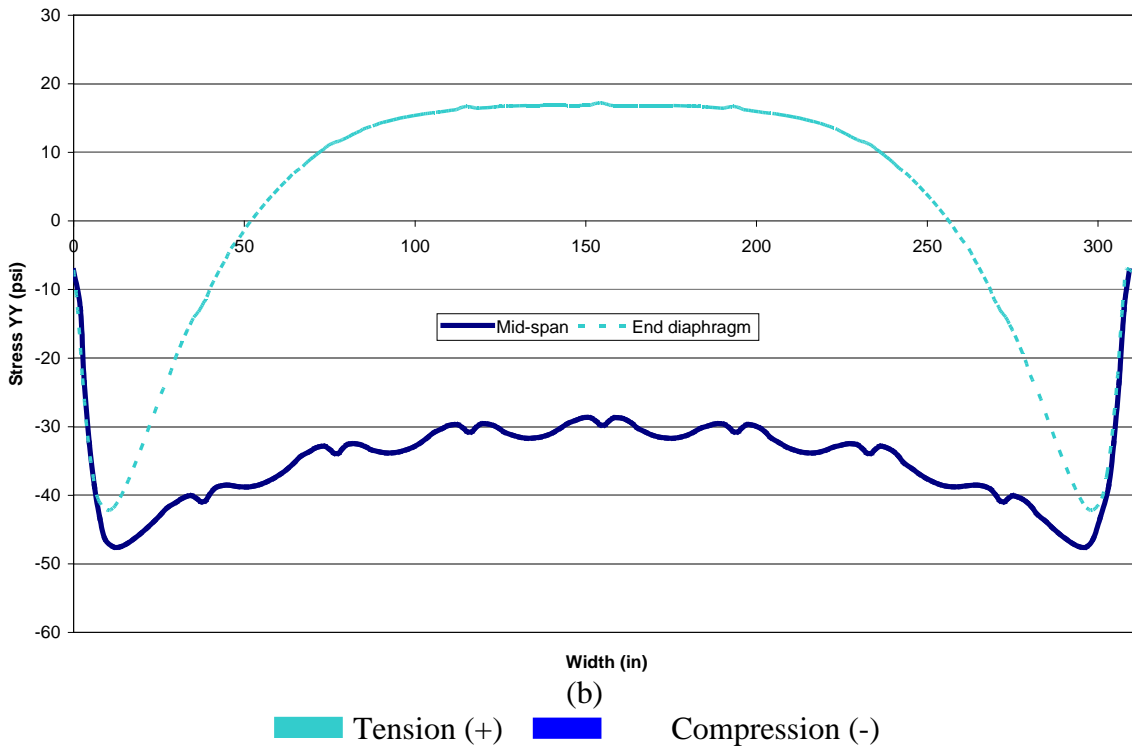
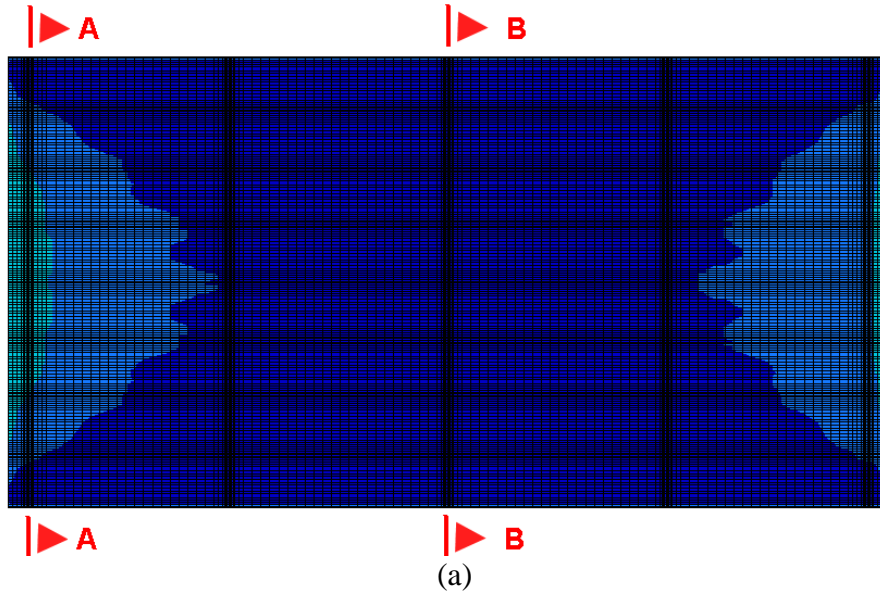


Figure 8-12. Transverse stress distribution (a) at the bottom surface of the 6-in thick deck and (b) along the width of the deck bottom surface over mid-span (Section B-B) and end-diaphragm (Section A-A) under Service I load combination 1

8.3.2 Load Combination 2: 1.0 DEAD + 1.0 PTG

In this combination, the system retains the stress state developed during construction, and positive thermal gradient loading is applied. Under this load, the deck's top fibers are now fully under compression (Figure 8-13) while tensile stresses forms on the bottom fibers of the 6-in.

thick deck (Figure 8-14). The maximum transverse tensile stress of 166 psi is documented at mid-span near the fascia beams (Figure 8-14). Tensile stresses are observed within the end diaphragms only at locations close to the fascia beams. Within the grout layers, between the fascia and the first interior beams, positive gradient loading increases both tensile and compressive stress magnitudes. Maximum tensile stress magnitudes increase to as much as 100 psi from -25 psi at the top of the shear key grout layers located between the fascia and the first interior beams (Figure 8-15).

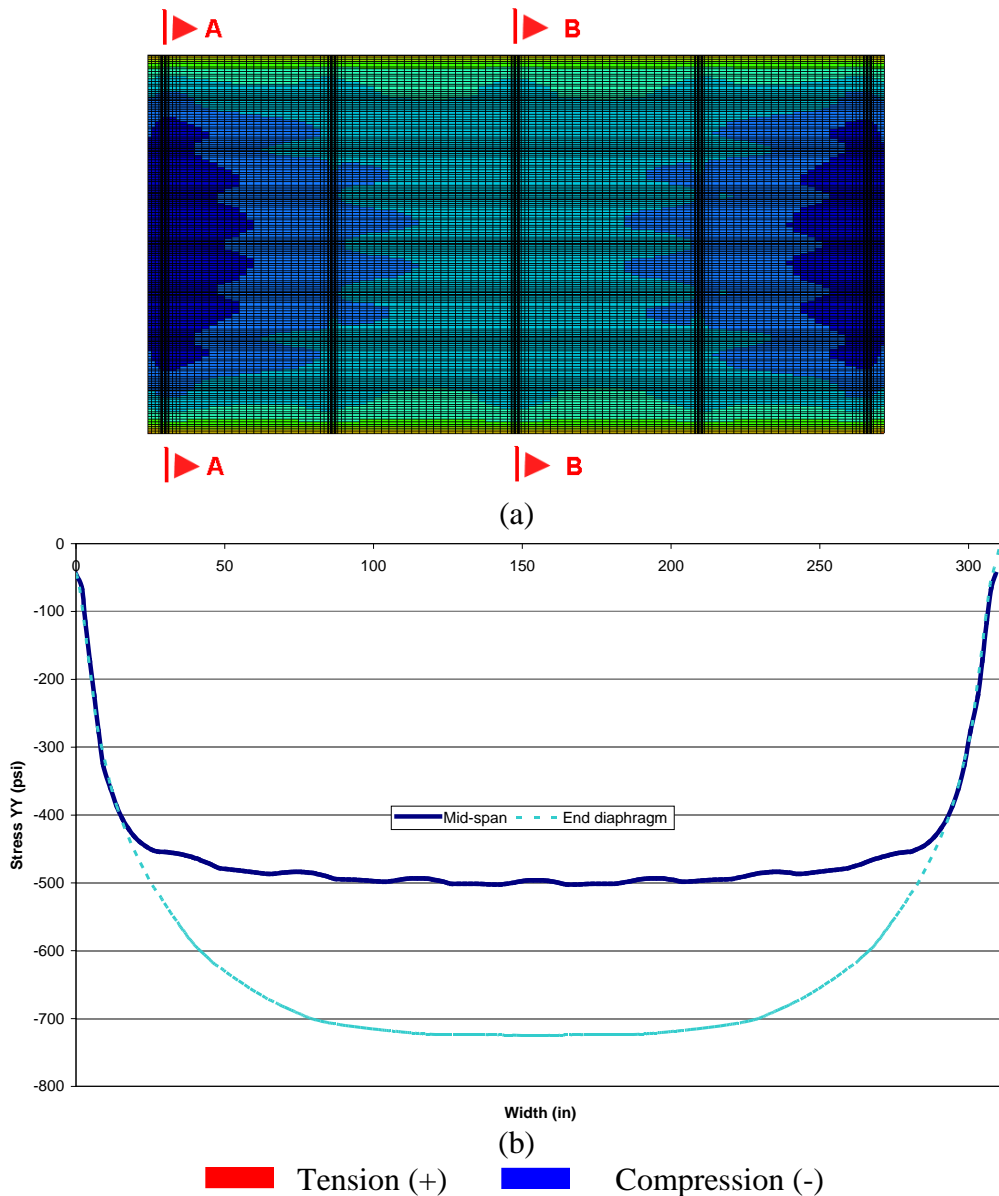
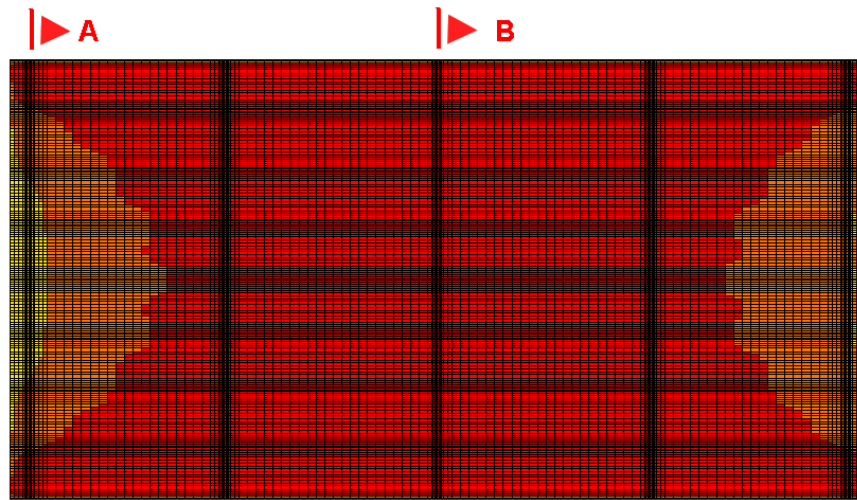
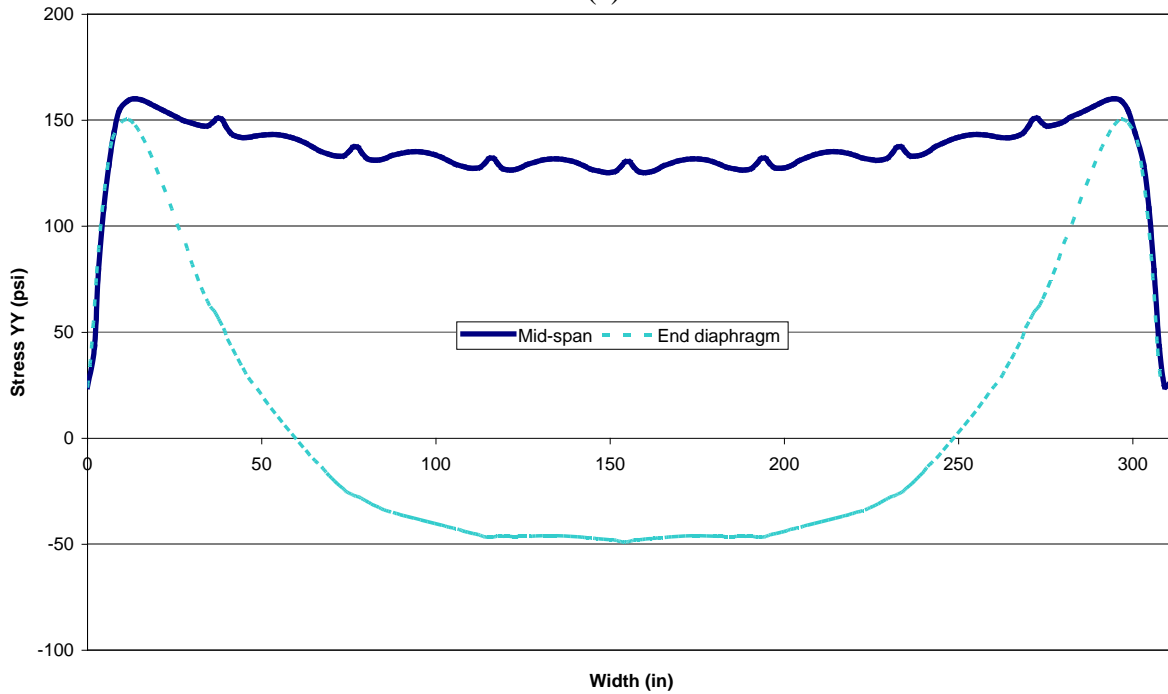


Figure 8-13. Transverse stress distribution (a) at the top surface of the deck and (b) along the width of the deck top surface over mid-span (Section B-B) and end-diaphragm (Section A-A) under Service I load combination 2



(a)



(b)

■ Tension (+) ■ Compression (-)

Figure 8-14. Transverse stress distribution (a) at the bottom surface of the deck and (b) along the width of the deck bottom surface over mid-span (Section B-B) and end-diaphragm (Section A-A) under Service I load combination 2

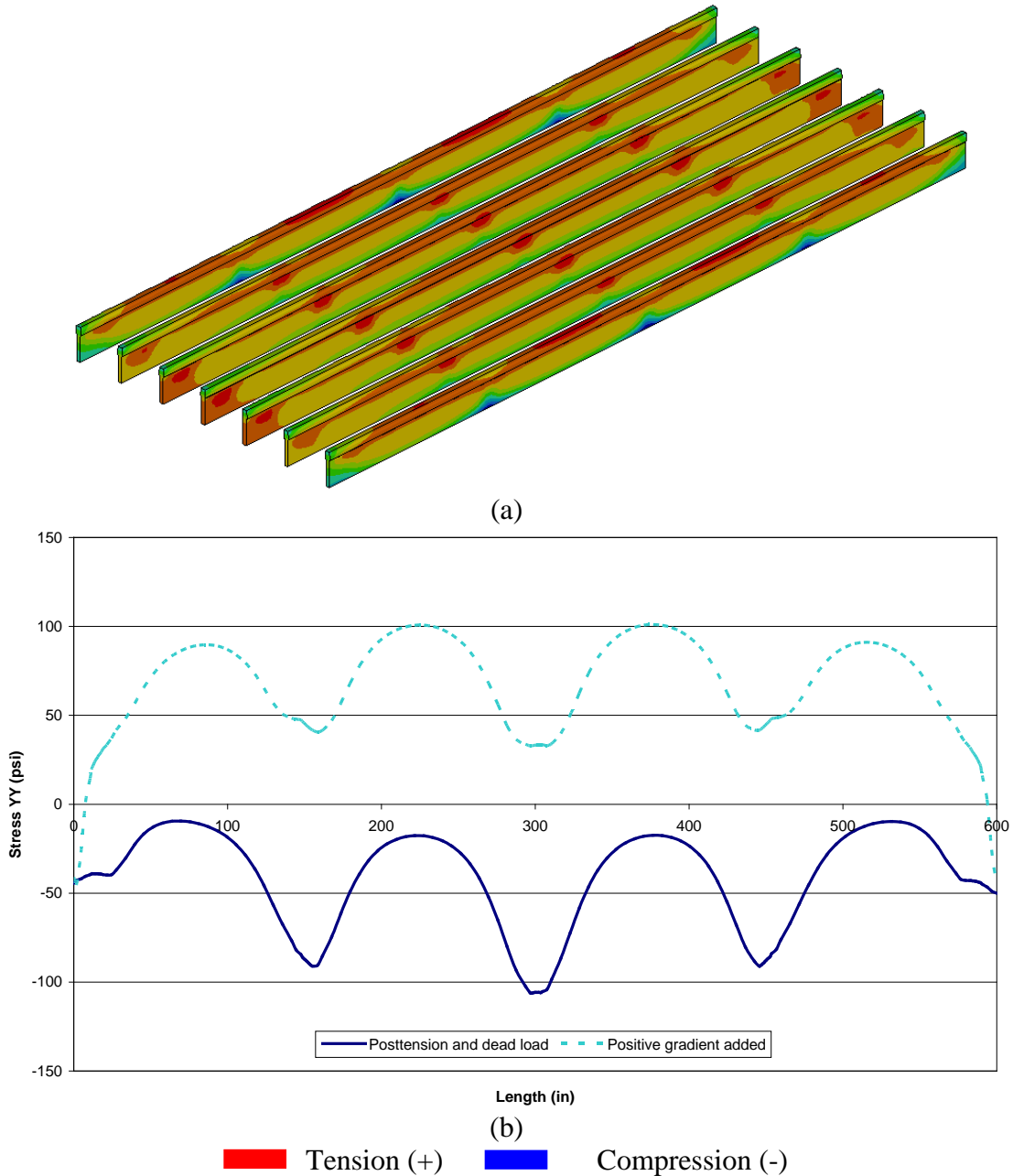


Figure 8-15. (a) Clamping stress distribution of grout layers under positive thermal gradient loading and (b) clamping stress distribution along the length of grout layers with and without the effect of positive gradient loading (stress plots are extracted using shear key top fiber nodes)

8.3.3 Load Combination 3: 1.0 DEAD + 1.0 LL

Single-Lane Loaded

In this combination, the system retains the stress state developed during construction, and HL-93 loading is applied on a single lane. This combination generated a maximum transverse tensile stress at the deck top fibers of about 32 psi over the end diaphragm and 22 psi at mid-span

(Figure 8-16). At the deck's bottom fibers, the maximum transverse tensile stresses are about 15 and 19 psi over the mid-span and end diaphragms, respectively (Figure 8-17). Live load on a single lane does not cause significant changes to grout clamping stresses. The maximum compressive clamping stress is increased to 189 psi from 164 psi; whereas tensile stress is increased to 16 psi from 6 psi.

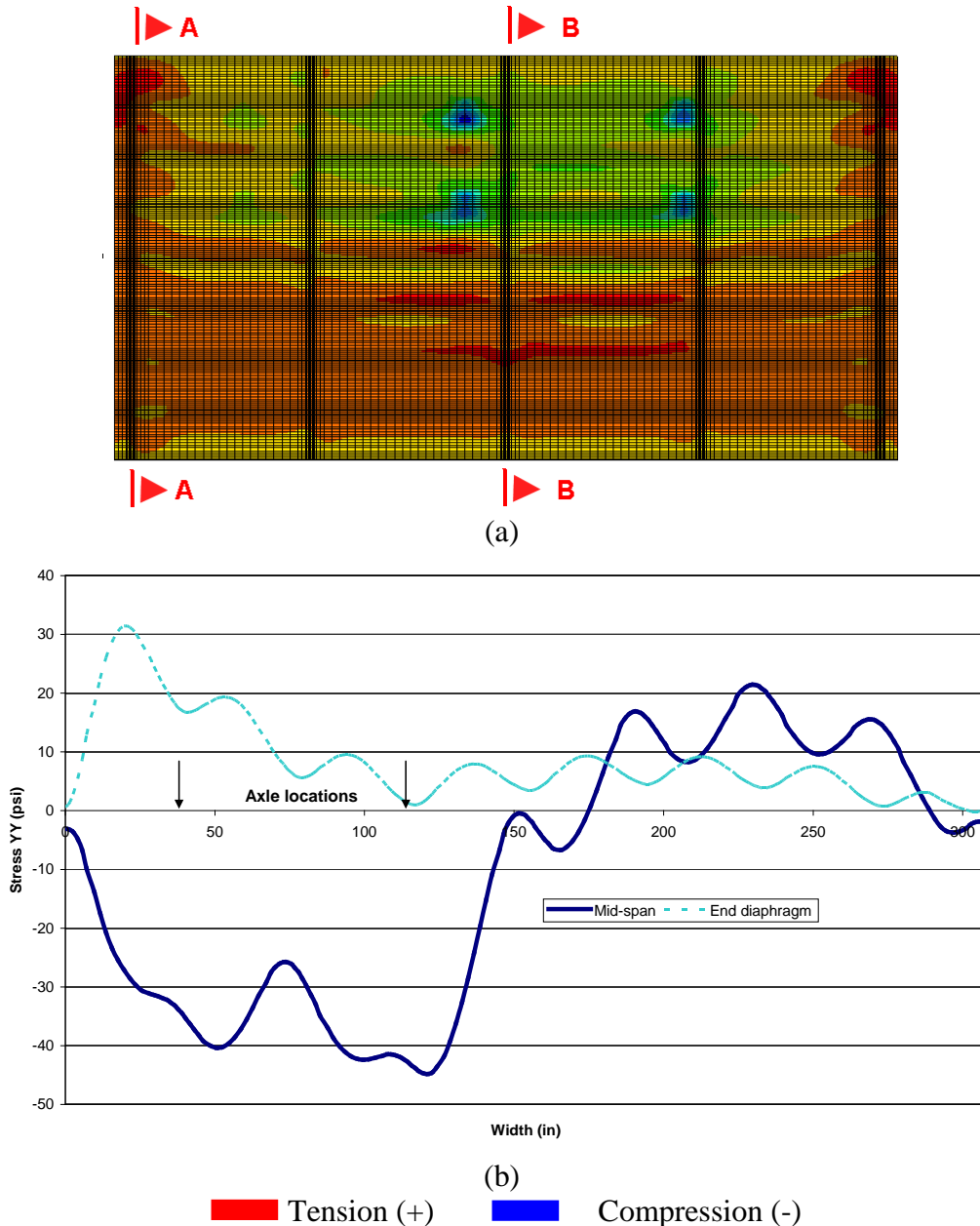


Figure 8-16. Transverse stress distribution (a) at the deck top surface and (b) along the width of the deck top surface over mid-span (Section B-B) and end-diaphragm centerline (Section A-A) under Service I load combination 3 with live load on a single lane

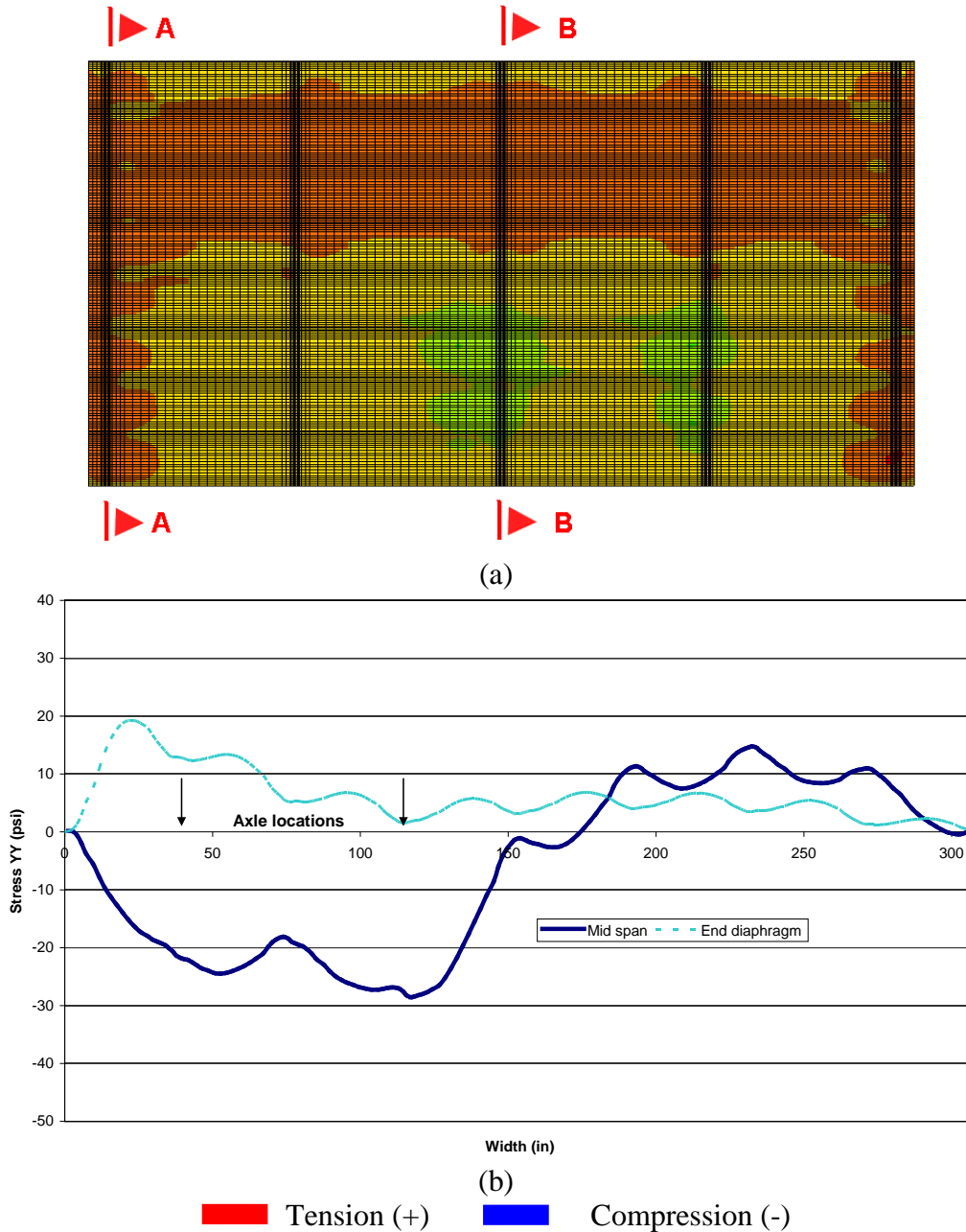


Figure 8-17. Transverse stress distribution (a) at the deck bottom surface and (b) along the width of the deck bottom surface over mid-span (Section B-B) and end-diaphragm centerline (Section A-A) under Service I load combination 3 with live load on a single lane

Two-Lane Loaded

In this combination, the HL-93 load is applied on both lanes. Under this load combination, the mid-span region is under compressive stress. However, both top and bottom surfaces of the 6-in thick deck located between two wheels of the same axle develop tensile stresses. Transverse tensile stress at these concentrated locations are no more than 10 psi at the top surface (Figure

8-18-a). Both top and bottom deck surfaces have transverse tensile stresses over the end diaphragms with maximum magnitudes of 25 and 15 psi, respectively (Figure 8-18 and Figure 8-19). The live load on both lanes does not significantly change clamping stresses developed in grout layers. The maximum compressive clamping stresses are within the grout layers located between the fascia and the first interior beams. Compressive stresses are increased to 189 psi from 164 psi; whereas tensile stresses are increased to 9.4 psi from 6.4 psi.

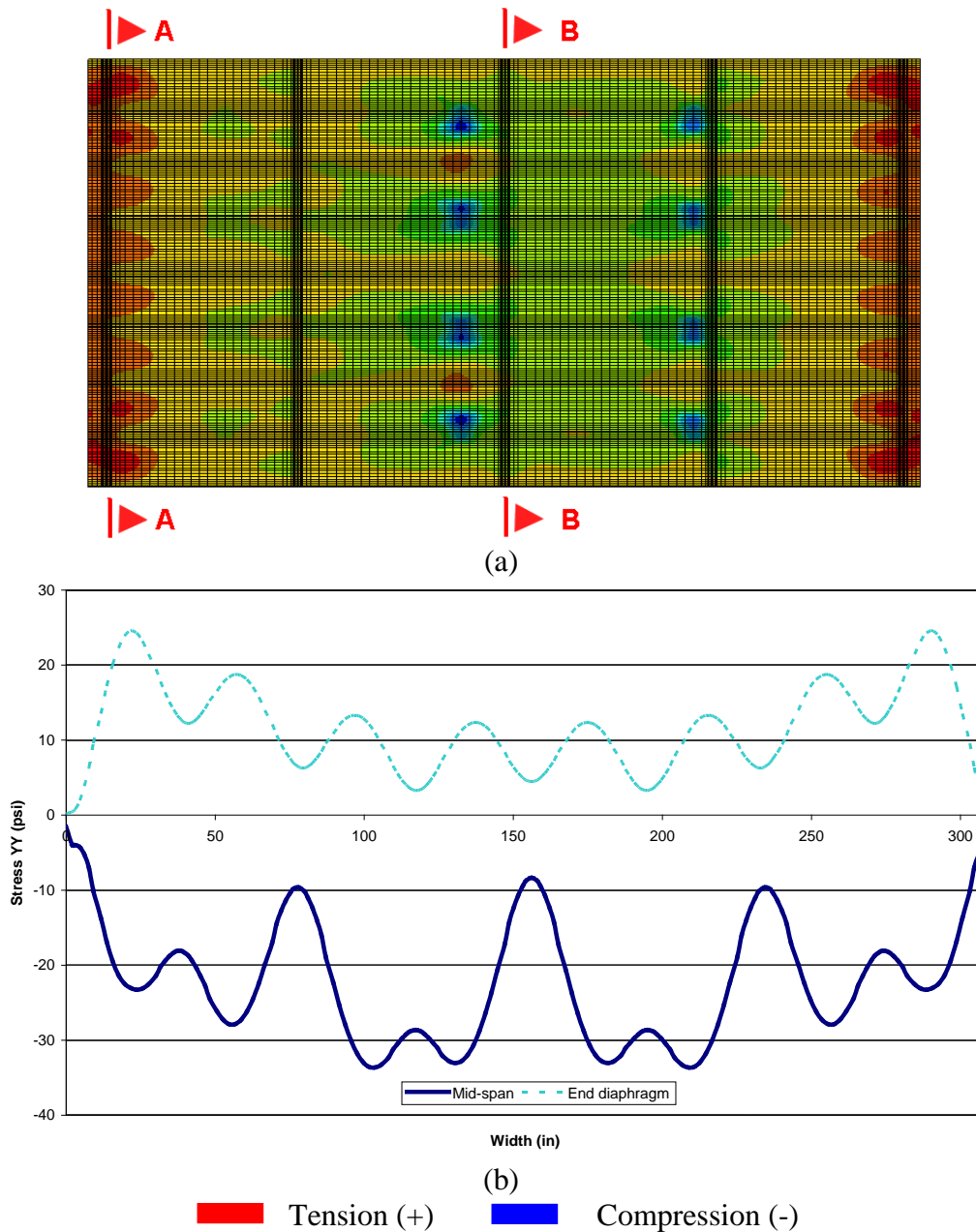


Figure 8-18. Transverse stress distribution (a) at the deck top surface and (b) along the width of the deck top surface over mid-span (Section B-B) and end-diaphragm (Section A-A) under Service I load combination 3 with live load on both lanes

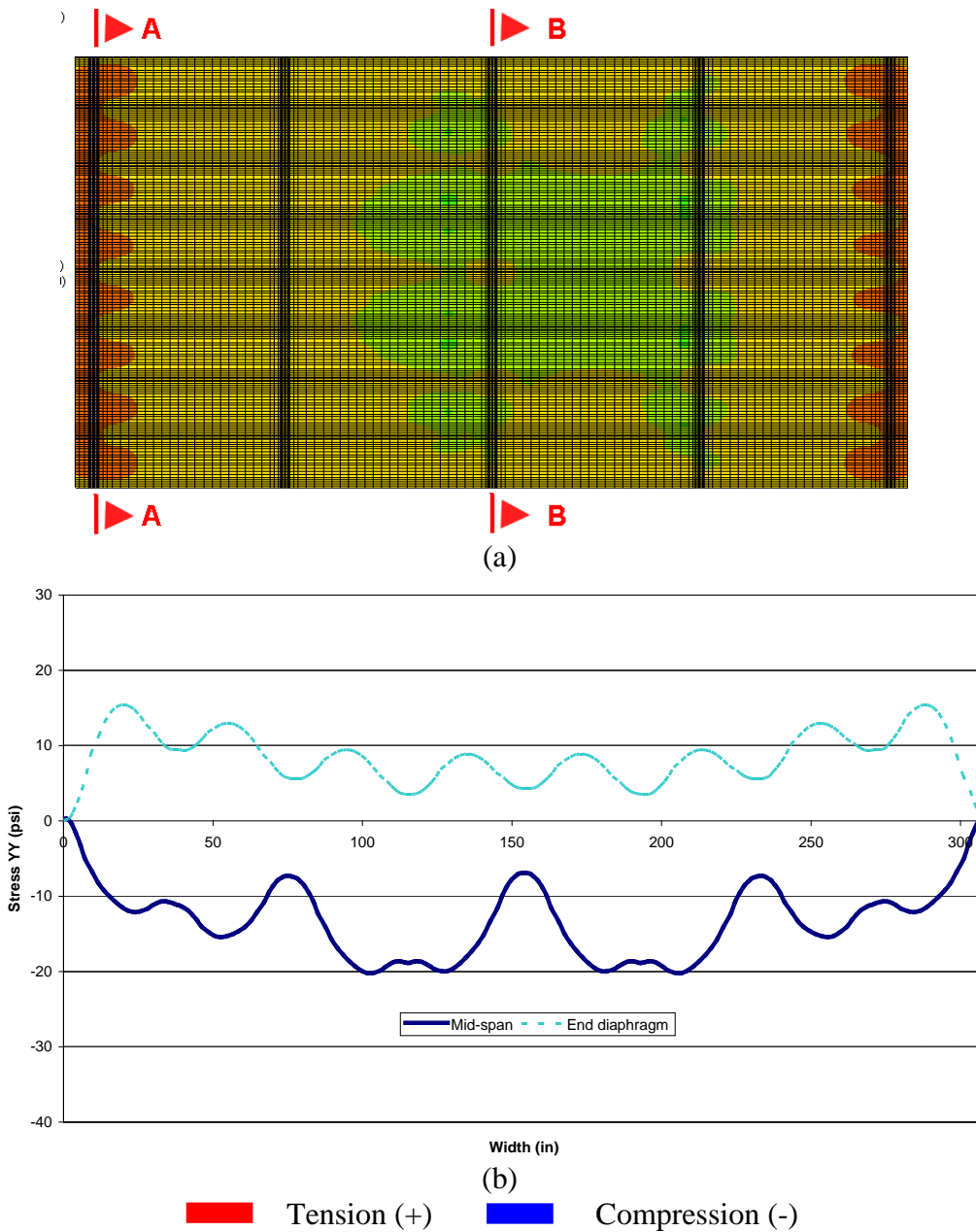


Figure 8-19. Transverse stress distribution (a) at the deck bottom surface and (b) along the width of the deck bottom surface over mid-span (Section B-B) and end-diaphragm (Section A-A) under Service I load combination 3 with live load on both lanes

8.4 SUMMARY AND CONCLUSIONS

FE analyses were carried out simulating the construction process sequences for the purposes of verifying the design assumptions that relate to performance expectations. Full 3-dimensional bridge models were subjected to the loads that develop during the stages of construction and later during operation of the bridge. Construction process sequences modeled are:

1. *Placing girders*
2. *Grouting shear keys*
3. *Applying posttension*
4. *Deck is cast but not hardened*
5. *Deck is hardened and barriers are placed.*

Service load analyses are performed considering the live and thermal gradient effects separately.

Load combinations were:

Combo 1: 1.0 DEAD + 1.0 NTG

Combo 2: 1.0 DEAD + 1.0 PTG

Combo 3: 1.0 DEAD + 1.0 LL

When thermal gradient and live load effects are considered simultaneously, the following load combinations are recommended in the AASHTO LRFD (2004):

Combo 4: 1.0 DEAD + 1.0 LL + 0.5 PTG or

Combo 5: 1.0 DEAD + 1.0 LL + 0.5 NTG

These combinations are not critical, and the combinations that include dead and thermal gradient effects (Combo 1 and Combo 2) generate much higher deck and grout stress magnitudes. Hence, Combo 4 and 5 were not considered in the analysis.

According to the analysis results:

1. Achieving a minimum clamping stress magnitude of 250 psi as required by the AASHTO at shear keys along the entire beam length would require a complete redesign of transverse posttension specifications.
2. Under posttensioning forces, clamping stresses are concentrated only within the width of diaphragms with the posttensioning strands.
3. Under posttensioning forces, clamping stress magnitudes within the shear keys increase towards the fascia beams (Figure 8-9 (b)).

4. Tensile stresses form both on top and bottom surfaces of the 6-in. deck under barrier loading, and increases potential for cracks reflecting from the shear keys (Figure 8-10).
5. The thermal gradient is the primary service loading that generates critical stresses within the deck and specific sections of shear key (Figure 8-11 through Figure 8-15).
6. Under negative thermal gradient loading, the top surface of the 6-in. deck is under tension; whereas bottom surface is under compression. Due to the fact that deck bottom surface is under compression, crack formation will be more random and not necessarily aligned with the shear keys (Figure 8-11 and Figure 8-12).
7. Under positive thermal gradient loading, the top surface of the 6-in. deck is under compression; whereas bottom surface is under tension (Figure 8-13, Figure 8-14 and Figure 8-15). Moreover, positive thermal gradient also creates tensile stresses at the top fibers of shear keys (Figure 8-15).
8. Under single lane loading, tensile stresses form both at mid-span and support regions of the 6-in. deck. With two-lane loading, tensile stresses only occur within the support regions (Figure 8-16 through Figure 8-19).

9 RATIONAL TRANSVERSE POSTTENSION DESIGN

9.1 OVERVIEW

Longitudinal reflective deck cracking is a recurring problem in Michigan and elsewhere even though many changes have been introduced to the empirical design procedures since 1950s (Aktan et al. 2005; Attanayake 2006). The finite element (FE) modeling and analysis of the construction sequences as well as post construction under live load discussed in chapter 8 showed that portions of the shear keys are under transverse tensile stresses. As a result, there is high potential for shear key-beam interface cracking and separation. A primary reason is that the shear keys are not uniformly compressed under transverse posttensioning. Conclusions derived from these analyses included the essential need to redesign the transverse posttensioning requirements. Moreover, it is documented that the transverse posttensioning requirements are based on empirical considerations without any regards to shear and moment demands and their variation on the shear keys. The shear key and deck longitudinal crack formation was observed and documented during construction monitoring of a side-by-side box-beam bridge project and is discussed in this chapter.

This chapter will present a rational analysis procedure for calculating the shear and bending moments at the shear keys from bridge load combinations. The rational analysis procedure is developed by the Western Michigan University project team and discussed in (Attanayake et al. 2008; Attanayake and Aktan 2008b; Attanayake 2006). This chapter will also present a rational design procedure based on the shear and moment demand envelopes at the shear key locations.

9.2 CONSTRUCTION MONITORING

Longitudinal reflective deck cracking was observed while monitoring the construction of a bridge that carries Oakland Drive over I-94 in Portage, Michigan (Figure 9-1). The construction scope included the full structure and substructure replacement. The bridge is straight and aligned in a north-south direction with two equal spans of 79 ft. There are six transverse posttension locations along each span. Each span width consists of 22 box-beams thus 21 shear keys. Each box-beam cross-section is 33×48-in. giving a full bridge width of 93 ft – 5 in. The bridge is designed for HS-25 loading; hence, posttension force magnitude applied at each location is 104.5 kips. There are two posttension locations at each diaphragm location. Therefore, the total

transverse posttension force magnitude is about 16 kips/ft. The bridge was originally designed for staged construction; hence, top posttension strands were discontinued at the bridge centerline while the bottom posttension strands were kept continuous (Figure 9-2). South span shear keys were grouted on May 11, 2007, and posttensioning was implemented on May 14, 2007. The project team inspected the shear keys on the same day just before and after posttensioning. Cracks along the interface between shear key and beam were observed before posttensioning and remained cracked after posttension (Figure 9-3). Shear keys were once again inspected three weeks after posttensioning (June 4th) but prior to deck placement. Cracks remained along the interface of every shear key (Figure 9-4).



Figure 9-1. Location of the new bridge



Figure 9-2. (a) Shear-key between beams 11 and 12 and (b) discontinued top posttension strands

The bridge deck was placed on June 6th and June 8th on north and south spans, respectively. The deck was moist cured with burlap cover and bleed hoses for seven days. Bridge deck concrete with a water/cementitious material ratio of 0.45 is specified as MDOT Grade D. The deck concrete developed compressive strength in excess of 5500 psi in 5 days and 6400 in 28 days.

The deck surface was inspected on June 22nd. Cracks were documented that stemmed from the top surface of the deck above the abutments, and they aligned with the shear keys. These cracks were observed before the approaches and barriers were placed. Specifically, the cracks developed before any barrier or live loading on the bridge deck. During this time, the deck was not subjected to live loads, only intrinsic material actions such as the heat of hydration and drying shrinkage. Calculations showed that the tensile stresses that developed on the deck, from posttension losses during the period of June 6 (deck placement) and June 22, are not significant enough to cause cracking.



Figure 9-3. Shear-key interface cracking observed on May 14th (a) before and (b) after posttension



Figure 9-4. Shear-key interface cracks observed on June 4th

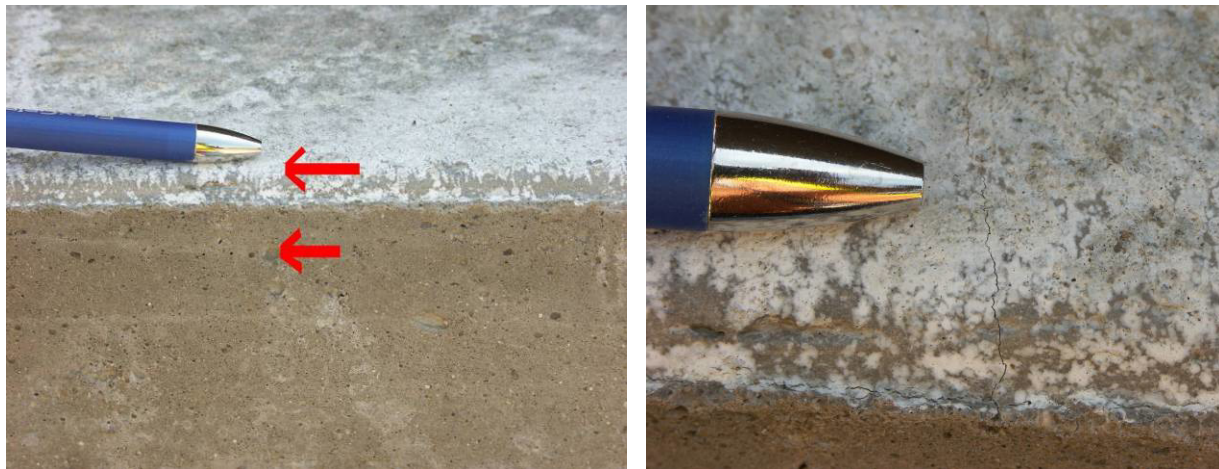


Figure 9-5. Deck cracking observed on June 22nd

9.3 MACROMECHANICAL MODEL

Construction process simulation results and observed performance of existing bridges show the need for a rational analysis model for orthotropic decks such as side-by-side box-beam bridge superstructures. Rational analysis model results will be utilized to rationally design transverse posttensioning. It should be mentioned that there is a rational transverse posttension design procedure given in the PCI Bridge Design Manual (2005) which is based on the grillage model proposed by El-Remaily et al. (1996). The grillage model, however, cannot sufficiently represent the load transfer response along the shear key due to simplified assumptions. Attanayake et al. (2008) developed a simple but refined analysis model using the concepts of mechanics of materials and macromechanics concepts. This model is referred to as the *macromechanical* model.

The first step in the macromechanical model development is to define the representative volume element (RVE) of the orthotropic deck; in this case, that is the side-by-side box-beam bridge deck (Figure 9-6). The RVE is defined by a shear key, halves of adjacent box-beams, and a portion of cast-in-place concrete deck. (Refer to the dashed box shown in Figure 9-6.) Hence, the width of the RVE is equal to the summation of a beam width and shear key thickness. In principle, the length of the RVE can be any value, yet it should be a reasonable ratio to the width since the RVE will be the building block of the bridge.

The analysis model development procedure from the RVE properties is depicted in Figure 9-6. The macromechanical modeling process is the calculation of stiffnesses of a finite portion of the original structure described by the RVE. The stiffnesses are normalized with respect to the length and width of the RVE. The normalized stiffness relations of RVE represent a thick plate with equal length and width dimensions of the orthotropic bridge superstructure system.

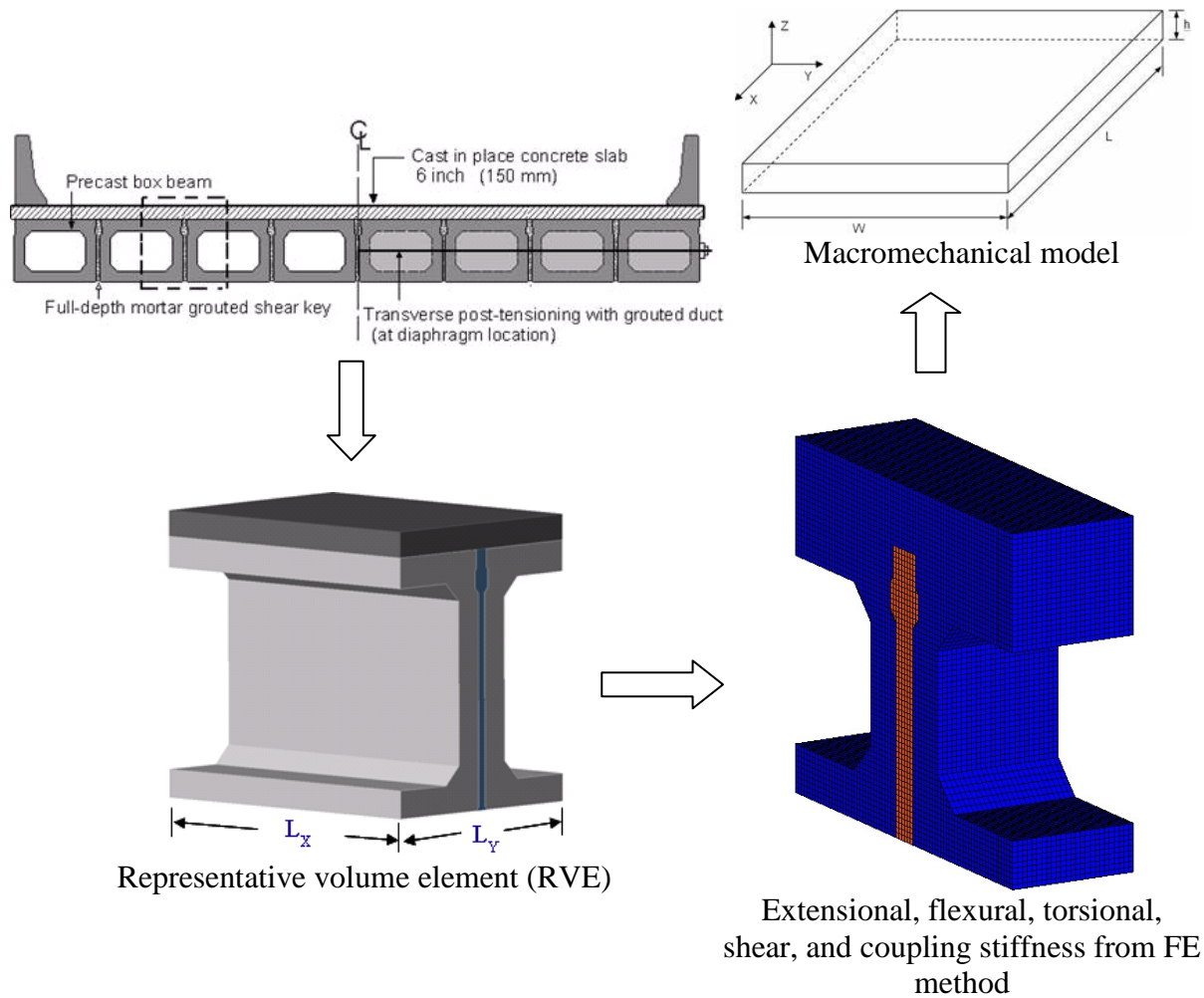


Figure 9-6. Concept of macromechanical model development procedure

The second step is to calculate the terms of the stiffness matrix given in Eq. 9-1 and Eq. 9-2. The stiffness matrix that is referred as the ABDE matrix consists of [A], [B], [D], and [E] sub matrices. The stiffness matrix defines the relationship between axial forces (N_1 and N_2) and axial strains (ϵ_1 and ϵ_2), in-plane shear force (N_{12}) and shear strain (γ_{12}), transverse shear forces (V_{13} and V_{23}) and transverse shear strains (γ_{13} and γ_{23}), moments (M_1 and M_2) and curvatures (k_1 and k_2), and torsional moment due to in-plane shear (M_{12}) and curvature (k_{12}). Definitions of forces and moments given in Eq. 9-1 are depicted in Figure 9-7. According to Eq. 9-1 and Eq. 9-2, the A_{ij} is in-plane stiffness, the B_{ij} is coupling stiffness, D_{ij} is flexural stiffness, and E_{ij} is the transverse shear stiffness (Kollar and Springer 2003; Jones 1975). The complete stiffness matrix of the RVE defined in Eq. 9-1 and Eq. 9-2 is referred to as the ABDE matrix.

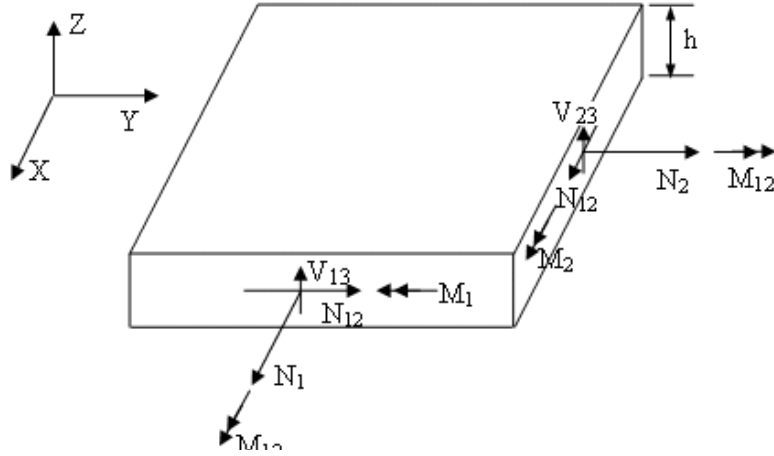


Figure 9-7. Notations – forces and moments acting on a plate element

The ABDE matrix of one RVE is established using the FE analysis. The FE model of the RVE is developed using continuum (8-node brick) elements with translational nodal degrees of freedom (ABAQUS 2008). Strains and curvatures are simulated with prescribed displacement profiles. Attanayake (2006) provides detailed procedure for developing ABDE matrix.

$$\begin{Bmatrix} N_1 \\ N_2 \\ N_{12} \\ M_1 \\ M_2 \\ M_{12} \\ V_{13} \\ V_{23} \end{Bmatrix} = \begin{bmatrix} A & B & 0 \\ B & D & 0 \\ 0 & 0 & E \end{bmatrix} \begin{Bmatrix} \varepsilon_1 \\ \varepsilon_2 \\ \gamma_{12} \\ k_1 \\ k_2 \\ k_{12} \\ \gamma_{13} \\ \gamma_{23} \end{Bmatrix} \quad (9-1)$$

where,

$$\begin{bmatrix} A & B & 0 \\ B & D & 0 \\ 0 & 0 & E \end{bmatrix} = \begin{bmatrix} A_{11} & A_{12} & A_{13} & B_{11} & B_{12} & B_{13} & 0 & 0 \\ A_{21} & A_{22} & A_{23} & B_{21} & B_{22} & B_{23} & 0 & 0 \\ A_{31} & A_{32} & A_{33} & B_{31} & B_{32} & B_{33} & 0 & 0 \\ B_{11} & B_{12} & B_{13} & D_{11} & D_{12} & D_{13} & 0 & 0 \\ B_{21} & B_{22} & B_{23} & D_{21} & D_{22} & D_{23} & 0 & 0 \\ B_{31} & B_{32} & B_{33} & D_{31} & D_{32} & D_{33} & 0 & 0 \\ 0 & 0 & 0 & 0 & 0 & 0 & E_{11} & 0 \\ 0 & 0 & 0 & 0 & 0 & 0 & 0 & E_{22} \end{bmatrix} \quad (9-2)$$

9.4 RATIONAL POSTTENSION DESIGN PROCEDURE

9.4.1 Overview

The rational transverse posttension design procedure is described in this report on a specific bridge design application. The bridge in this example is a side-by-side box-beam in length and width of 600 in. and 309 in., respectively. The bridge cross-section consists of eight 27 in. deep and 36 in. wide box-beams with 3 in. wide full-depth shear keys and a 6-in thick reinforced concrete deck as shown in Figure 9-8. Grouted joints (shear keys) transfer loads (moment and shear) while providing tight moisture seal between the beams. To assure tight moisture seal, the joint should not be allowed to develop cracks at the interface. Therefore, the grout-beam interface needs to be modeled as a tightly bonded joint. Current side-by-side box-beam superstructure configuration consists of rigid diaphragms at predefined locations that are established based on the span length. Intermediate diaphragms are provided to facilitate posttension applications. Posttension is to facilitate load transfer between the girders through the grouted shear keys. The service state expectation from the transverse posttension is to provide a box-beam assemblage that acts as a single unit without developing cracks at the joints. Assuming tightly bonded joints in the model satisfies the envisioned behavior by posttensioning; thus, diaphragms and posttension are not incorporated in the model.

Following the procedure discussed in Attanayake (2006), [A], [B], [D], and [E] matrices are developed for the RVE shown in Figure 9-9. Two different RVE configurations are considered in order to establish transverse posttensioning in two stages: with and without the cast-in-place concrete deck. Elasticity modulus of concrete (both cast-in-place deck and the box-beams) and grout are taken as 5000 psi and 3600 psi, respectively. Poisson's ratio of both concrete and grout is assumed 0.2. The resulting [ABDE] matrices for two different RVE configurations are given in Eq. 9-3 and Eq. 9-4. The coupling matrix [B] is zero (Attanayake 2006; Jones 1975; and Kollar and Springer 2003).

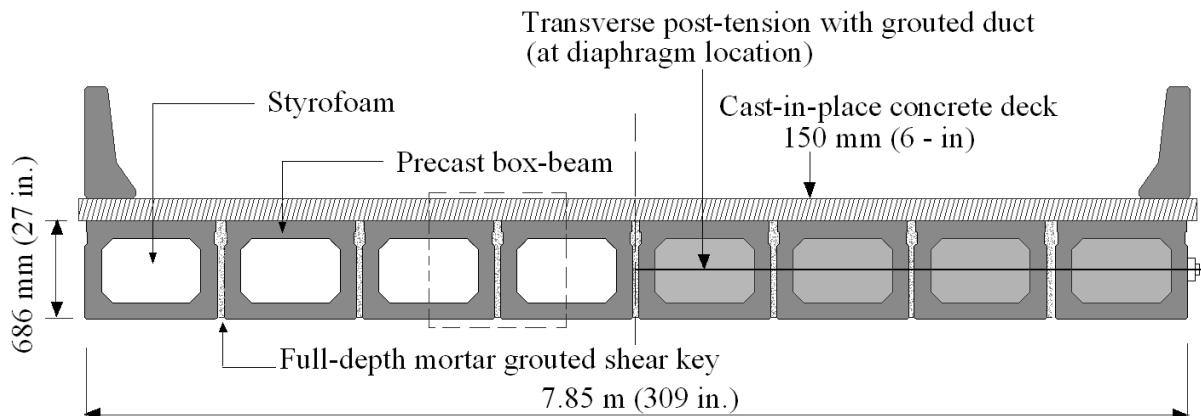


Figure 9-8. Side-by-side box-beam configuration

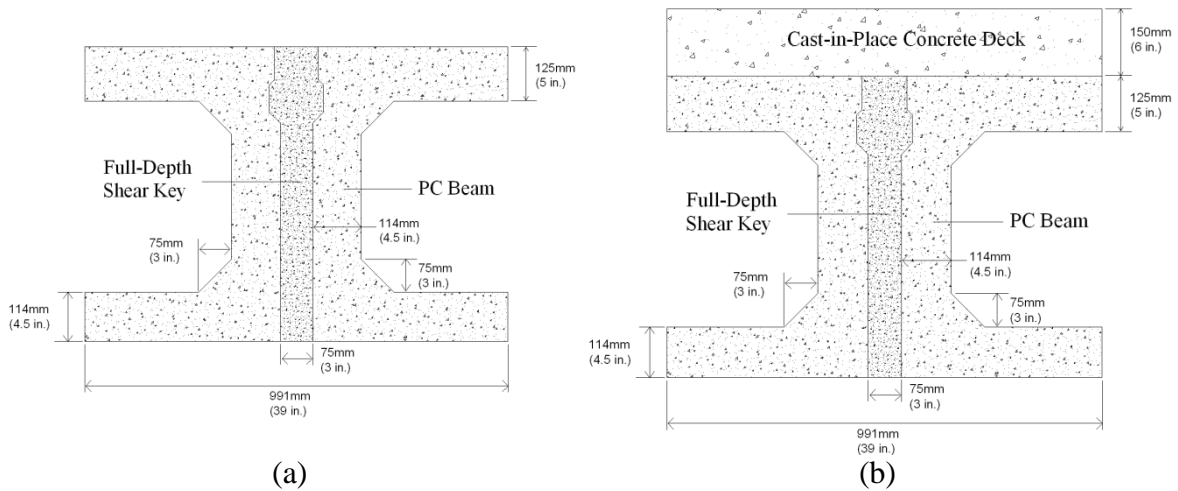


Figure 9-9. Cross-section of the RVE (a) without and (b) with deck.

Stiffness Matrix of RVE without Deck

$$\begin{bmatrix} A & B & 0 \\ B & D & 0 \\ 0 & 0 & E \end{bmatrix} = 10^7 \times \begin{bmatrix} 7.55 & 1.03 & 0 & 0 & 0 & 0 & 0 & 0 \\ 1.03 & 5.13 & 0 & 0 & 0 & 0 & 0 & 0 \\ 0 & 0 & 3.05 & 0 & 0 & 0 & 0 & 0 \\ 0 & 0 & 0 & 682.98 & 125.35 & 0 & 0 & 0 \\ 0 & 0 & 0 & 125.35 & 627.29 & 0 & 0 & 0 \\ 0 & 0 & 0 & 0 & 0 & 256.88 & 0 & 0 \\ 0 & 0 & 0 & 0 & 0 & 0 & 2.93 & 0 \\ 0 & 0 & 0 & 0 & 0 & 0 & 0 & 2.93 \end{bmatrix} \begin{matrix} lb/in \\ lb/in \\ lb/in \\ in-lb \\ in-lb \\ in-lb \\ lb/in \\ lb/in \end{matrix} \quad (9-3)$$

Stiffness Matrix of RVE with Deck

$$\begin{bmatrix} A & B & 0 \\ B & D & 0 \\ 0 & 0 & E \end{bmatrix} = 10^7 \times \begin{bmatrix} 10.68 & 1.67 & 0 & 0 & 0 & 0 & 0 & 0 \\ 1.67 & 8.35 & 0 & 0 & 0 & 0 & 0 & 0 \\ 0 & 0 & 4.30 & 0 & 0 & 0 & 0 & 0 \\ 0 & 0 & 0 & 1282.7 & 232.45 & 0 & 0 & 0 \\ 0 & 0 & 0 & 232.45 & 1162.8 & 0 & 0 & 0 \\ 0 & 0 & 0 & 0 & 0 & 477.4 & 0 & 0 \\ 0 & 0 & 0 & 0 & 0 & 0 & 4.31 & 0 \\ 0 & 0 & 0 & 0 & 0 & 0 & 0 & 4.31 \end{bmatrix} \begin{matrix} lb/in \\ lb/in \\ lb/in \\ in-lb \\ in-lb \\ in-lb \\ lb/in \\ lb/in \end{matrix} \quad (9-4)$$

9.4.2 Analysis and Design Procedure

The resulting analysis model assembled with the [ABDE] matrix (i.e., the macromechanical model) is simply a thick continuous plate. Live load combinations are applied satisfying the AASHTO LRFD (2004) requirements to generate maximum load effect without any restrictions. Analysis results under dead loads and HL-93 load represent the moment and shear distribution throughout the plate. Hence, moments and shear acting at the shear key locations can be determined. Knowing load demand at the longitudinal joints between precast beams (i.e., the shear key locations), any other joint detail can be developed.

In this example, the design procedure is illustrated using the most common transverse connection design configuration: i.e., the transverse posttension application through discrete diaphragms of the beams with full-depth grouted shear keys. The example uses five discrete diaphragms along the span: two 24 in. wide end diaphragms and three 14 in. wide intermediate diaphragms located at mid-span and one-fourth location along the span (Figure 9-10).

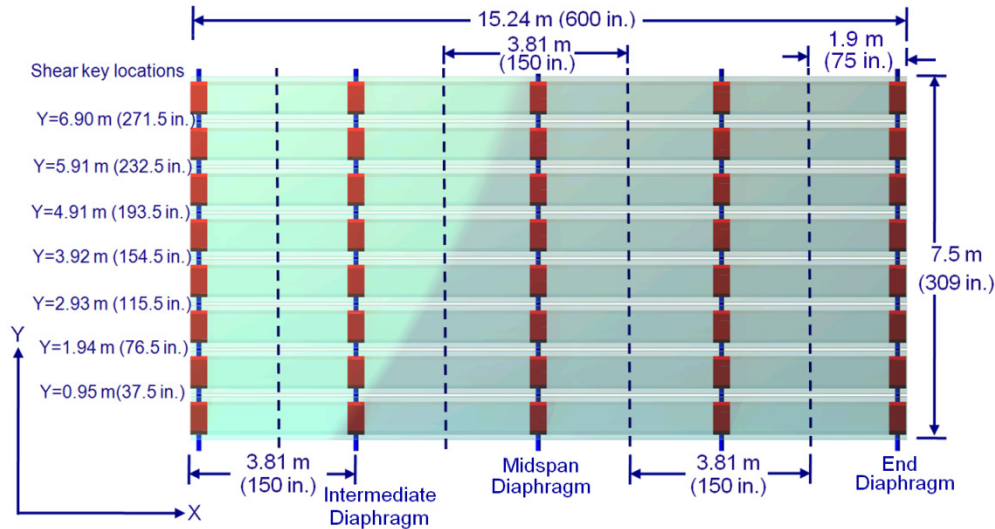


Figure 9-10. Diaphragm and shear key locations.

To determine the first stage of posttension, the macromechanical model with stiffness properties of RVE without a deck is analyzed under dead load corresponding to cast-in-place concrete deck. Concrete self weight is assumed to be 150 lb/ft^3 . For the second stage, the stiffness properties of RVE with a deck are assigned to the macromechanical model and analyzed under barrier load (New Jersey Type 4, Figure 9-11), and HS-20 truck and lane load (i.e., HL-93). HS-20 truck position on a single lane (Figure 9-12) and two lanes are considered. In order to determine the transverse posttension force requirement at each diaphragm location, the nominal moment acting within the half distance between diaphragms is calculated as given in Table 9-1. Critical moment combinations are recognized for calculating posttension force demand at the diaphragms before and after deck placement.

AASHTO LRFD (2004) does not provide an explicit service load criteria for longitudinal joint design. Hence, service I and III limit states are considered for limiting the stresses at the longitudinal joints. When load factors are considered, service I criteria obviously controls the design. The joint design criteria used here is crack prevention; hence, posttension is designed based on no tension. Based on AASHTO LRFD (2004) Section 3.6.1.1.2, multiple presence factors of 1.2 and 1.0 are considered for the condition of one and two lanes of vehicular live loads, respectively. Also, section 3.6.2.1 of AASHTO LRFD (2004) recommends using 1.75 as the dynamic load allowance factor for deck joints. Transverse posttension force magnitudes at each diaphragm location are calculated following service I limit state requirements, critical

transverse moments at the joints, and the AASHTO LRFD (2004) specification stipulations. The Michigan Bridge Design Guide (2005) specifies transverse posttension application at two locations along the height of 33 in. or deeper beams. Considering the impact of applying posttension at two locations along the beam height on moment transfer across the joint, a similar practice is maintained in this example as shown in Table 9-2.

Transverse posttension force magnitudes at each diaphragm location are calculated following Service I limit state requirements, critical transverse moments at the joints, and the AASHTO LRFD (2004) specification stipulations. The results are summarized in Table 9-3. A detailed calculation procedure developed by Attanayake and Aktan (2009) is provided in Appendix J.

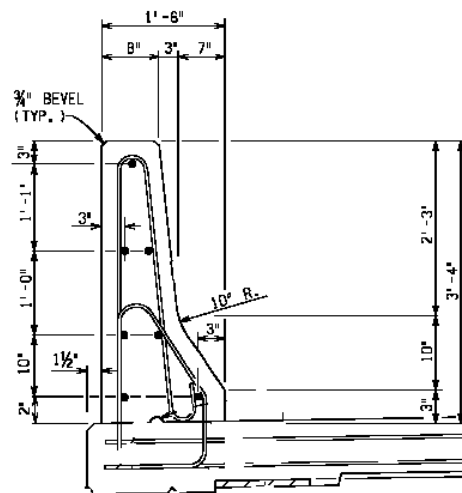


Figure 9-11. New Jersey Type 4 barrier (Note: 1 in. = 25.4 mm)

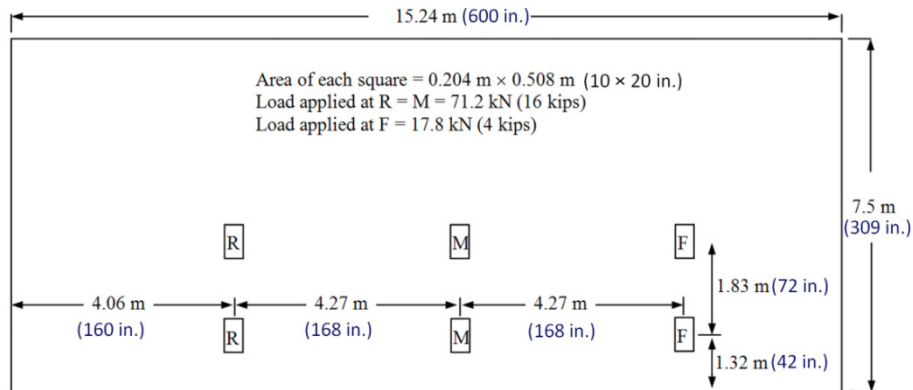


Figure 9-12. Position of a single HS-20 truck

Table 9-1. Averaged Transverse Moment, N-m/m (in-lb/in)

Row No.	Shear key location m (in.)	End Diaphragm Moment Averaged within 1.91m (75 in.)						Intermediate Diaphragm Moment Averaged within 3.81 m (150 in.)						Mid-span Diaphragm Moment Averaged within 3.81 m (150 in.)					
		Loads						Loads						Loads					
		Deck (a)	Barrier (b)	1 truck (c)	1 lane (d)	2 trucks (e)	2 lanes (f)	Deck (g)	Barrier (h)	1 truck (i)	1 lane (j)	2 trucks (k)	2 lanes (l)	Deck (m)	Barrier (n)	1 truck (o)	1 lane (p)	2 trucks (q)	2 lanes (r)
1	0.95 (37.5)	-730 (-164)	-2982 (-670)	-2728 (-613)	-547 (-123)	-1838 (-413)	-263 (-59)	2283 (513)	-2332 (-524)	8669 (1948)	2532 (569)	7432 (1670)	2078 (467)	3039 (683)	-2554 (-574)	10992 (2470)	3244 (729)	9372 (2106)	2657 (597)
2	1.94 (76.5)	779 (175)	-2439 (-548)	739 (166)	863 (194)	988 (222)	828 (186)	3974 (893)	-4303 (-967)	10805 (2428)	3872 (870)	9919 (2229)	3453 (776)	5224 (1174)	-5006 (-1125)	14098 (3168)	4873 (1095)	13087 (2941)	4406 (990)
3	2.93 (115.5)	1460 (328)	-2194 (-493)	1833 (412)	1095 (246)	2390 (537)	1077 (242)	5002 (1124)	-5304 (-1192)	13025 (2927)	3484 (783)	14374 (3230)	3698 (831)	6501 (1461)	-6439 (-1447)	16105 (3619)	4388 (986)	18165 (4082)	4810 (1081)
4	3.92 (154.5)	1606 (371)	-2140 (-481)	1384 (311)	360 (81)	2768 (622)	721 (162)	5345 (1201)	-5611 (-1261)	5994 (1347)	1571 (353)	11988 (2694)	3142 (706)	6920 (1555)	-6906 (-1552)	7939 (1784)	2145 (482)	15878 (3568)	4294 (965)
5	4.91 (193.5)	1460 (328)	-2194 (-493)	552 (124)	-18 (-4)	2390 (537)	1077 (242)	5002 (1124)	-5304 (-1192)	1348 (303)	209 (47)	14374 (3230)	3698 (831)	6501 (1461)	-6439 (-1447)	2060 (463)	423 (95)	18165 (4082)	4810 (1081)
6	5.91 (232.5)	779 (175)	-2439 (-548)	249 (56)	-36 (-8)	988 (222)	828 (186)	3974 (893)	-4303 (-967)	-886 (-199)	-414 (-93)	9919 (2229)	3453 (776)	5224 (1174)	-5006 (-1125)	-1010 (-227)	-467 (-105)	13087 (2941)	4406 (990)
7	6.9 (271.5)	-730 (-164)	-2982 (-670)	890 (200)	285 (64)	-1838 (-413)	-263 (-59)	2283 (513)	-2332 (-524)	-1237 (-278)	-454 (-102)	7432 (1670)	2078 (467)	3039 (683)	-2554 (-574)	-1620 (-364)	-587 (-132)	9372 (2106)	2657 (597)

Note: Negative (-) moments develop tension on top of the deck

Highlighted cells contain the critical moments for AASHTO LRFD (2004) Service I combination

Table 9-2. Geometric Parameters of Diaphragms and Transverse Posttension Locations along Beam Height

Transverse Posttension Locations along Beam Height		
Diaphragm Cross-Section without Deck		
	End Diaphragm (a)	Intermediate and Mid-span Diaphragms (b)
1. Cross-Section Area (A) mm ²	4.356×10^5	2.442×10^5
2. Moment of Inertia (I) mm ⁴	1.708×10^{10}	9.557×10^9
3. Neutral Axis Depth (y) mm	343	343
Diaphragm Cross-Section with Deck		
4. Cross-Section Area (A) mm ²	5.321×10^5	2.983×10^5
5. Moment of Inertia (I) mm ⁴	3.114×10^{10}	1.746×10^{10}
6. Miscellaneous Parameters		

Table 9-3. Posttension Force Requirement for the Sample Bridge

		Posttension Force at Diaphragm (P), kips		
		End Diaphragm	Intermediate Diaphragm	Middle Diaphragm
Before deck placement		7	41	52
After deck placement		63	105	130
Total		70	146	182
Total (empirical) MDOT ⁺	HS-20	82.5	82.5	82.5
	HS-25	104.5	104.5	104.5

+ Michigan DOT applies the highest level of posttension in the US. Posttension force magnitudes are recommended based on empirical methods and applied before deck placement (*Attanayake and Aktan 2008*)

9.5 CONSTRUCTION SIMULATION WITH STAGED POSTTENSION

Construction simulation discussed in chapter 8 is based on the current Michigan DOT practice. Transverse connection design, as specified in the MDOT design manual, is empirical and applied in a single stage. The rational design procedure discussed in section 9.4 recommends staged posttension to precompress the deck before casting barriers and applying live load. Finite element simulation of the proposed procedure and results are discussed in this section.

The first two stages of the construction process are the same as those discussed in Chapter 8. That is: beams are erected and then shear keys are grouted. Given below are the analyses performed for the following stages:

Stage 3: Posttension application before 6-in. thick deck placement

Following the proposed procedure, two posttension locations are considered along the beam height. The first posttension location is placed seven inches below the top of the beam. The second location is seven and a half inches above the bottom fiber of the beam (Figure 9-13). (Note: 7.5 in. distance is selected based on the limitations of the FE mesh size.) Posttension load magnitudes are established from the rational design example as given in Table 9-3.

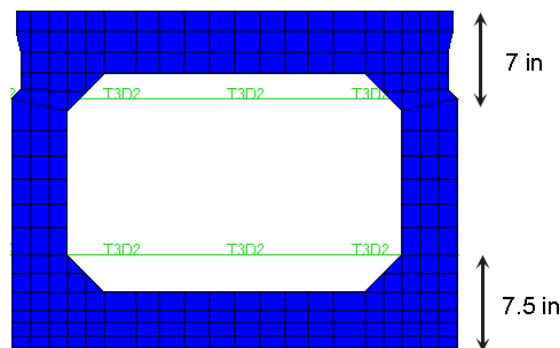


Figure 9-13. Transverse posttension locations along the beam height

Clamping stress distribution of the shear key located between fascia and the first interior beams is shown in Figure 9-14a. At the shear key located between fascia and the first interior beams, the maximum compressive clamping stress magnitude of 61 psi and tensile stress magnitude of 3.2 psi are obtained. The magnitude of posttension applied at the mid-span diaphragm is greater than the intermediate and end diaphragms; hence, the maximum clamping stress occurs at mid-span instead of end-diaphragms (Figure 9-14b).

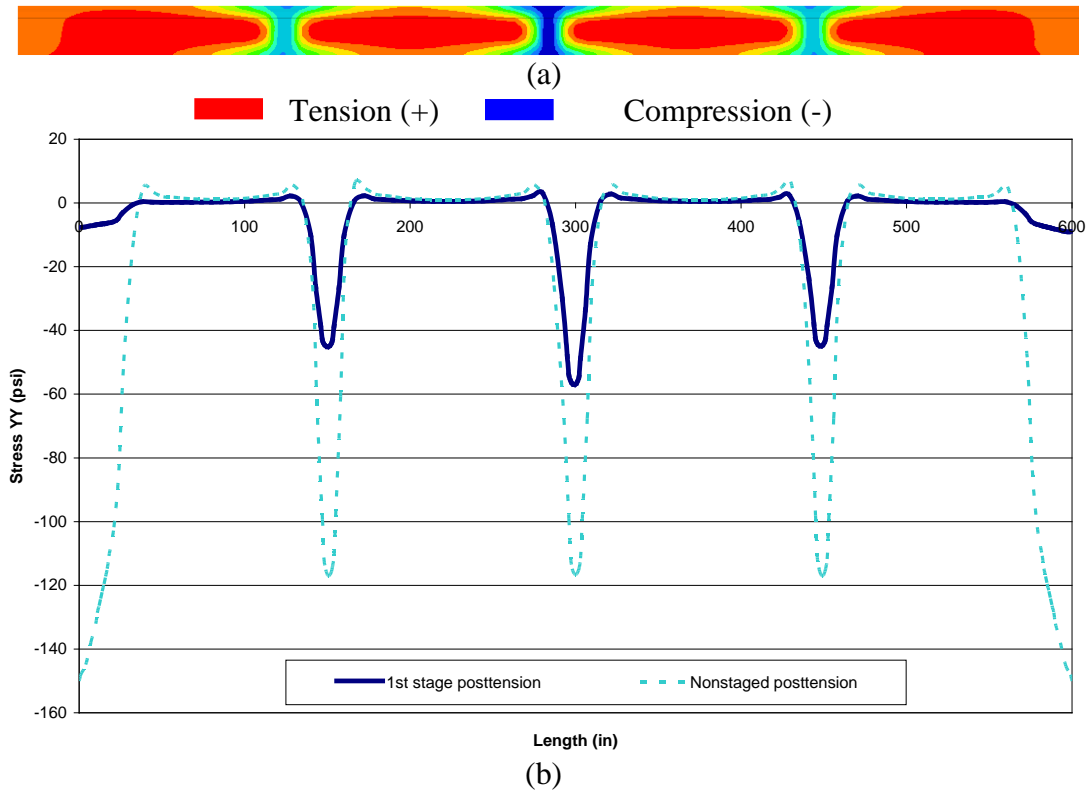


Figure 9-14. Clamping stress (a) contours at shear key after the first stage posttension and (b) distribution along the length of the shear key with or without staged posttension (stresses are extracted using shear key mid-height nodes)

Stage 4: Deck placement

After application of the first stage posttension, a 6-in. thick concrete deck is cast. Hence, dead load of the deck is acting on the beam-shear key system, but deck elements are not activated and are free of stresses. Applying deck as dead load causes minor changes to the shear key clamping stresses. Specifically, compressive clamping stresses are increased to 68 psi from 61 psi, whereas tensile stress magnitudes increased to 9 psi at locations close to end diaphragms where initial posttension magnitudes are low.

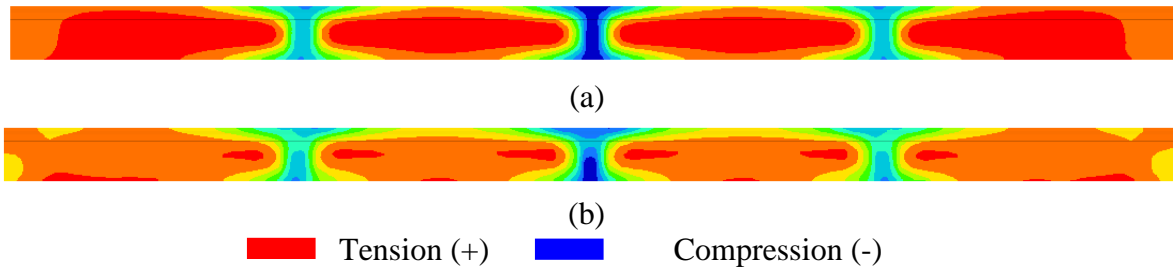


Figure 9-15. Clamping stress distribution along the shear key between fascia and the first interior beams under (a) posttension and (b) posttension and deck dead load

Stage 5: Deck concrete is hardened

To simulate the behavior of a bridge superstructure with hardened concrete deck, deck elements are activated. No loads are defined within this step. Any further loads applied will now act on the composite system.

Stage 6: Posttension application upon deck placement

Upon second stage posttension, clamping stress magnitudes at the shear key between fascia and the first interior beams are increased (Figure 9-16). Compressive clamping stress increases to 231 psi from 61 psi, whereas tensile stress magnitude remains the same at 9 psi. With the application of second stage posttension after deck placement, a greater part of the deck is compressed with maximum stress magnitude reaching 100 psi around mid-span. Maximum tensile stress magnitude of 18 psi develops in regions close to fascias at mid-span diaphragm location (Figure 9-17b). Tensile stresses that develop between the diaphragms (dark red contours in Figure 9-17a) and Figure 9-18a) correspond to magnitudes of less than 6 psi. Transverse stress distribution along the width of the deck is given in Figure 9-17 and Figure 9-18 for the top and bottom surfaces of the 6-in. thick cast-in-place deck, respectively.

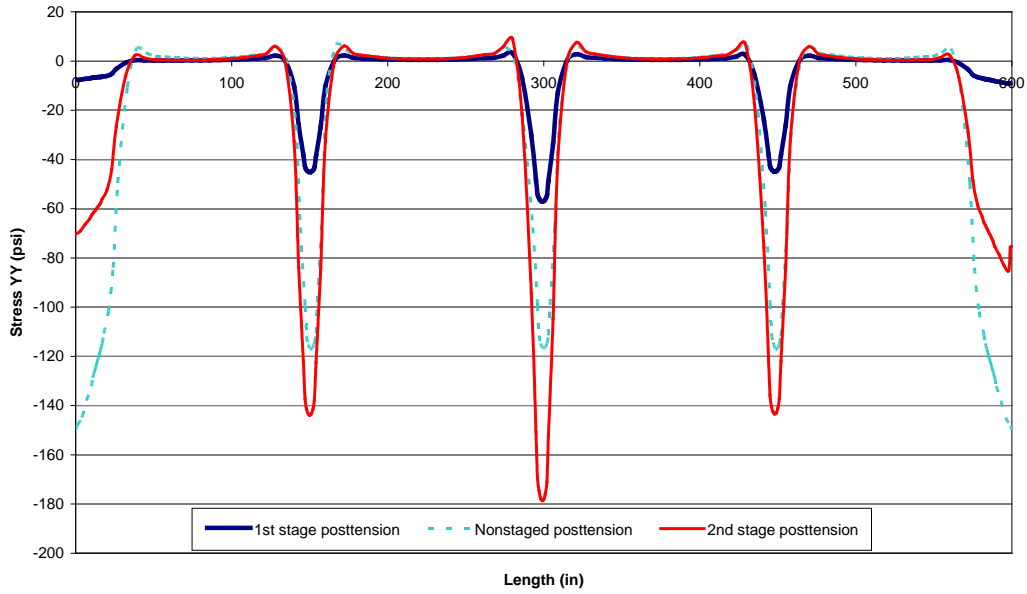


Figure 9-16. Clamping stress distribution along the length of the shear key with or without staged posttension (stresses are extracted using shear key mid-height nodes; compression-negative, tension-positive)

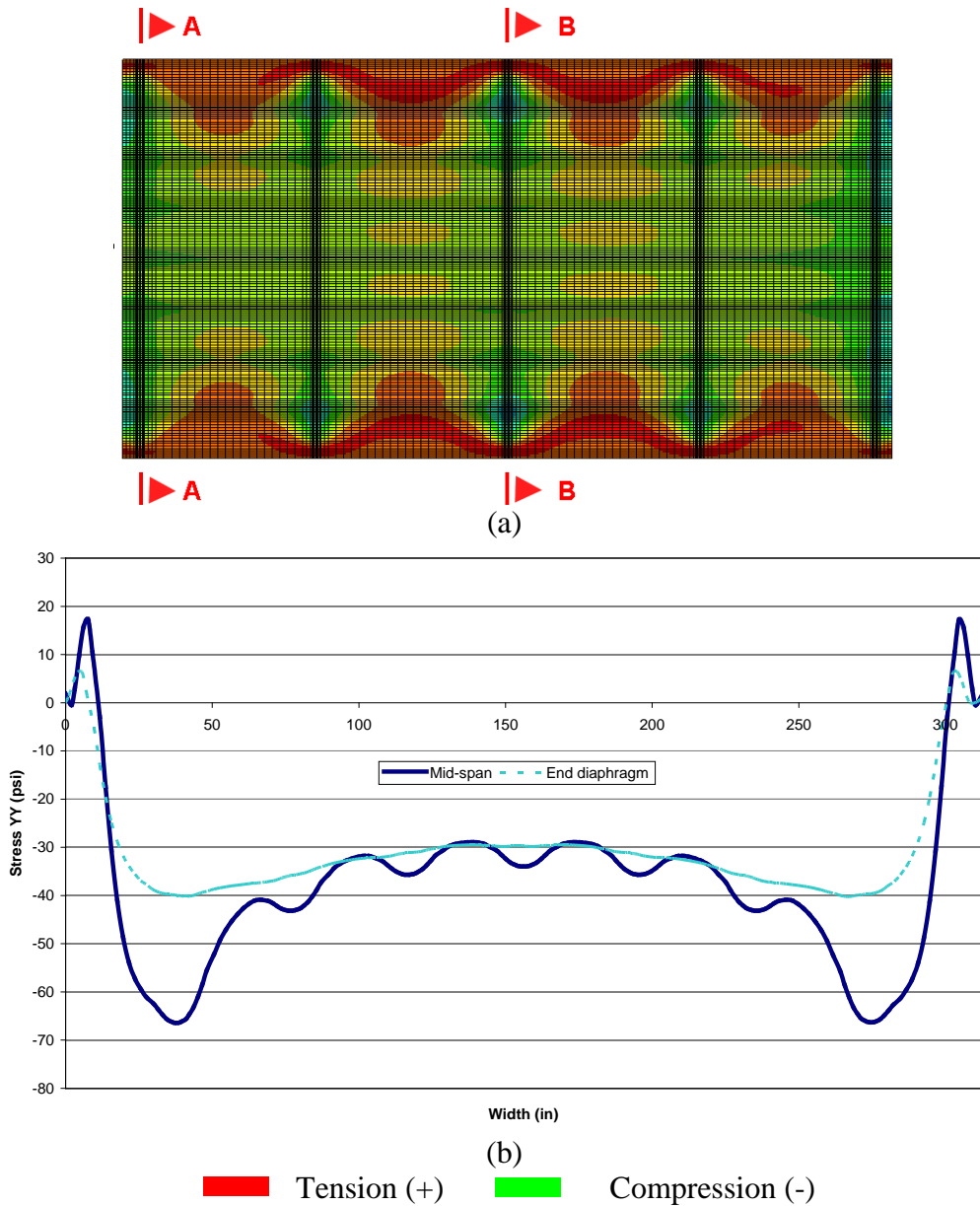


Figure 9-17. Transverse stress distribution (a) at the deck top surface and (b) along the width of the deck top surface over mid-span (Section B-B) and end-diaphragm (Section A-A) after second stage posttension

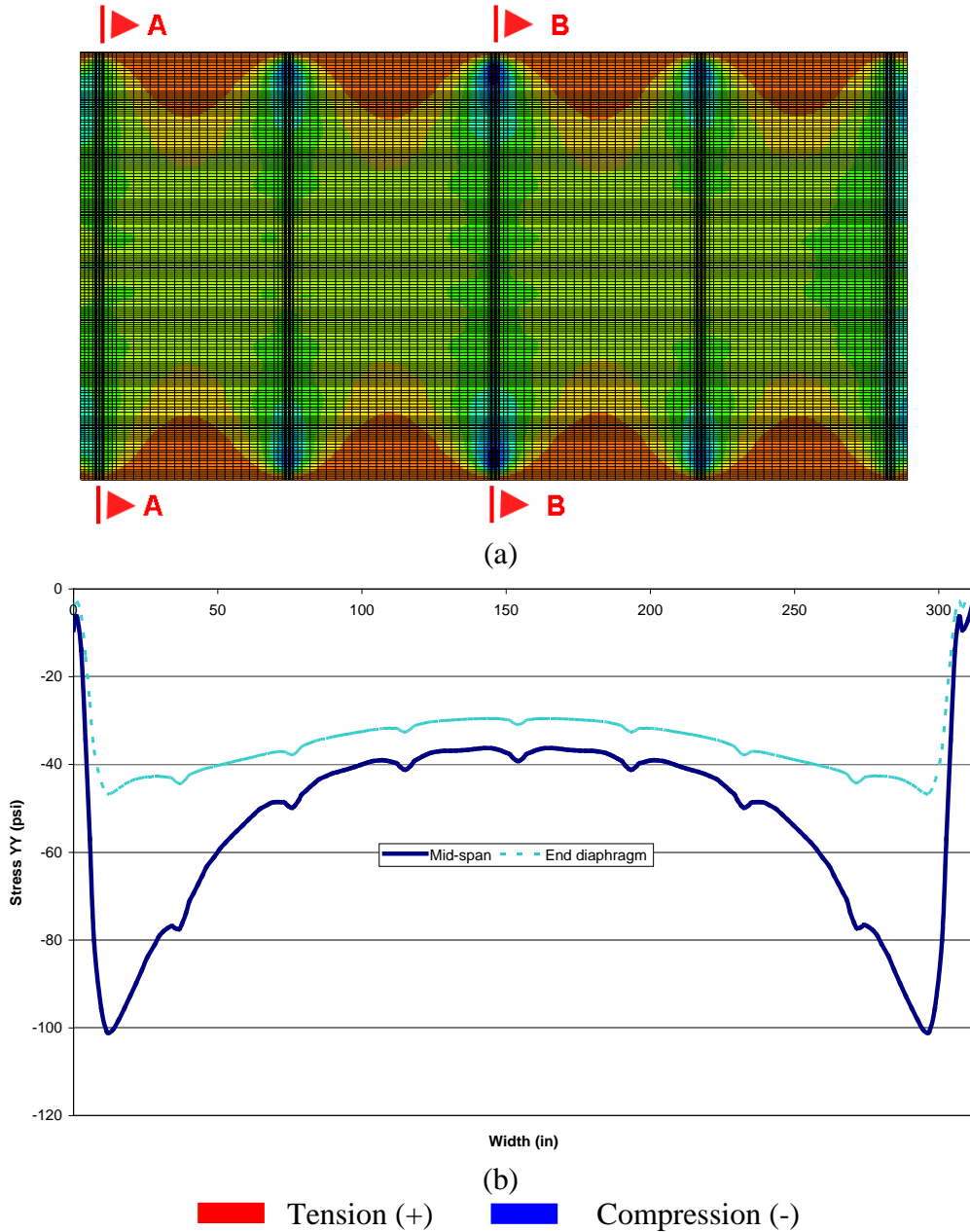


Figure 9-18. Transverse stress distribution (a) at the deck bottom surface and (b) along the width of the deck bottom surface over mid-span (Section B-B) and end-diaphragm (Section A-A) after second stage posttension

Stage 7: Barriers are placed

Analysis in Chapter 8 showed that with single-stage posttension application (current MDOT practice), barrier loads generated tensile stresses within the 6-in thick cast-in-place concrete deck, particularly close to interior beams at mid-span. During this analysis step, barrier load is applied to the structure that is posttensioned following the proposed two-staged procedure. The maximum compressive stress within the 6-in. thick concrete deck remains at 75 psi; whereas

tensile stress magnitudes are increased to 14 psi from 6 psi (Figure 9-19). Also, clamping compressive stress in shear keys between the fascia and the first interior beams increases to 241 psi from 231 psi; whereas tensile stress remains at 8 psi.

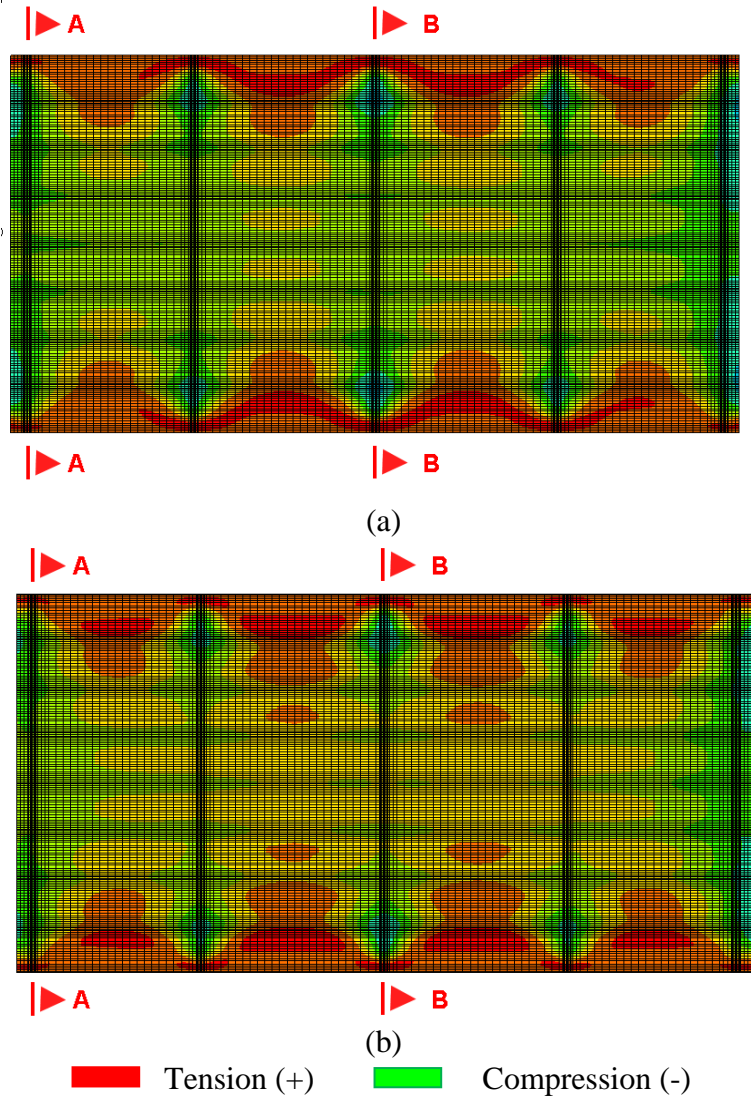


Figure 9-19. Transverse stress distribution at the cast-in-place concrete deck top surface (a) before and (b) after the barriers are placed

9.5.1 Service Load Analysis

Service I load combinations utilized in the analysis are as follows:

- Combo 1: 1.0 DEAD + 1.0 NTG
- Combo 2: 1.0 DEAD + 1.0 PTG
- Combo 3: 1.0 DEAD + 1.0 LL

where

NTG: Negative thermal gradient loading

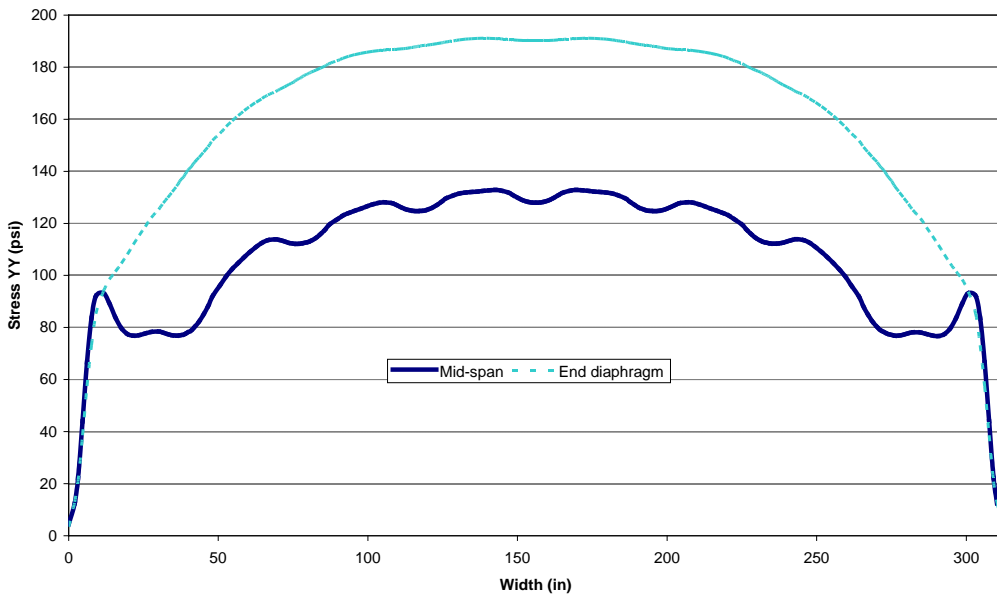
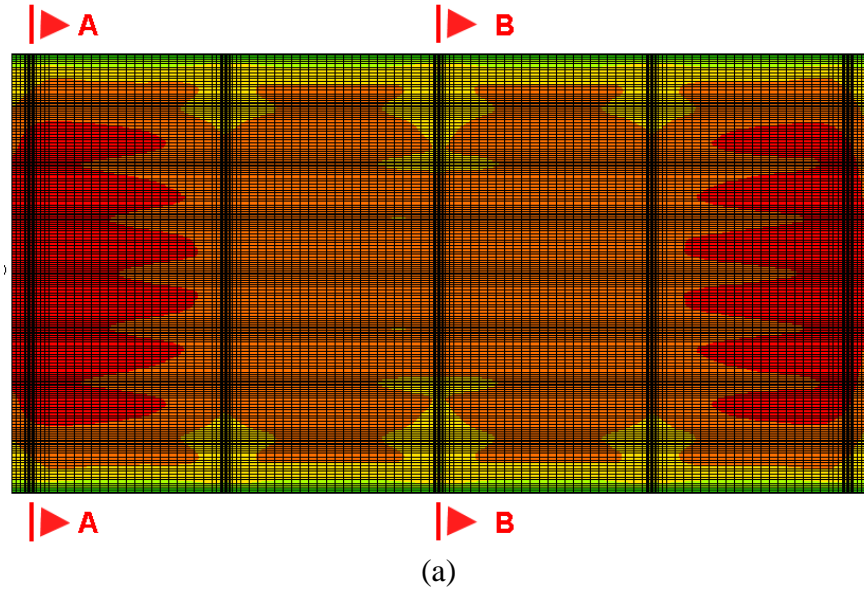
PTG: Positive thermal gradient loading

DEAD: Dead load of all components

LL: HL-93 live load with impact and multiple presence factors

9.5.1.1 Load Combination 1: 1.0 DEAD + 1.0 NTG

Negative thermal gradient loading is applied to the composite beam-shear key-deck assemblage while the stresses generated under dead loads are retained. Transverse stress distribution at the deck top surface is given in Figure 9-20 (a), and the stress variations at selected sections along the width of the top surface are given in Figure 9-20 (b). Transverse tensile stress of 160 psi is calculated at mid-span close to the interior girders in single-stage posttension application (i.e., according to current MDOT practice). These stresses are decreased to 130 psi in the staged posttension application. Tensile stress of 230 psi documented over the end-diaphragms with single-stage posttension is also decreased to 190 psi when the proposed two-stage posttension is applied. Tensile stresses that are developed at the bottom face of the 6-in cast-in-place slab with single-stage posttension are now completely diminished (Figure 9-21b). Clamping stresses developed in the shear keys are minimally affected by the negative thermal gradient loading. The maximum clamping compressive stress at the shear key located between fascia and the first interior beams is decreased to 217 psi from 241 psi, whereas tensile stress remains at 8 psi.



(b)

■ Tension (+) ■ Compression (-)

Figure 9-20. Transverse stress distribution (a) at the top surface of the deck and (b) along the width of the deck top surface over mid-span (Section B-B) and end-diaphragm (Section A-A) under service I load combination 1

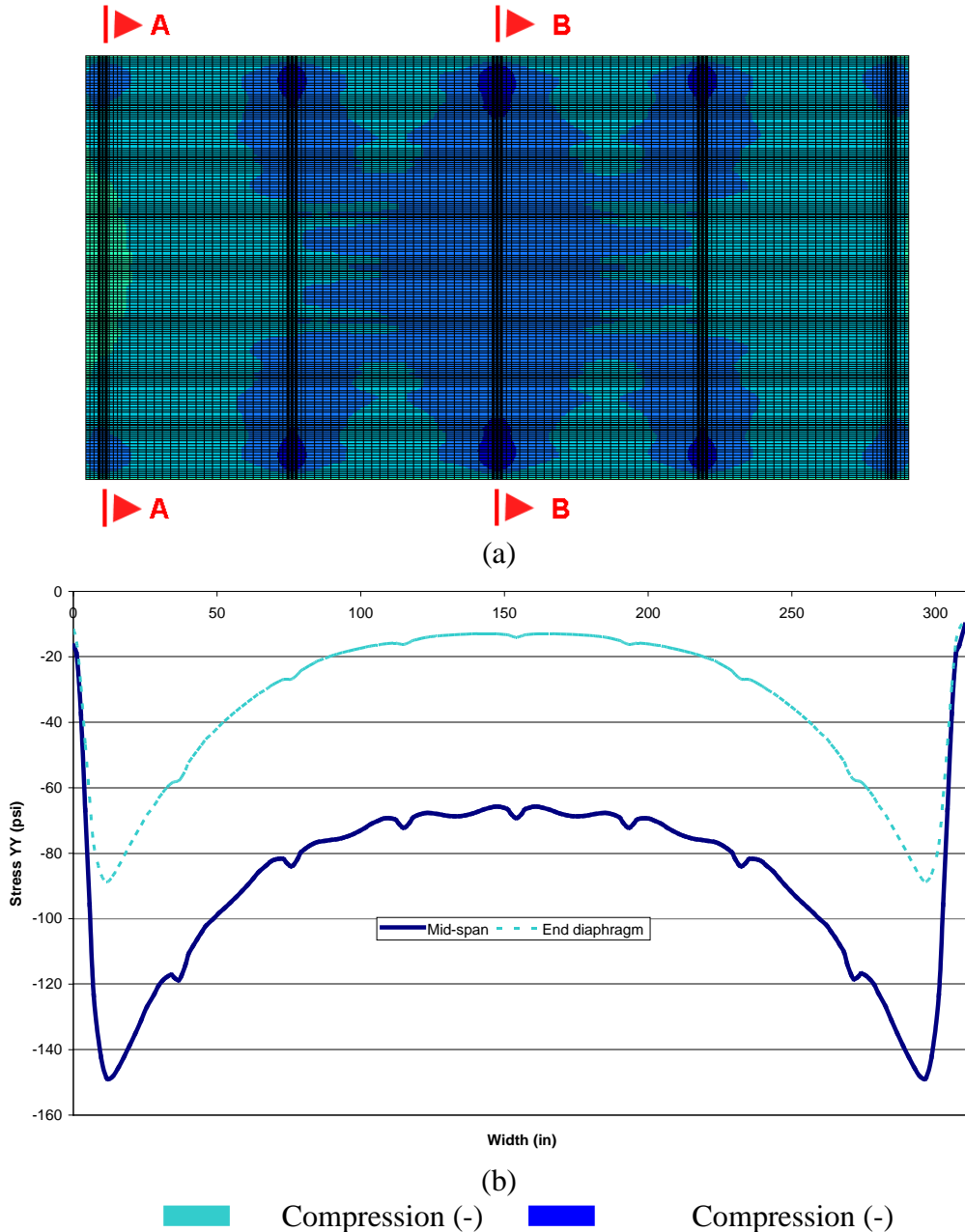


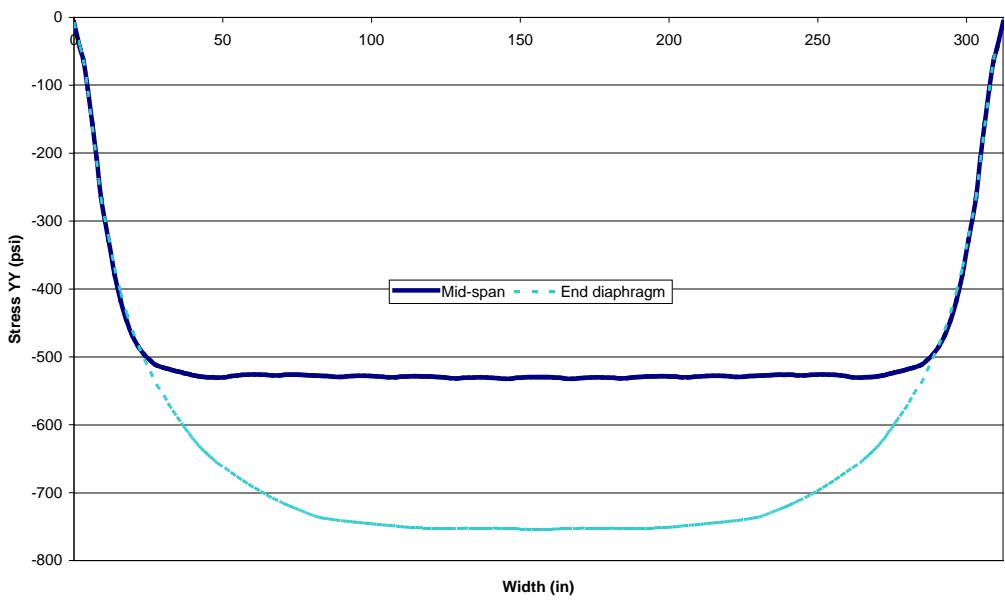
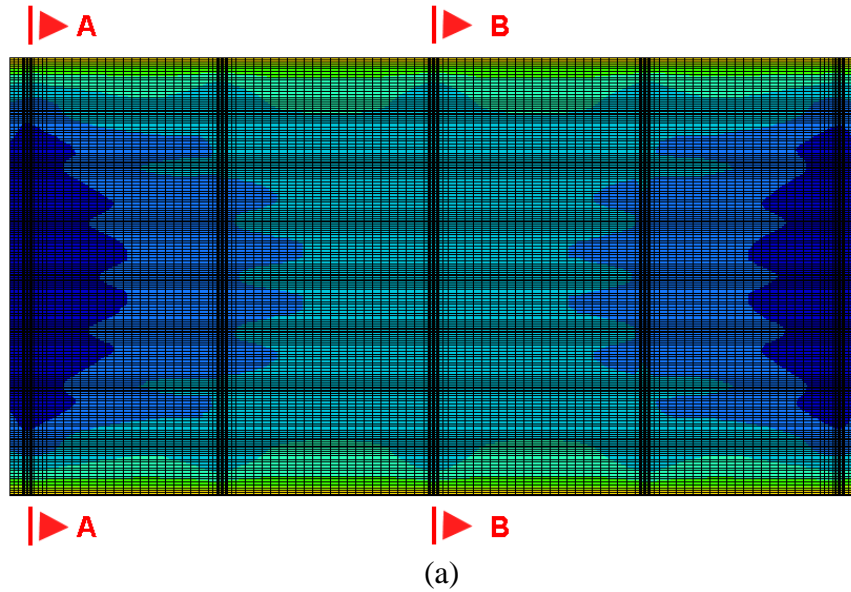
Figure 9-21. Transverse stress distribution (a) at the bottom surface of the 6-in thick deck and (b) along the width of the deck bottom surface over mid-span (Section B-B) and end-diaphragm (Section A-A) under service I load combination 1

9.5.1.2 Load Combination 2: 1.0 DEAD + 1.0 PTG

Negative thermal gradient loading is removed, and positive thermal gradient loading is applied to the composite beam-shear key-deck assemblage while the stresses generated under dead loads are retained. The deck top surface is now uniformly under compression (Figure 9-22) while tensile stresses form at portions of the 6-in. thick deck bottom surface (Figure 9-23).

Compressive stress magnitudes calculated at the top surface of the deck under single-stage posttension are increased by more than 30 psi when two-stage posttension is implemented. The maximum transverse tensile stress magnitude of 166 psi developed at mid-span during single-stage posttension is now decreased to lower than 100 psi. At end diaphragm locations, only at locations close to the fascia beams, tensile stresses are observed with a maximum magnitude of 106 psi (Figure 9-23b).

The application of positive gradient loading affects the clamping stresses in the shear keys between the fascia and the first interior beams. The maximum tensile stress magnitudes at the top of grout layers located between the fascia and the first interior beams increased to 100 psi from -10 psi (Figure 9-24). For this particular load case, precompressing the deck did not help reduce the tensile stress magnitudes developed at the top of shear keys.



■ Tension (+) ■ Compression (-)

Figure 9-22. Transverse stress distribution (a) at the top surface of the deck and (b) along the width of the deck top surface over mid-span (Section B-B) and end-diaphragm (Section A-A) under service I load combination 2

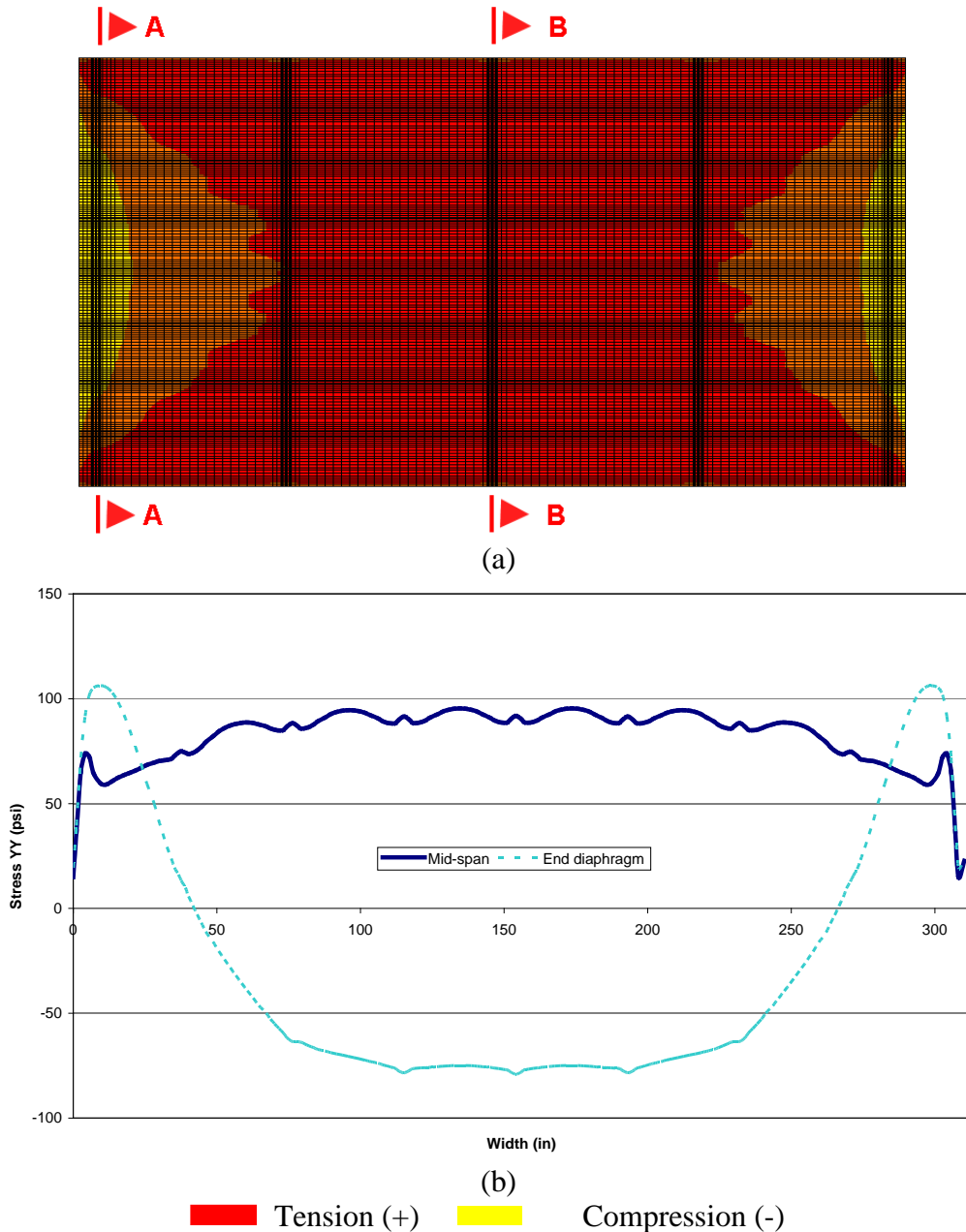


Figure 9-23. Transverse stress distribution (a) at the bottom surface of the cast-in-place deck and (b) along the width of the deck bottom surface over mid-span (Section B-B) and end-diaphragm (Section A-A) under service I load combination 2

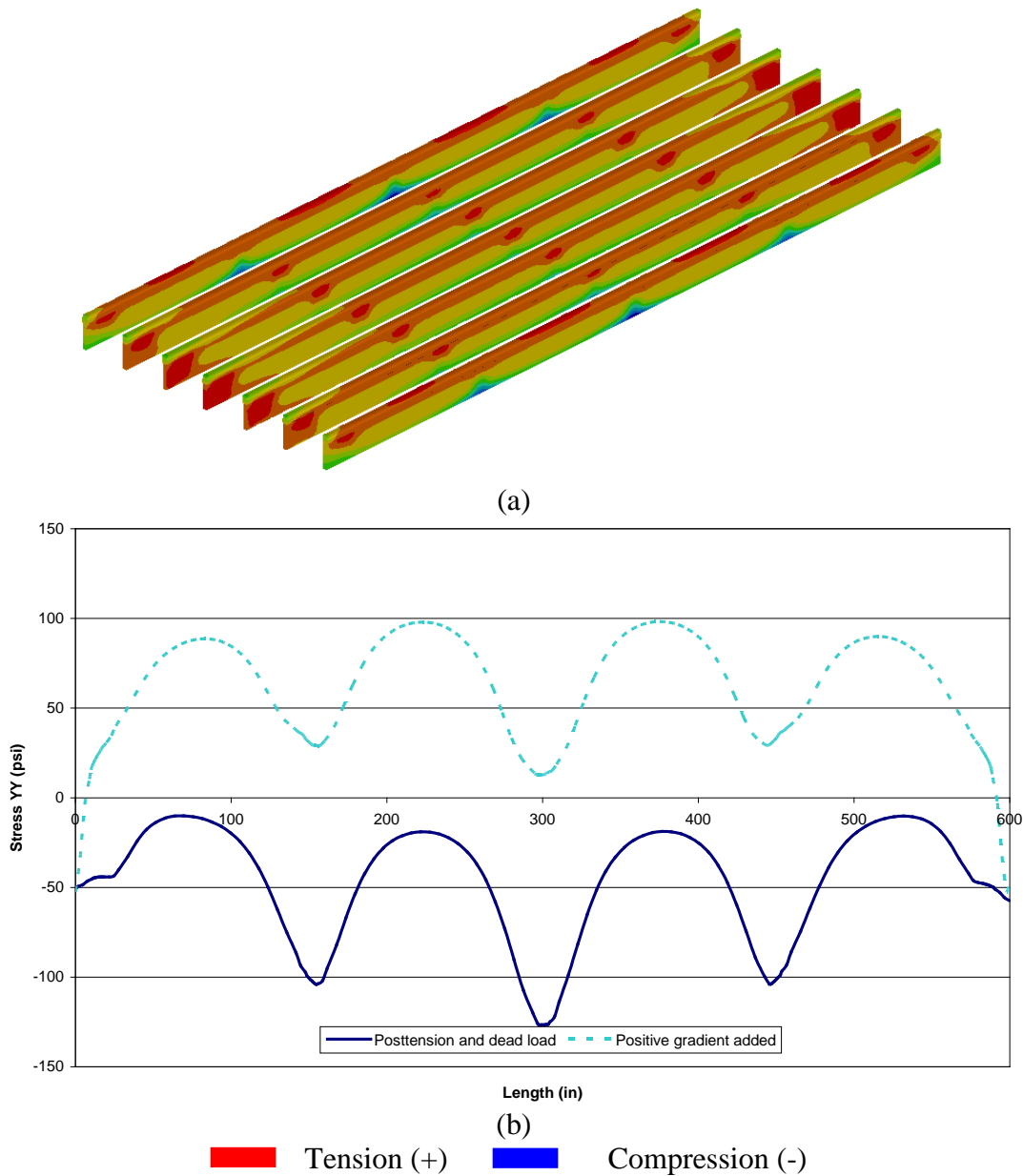


Figure 9-24. Clamping stress (a) profile on grout layers under positive thermal gradient loading and (b) distribution along the length of grout layers with and without positive gradient loading (stress plots are extracted using shear key top fiber nodes; compression-negative, tension-positive)

9.5.1.3 Combination 3: 1.0 DEAD + 1.0 LL

Single-Lane Loaded

At this step, the thermal gradient load is removed, and the HL-93 load is applied on a single lane of the bridge while the dead load stresses generated in the earlier stages are retained. The maximum transverse tensile stress at the top surface of the deck over the end diaphragm is decreased to 12 psi from 30 psi; whereas it is reduced from 20 psi to 11 psi at mid-span (Figure

9-25). Transverse tensile stresses are completely diminished at the cast-in-place deck bottom surface (Figure 9-26). Grout clamping stresses do not change significantly under a single lane live load. On the grout layers between the fascia and the first interior beams, the maximum compressive clamping stress is increased to 273 psi from 241 psi; whereas tensile stress magnitude is increased to 10 psi.

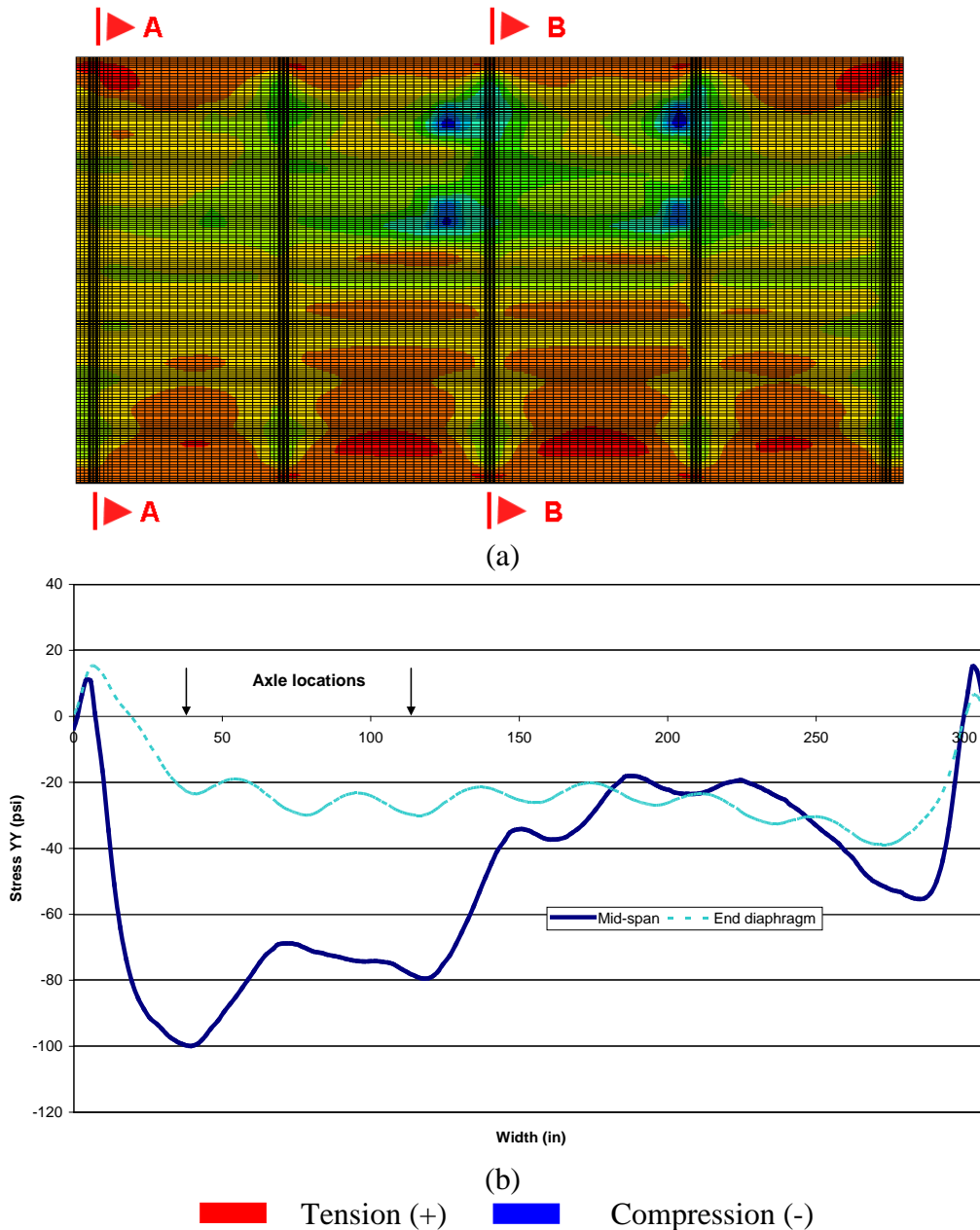


Figure 9-25. Transverse stress distribution (a) at the deck top surface and (b) along the width of the deck top surface over mid-span (Section B-B) and end-diaphragm centerline (Section A-A) under service I load combination 3 with a single lane live load

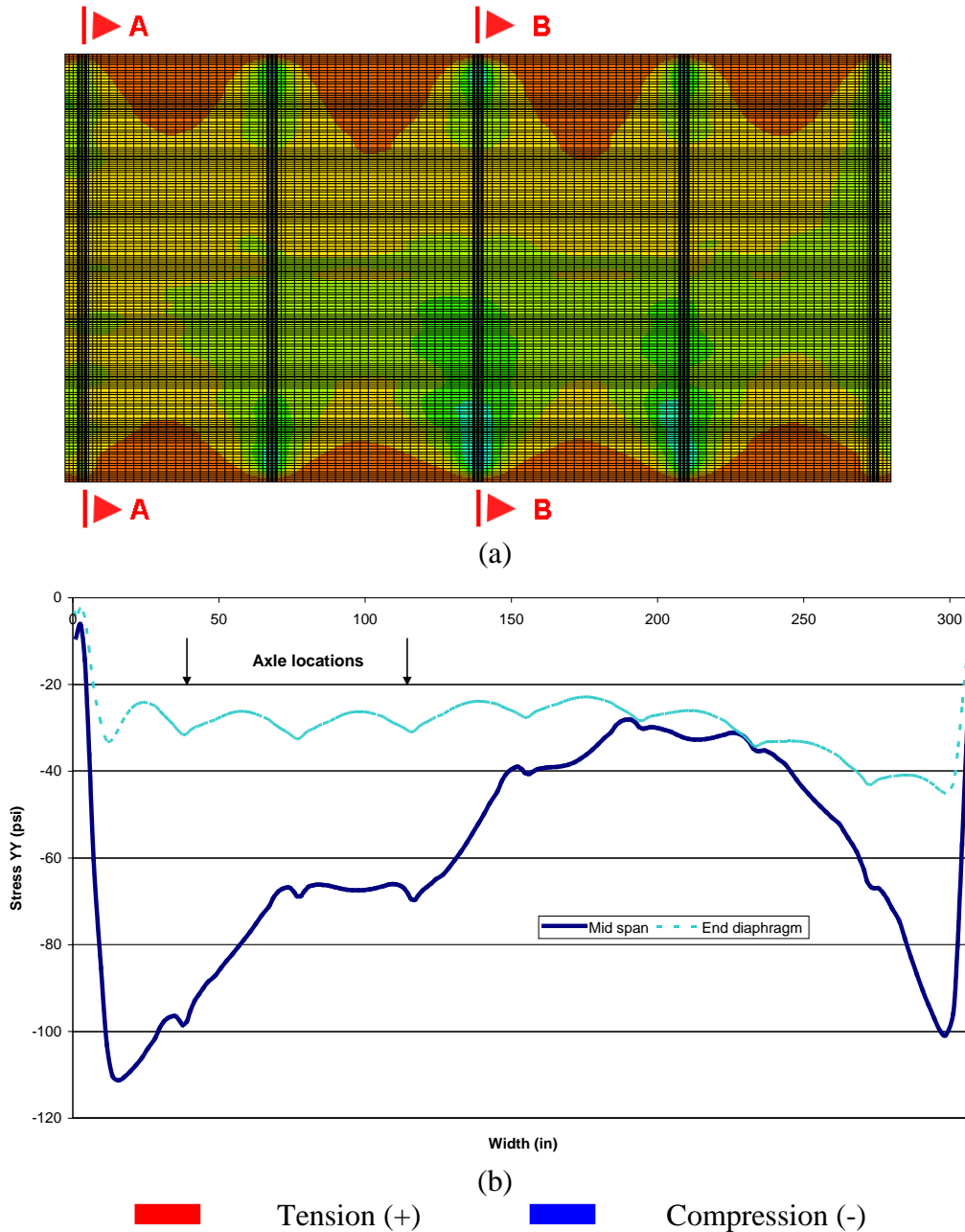


Figure 9-26. Transverse stress distribution (a) at the 6-in. deck bottom surface and (b) along the width of the deck bottom surface over mid-span (Section B-B) and end-diaphragm centerline (Section A-A) under service I load combination 3 with a single lane live load

Two-Lane Loaded

With the live load on both lanes of the bridge, mid-span regions of both top and bottom surfaces of the 6-in thick deck are now under compression. Transverse tensile stresses at the deck top surface and at specific concentrated locations are observed with a maximum of 21 psi (Figure 9-27-a). The entire bottom surface of the cast-in-place deck is under compression (Figure 9-28).

Under this load combination, grout clamping stresses do not change significantly. On the grout layers between the fascia and the first interior beams, the maximum compressive clamping stress is increased to 248 psi from 241 psi, and tensile stress magnitude remained at 10 psi.

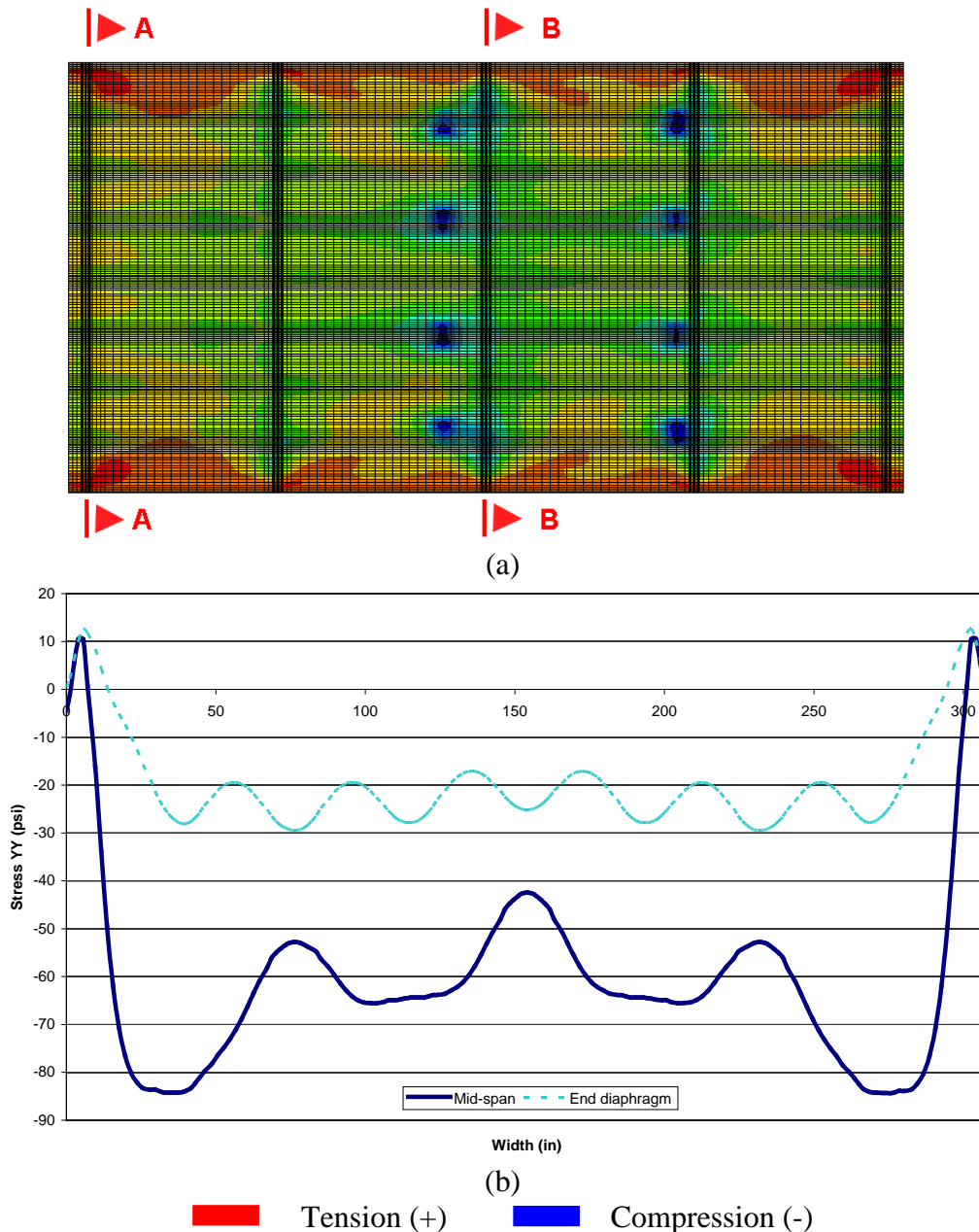


Figure 9-27. Transverse stress distribution (a) at the deck top surface and (b) along the width of the deck top surface over mid-span (Section B-B) and end-diaphragm (Section A-A) under service I load combination 3 with live load on two lanes

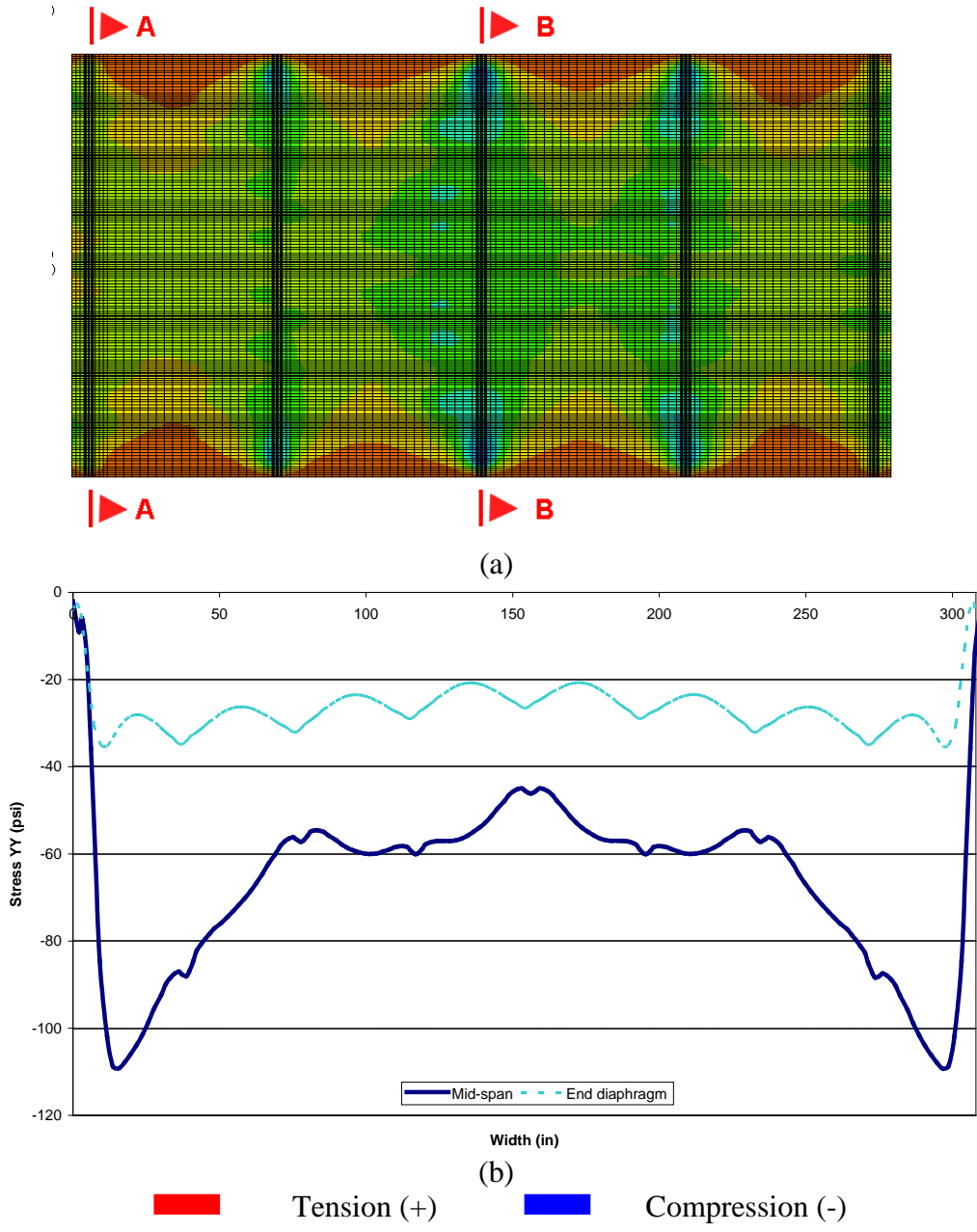


Figure 9-28. Transverse stress distribution (a) at the 6-in. deck bottom surface and (b) along the width of the deck bottom surface over mid-span (Section B-B) and end-diaphragm (Section A-A) under service I load combination 3 with live load on two lanes

9.6 SUMMARY AND CONCLUSIONS

In order to identify and document the longitudinal reflective deck crack initiation and progression, the bridge that carries Oakland Drive over I-94 in Portage, Michigan was monitored during construction. Cracks along the beam-shear key interface were observed before posttensioning and remained cracked after posttension. Cracks that stemmed from the top surface of the deck above the abutments were documented before any live or barriers loads. An analysis model, herein referred to as the macromechanical model was presented. The analysis model is suitable for calculating the required posttension levels using the concepts of mechanics of materials and macromechanics. Based on the results of the macromechanical model analysis, further FE analysis was performed evaluating the effects of staged posttension application on the deck and grout stresses.

Stress analyses of the single-stage and two-stage posttension are compared to document the effectiveness of two-stage posttension. Under thermal gradient loads, transverse stresses along the bottom surface of the deck and at the top deck surface undoubtedly diminished with the application of two-stage posttension (Figure 9-29 and Figure 9-30). Observed deck top surface tensile stresses at mid-span and end-diaphragm locations with single-stage posttension and single lane live load are completely diminished (Figure 9-31). With two-stage posttension, tensile stresses only developed at regions within the proximity of the fascias.

The application of second stage of posttension following deck placement reduced deck stresses under dead and live loads. A similar benefit is not observed under positive gradient loading and transverse tensile stress magnitudes calculated along the top of the shear keys closest to fascias increased by 5 psi. Compressive stress magnitudes decreased by about the same amount (Figure 9-32).

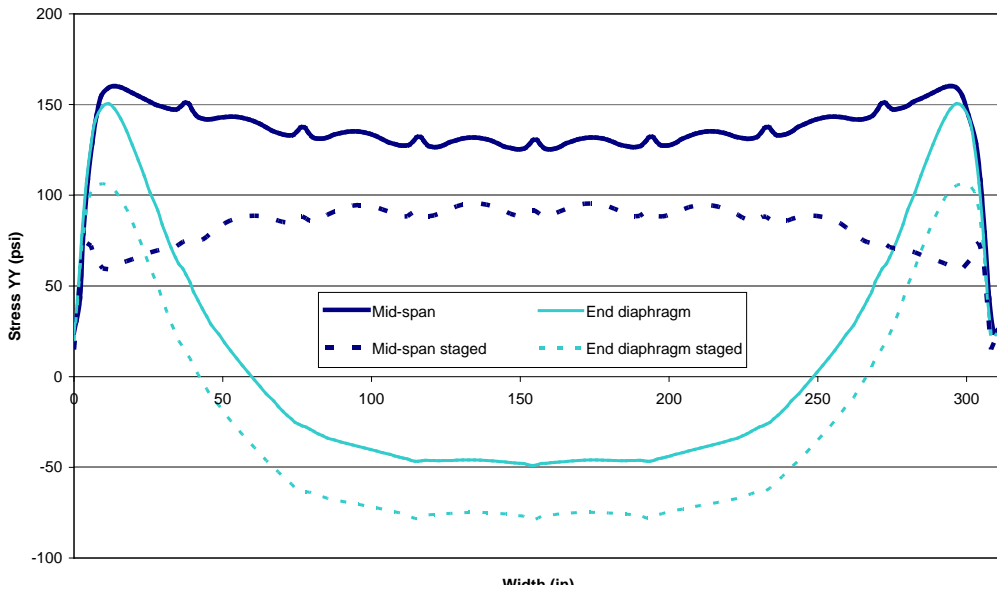


Figure 9-29. Transverse stress distribution along the width of the 6-in cast-in-place concrete deck bottom surface with and without staged posttension under service I load combination 2

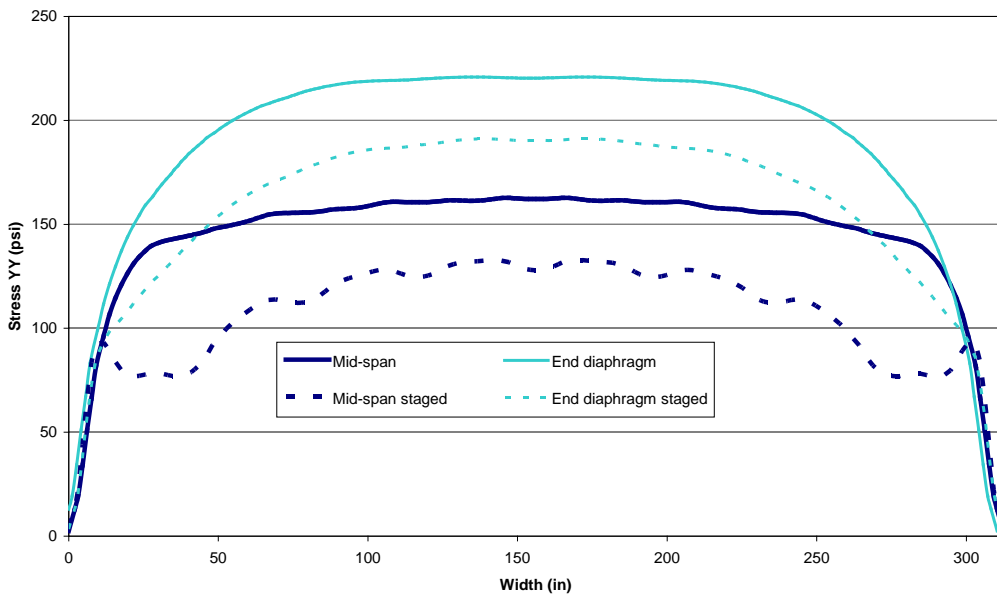


Figure 9-30. Transverse stress distribution along the width of the deck top surface with and without staged posttension under service I load combination 1

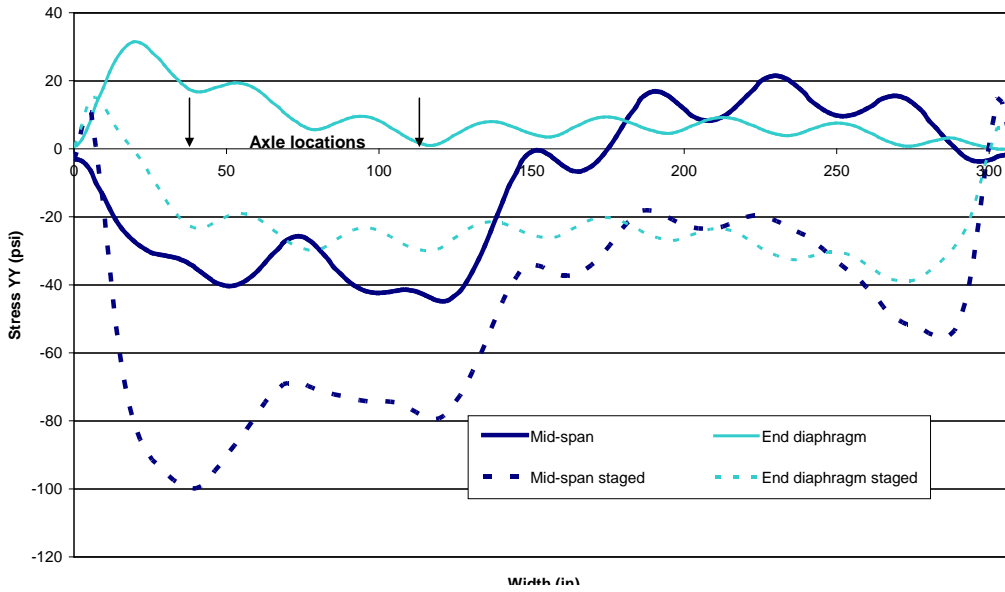


Figure 9-31. Transverse stress distribution along the width of the deck top surface with and without staged posttension under service I load combination 3 with a single lane live load

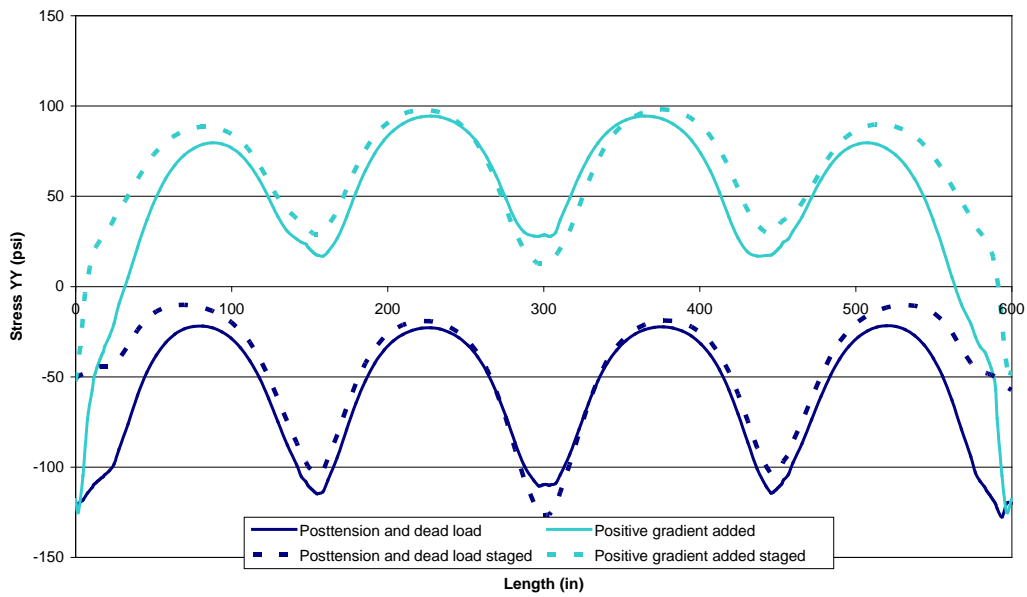


Figure 9-32. Clamping stress distribution along the length of the shear key top surface with and without staged posttension under positive gradient loading

The following conclusions and recommendations are generated from the derivations and analyses presented in this chapter:

1. The macromechanical model, once the ABDE matrices are provided, becomes a very useful and simplified tool in developing an analysis model for orthotropic deck systems such as the side-by-side box-beam bridge decks.
2. The critical moment and shear along the shear keys can be calculated from the analysis results obtained from the macromechanical models of the side-by-side box beam bridge.
3. The critical moments and shear along the shear keys can be used for calculating the transverse posttension requirements based on the proposed service criteria of zero tensile stress on the deck under gravity loading. This process will most likely abate reflective deck cracking.
4. A two-stage transverse posttensioning is recommended corresponding to before and after the six-inch concrete deck is placed.
5. Transverse tensile deck stresses that occur under live load can be eliminated except at specific isolated regions within the proximity of the fascias when recommended two-stage posttensioning is implemented.
6. There is no effective way of reducing tensile stresses in the deck that occur under positive thermal gradient loading.

10 CAPACITY EVALUATION OF A BOX-BEAM BRIDGE WITH DISTRESSED BEAMS

10.1 OVERVIEW

The objective of finite element (FE) modeling and analysis of distressed beams is to simulate various damaged scenarios under dead and live loads. Rating trucks recommended in the MDOT Analysis Guide (2003) and the AASHTO LRFR (2003) are used. Simulation of beam damage scenarios in a full bridge superstructure model helps develop recommendations for load rating considering the structural system interaction rather than the behavior of a single box-beam.


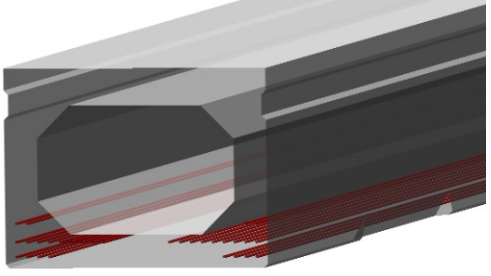

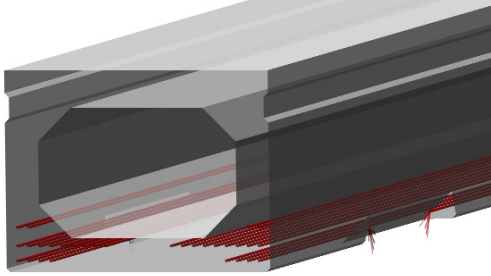

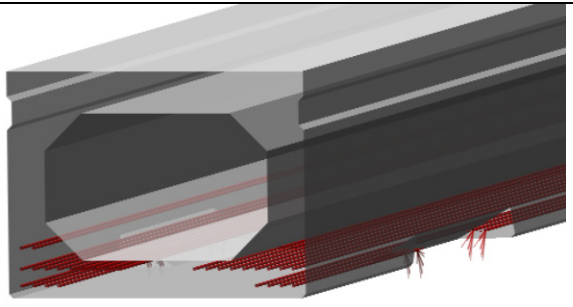
Distresses commonly observed during bridge inspections are incorporated into the full bridge FE models following similar procedures used in Phase I of this project. In the case of flexure critical models, distresses are incorporated at mid-span and quarter point locations of a beam. In the shear critical models, distresses are incorporated at beam ends. Concrete distress is modeled by gradually reducing the elasticity modulus from a depth of distress penetration to the surface. In the case of a broken tendon, strands are discontinued within the distress zone.

Four different distress levels are modeled (Table 10-1 and Table 10-2) again corresponding to the observed states during field inspection. Level one designates the undamaged sound box-beam. Level two is limited to the concrete section loss due to minor spall along bottom corners of a box beam cross-section. Level three designates similar spall as in level two but with one broken tendon within the distressed region. The distress length along the beam is taken as 50 inches for flexure and 17 inches for shear for both level two and three (Figure 10-1). Level four represents a major spall incorporating two broken tendons along the bottom corner of the distressed region. At level four, the length of distress along the beam is increased to 62 and 23 inches for flexure and shear critical models, respectively (Figure 10-2).

Table 10-1. Distress Level Summary in FE Analysis

Case	Distress Level Summary	Figure
1	Control condition; as built properties, no loss of prestressing strand.	None
2	Spall along bottom corner of box-beam. Length of spall is 50 inches and 17 inches for flexure critical and shear critical models, respectively.	Figure 10-1
3	Spall along bottom corner of box-beam. Length of spall is 50 inches and 17 inches for flexure critical and shear critical models, respectively. One broken tendon within distressed zone.	Figure 10-1
4	Spall along bottom corner of box-beam. Length of spall is 62 inches and 23 inches for flexure critical and shear critical models, respectively. Two broken tendons within distressed zone.	Figure 10-2

Table 10-2. Distress Observed During Field Inspection and Used in FE Models

Distress Level	Observed During Field Inspection	Finite Element Model
2		
3		
4		

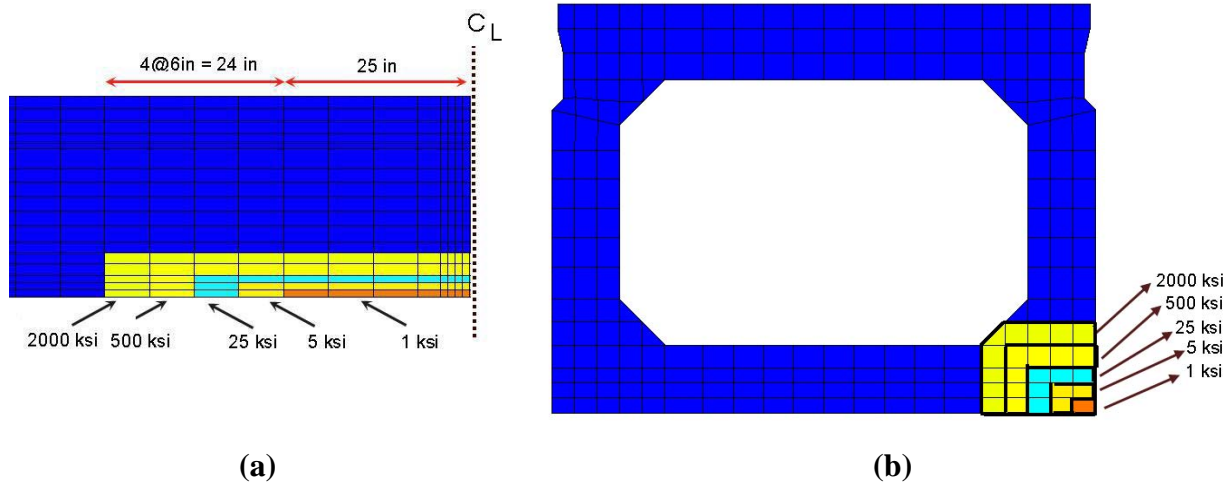


Figure 10-1. Finite element model of distress levels 2 and 3: (a) enlarged view of half of the distressed zone along length and (b) section view of the distressed zone (note: broken strands are not visible)

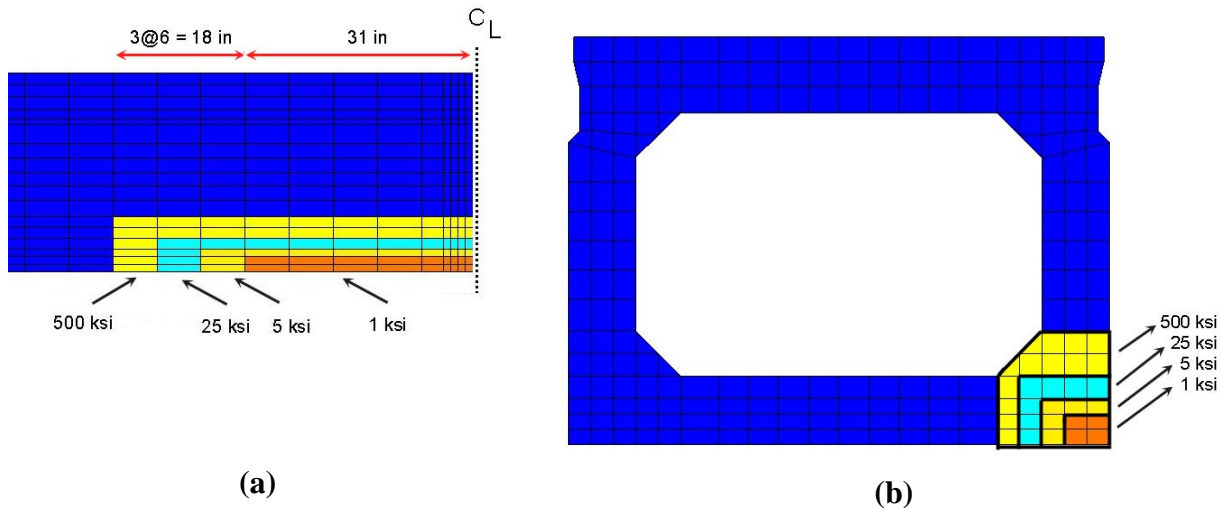


Figure 10-2. Finite element model of distress level 4: (a) enlarged view of half of the distressed zone along length and (b) section view of the distressed zone (note: broken strands are not visible)

This chapter also investigates the influence of posttension and grout loss in the shear key as another form of distress. The length of the grout void in shear keys due to loss of grout is taken equal to the length of the beam distress zone.

The details of the configuration and the material properties of a side-by-side box-beam bridge for construction simulation and service load analysis was given in Chapter 8. The same bridge configuration is used in this chapter for capacity evaluation and load rating following the AASHTO LRFR (2003) procedures. Michigan specific rating trucks are selected from the MDOT Bridge Analysis Guide (2003). According to the AASHTO LRFR (2003), the

methodology for the Load and Resistance Factor Rating (LRFR) of a bridge is comprised of three distinct procedures: (1) design load rating, (2) legal load rating, and (3) permit load rating (Figure 10-3).

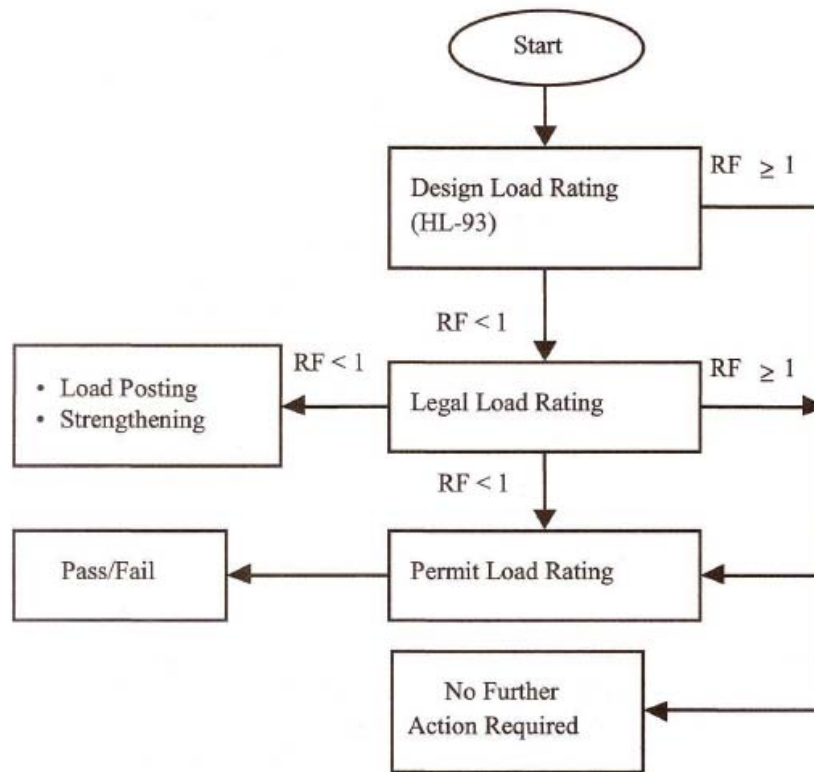


Figure 10-3. LRFR decision making flow chart (AASHTO LRFR 2003)

Design load rating serves as the first-level of load capacity assessment of existing bridges with respect to the design loads given in the AASHTO LRFD bridge design specifications. Permit load rating is required for the review of permit applications for a passage of vehicles with special axle configurations and/or weight limits. Legal load rating provides a safe load capacity for a given AASHTO or state specific truck configuration.

In this project, design load rating is performed using the AASHTO LRFD (2004) live load configuration (i.e., HL-93). Legal load configurations given in the AASHTO LRFR (2003) and the Michigan Bridge Analysis Guide (MDOT 2003) are considered for legal load rating. This analysis considers truck # 21 of the Michigan Bridge Analysis Guide, which shows that a moment of 769 k-ft with a weight of 151.4 kips and a moment/weight ratio of 5.08 governs the legal load rating for the bridge configuration. In both flexure and shear critical configurations,

truck positions generating maximum internal stress resultants (bending moment and shear) are established (Figure 10-4 through Figure 10-8). Analysis is performed by incrementally and uniformly increasing the HL-93 load while monitoring stresses within the fracture critical zone. The analysis is terminated when the tensile stress within the fracture critical zone reached the tensile stress limit.

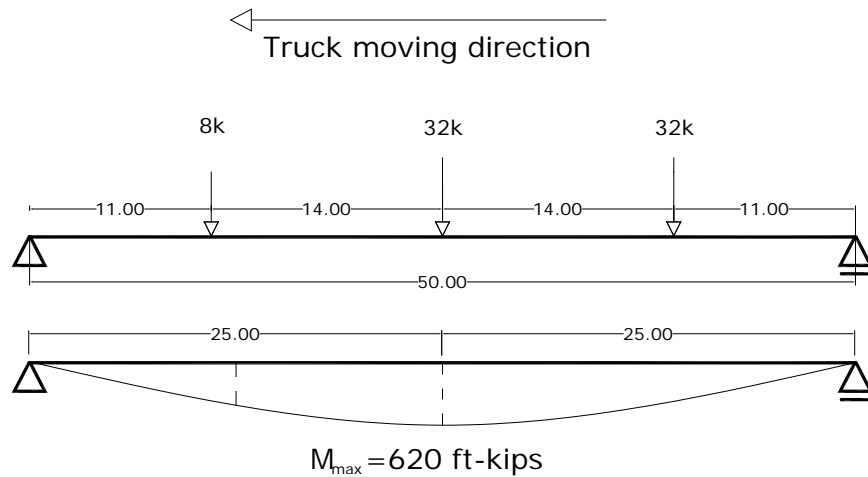


Figure 10-4. Axle load configuration of HL-93 generating maximum moment at mid-span (Note: Lane load that generates additional 200 ft-kips moment at mid-span is not shown)

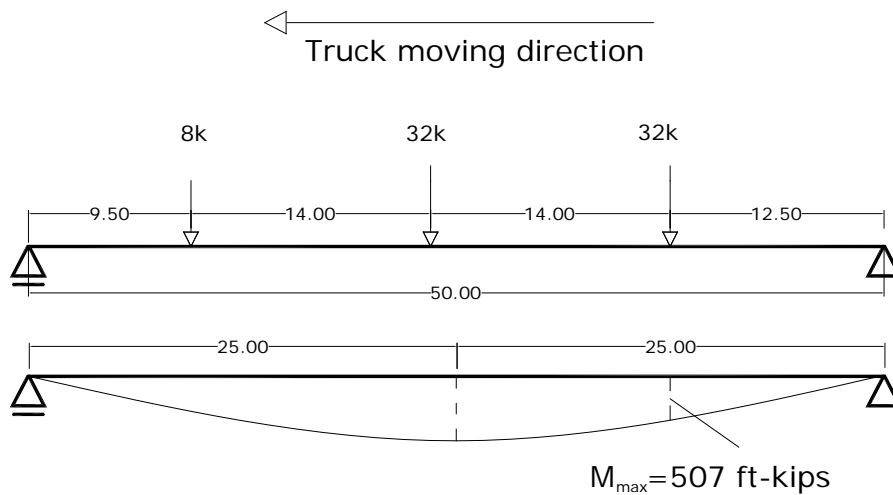


Figure 10-5. Axle load configuration of HL-93 generating maximum moment at quarter point (Note: Lane load that generates additional 150 ft-kips moment at quarter point is not shown)

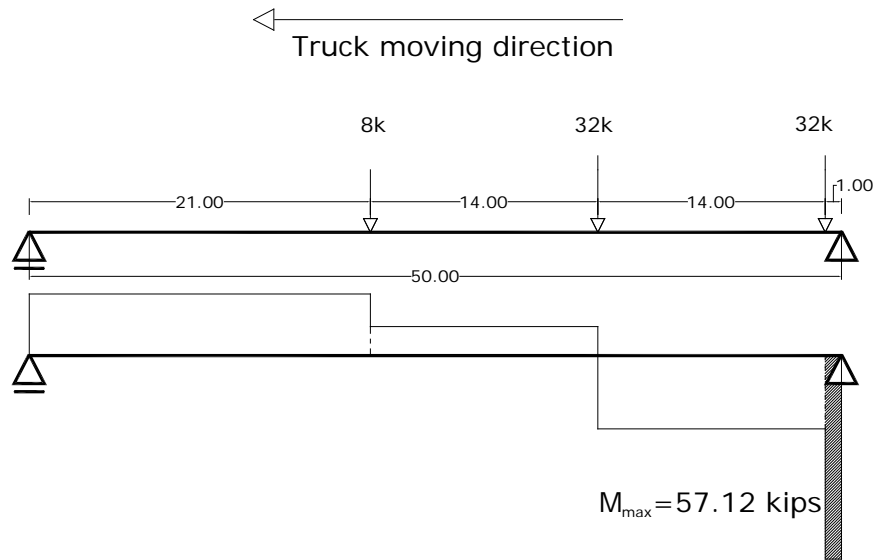


Figure 10-6. Axle load configuration of HL-93 generating maximum shear 1 ft away from the support (Note: Lane load that generates additional 15.36 kips shear 1 ft away from the support is not shown)

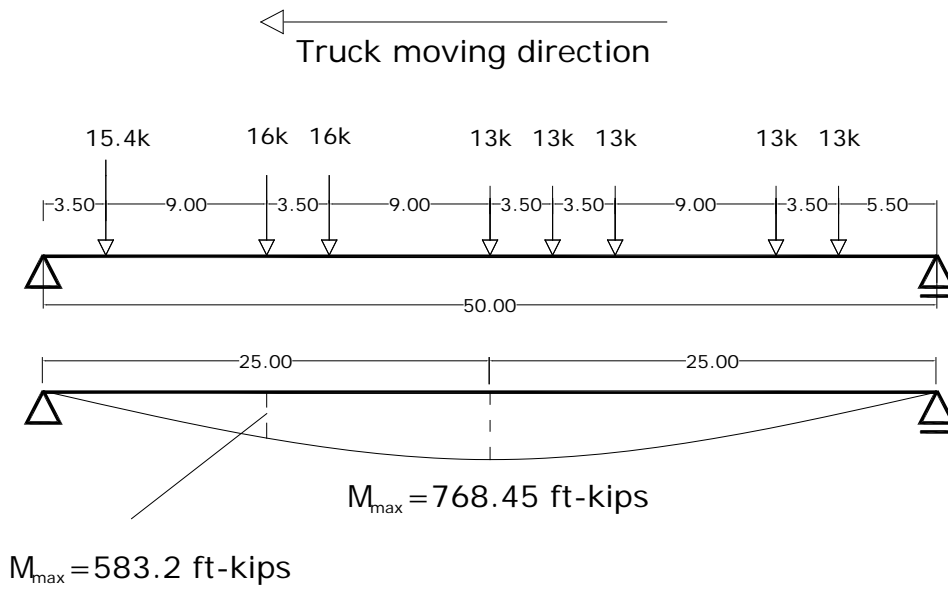


Figure 10-7. Axle load configuration of Truck 21 generating maximum moment at mid-span and quarter point

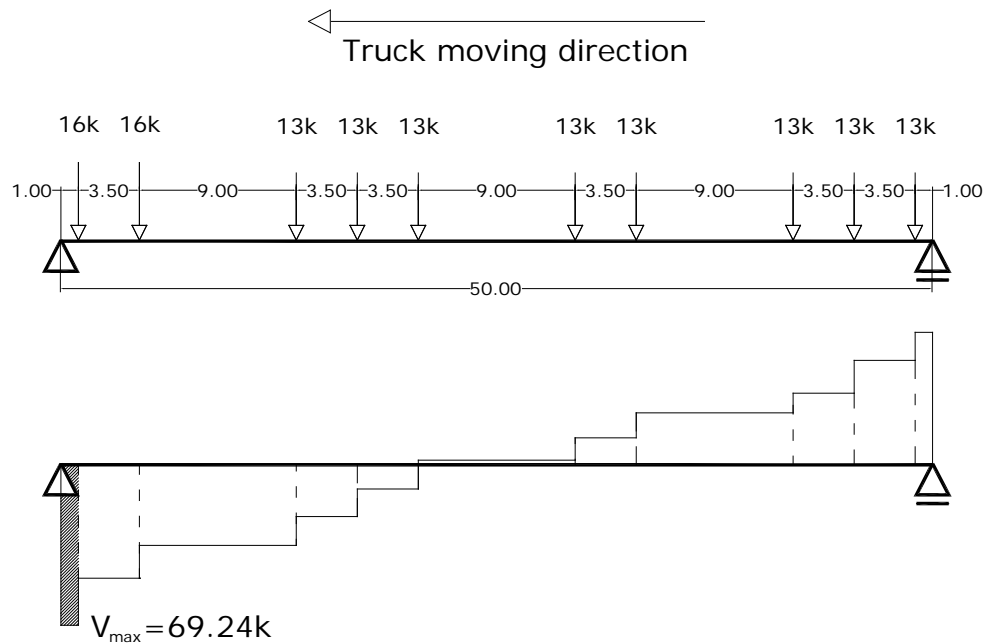


Figure 10-8. Axle load configuration of Truck 21 generating maximum shear 1 ft away from the support

The nonlinear nature of this bridge structural system also requires stages analysis. The first three steps of simulation included positioning box-beams, mortar grouting shear keys, and applying transverse posttension. Next, deck elements and barrier loads are activated resulting in the beam stresses due to the dead load of the structure. Finally, 150 percent of the live load is applied within six increments. This allows calculation of the beam stress levels at 25, 50, 75, 100, 125 and 150 percent of the live load. Design and evaluation is governed by Service III limit state. Hence, the maximum load applied on the bridge is determined when the beam stress reaches the threshold tensile stress limit of $0.19\sqrt{f'_c}$ (ksi). The moment acting on the beam is calculated using element stresses when maximum tensile stress limit is reached; hence the service moment capacity. It should be noted that live load demand is obtained when 100 percent of the live load is acting on the bridge, yet the bridge still may not have reached its ultimate capacity. The behavior is linearly elastic until the first crack occurs, and thus superposition is valid within the live load increments. This means, with the bridge response being D at the end of the dead load

step and (D+L) at the increment when 100 percent of the live load is acting, live load demand can be found by subtracting dead load demand from the total demand (i.e., $D+L-D = L$).

Beam capacities are defined independently for the flexure critical and shear critical beams. In flexural critical beams, live load capacity is defined as the percentage of truck load that generates a maximum tensile stress equal to the allowable tensile stress limit of $0.19\sqrt{f'_c}$, for moderate corrosion conditions, at or near the bottom fibers (AASHTO LRFD Section 5.9.4.2). In shear critical beams, the fracture critical zone is defined between 12 to 21 inches from the support. Within this zone, principal stresses are calculated. The beam live load capacity is defined as the percentage of truckload generating a maximum tensile principal stress of $0.19\sqrt{f'_c}$ on the web and within the fracture critical zone.

10.2 FLEXURE CRITICAL DISTRESS AND ASSOCIATED BOX BEAM CAPACITIES

The stress and deformation calculations under dead and live loads are performed assuming elastic behavior of both materials (prestressing steel and concrete). Distress types discussed in Table 10-1 and Table 10-2 are incorporated into a fascia beam of a full bridge model (Figure 10-9). Live loads applied to the FE models are scaled to a proportion of the live load that would generate the allowable tensile stress of 424 psi ($0.19\sqrt{f'_c}$ ksi for 5 ksi concrete).

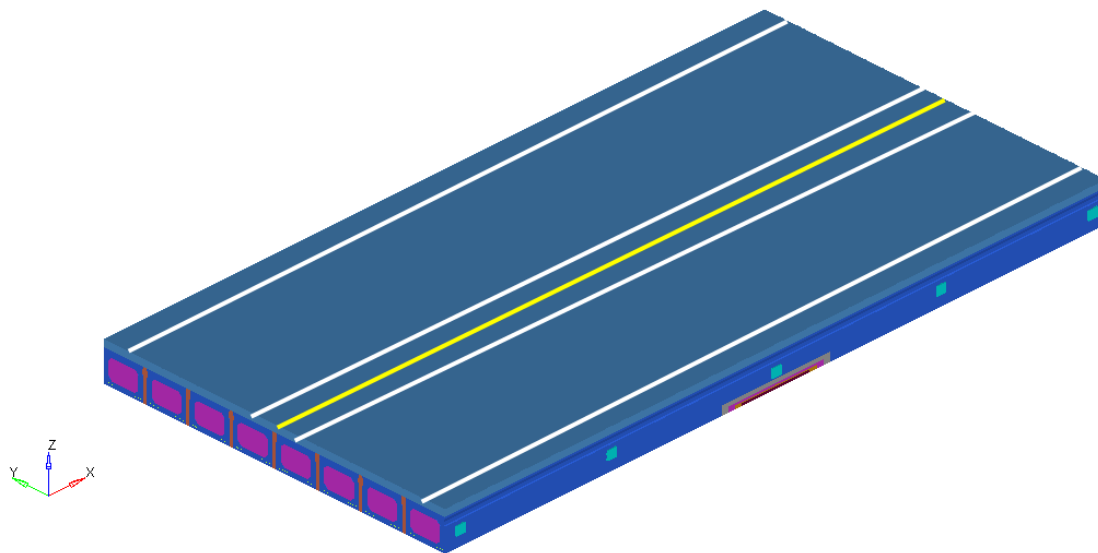


Figure 10-9. 3D view of the model showing distress on fascia beam and design lanes

Table 10-3 shows the service moment capacities calculated from the sectional stress distribution obtained from the FE analysis. The moment capacities are calculated at critical cross-sections by taking moments about the strand axis utilizing the longitudinal element stresses. Critical cross-sections are 13 inches away from the mid-span and the quarter points to avoid interfering with the solid diaphragms. In calculating moment capacities, contribution of concrete tensile stresses is neglected. It should be noted that when the tensile stresses below the neutral axis are neglected, assuming a cracked section, the resulting moment capacities calculated from sectional analysis will be lower than equivalent static moment values..

Table 10-3. Service Moment Capacities for Box-beams at Various Distress Levels (ft-kips)

Level	Beam condition	Service moment capacities of beam with distress at specified locations			
		Live load			
		HL-93		Truck 21	
		Distress location		Distress location	
		Mid-span	Quarter point	Mid-span	Quarter point
1	Undamaged	609	610	610	610
2	Spall	594	611	596	610
3	Spall + 1 broken tendon	559	615	560	615
4	Spall + 2 broken tendons	522	616	524	615

According to Table 10-3, when the distress is at the mid-span, the moment capacity of the section decreases with increasing level of distress. When the distresses are at the quarter point, greater live loads are required to reach the threshold tensile stress level of 424 psi at the beam bottom flange, thus the beam capacity remains practically unchanged (610 – 616 ft-kips). According to the analysis results, the quarter point distress does not control beam capacity. When simulating distress levels 3 and 4, FE models allowed redevelopment of strands beyond the distress regions. However, there are no studies on strand redevelopment, and it is advised to remove strands when evaluating beam capacity with broken strands.

It should also be noted that, in calculating the service moment capacity from the FE analysis results, prestressing strand stress (f_{pe}), after all losses, is taken as 163.4 ksi. In the AASHTO LRFR strength limit state, the average stress in prestressing steel at the time for which the

nominal resistance of the member required (f_{ps}) should be used. For the cross-section, this value is calculated analytically as 262 ksi with the following formulas:

$$f_{ps} = f_{pu} \left(1 - k \frac{c}{d_p}\right) \quad (10-1)$$

$$c = \frac{A_{ps} f_{pu}}{0.85 f_c' \beta_1 b + k A_{ps} \frac{f_{pu}}{d_p}} \quad (10-2)$$

Where:

A_{ps} = area of prestressing steel (1.53 in²)

b = width of beam (36 in.)

c = distance from the extreme compression fiber to neutral axis (for rectangular section behavior)

d_p = distance from the extreme compression fiber to the centroid of prestressing tendons (31 in.)

f_c' = specified concrete compressive strength at 28 days (5 ksi)

f_{pe} = average stress in prestressing steel after all losses (163.4 ksi)

f_{ps} = average stress in prestressing steel at the time for which the nominal resistance of member is required

f_{pu} = specified tensile strength of prestressing steel (270 ksi)

k = factor used in calculation of average stress in prestressing steel for Strength Limit State (0.28 for low-relaxation strands)

β_1 = factor for concrete strength (0.8)

Then, the nominal flexural capacity of the section is calculated analytically as 992 ft-kips with;

$$M_n = A_{ps} f_{ps} \left(d_p - \frac{\beta_1 c}{2}\right) \quad (10-3)$$

The nominal moment capacities of box beams with various distress levels are shown in Table 10-4. Although the section is selected 13 inches away from the mid-span of the FE model,

nominal moment capacity of the undamaged beam, calculated using FE analysis results, is 98 percent accurate when compared with the analytical results (i.e. $976/992 \times 100 = 98.3\%$).

Table 10-4. Nominal Moment Capacities of Box-beams with Various Distress Levels (ft-kips)

Level	Beam condition	Nominal moment capacities of beam with distress at specified locations			
		Live load			
		HL-93 loading		Truck 21	
		Distress location		Distress location	
		Mid-span	Quarter point	Mid-span	Quarter point
1	Undamaged	976	979	979	979
2	Spall	953	979	956	979
3	Spall + 1 broken tendon	896	986	898	986
4	Spall + 2 broken tendons	838	987	840	987

When distress is defined at mid-span, the nominal moment capacity of the beam decreases gradually as the level of damage increases. When distresses occur at the quarter point, moment capacity of the beam is independent of the damage level and remains constant. Moment capacity with quarter point distresses is governed by the mid-span stresses.

Demands under dead load and 100 percent of live load are given in Table 10-5 and Table 10-6 for mid-span and quarter point distresses, respectively. Demand under dead and live load varies within each distress level due to change in the stiffness of the fascia beam. There is a slight difference in the HL-93 and Truck 21 demands, since Truck 21 causes slightly greater moments within the critical section investigated. Maximum demands occur at regions close to mid-span, irrespective of damage level at quarter point.

Table 10-5. Moment Demands for Distress Levels One through Four at Mid-span

Level	Beam condition	Moment demand at critical section (ft-kips)			
		DL	LL (HL-93)	DL	LL MDOT Truck 21)
1	Undamaged	320	238	320	243
2	Spall	324	228	324	232
3	Spall + 1 broken tendon	312	229	312	233
4	Spall + 2 broken tendons	300	225	300	228

Table 10-6. Moment Demands for Distress Levels One through Four at Quarter Point

Level	Beam condition	Moment demand at critical section (ft-kips)			
		DL	LL (HL-93)	DL	LL (MDOT Truck 21)
1	Undamaged	320	238	320	243
2	Spall	319	239	319	243
3	Spall + 1 broken tendon	320	239	320	243
4	Spall + 2 broken tendons	320	239	320	243

The flexural load rating factor for each level of distress is calculated according to the rating formulas given in the AASHTO LRFR (2003) and the MDOT Bridge Analysis Guide (2003). Following AASHTO LRFR procedures, Strength I and Service III Limit States are considered for design and legal load rating calculations. Design and legal load ratings of the box-beam are calculated using the following equation:

$$RF = \frac{C - (\gamma_{DC})DC - (\gamma_{DW})DW \pm (\gamma_P)P}{(\gamma_L)(LL + IM)} \quad (10-4)$$

For the strength limit states

$$C = \phi_c \phi_s \phi R_n \quad (10-5)$$

Where the lower limit shall apply:

$$\phi_c \phi_s \geq 0.85 \quad (10-6)$$

For the Service Limit States:

$$C = f_R \quad (10-7)$$

Where:

RF = Rating factor

C = Capacity

f_R = Allowable stress in the LRFD code

R_n = Nominal member resistance (as inspected)

DC = Dead-load effect due to structural components and attachments

- DW = Dead-load effect due to wearing surface and utilities
- P = Permanent loads other than dead loads
- LL = Live load effect
- IM = Dynamic load allowance (0.33)
- γ_{DC} = LRFD load factor for structural components and attachments (1.25 for Strength I, 1.0 for Service III Limit States)
- γ_{DW} = LRFD load factor for wearing surface and utilities
- γ_p = LRFD load factor for permanent loads other than dead loads = 1.0
- γ_L = Evaluation live-load factor
 1.75 for design inventory,
 1.35 for design operating,
 1.80 for legal live loads of unknown ADTT,
 0.80 for design loads of Service III
 1.00 for legal loads of Service III
- ϕ_c = Condition factor (1.0)
- ϕ_s = System factor (1.0)
- ϕ = LRFD resistance factor (1.0)

Michigan operating load ratings based on the load factor method are calculated according to the following formula (Michigan Bridge Analysis Guide 2003):

$$RF = (C - A_1 D) / [A_2 L (1 + I)] \quad (10-8)$$

Where:

RF = the rating factor for the live-load carrying capacity

C = the capacity of the member, M_n

D = the dead load effect on the member, M_{DL}

L = the live load effect on the member, M_{LL}

I = impact factor

A_1 = factor for dead load

A_2 = factor for live load

Rating factors are given in Table 10-7 and Table 10-8 for distresses at mid-span and quarter point locations, respectively. Although AASHTO LRFR does not require checking legal load rating if the load factor for inventory design load rating is greater than 1.0, legal load ratings are also calculated for comparison purposes. Rating factors decrease as expected with the increased level of damage at mid-span. The Service III legal load rating gives an indication of how much reserve capacity is left for Truck 21 since it uses factor 1.0 for both dead and live loads. For the undamaged case, while the system can carry an additional 20 percent of Truck # 21 at level 4 its capacity to satisfactorily carry the truck decreases by about 2 percent. Spall alone (Level 2) is not a major cause of capacity degradation. Beam capacity reduction is significant if broken tendons are present (Level 3 and 4). Distress at quarter points is not of major concern since the system behavior is still governed by the stresses within the mid-span region. Rating factors remain an almost constant; independent of any damage observed at quarter points (Table 10-8).

Table 10-7. Rating Factors for Distress Levels One through Four at Mid-span

Level	Beam condition	Design Load Rating* (HL-93)		Legal Load Rating (Truck 21)		MDOT Operating Rating (Truck 21)
		Strength I	Service III	Strength I	Service III	
1	Undamaged	1.38	1.51	1.32	1.20	1.79
2	Spall	1.37	1.48	1.32	1.17	1.78
3	Spall + 1 broken tendon	1.26	1.35	1.21	1.07	1.63
4	Spall + 2 broken tendons	1.18	1.24	1.13	0.98	1.52

* For operating, multiply the Strength I Limit State rating with 1.75/1.35

Table 10-8. Rating Factors for Distress Levels One through Four at Quarter Points

Level	Beam condition	Design Load Rating* (HL-93)		Legal Load Rating (Truck 21)		MDOT Operating Rating (Truck 21)
		Strength I	Service III	Strength I	Service III	
1	Undamaged	1.39	1.53	1.32	1.20	1.79
2	Spall	1.39	1.53	1.32	1.20	1.78
3	Spall + 1 broken tendon	1.40	1.54	1.34	1.21	1.80
4	Spall + 2 broken tendons	1.41	1.55	1.34	1.21	1.81

* For operating, multiply the Strength I Limit State rating with 1.75/1.35

10.3 SHEAR CRITICAL DISTRESS AND BOX BEAM CAPACITIES

In the analysis, the PC box-beam is assumed to reach shear capacity upon the crack formation within the shear critical region of the beams. The diagonal tension crack initiates when principal tensile stress reaches the critical tensile stress of 424 psi within the shear critical region.

Under the investigated set of moving loads and span length, critical principal stresses occur near mid-span irrespective of the distress levels at beam ends. The beams are expected to fail under flexure rather than shear. Thus, rating factors (Table 10-7 and Table 10-8) calculated using limiting stresses at the beam mid-span should be considered when evaluating a bridge with flexure-critical span length.

10.4 INFLUENCE OF GROUT LOSS AND BROKEN POSTTENSION STRANDS

Other damage parameters of interest include evaluation of the effect of shear key grout loss and broken transverse posttension strands on the box-beam capacity. Analysis of moment and shear critical distress scenarios demonstrated that flexure governs beam capacity for the selected span. Hence, the effect of shear key grout and/or posttension loss only at the mid-span will be analyzed. Inspection of bridges built in the 1950s with partial depth shear keys showed that the shear key itself was primarily intact (Figure 10-10). Current Michigan box-beam bridges utilize full-depth shear keys. Inspection of a box-beam bridge with full-depth shear key shows grout spall (Figure 10-11). Hence, the impact of grout loss on structural capacity is evaluated. Only grout loss below the first seven inches from the top of the beam is considered in the analysis. In order to define shear key grout loss, the elasticity modulus of the grout is reduced gradually following a similar approach that was applied for distress definition in box beams (Figure 10-12). Grout loss is defined on shear key elements between the investigated fascia and the first interior beam at mid-span (Figure 10-13).

Broken posttension strands at one location are incorporated by removing the horizontal force at the mid-span diaphragm location. A final evaluation included the investigation of broken posttension strands and grout loss simultaneously. The purpose of the analysis is to develop an understanding of the influence of the loss of grout and/or posttension on beam capacity; hence undamaged beam configuration is used in the investigations.



Figure 10-10. a) A portion of shear key grout remain intact with the beam and (b) beam surface after shear key grout cleanly fall off



Figure 10-11. Shear key grout loss

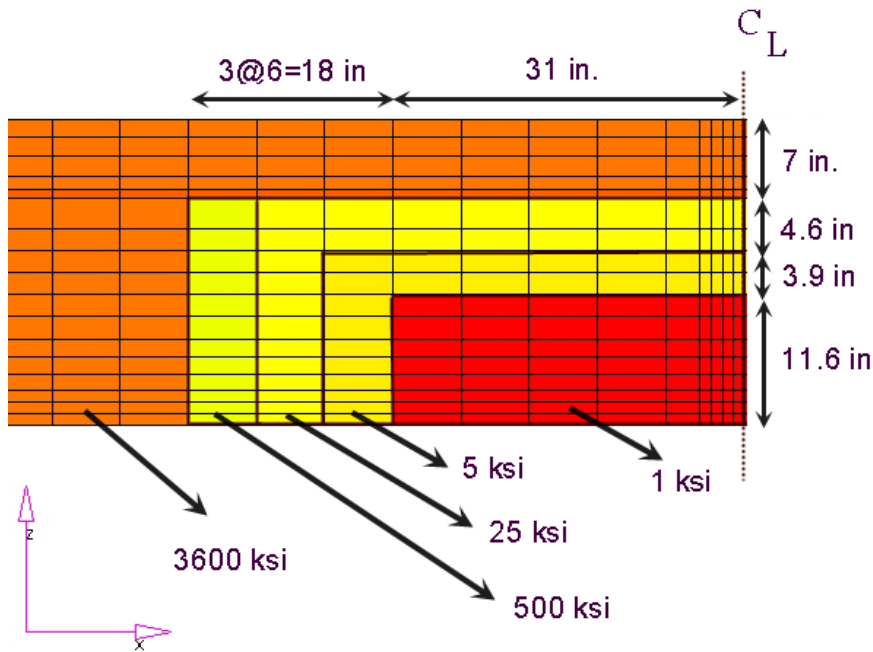


Figure 10-12. Shear key grout loss definition

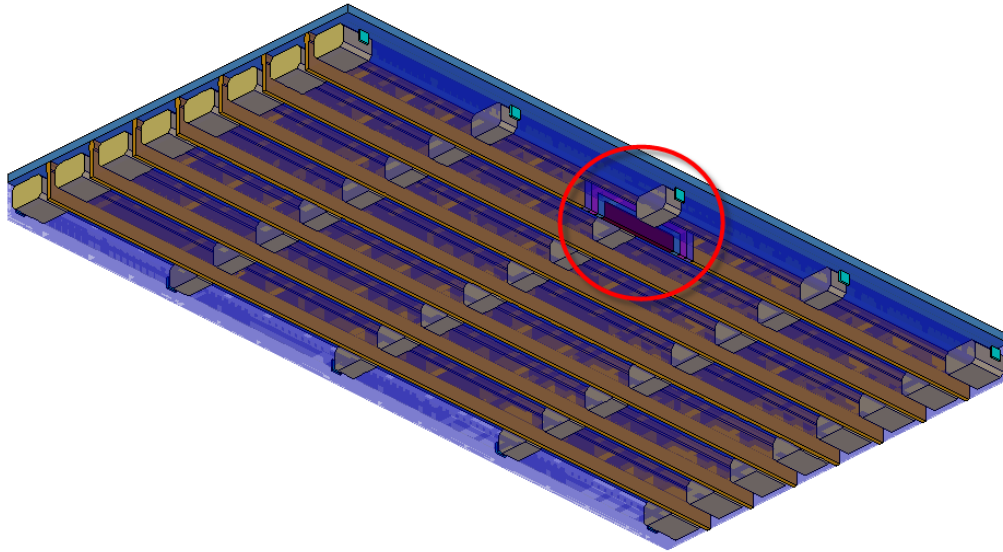


Figure 10-13. Distress at shear key between a fascia and the first interior beam at mid-span

Analysis results of the investigated cases are summarized in Table 10-9: moment due to dead load and 100 percent live load (HL-93), nominal moment capacity, and inventory design load rating. Results of the undamaged beam with no grout or posttension loss are also included for comparison purposes.

Table 10-9. Moments due to Dead and Live Loads, Nominal Moment Capacities, and Rating Factors for Distress at Mid-span

Damage parameter investigated	Moment demand at critical section under dead and live loads (ft-kips)		Nominal Moment Capacity (ft-kips)	Inventory Design Load Rating* (HL-93)	
	DL	LL (HL-93)		Strength I	Service III
Undamaged structure	320	238	976	1.38	1.51
Grout loss	330	233	975	1.38	1.49
Broken PT strand	298	238	928	1.33	1.47
Grout loss + broken PT	304	234	928	1.34	1.46

* For operating, multiply the Strength I Limit State rating with 1.75/1.35

The nominal moment capacity of the fascia beam is independent of the damage to the grout layer. With relatively less stiff connection between the fascia and the first interior beam, the dead load demand increases by around 3 percent due to partial distribution of barrier weight. Due to restrictions in the AASHTO LRFD for positioning live loads close to the barriers and considering tire contact area, a major portion of the wheel loads is placed on the first interior

beam. With the reduction in shear key stiffness due to grout loss, there is a 2 percent reduction in live load demand on the fascia beam.

In the case of broken posttension strands, the nominal moment capacity of the beam decreases by about 5 percent (i.e., from 976 ft-kips to 928 ft-kips). When posttension is applied, transverse compressive stresses develop in the beams. Due to Poisson's effect, longitudinal compressive stresses develop in the beam compensating some of the tensile stresses developed under applied loads (Figure 10-13 and Figure 10-14). Therefore, transverse posttension helps increase the nominal moment capacity of the beam. When transverse posttension is broken, structural system stiffness does not change because perfect bond between beams and shear keys is assumed in the analysis. There is no change in load distribution, but loss of posttension altered the beam stress distributions and resulted in lower dead load moments. Live load (HL-93) demand remains the same for both undamaged and broken posttension strand cases. This is because posttension acting on the mid-span diaphragm location first increases the beam capacity; then the beam capacity returns to original because of posttension loss. Normal stress distribution along the beam height, under 100 percent HL-93 load, remains the same for both undamaged and broken posttension strand cases (Figure 10-15).

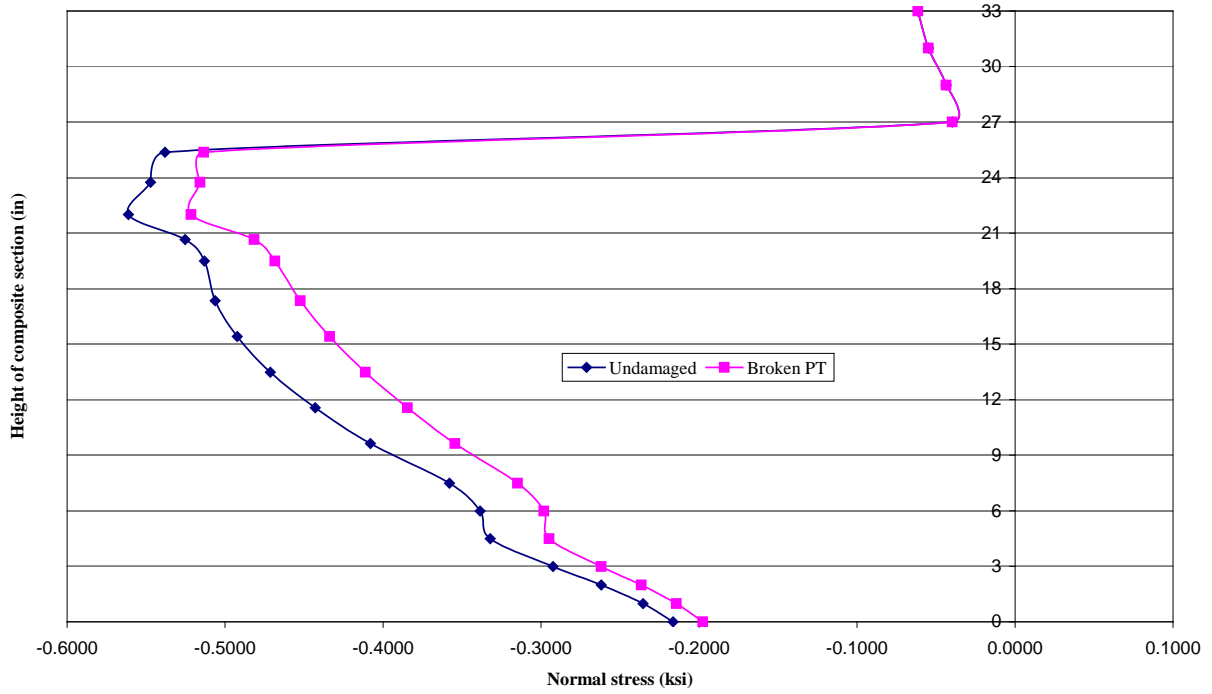


Figure 10-14. Normal stress distribution through the depth of deck-beam composite cross-section under dead load + prestress (tensile +; compression -)

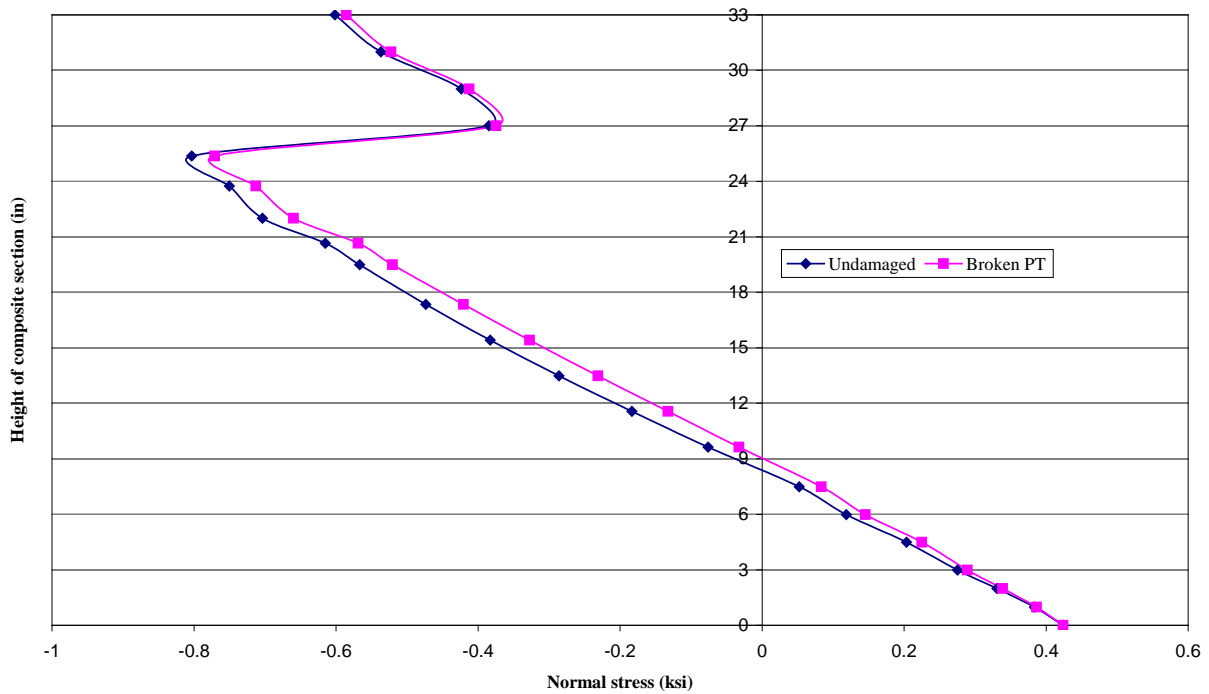


Figure 10-15. Normal stress distribution through the depth of deck-beam composite cross-section under service loads that develop 424 psi extreme fiber tensile stress (Tensile +, Compressive -)

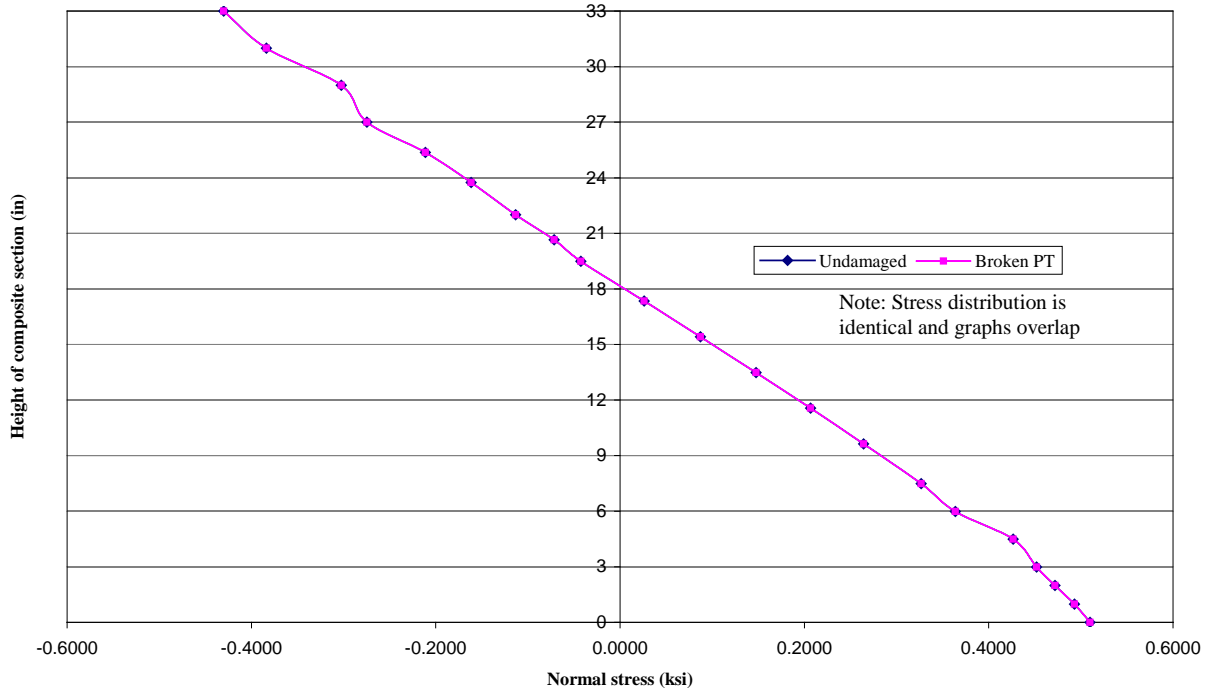


Figure 10-16. Normal stress distribution through the depth of deck-beam composite cross-section only under 100 percent live load (Tensile +, Compressive -)

When all the damage scenarios are considered, most critical is the loss of grout, provided that the bond between shear keys and the beams remain intact once the posttension is lost.

10.5 SUMMARY AND CONSLUSIONS

FE analyses are carried out investigating the effects of various distresses that may occur within the beam or some other components such as the shear key and posttension strands. FE modeling and analysis is performed for an eight-beam, two-lane, 50-ft long bridge under dead loads and live loads, as recommended in the AASHTO LRFD (2004) and the Michigan Bridge Analysis Guide (MDOT 2003). The live load is applied in increments until the tensile stress limit of $0.19\sqrt{f'_c}$ (424 psi) is reached. Flexural capacity is calculated from sectional analysis utilizing the uniaxial stress data obtained from FE analysis. Nominal moment capacity and load demands for distress levels one through four at mid-span are given in Table 10-10.

Table 10-10. Nominal Moment Capacity and Load Demands Based on FE Results (Distress at Mid-span)

Distress Level	Beam condition	Moment Capacity (ft-kips)	Dead Load Demand (ft-kips)	Live Load Demand (ft-kips)	
				HL-93	Truck 21
1	Undamaged	976	320	238	243
2	Spall	953	324	228	232
3	Spall + 1 broken tendon	896	312	229	233
4	Spall + 2 broken tendons	838	300	225	228

Flexural capacities of box beams with distresses at mid-span as well as the dead and live load demands are also calculated at the critical cross-section, in accordance with the AASHTO LRFD (2004) (Table 10-11). Beam distress is defined by reducing the distress width considering the modular ratio between sound concrete and distressed region. The number of prestressing tendons is modified to model the broken tendon cases. Dead load demand is calculated for two separate cases: where barrier load is equally distributed over eight beams, or is solely acting on fascias (i.e., no load transfer). These dead load distributions defined the upper and lower bounds of the dead load demands.

Table 10-11. Nominal Moment Capacity and Load Demands Based on the AASHTO LRFD (2004) (Distress at Mid-span)

Distress Level	Beam condition	Moment Capacity (ft-kips)	Dead Load Demand (ft-kips)		Live Load Demand (ft-kips)	
			Barrier Load Distributed (Lower Bound)	Barrier Load Not Distributed (Upper bound)	HL-93	Truck 21
1	Undamaged	992	282	394	266	269
2	Spall	975	282	394	266	269
3	Spall + 1 broken tendon	886	282	394	266	269
4	Spall + 2 broken tendons	793	282	394	266	269

Capacities obtained from the FE models and the AASHTO LRFD closely correlate with a minimum accuracy of 95% for distress level 4 (i.e. $793/838 \times 100 = 94.6\%$). For distress levels 3 and 4, where broken tendons are present, capacities obtained from FE results exceed those obtained from LRFD due to stress redistribution of broken tendons. However, with LRFD, only sectional analysis can be performed, and it is assumed that tendons are lost through the beam

length. Dead load demands obtained from FE fall within the upper and lower bounds established based on load distribution. Live load demands obtained by LRFD are 11% percent higher than those calculated by FE results. Analytical calculations are based on the distribution factors recommended by the AASHTO LRFD (2004), whereas FE analysis is more refined and accounts for the structural system behavior of Michigan design.

Rating factors given in Table 10-7 for distresses at mid-span are presented again in Table 10-12 for comparison purposes. Load ratings performed with analytical results of lower and upper bound dead load demands are given in Table 10-13 and Table 10-14, respectively.

Table 10-12. Rating Factors for Distress Levels One through Four at Mid-span Obtained from FE Results

Distress Level	Beam condition	Design Load Rating (HL-93)		Legal Load Rating (Truck 21)		MDOT Operating Rating (Truck 21)
		Strength I	Service III	Strength I	Service III	
1	Undamaged	1.38	1.51	1.32	1.20	1.78
2	Spall	1.37	1.48	1.32	1.17	1.78
3	Spall + 1 broken tendon	1.26	1.35	1.21	1.07	1.63
4	Spall + 2 broken tendons	1.18	1.24	1.13	0.98	1.52

Table 10-13. Rating Factors for Distress Levels One through Four at Mid-span Obtained Analytically Using AASHTO LRFR Specifications for Lower Bound Dead Load Demand

Distress Level	Beam condition	Design Load Rating (HL-93)		Legal Load Rating (Truck 21)		MDOT Operating Rating (Truck 21)
		Strength I	Service III	Strength I	Service III	
1	Undamaged	1.37	1.58	1.32	1.25	1.79
2	Spall	1.34	1.53	1.28	1.21	1.74
3	Spall + 1 broken tendon	1.15	1.27	1.10	1.01	1.48
4	Spall + 2 broken tendons	0.95	1.00	0.91	0.79	1.22

Table 10-14. Rating Factors for Distress Levels One through Four at Mid-span Obtained Analytically Using AASHTO LRFR Specifications for Upper Bound Dead Load Demand

Distress Level	Beam condition	Design Load Rating (HL-93)		Legal Load Rating (Truck 21)		MDOT Operating Rating (Truck 21)
		Strength I	Service III	Strength I	Service III	
1	Undamaged	1.07	1.06	1.03	0.83	1.37
2	Spall	1.04	1.01	1.00	0.80	1.32
3	Spall + 1 broken tendon	0.84	0.74	0.81	0.59	1.07
4	Spall + 2 broken tendons	0.65	0.47	0.62	0.37	0.80

For cases where it is assumed that the barrier load is distributed uniformly to the eight beams, load ratings obtained from FE results and analytical calculations are very close to each other for distress levels one and two (Table 10-12 and Table 10-13). The discrepancy between the two ratings is higher when broken tendons are involved (Level 3 and 4). This is again due to stress redistribution of prestressing tendons in FE analysis and constant demand under dead and live load in analytical calculations regardless of distress observed. When barrier load is acting solely on the fascia beam, critical ratings are observed. For legal load rating, a rating factor less than one is observed even for the undamaged scenario (Table 10-14) since dead load demand is increased by around 40 percent (i.e. 282 ft-kips to 394 ft-kips) while the live load factor is increased to 1.0 from 0.80

According to the results:

1. Nominal moment capacity and hence the load rating of the beam decreases gradually as the level of distress increases at mid-span. Beam capacity reduction is significant when broken strands are present (Level 3 and 4).
2. When distresses occur at quarter points, the moment capacity of the beam is governed by the stresses that occur close to mid-span (i.e., beam capacity is independent of the quarter point damage level considered in this analysis). Rating factors remain almost constant with the quarter point damage scenarios considered in this analysis. Two broken strands with some spall constitute the most critical damage considered in the analysis (Table 10-8).

3. For the investigated set of moving loads and span length, critical principal stresses occur near mid-span irrespective of the beam end distress levels considered in this study. The rating factors calculated for the example bridge are independent of the beam end distresses (Table 10-7 and Table 10-8).
4. Loss of grout influences the load demands on the fascia beam; thus load distribution. The fascia beam has to carry greater dead load due to barrier weight and less live load since majority of the axle loads are acting on the interior beams.
5. Posttension does not influence load distribution if shear keys are intact. However, it helps increase beam capacity by countering the tensile stresses.
6. Lateral posttension is required to increase the system redundancy and is important when the bond between beams and the shear key is not capable of transferring tensile stresses.

11 SUMMARY AND CONCLUSIONS

This project consisted of six tasks. The first task was the review and synthesis of literature. Capacity evaluation and load testing of distressed bridges or beams, properties of shear key and repair materials, durability of shear key and repair materials, properties of cementitious materials that have a potential to be used for shear keys, and design parameters for the transverse design of box-beam bridge superstructures are the topics covered under literature review. The literature review was jointly conducted by Western Michigan University (WMU) and Michigan Technological University (MTU). The WMU research team synthesized the information related to capacity evaluation and load testing of distressed bridges or beams, mechanical properties of shear key grout and repair materials, properties of cementitious materials that have a potential use as shear key grout, and design parameters for the transverse design of box-beam bridge superstructures.

Literature revealed that for uncracked beams fatigue is not a concern. Fatigue may become a concern for bridges subjected to frequent loading generating tensile fiber stress in excess of $6(f_c')^{1/2}$ psi or strand stress greater than $0.06f_{pu}$. Transverse connection of precast elements in a box-beam bridge governs the load transfer between beams. Transverse connection is established by the contribution and interaction of grouted full-depth shear keys, transverse posttension and a cast-in-place concrete deck. The effectiveness of transverse connection is a function of the shear key grout and posttension spacing. In this case, when the elasticity modulus of the shear key grout is lower than the parent material, the transfer connection efficiency of the shear key at a posttension location increases with decreasing thickness. Specifically, mechanical properties of grout material at the time of posttension govern the stress distribution along the joint; hence the load transfer and the tightness of the joint to prevent moisture ingress. Shear key grout mixes can be specified for required strength and modulus at the time of transverse posttension application.

The second task was to evaluate the load capacity of a salvaged box-beam. WMU was solely responsible for performing the task and deliverables. A 50-year old box-beam was salvaged from the bridge (S11-38101) that carries Hawkins road over I-94 during a beam replacement activity. The visible beam distress, specifically wide longitudinal cracking at the beam soffit, was the reason for replacement. The beam was carefully removed and load testing was

performed. Analysis of load test data indicated that with all the visible distress, the beam capacity still exceeded the required design capacity. However, the beam was designed for a lower load (i.e., H-15) than the currently required load. A related finding that will be helpful in load capacity assessment was the use of camber measurement for calculating remaining prestress. Prestress estimation using camber measurements overestimated the remaining prestress by 40 to 50 percent. The testing of the salvaged beam also demonstrated the need to implement inspection procedures that will help reveal concealed corrosion, characterize material properties, and also quantify the load transfer ability along the shear keys.

The third task was MTU responsibility. This task included conducting a survey of commonly used repair materials and shear key grouts for prestressed box beam bridges, and a laboratory evaluation of selected materials. The intended result of the laboratory evaluation was development of required material characteristics from the perspective of dimensional stability and durability of prestressed box beam bridges. Based on the survey conducted at the start of the project, four repair materials and three shear key grouts were selected for evaluation. Detailed evaluation of fresh and hardened concrete properties was conducted in the laboratory. An extensive durability evaluation was performed to assess sorptivity, shrinkage, and resistance to freezing and thawing cycles of repair materials as well as shear key grouts. It was observed that the selected materials showed variations in performance in comparison with each other.

The laboratory analysis indicated that selection of a particular repair material would depend upon the intended application. All repair materials exhibited lower sorption values in comparison to normal concrete but exhibited a large variation in shrinkage values in comparison with normal concrete. Among the shear key grouts evaluated, it was observed that the masonry cement based grout exhibited the lowest strengths whereas SET 45 exhibited higher strengths as well as lower shrinkage values.

The fourth task was to evaluate mechanical properties of shear key grout and specified repair materials. WMU was responsible for performing the task and deliverables. Mechanical properties of repair and manufactured grout materials (e.g., set gout and set-45) identified for this propose were documented based on manufacturers' technical data sheets. To form the shear-keys, type R-2 grout mix is specified and commonly used in Michigan box-beam bridges.

Specimens were prepared and tests were performed to document the mechanical properties of R-2 grout. The compressive strength of grout was evaluated. In addition, an ultrasonic pulse velocity (UPV) test was performed in compliance with ASTM C597 to determine the dynamic modulus of elasticity and the Poisson's ratio of the Type R-2 grout. In cementitious materials, the dynamic modulus determined in accordance with ASTM C469 is expected to be greater than the static modulus. However, for the grout materials the measured dynamic modulus was lower than the static modulus determined following the ASTM C469 procedure. Additional testing was performed for investigative purposes. The uniaxial stress-strain response showed a hysteretic strain hardening behavior not expected of sound cementitious material. Consequently, the elastic modulus at low strain is lower than at high strain during the load cycle. The static modulus test (ASTM C469) cannot capture this behavior and calculates a nominal modulus value. Other repair materials also showed a similar behavior, and further investigations are recommended.

The fifth task was the simulation of construction process stages. WMU was responsible for performing the task and deliverables. While simulating the construction process stages, box-beam bridge transverse connection design and material parameters were also investigated using sub-assembly models. The parameters investigated in these simulations were: grout mechanical properties, posttension force magnitude and location, number of diaphragms, and the bridge width. The sub-assembly models developed for this purpose were 50 ft. long, 27×36-in. box beams connected with shear keys and posttension at diaphragm locations. Two sub-assembly models were developed, one with three beams and the other with four beams. Simulations showed that load transfer occurs primarily through the stiffer portions of the bridge superstructure (i.e., through the diaphragms). In this respect, the AASHTO LRFD (2004) Section 5.14.1.2.8 recommendations regarding transverse normal interface stress distribution were found to be vague. Compliance with this recommendation, requiring the development of a minimum clamping stress of 250 psi at shear keys along the beam length, could not be achieved with the current beam and posttension provisions. A comprehensive redesign of transverse connection is needed for achieving this level of uniform clamping stress along the shear key. Every stage of the side-by-side box-beam construction process was simulated using advanced pre/post processing capabilities of HyperMesh and FE analysis capabilities of ABAQUS. Stresses

developed in beams, shear keys, and the deck were evaluated and documented. Further, to assure shear key functionality and strength requirements, a rational analysis and design model was developed. Changes to construction procedures were suggested, and these suggested changes were re-evaluated with construction process simulations. The proposed rational design procedure established the posttension requirements based on minimizing the tensile stresses at the shear key under gravity loading. With the proposed design, posttension application is recommended in two stages before and after 6-in. cast-in-place concrete deck placement. With the two-stage posttension scheme, transverse tensile deck stresses that occur under live load were eliminated except at some isolated regions within the proximity of the fascias.

The sixth and final task was to evaluate flexural and shear capacity of distressed beams considering structural system behavior. WMU was responsible for performing the task and deliverables. Effects of three major distress types were evaluated. These were spall, spall with single broken strand, and spall with two broken strands. Distresses were incorporated along the corner of the beam's bottom flange. In addition to beam distresses, impact of the shear key grout loss and/or transverse posttension loss on beam capacity was investigated. Analysis results showed that, for the selected span length of 50 ft., the capacity was reduced only when the distresses were at the midspan. Partial loss of grout alters the dead and live load demands on the fascia beam due to reduced stiffness. It was shown that posttension did not influence the load distribution provided that shear keys were intact. However, posttension contributes to the beam capacity and provides redundancy to the systems especially when a weak bond exists between the grout and beams.

11.1 RECOMMENDATIONS

The following key recommendations are based on the findings from the project tasks of the literature review, load testing of a salvaged box-beam, testing of grout and repair material properties, and the development of subsequent finite element modeling and simulations:

1. Among the fresh properties of utmost importance is workability in case of polymer based repair materials. Repair materials which do not need excessive force for proper placement and consolidation should be selected.

2. Repair materials with shrinkage values comparable to the substrate concrete should be selected. In this study all the repair materials did not necessarily exhibit the required behavior and, hence, it is essential to select a repair material based on its intended use. It is necessary to evaluate the shrinkage behavior of a selected repair material prior to application on site.
3. To protect exposed steel from corrosion, repair materials evaluated in this study can be adopted for use because all of them exhibited high resistance to chloride ion transport as well as low sorption values.
4. When selecting a shear key grout it is essential to determine the early age compressive strength as well as its early age shrinkage properties based on the load applied to it. A more detailed understanding of shear key grout from a material standpoint as well as the total design of the shear key itself is recommended.
5. Adequate load transfer and achieving a watertight connection along the transverse joint cannot be achieved with the currently specified grout with nonlinear hysteretic behavior. Revisions to grout material specifications are recommended.
6. In-service bridge beam load capacity assessment should be based on material characterization, load transfer evaluation along the shear keys, and estimation or assessment of concealed corrosion.
7. The recommended load analysis procedure and the associated design criteria requiring a two-stage posttension process should be implemented for improved durability performance of side-by-side box-beam bridges.

Intentionally left blank

12 SUGGESTIONS FOR FUTURE RESEARCH

The focus of this work has been the investigation of safety of in-service side-by-side box-beam bridges with distressed beams, selection of materials for repair and the repair techniques, and investigation of drawbacks as well as benefits of current design and construction procedures. As with similar projects dealing with complex bridge structures, several questions remain unanswered, and continuation work is needed. The list of tasks that is outlined below should be considered.

- Load testing data of a fifty-year old salvaged beam indicated that, even with a wide long longitudinal crack at the bottom flange, the experimental beam capacity exceeded the design capacity. Visual inspection of the salvaged beam while in place was not adequate to identify/evaluate the strand corrosion, condition of transverse tie rods, and other material related distress within the box-beam cavity. Further, there was no quantifiable evaluation of load transfer between girders. Future projects are suggested for incorporating inspection procedures based on innovative technologies for acquiring quantifiable data for load rating of bridges.
- Shear key grout specifications need to be reevaluated and revised. For example, the required grout compressive strength in 24 hours is 4000 psi according to the AASHTO LRFD (2004) Section 5.14.1.2.8. The AASHTO Standard Specifications (2002) require 5000 psi in 24 hours. Grout materials tested during this project could not satisfy the strength required by the AASHTO LRFD or Standard. Also, AASHTO LRFD (2004) requires a clamping stress level of 250 psi at the shear key upon posttension application. The concern with the grout materials tested is not their strength, but the nonlinear strain hardening behavior. Consequently, grout modulus under levels of posttension stresses is very low. Grout modulus at the time of posttension is important as it governs the load distribution between the beams as well as tightening the joint for water intrusion. A future project is suggested to formulate grout composition, mechanical property variation with time, behavior under various load levels, and appraisal of AASHTO stipulations.
- Construction process numerical simulation results illustrated the benefits of implementing two-stage transverse posttension on side-by-side box-beam bridges. First, an implementation project is recommended utilizing the design and posttension

stipulations developed in this study. Also, development of design charts is proposed for a robust design of unremarkable side-by-side box beam bridges. These should be based on the recommended analysis and posttension design procedures. Hence, three future projects are recommended: an implementation project for developing design charts to be included in the MDOT Bridge Design Guide, the implementation of the proposed design and construction procedures on a new superstructure replacement construction, and the instrumentation and monitoring of the replacement bridge for long-term performance.

13 REFERENCES

- AASHTO. (2002). *Standard Specifications for Highway Bridges*, 17th Edition, American Association of State Highway and Transportation Officials, 444 North Capitol Street, N.W., Suite 249, Washington, D. C.
- AASHTO. (2004). *AASHTO LRFD Bridge Design Specifications*, Third Edition, American Association of State Highway and Transportation Officials, 444 North Capitol Street, N.W., Suite 249, Washington, D. C.
- ABAQUS/Standard User's Manual - Version 6.7. (2008). Hibbitt, Karlson & Sorensen, Inc., Pawtucket, RI. (<http://www.abaqus.com>).
- ACI. (2005). "ACI 548 Polymer Modified Concrete ". American Concrete Institute, Detroit, MI.
- ACI 503.1 (1992). "Standard specification for bonding hardened concrete, steel, wood, brick and other materials to hardened concrete with a multi-component epoxy adhesive." American Concrete Institute, Detroit, MI, 1992.
- Aktan, H., Ahlborn, T. M., Gilbertson, C. G., and Attanayake, U. (2005) "Condition Assessment and Methods of Abatement of Prestressed Concrete Box-Beam Deterioration – Phase I." *MDOT RC-1470*, Michigan Department of Transportation, Lansing, MI.
- Al-Zahrani, M. M., Maselhuddin, M., Al-Duaijan, A. U., and Ibrahim, M. (2003). "Mechanical Properties and Durability Characteristics of Polymer-and Cement-Based Materials." *Cement and Concrete Composites*, 25, 527-537.
- Arandigoyen, M., Alvarez, J. I. (2007). "Pore structure and mechanical properties of cement–lime mortars." *Cement and Concrete Research* 37 (2007) 767–775.
- Attanayake, U. (2006). "Macromechanical modeling of precast orthotropic bridge superstructure systems." *Ph.D Dissertation*, Wayne State University, Detroit, Michigan.
- Attanayake, U. and Aktan, H. M. (2009). "Side-by-side Box-beam Bridge Superstructure – Rational Transverse Posttension Design," *CD-ROM, paper # 09-3420*, 88th TRB Annual Meeting, Transportation Research Board of National Academies, Washington, D. C.
- Attanayake, U. and Aktan, H. (2008). "Issues with Reflective Deck Cracks in Side-by-Side Box-Beam Bridges." *The 4th Concrete Bridge Conference*, Hyatt Regency, St. Louis, Missouri, May 4 – 7.
- Attanayake, U. and Aktan, H. M. (2007). "Macromechanical modeling of precast orthotropic bridge superstructure systems." *CD-ROM, paper # 07-3209*, 86th Annual Meeting, Transportation Research Board of National Academies, Washington, D. C.

- Baluch, M. H., Rahman, M. K., and Al-Gadhib, A. H. (2002). "Risks of Cracking and Delamination in Patch Repair." *Journal of Materials in Civil Engineering* 14(4), 294-302.
- Barboza, A. d. S. R. and El Debs, E. E. (2006). "Load-bearing capacity of mortar joints between precast elements." *Magazine of Concrete Research*, 58 (9), 589-599.
- Beushausen, H.-D., and Alexander, M. G. (2007). "Performance of Concrete Patch Repair System" *Advances in Construction Materials 2007*, C. U. Grosse, ed., Springer 255-262.
- Civjan, S. A., Jirsa, J. O., Carrasquillo, R. L., and Fowler, D. W. (1998). "Instrument to Evaluate Remaining Prstress in Damaged Prestressed Concrete Bridge Girders." *PCI Journal*, 43(2), 62-71.
- Deshpande, Y. S. (2006). "Evaluation of Commercial Rapid-Setting Materials and Development of Rapid-Setting Self-Compacting Concrete for Dowel Bar Retrofit Applications " Ph.D., Purdue University.
- Dong, X. (2002). "Traffic forces and temperature effects on shear key connection for adjacent box girder bridge." Ph.D Dissertation, University of Cincinnati, Ohio.
- Dragosavic, M. (1978). "Load bearing capacity of joints between precast elements." *RILEM-CEB-CIB Symposium Mechanical and Insulating Properties of Joints of Precast Reinforced Concrete Elements*. RILEM/CEB, Athens. pp. 29-40.
- El-Remaily, A., Tadros, M. K., Yamane, T., and Krause, G. (1996). "Transverse Design of Adjacent Precast Prestressed Concrete Box-beam Bridges." *PCI Journal*, 41(4), 96-113.
- Emberson, N. K., and Mays, G. C. (1990). "Significance of property mismatch in the patch repair of structural concrete Part I: Properties of Repair Systems." *Magazine of Concrete Research*, 45(152), 147-160.
- Ghrici, M., Kenai, S., Said-Mansour, M. (2007). "Mechanical properties and durability of mortar and concrete containing natural pozzolana and limestone blended cements." *Cement & Concrete Composites* 27(2007) 542–549.
- Gulyas, R. J., Wirthlin, G. J., and Champa, J. T. (1995). "Evaluation of keyway grout test methods for precast concrete bridges." *PCI Journal*, Vol. 40, No. 1, pp. 44-57.
- Harries, K. A. (2006). "Full-scale Testing Program on De-commissioned Girders from the LakeView Drive Bridge." FHWA-PA-2006-008-EMG001, University of Pittsburgh, Department of Civil and Environmental Engineering, 949 Benedum Hall, Pittsburgh, PA 15261.
- Hassan, K. E., Robery, P. C., and Al-Alawi, L. (2000). "Effect of Hot-Dry Curing Environment on the Intrinsic Properties of Repair Materials " *Cement and Concrete Composites*, 22, 453-458.

Hawkins, N.M., and Fuentes, B.F. (2003). "Structural Condition Assessment and Service Load Performance of Deteriorated Pretensioned Deck Beam Bridges." FHWA-IL-UI-285, Illinois Department of Transportation, Springfield, IL 62704.

<http://www.fhwa.dot.gov/hfl/about.cfm> (Accessed: September 2008).

<http://www.trb.org/trbnet/ProjectDisplay.asp?ProjectID=1673> (Accessed: September 2008)

Huckelbridge, A. A. Jr., El-Esnawi, H., and Moses, F. (1995). "Shear-Key Performance in Multibeam Box-beam Bridges." *Journal of Performance of Constructed Facilities*, 9(4), 271-285.

HyperMesh user's manual – version 8.0. (2007). Altair Engineering, Inc., 1820 E Big Beaver, Troy, Michigan 48083. (<http://www.altair.com>).

Issa, M.A., Valle, C.L., Abdalla, H.A., Islam, S., and Issa, M.A. (2003). "Performance of Transverse Joint Grout Materials in Full-Depth Precast Concrete Bridge Deck Systems." *PCI Journal*, Vol. 48, No. 4, pp.92-103.

Jones, R. M. (1975). *Mechanics of composite Materials*, first edition, McGraw-Hill, New York.

Kollar, L. P. and Springer, G. S. (2003). *Mechanics of Composite Structures*. Cambridge University press.

Kosednar, J., and Mailvaganam, N. P. (2005). "Selection and Use of Polymer-Based Materials in the Repair of Concrete Structures." *Journal of Performance of Constructed Facilities*, 19(3), 229-233.

Kuhlmann, L. A., and Foor, N. C. (1984). "Chloride Permeability Versus Air Content of Latex Modified Concrete." *Cement, Concrete, and Aggregates*, 6(1), 11-16.

Kuhn, P., and Chiarto, P. T., "Shear Lag in Box-beams Methods of Analysis and Experimental Investigations." Report No 739, *National Advisory Committee of Aeronautics*.

Lall, J., Alampalli, S., and DiCocco, E. F. (1998). "Performance of Full-Depth Shear Keys in Adjacent Prestressed Box Beam Bridges," *PCI Journal*, Vol. 43, No. 2, pp. 72-79.

Lavelle, J. A. (1988). "Acrylic latex-Modified Portland Cement " *ACI Materials Journal* (1), 4-8.

Mangat, P. S., and O'Flaherty, F. J. (2000). "Influence of Elastic Modulus on Stress Redistribution and Cracking in Repair Patches " *Cement and Concrete Research*, 30(1), 125-136.

MDOT. (2003a). *Bridge Design Manual*. Michigan Department of Transportation, Lansing, Michigan.

MDOT. (2003b). *Standard Specification for Construction*. Michigan Department of Transportation, Lansing, Michigan.

MDOT. (2005a). *Bridge Design Guide*. Michigan Department of Transportation, Lansing, Michigan.

MDOT. (2005b). *Bridge Analysis Guide*. Michigan Department of Transportation, Lansing, Michigan.

Miller, R., Hlavacs, G. M., Long, T., and Greuel, A. (1999). "Full-Scale Testing of Shear-Keys for Adjacent Box-beam Bridges." *PCI Journal*, 44(6), 80-90.

Miller, R., and Parekh, K. (1994). "Destructive Testing of Deteriorated Prestressed Box Bridge Beam." *Transportation Research Record 1460*, Transportation Research Board, 2101 Constitution Avenue, NW, Washington, DC.

Mirza, J., Mirza, M. S., and Lapointe, R. (2002). "Laboratory and Field Performance of Polymer-Modified Cement-Based Repair Mortars in Cold Climates." *Constructino and Building Materials* (16), 363-374.

Ohama, Y. (1995a). *Handbook of Polymer-Modified Concrete and Mortars-Properties and Process Technology* Noyes Publication Park Ridge, New Jersey

Ohama, Y. (1995b). "Polymer-Modified Mortars and Concretes." *Concrete Admixtures Handbook*, V. S. Ramachandran, ed., Noyes Publications, Park Ridge, N.J.

Parameswaran, S. (2004). "Investigating the Role of Material Properties and Their Variability in the Selection of Repair Material," Purdue University West Lafayette.

PCI (2003). *Precast Prestressed Bridge Design Manual*. Precast/Prestressed Concrete Institute, 175 W. Jackson Boulevard, Chicago, IL 60604

Pinelle, D. J. (1995). "Curing Stresses in Polymer-Modified Repair Mortars." *Cement, Concrete, and Aggregates*, 17(2), 195-200.

Rao, C., and Frantz, G. C. (1996). "Fatigue Tests of 27-Year-Old Prestressed Concrete Bridge Box-beams." *PCI Journal*, 41(5), 74-83.

Scholz. D. P., Wallenfelsz, J. A., Lijeron, C., and Roberts-Wallmann, C. (2007). "Recommendations for the Connection Between Full-Depth Precast BridgeDeck Panel Systems and Precast I-Beams." FHWA/VTRC 07-CR17, Virginia Transportation Research Council, 530 Edgemont Road, Charlottesville, VA 22903.

Vambersky, J. N. J. A. (1990). "Mortar Joints Loaded in Compression." *Proceeding of International Seminar on Prefabrication of Concrete Structures*. Delft University Press. pp. 167-180.

Vaysburd, A. M. (2006). "Holistic system approach to design and implementation of concrete repair." *Cement and Concrete Composites*, 28, 671-678.

Young, B., and Kreider, R. (2006). "Laboratory and Field Evaluations of Rapid Setting Patching Materials for Portland Cement Concrete." NTPEP Report 9005.1, AASHTO.

Yurtdas, I., Peng, H., Burlion, N., Skoczylas, F. (2005). "Influence of water by cement ratio on mechanical properties of mortars is submitted by drying." *Cement and Concrete Research* 36 (2006) 1286–1293.



MDOT RC-1527

**CONDITION ASSESSMENT AND METHODS
OF ABATEMENT OF PRESTRESSED
CONCRETE BOX-BEAM DETERIORATION**

Phase II

**FINAL REPORT
(APPENDICES)**



MichiganTech

Center for Structural Durability
A Michigan DOT Center of Excellence

Research

CONDITION ASSESSMENT AND METHODS OF ABATEMENT OF PRESTRESSED CONCRETE BOX- BEAM DETERIORATION

Phase II

Project Manager: Mr. Steve Kahl, P.E.

Submitted to:



Submitted by



Western Michigan University
Department of Civil & Construction Engineering
College of Engineering and Applied Sciences
Kalamazoo, MI 49008
Fax: (269) – 276 – 3211

Dr. Haluk Aktan, P.E.
Professor & Chair
(269) – 276 – 3206
haluk.aktan@wmich.edu

Dr. Upul Attanayake
Assistant Professor
(269) – 276 – 3217
upul.attanayake@wmich.edu

Mr. Evren Ulku
Graduate Research Assistant
(313) – 577 – 3785
evren@eng.wayne.edu

MichiganTech

Michigan Technological University
Dept. of Civil & Environmental Engineering
1400 Townsend Drive
Houghton, MI 49931
Fax: (906) – 487 – 1620

Dr. Theresa M. Ahlborn, P.E.
Associate Professor
(906) – 487 – 2625
tess@mtu.edu

Dr. Yogini Deshpande
Post Doctoral Researcher
(906) – 487 – 1474
yogini@mtu.edu

Intentionally left blank

Contents

Appendix A: Material Data Sheets

**Appendix B: Repair Material and Shear Key Grout Volume Required for
Each Test**

**Appendix C: Compressive Strength of Repair Materials and Shear Key
Grouts**

Appendix D: Slant Shear Bond Strength

**Appendix E: Free Shrinkage Data for Repair Mortar and Shear Key
Grouts**

Appendix F: Resistance to Freezing and Thawing

appendix G: Air Content of Repair Materials and Shear Key Grouts

appendix H: Coefficient of Thermal Expansion

Appendix I: Sorptivity

Appendix J: Rational Transverse Posttension Design

Intentionally left blank

APPENDIX A: MATERIAL DATA SHEETS

Construction

Product Data Sheet
Edition 8.2003
Identification no. 539
SikaRepair SHA

SikaRepair® SHA

Fast-setting, one component, cementitious repair mortar with superior high build properties

Description	SikaRepair SHA is a fast-setting, one-component, cementitious ready to use repair mortar. The incorporation of low density aggregates allows high build applications on vertical and overhead surfaces. SikaLatex R or SikaLatex may be used instead of water for a two component, polymer-modified repair mortar.
Where to Use	<ul style="list-style-type: none"> ■ Fast repairs to overhead and vertical concrete and mortar surfaces on grade, above and below grade. ■ As a repair material for building facades, parking structures, industrial plants, bridges, etc.
Advantages	<ul style="list-style-type: none"> ■ Minimal time required between lifts. ■ Fast finishing time. ■ Time/labor-saving material; application up to 3 inches on vertical surfaces in one layer. ■ Easy to use; just add water. ■ High bond strength ensures excellent adhesion. ■ Good, early and ultimate strength. ■ Increased freeze/thaw durability and resistance to deicing salts. ■ Easy to clean. ■ Suitable for exterior and interior applications. ■ Not a vapor barrier.
Yield	0.55 cu. ft./bag
Packaging	Sika Repair SHA: 25 lb. bag, 60/pallet; 50 lb. (22.7 kg.) multi-wall bag. SikaLatex (R): 1 gal. plastic jug; 4/carton, 5 gal. pails.

Typical Data (Material and curing conditions @ 73°F (23°C) and 50% R.H.)

Shelf Life	One year in original, unopened bags.	
Storage Conditions	Store dry at 40°-95°F (4°-35°C). Condition material to 65°-75°F before using.	
Color	Concrete gray.	
Mixing Ratio	1 50 lb. bag SikaRepair SHA + 3/4 gal. to 1 gal. of liquid	
Density (Wet mix)	106 lbs./cu. ft. (1.70 kg./l)	
Application Time	Approximately 20-30 minutes.	
Finishing Time	30-40 minutes	
Time Between Lifts	Less than 1 hour	
Compressive Strength (ASTM C-109)		with Latex R
1 day	2,000 psi (13.8 MPa)	2,500 psi (17.2 MPa)
7 days	3,000 psi (20.7 MPa)	3,500 psi (24.1 MPa)
28 days	4,500 psi (31.0 MPa)	5,000 psi (34.5 MPa)
Flexural Strength (ASTM C-293)		
28 days	800 psi (5.5 MPa)	1,100 psi (9.7 MPa)
Bond Strength* (ASTM C-882 modified)		
28 days	1,000 psi (6.8 MPa)	1,800 psi (12.4 MPa)

*Mortar scrubbed into substrate

How to Use

Substrate Concrete, mortar, and masonry products.

Surface Preparation - Concrete/Mortar: Remove all deteriorated concrete, dirt, oil, grease, and all bond-inhibiting materials from surface. Preparation work should be done by high pressure water blast, scabblor or other appropriate mechanical means to obtain an exposed aggregate surface profile of ±1/16-in. (CSP-5). After preparation, substrate strength should be verified prior to patch placement. Substrate should be saturated surface dry (SSD) with no standing water during application.

Reinforcing Steel: Steel reinforcement should be thoroughly prepared by mechanical cleaning to remove all traces of rust. Where corrosion has occurred due to the presence of chlorides, the steel should be high pressure washed with clean water after mechanical cleaning. For priming of reinforcing steel use Sika Armatec 110 EpoCem (consult Technical Data Sheet).



Concrete Substrate: Prime the prepared substrate with a brush or sprayed applied coat of Sika Armatec 110 EpoCem (consult Technical Data Sheet). Alternately, a scrub coat of Sika Repair SHA can be applied prior to placement of the mortar. The repair mortar has to be applied into the wet scrub coat before it dries.

Mixing	<p>With water: Pour 3/4 of one gallon of water into the mixing container. Add powder while mixing continuously. Mix mechanically with a low-speed drill (400-600 rpm) and mixing paddle or in an appropriate mortar mixer. Add more water to obtain desired consistency of the mortar. <u>Do not exceed one gallon per bag.</u> Mix to uniform consistency, maximum 3 minutes. Manual mixing can be tolerated only for less than a full unit. Thorough mixing and proper proportioning is necessary.</p> <p>With Latex R: Pour 3/4 gallon of Sika Latex R into the mixing container. Slowly add powder and mix as above.</p> <p>With diluted Latex R: Sika Latex R may be diluted up to 5:1 (water: Sika Latex R) for projects requiring minimal polymer-modification. Pour 3/4 gallon of the mixture into the mixing container. Slowly add powder and mix as above.</p> <p>Note: SikaLatex R must be protected from freezing. If frozen, discard.</p>
Application & Finish	<p>The mixed SikaRepair SHA must be worked well into the primed substrate, filling all pores and voids. Compact well. Force material against edge of repair working towards the center. Thoroughly compact the mortar around exposed reinforcement. After filling repair, consolidate, then screed. Finish with steel, wood, plastic floats, or damp sponges, depending on the desired surface texture. Where multiple lifts are required, score top surface on each lift to produce a roughened substrate for next lift. Allow preceding lift to harden before applying fresh material. Saturate surface of the lift with clean water. If previous layers are over 48 hours old, mechanically prepare the substrate and dampen.</p>
Curing	<p>As per ACI recommendations for portland cement concrete, curing is required. Moist cure with wet burlap and polyethylene, a fine mist of water or a water based* compatible curing compound. Curing compounds adversely affect the adhesion of following lifts of mortar, leveling mortar or protective coatings. Moist curing should commence immediately after finishing. Protect freshly applied mortar from direct sunlight, wind, rain and frost.</p> <p>*Pretesting of curing compound is recommended.</p>
Limitations	<ul style="list-style-type: none"> ■ Application thickness: Minimum: With water: 1/4 inch (6 mm). With Latex R: 1/8" (3 mm). Maximum in one lift: 3 inches (75 mm) vertical, 1.5 inches (38 mm) overhead. ■ Minimum ambient and surface temperatures 45°F (7°C) and rising at time of application. ■ Do not use solvent based curing compounds. As with all cement based materials, avoid contact with aluminum to prevent adverse chemical reaction and possible product failure. Insulate potential areas of contact by coating aluminum bars, rails, posts etc. with an appropriate epoxy such as Sikadur Hi-Mod 32.
Caution	<p>Irritant</p> <p>Suspect carcinogen - Contains portland cement and sand (crystalline silica). Skin and eye irritant. Avoid contact. Dust may cause respiratory tract irritation. Avoid breathing dust. Use only with adequate ventilation. May cause delayed lung injury (silicosis). IARC lists crystalline silica as having sufficient evidence of carcinogenicity in laboratory animals and limited evidence of carcinogenicity in humans. NTP also lists crystalline silica as a suspect carcinogen. Use of safety goggles and chemical resistant gloves is recommended. If PELs are exceeded, an appropriate NIOSH approved respirator is required. Remove contaminated clothing.</p>
First Aid	<p>In case of skin contact, wash thoroughly with soap and water. For eye contact, flush immediately with plenty of water for at least 15 minutes, and contact a physician. For respiratory problems, remove person to fresh air.</p>
Clean Up	<p>In case of spillage, scoop or vacuum into appropriate container, and dispose of in accordance with current, applicable local, state and federal regulations. Keep container tightly closed and in an upright position to prevent spillage and leakage.</p> <p>Mixed material: Uncured material can be removed with water. Cured material can only be removed mechanically.</p>

KEEP CONTAINER TIGHTLY CLOSED
NOT FOR INTERNAL CONSUMPTION
CONSULT MATERIAL SAFETY DATA SHEET FOR MORE INFORMATION

KEEP OUT OF REACH OF CHILDREN
FOR INDUSTRIAL USE ONLY

Sika warrants this product for one year from date of installation to be free from manufacturing defects and to meet the technical properties on the current technical data sheet if used as directed within shelf life. User determines suitability of product for intended use and assumes all risks. Buyer's sole remedy shall be limited to the purchase price or replacement of product exclusive of labor or cost of labor.

NO OTHER WARRANTIES EXPRESS OR IMPLIED SHALL APPLY INCLUDING ANY WARRANTY OF MERCHANTABILITY OR FITNESS FOR A PARTICULAR PURPOSE. SIKA SHALL NOT BE LIABLE UNDER ANY LEGAL THEORY FOR SPECIAL OR CONSEQUENTIAL DAMAGES.

Visit our website at www.sikausa.com

1-800-933-SIKA NATIONWIDE

Regional Information and Sales Centers. For the location of your nearest Sika sales office, contact your regional center.

Sika Corporation
201 Polito Avenue
Lyndhurst, NJ 07071
Phone: 800-933-7452
Fax: 201-933-6225

Sika Canada Inc.
601 Delmar Avenue
Pointe Claire
Quebec H9R 4A9
Phone: 514-897-2610
Fax: 514-694-2792

Sika Mexicana S.A. de C.V.
Carretera Libre Calaya Km. 8.5
Corregidora, Queretaro
C.P. 76920 A.P. 136
Phone: 52 42 25 0122
Fax: 52 42 25 0537



Quality Certification Numbers: Lyndhurst: FM 69711 (ISO 9000), FM 70421 (QS 9000), Marion: FM 69715, Kansas City: FM 68107, Santa Fe Springs: FM 69408

Sika and SikaRepair are registered trademarks. Made in USA. Printed in USA.

Product Data Sheet
Edition 8.2003
Identification no. 188
SikaTop 123 *Plus*

SikaTop® 123 PLUS

Two-component, polymer-modified, cementitious, non-sag mortar plus FerroGard 901 penetrating corrosion inhibitor

Description	SikaTop 123 <i>PLUS</i> is a two-component, polymer-modified, portland cement, fast-setting, non-sag mortar. It is a high performance repair mortar for vertical and overhead surfaces, and offers the additional benefit of FerroGard 901, a penetrating corrosion inhibitor.		
Where to Use	<ul style="list-style-type: none"> ■ On grade, above, and below grade on concrete and mortar. ■ On vertical and overhead surfaces. ■ As a structural repair material for parking structures, industrial plants, water/waste water treatment facilities, roads, walkways, bridges, tunnels, dams, ramps, etc. ■ Approved for repairs over cathodic protection systems. 		
Advantages	<ul style="list-style-type: none"> ■ High compressive and flexural strengths. ■ High early strengths. ■ Increased freeze/thaw durability and resistance to de-icing salts. ■ Compatible with coefficient of thermal expansion of concrete - Passes ASTM C-884 (modified). ■ Increased density - improved carbon dioxide resistance (carbonation) without adversely affecting water vapor transmission (not a vapor barrier). ■ Enhanced with FerroGard 901, a penetrating corrosion inhibitor - reduces corrosion even in the adjacent concrete. ■ Not flammable, non-toxic. ■ Conforms to ECA/USPHS standards for surface contact with potable water. ■ USDA approved. ■ ANSI/NSF Standard 61 potable water approved. 		
Yield	0.39 cu. ft./unit.		
Packaging	Component 'A' - 1 gal. plastic jug; 4/carton. Component 'B' - 44 lb. multi-wall bag.		
Typical Data (Material and curing conditions @ 73°F (23°C) and 50% R.H.)			
Shelf Life	One year in original, unopened packaging.		
Storage Conditions	Store dry at 40°-95°F. Condition material to 65°-75°F. before using. Protect Component 'A' from freezing. If frozen, discard.		
Color	Concrete gray when mixed.		
Mixing Ratio	Plant-proportioned kit.		
Application Time	Approximately 15 min. after adding Component 'B' to Component 'A'. Application time is dependent on temperature and relative humidity.		
Finishing Time	20 to 60 min after combining components: depends on temperature, relative humidity, and type of finish desired.		
Density (wet Mix)	132 lbs./cu. ft. (2.2 kg./l)		
Flexural Strength (ASTM C-293)	28 days	2,000 psi (13.8 MPa)	
Splitting Tensile Strength (ASTM C-496)	28 days	900 psi (6.2 MPa)	
Bond Strength* (ASTM C-882 modified)	28 days	2,200 psi (15.2 MPa)	
Compressive Strength (ASTM C-109)			
	1 day	3,500 psi	(24.1 MPa)
	7 days	6,000 psi	(41.4 MPa)
	28 days	7,000 psi	(48.3 MPa)
Permeability (AASHTO-277)	28 days Approximately 500 Coulombs. Electrical resistivity (ohm-cm) 27,000		
Freeze/Thaw Resistance (ASTM C-666)	300 cycles	98%	
Corrosion Testing for FerroGard 901			
Cracked Beam Corrosion Tests:	Reduced corrosion rates 63% versus control specimens. ASTM G109 modified after 400 days		
<small>* Mortar scrubbed into substrate.</small>			
Substrate	Concrete, mortar, and masonry products.		



How to Use

Surface Preparation Concrete/Mortar: Remove all deteriorated concrete, dirt, oil, grease, and all bond-inhibiting materials from surface. Be sure repair area is not less than 1/8 inch in depth. Preparation work should be done by high pressure water blast, scabblor, or other appropriate mechanical means to obtain an exposed aggregate surface with a minimum surface profile of ±1/16 in. (CSP-5) Saturate surface with clean water. Substrate should be saturated surface dry (SSD) with no standing water during application.
Reinforcing Steel: Steel reinforcement should be thoroughly prepared by mechanical cleaning to remove all traces of rust. Where corrosion has occurred due to the presence of chlorides, the steel should be high-pressure washed with clean water after mechanical cleaning. For priming of reinforcing steel use Sika Armatec 110 EpoCem (consult Technical Data Sheet).

Priming **Concrete Substrate:** Prime the prepared substrate with a brush or sprayed applied coat of Sika Armatec 110 EpoCem (consult Technical Data Sheet). Alternately, a scrub coat of Sika Top 123 can be applied prior to placement of the mortar. The repair mortar has to be applied into the wet scrub coat before it dries.

Mixing Pour Component 'A' into mixing container. Add Component 'B' while mixing continuously. Mix mechanically with a low-speed drill (400 - 600 rpm) and mixing paddle or mortar mixer. Mix to a uniform consistency, maximum 3 minutes. Manual mixing can be tolerated only for less than a full unit. Thorough mixing and proper proportioning of the two components is necessary.

Application & Finish SikaTop 123 PLUS **must be scrubbed** into the substrate, filling all pores and voids. Force material against edge of repair, working toward center. After filling repair, consolidate, then screed. Material may be applied in multiple lifts. The thickness of each lift, not to be less than 1/8 inch minimum or more than 1.5 inches maximum. Where multiple lifts are required score top surface of each lift to produce a roughened surface for next lift. Allow preceding lift to reach final set, 30 minutes minimum, before applying fresh material. Saturate surface of the lift with clean water. Scrub fresh mortar into preceding lift. Allow mortar or concrete to set to desired stiffness, then finish with wood or sponge float for a smooth surface.

Curing As per ACI recommendations for portland cement concrete, curing is required. Moist cure with wet burlap and polyethylene, a fine mist of water or a water based*, compatible curing compound. Curing compounds adversely affect the adhesion of following lifts of mortar, leveling mortar or protective coatings. Moist curing should commence immediately after finishing. If necessary protect newly applied material from direct sunlight, wind, rain and frost.

*Pretesting of curing compound is recommended.

Limitations

- **Application thickness:** Minimum 1/8 inch (3 mm). Maximum in one lift - 1.5 in. (38 mm).
- Minimum ambient and surface temperatures 45°F (7°C) and rising at time of application.
- Do not use solvent-based curing compound.
- Size, shape and depth of repair must be carefully considered and consistent with practices recommended by ACI. For additional information, contact Technical Service.
- For additional information on substrate preparation, refer to ICRI Guideline No. 03732 Coatings, and Polymer Overlays".
- If aggressive means of substrate preparation is employed, substrate strength should be tested in accordance with ACI 503 Appendix A prior to the repair application.
- As with all cement based materials, avoid contact with aluminum to prevent adverse chemical reaction and possible product failure. Insulate potential areas of contact by coating aluminum bars, rails, posts etc. with an appropriate epoxy such as Sikadur Hi-Mod 32.

Caution **Component 'A' - Irritant** - May cause skin/eye/respiratory irritation. Avoid breathing vapors. Use with adequate ventilation. Avoid skin and eye contact. Safety goggles and rubber gloves are recommended. **Component 'B' - Irritant; suspect carcinogen** - Contains portland cement and sand (crystalline silica). Skin and eye irritant. Avoid contact. Dust may cause respiratory tract irritation. Avoid breathing dust. Use only with adequate ventilation. May cause delayed lung injury (silicosis). IARC lists crystalline silica as having sufficient evidence of carcinogenicity in laboratory animals and limited evidence of carcinogenicity in humans. NTP also lists crystalline silica as a suspect carcinogen. Use of safety goggles and chemical resistant gloves is recommended. If PELs are exceeded, an appropriate, NIOSH approved respirator is required. Remove contaminated clothing.

First Aid In case of skin contact, wash thoroughly with soap and water. For eye contact, flush immediately with plenty of water for at least 15 minutes, and contact a physician. For respiratory problems, remove person to fresh air.

Clean Up In case of spillage, scoop or vacuum into appropriate container, and dispose of in accordance with current, applicable local, state and federal regulations. Keep container tightly closed and in an upright position to prevent spillage and leakage.

Mixed components: Uncured material can be removed with water. Cured material can only be removed mechanically.

KEEP CONTAINER TIGHTLY CLOSED
 NOT FOR INTERNAL CONSUMPTION
 CONSULT MATERIAL SAFETY DATA SHEET FOR MORE INFORMATION

KEEP OUT OF REACH OF CHILDREN
 FOR INDUSTRIAL USE ONLY

Sika warrants this product for one year from date of installation to be free from manufacturing defects and to meet the technical properties on the current technical data sheet if used as directed within shelf life. User determines suitability of product for intended use and assumes all risks. Buyer's sole remedy shall be limited to the purchase price or replacement of product exclusive of labor or cost of labor.

NO OTHER WARRANTIES EXPRESS OR IMPLIED SHALL APPLY INCLUDING ANY WARRANTY OF MERCHANTABILITY OR FITNESS FOR A PARTICULAR PURPOSE. SIKA SHALL NOT BE LIABLE UNDER ANY LEGAL THEORY FOR SPECIAL OR CONSEQUENTIAL DAMAGES.

Visit our website at www.sikausa.com

1-800-933-SIKA NATIONWIDE

Regional Information and Sales Centers. For the location of your nearest Sika sales office, contact your regional center.

Sika Corporation
 201 Polito Avenue
 Lyndhurst, NJ 07071
 Phone: 800-933-7452
 Fax: 201-933-6225

Sika Canada Inc.
 601 Delmar Avenue
 Pointe Claire
 Quebec H9R 4A9
 Phone: 514-697-2610
 Fax: 514-694-2792

Sika Mexicana S.A. de C.V.
 Carretera Libre Celaya Km. 8.5
 Corregidora, Queretaro
 C.P. 76920 A.P. 136
 Phone: 52 42 25 0122
 Fax: 52 42 25 0537



T E C H N I C A L D A T A S H E E T



Conpatch VO Vertical and overhead repair mortar

PRODUCT DESCRIPTION

Conspec Conpatch V/O is a single component, cement based, polymer modified patching and render repair mortar developed for vertical and overhead, thin to thick surface applications. Conpatch V/O's unique rapid setting, shrinkage compensating formulation offers excellent durability and ease of application without the use of forms. If required the material may be mixed with Corrosion Inhibitor admixture using proven calcium nitrite technology.

USE

Conpatch V/O is specifically formulated to repair vertical and overhead concrete. Surfaces subjected to severe freeze-thaw and de-icing salts such as bridge columns, parking structures columns, spandrels beams, concrete ceilings, tunnels, pipes, pilings and any other vertical or overhead application where excellent durability and strength is required.

BENEFITS

- ◇ Standard product is one-component; just add water
- ◇ Can be used as a two-component repair mortar with approved admixture
- ◇ Excellent resistance to freeze-thaw and de-icing salts
- ◇ Available with proven calcium nitrite corrosion technology
- ◇ Designed for Vertical and Overhead Patching
- ◇ Interior and exterior applications
- ◇ Can be extended for deep patches
- ◇ Rapid set and strength gain for multi-lift and structural repairs
- ◇ Is shrinkage compensated, helping to assure a tight contact with surrounding substrate
- ◇ High bond strength
- ◇ Thermal expansion similar to concrete for long term durability
- ◇ For overhead, vertical and horizontal applications
- ◇ Can be pumped and sprayed through small volume pneumatic equipment

PROPERTIES, TEST DATA

Initial Set 30 minutes

Final Set 60 minutes

Compressive Strength (ASTM C - 109)

24 hours >4500 psi (31 MPa)

7 days >7000 psi >(48 MPa)

28 days >8000 psi >(55 MPa)

Flexural Strength (ASTM C -78)

1 Day 850 psi

7 Day 1,000 psi

28 day 1,200 psi

Splitting Tensile Strength (ASTM C-496)

1 Day 240 psi

7 Day 540 psi

28 Day 650 psi

Direct Tensile Strength (CRD C164)

1 Day 170 psi

7 Day 200 psi

28 Day 240 psi

Modulus of Elasticity (ASTM C469)

28 Days 3.9x10⁶

Bond Strength (ACI 503R Direct Tensile)

1 Day 200 psi

7 Day 245 psi

28 Day 300 psi

Coefficient of Thermal Expansion (CRD C-39 modified)

4.4x10⁻⁶

Freeze Thaw Resistance (ASTM C666, Procedure A)

300 cycles >96%

Scaling Resistance (ASTM C672)

50 cycles 0 Rating

Rapid Chloride Permeability (ASTM C1202)

28 Days 430 Coulombs

APPLICATION

Surface Preparation

The concrete must be sound and free of all foreign material, including oil, grease, dust, laitance, or other surface contaminants. We recommend surface prep per ICRI Guideline 03730. Saw cut the perimeter of the repair to a maximum depth of 1/2" (1.3 cm). Best results will be obtained by abrasive blasting the area to be repaired, providing uniform depth, a high surface profile and a firm bonding area. All surfaces to be repaired should be in a saturated-surface-dry (SSD) condition with no standing water on the surface.

Mixing

Ratios:

Standard Mix: Add 6.25 - 6.75 pints (2.94-3.19 L) of clean potable water per 50 lb. (22.7 kg) bag or 20-24 oz. (0.59-.70 L) per 10 lbs. (4.5 kg) of Conpatch V/O material.

Acrylic Admix: Add 6.5-6.75 pints (3.08-3.19 L) of Strong Bond diluted 1:1 with clean potable water per 50 lb. (22.7 kg) bag.

Corrosion Inhibitor: 6.5-6.75 pints (3.08-3.19 L) of Special Bond CI neat per 50 lb. (22.7 kg) bag.

Mixing: Mix with a low speed drill or, for larger projects, a mortar mixer. Add recommended amount of clean water or Special Bond CI into the container followed by the Conpatch V/O. Mix 2 to 3 minutes. Mix only what can be applied within the setting period. Work time is approximately 15-25 minutes.

Scrub-coat: Using freshly mixed Conpatch V/O, scrub a thin layer into the SSD substrate with a stiff fiber brush and

Refer to www.daytonsuperiorchemical.com for latest Technical Data Sheet and MSDS
Conspec a brand of Dayton Superior Corporation • 4226 Kansas Ave. Kansas City, KS 66106
Phone: (877) 416- 3439 • www.daytonsuperiorchemical.com • Fax: (913) 279- 4806

place the Conpatch V/O before the scrub coat dries. In certain conditions the use of an approved bonding agent, i.e. Spec Bond 100 surface applied epoxy or Special Bond CI integral mix, may be required. Contact technical services for further information.

Application Temperature Range: Ideal installation temperatures are from 50°F (10°C) to 80°F (27°C). Cooler temperatures will slow set-time and strength gain. Hot temperatures will accelerate set time.

Placement

Place the Conpatch V/O by trowel or hand before the scrub coat dries. On patching applications, trowel the Conpatch V/O onto the surface to a minimum thickness of 1/4" (0.6 cm) and a maximum neat thickness of 2". Additional lifts can be placed up to 6 inches and between each lift, the substrate must be left roughened or scarified. Prior to each lift, the surface must be in a SSD condition and a scrub coat applied immediately prior to the next lift being applied.

Curing

Conpatch V/O is self-curing under most conditions. Thin applications will require actions for curing. To assure maximum durability under severe drying conditions (high wind and temperature, low humidity), moist cure or use approved ASTM C-309 Conspec water based curing compound.

Clean Up

Use water when material is wet. Hardened material requires abrasive methods.

WASTE DISPOSAL

Dispose of waste material and empty packaging in accordance with all Federal, State and Local requirements. Refer to the product's MSDS for further information.

ESTIMATED YIELD

0.37 ft³ (0.01 m³)

PACKAGING

ITEM #	Package	Weight	
		lb.	kg
300437	Bags	50	22.7

STORAGE

Shelf life of unopened bags, when stored in a dry facility, is 12 months. Excessive temperature differential and/or high humidity can shorten the shelf life expectancy. Store in a cool, dry area free of direct sunlight.

LIMITATIONS

When using less than one bag always dry mix the full bag. Supported patches deeper than 2" (5 cm) may require reinforcement or anchorage. Applications for unsupported repairs exceeding 1" (2.54 cm) in thickness may require anchorage and should be designed in accordance with the provisions of SEI/ASCE 7-02, Section 9.6.1.6. Please consult the engineer of record for special requirements that may be required. DO NOT place at unprotected

temperatures below 40°F(5°C) or if the temperature is expected to drop below 40°F(5°C) in the next twenty-four hour period. In hot weather, follow ACI Committee 305 recommended procedures. Do not apply over smooth hard trowelled surfaces without roughening.

PRECAUTIONS

Contains Portland cement and sand. Cement will cause irritation. Avoid contact. Use of a dust respirator, safety goggles and rubber gloves is recommended. Avoid prolonged contact with eyes, immediately flush with water for at least 15 minutes. Get prompt medical attention. DO NOT wear contact lenses when working with this product. DO NOT take internally. Keep out of reach of children. Avoid hazards by following all precautions found in the Material Safety Data Sheet (MSDS), product labels and technical literature. Please read this information prior to using the product.

MANUFACTURER

Conspec a brand of Dayton Superior Corporation
 4226 Kansas Avenue
 Kansas City, KS 66106
 Customer Service: 877-416-3439
 Technical Service: 877-416-3439
 Website: www.daytonsuperiorchemical.com

WARRANTY

Dayton Superior Corporation ("Dayton") warrants for 12 months from the date of manufacture or for the duration of the published product shelf life, whichever is less, that at the time of shipment by Dayton, the product is free of manufacturing defects and conforms to Dayton's product properties in force on the date of acceptance by Dayton of the order. Dayton shall only be liable under this warranty if the product has been applied, used, and stored in accordance with Dayton's instructions, especially surface preparation and installation, in force on the date of acceptance by Dayton of the order. The purchaser must examine the product when received and promptly notify Dayton in writing of any non-conformity before the product is used and no later than 30 days after such non-conformity is first discovered. If Dayton, in its sole discretion, determines that the product breached the above warranty, it will, in its sole discretion, replace the non-conforming product, refund the purchase price or issue a credit in the amount of the purchase price. This is the sole and exclusive remedy for breach of this warranty. Only a Dayton officer is authorized to modify this warranty. The information in this data sheet supersedes all other sales information received by the customer during the sales process. THE FOREGOING WARRANTY SHALL BE EXCLUSIVE AND IN LIEU OF ANY OTHER WARRANTIES, EXPRESS OR IMPLIED, INCLUDING WARRANTIES OF MERCHANTABILITY AND FITNESS FOR A PARTICULAR PURPOSE, AND ALL OTHER WARRANTIES OTHERWISE ARISING BY OPERATION OF LAW, COURSE OF DEALING, CUSTOM, TRADE OR OTHERWISE.

LIMITATION OF LIABILITY

Dayton shall not be liable in contract or in tort (including, without limitation, negligence, strict liability or otherwise) for loss of sales, revenues or profits; cost of capital or funds; business interruption or cost of downtime, loss of use, damage to or loss of use of other property (real or personal); failure to realize expected savings; frustration of economic or business expectations; claims by third parties (other than for bodily injury), or economic losses of any kind; or for any special, incidental, indirect, consequential, punitive or exemplary damages arising in any way out of the performance of, or failure to perform, its obligations under any contract for sale of product, even if Dayton could foresee or has been advised of the possibility of such damages. The Parties expressly agree that these limitations on damages are allocations of risk constituting, in part, the consideration for this contract, and also that such limitations shall survive the determination of any court of competent jurisdiction that any remedy provided in these terms or available at law fails of its essential purpose.

Refer to www.daytonsuperiorchemical.com for latest Technical Data Sheet and MSDS
 Conspec a brand of Dayton Superior Corporation • 4226 Kansas Ave. Kansas City, KS 66106
 Phone: (877) 416- 3439 • www.daytonsuperiorchemical.com • Fax: (913) 279- 4806



The Chemical Company

PRODUCT DATA

3^{03 01 20} Concrete Rehabilitation

HB2 REPAIR MORTAR

Polymer-modified high-build repair mortar

Description

HB2 Repair Mortar is a two-component polymer-modified high-build, lightweight repair mortar. It is designed for repairing vertical and overhead concrete surfaces in deep lifts—up to 3" on vertical and 1-1/2" on overhead surfaces. It can be applied by hand, trowel, or low-velocity wet spraying.

Yield

No. 1 Kit:
0.50 ft³ (0.015 m³ per 45 lb bag)
No. 2 Kit:
2.50 ft³ (0.076 m³ per 225 lb bag)

Packaging

No. 1 Kit
45 lbs (20.4 kg) powder
1 gallon (3.8 L) liquid

No. 2 Kit
225 lbs (102 kg) powder
5 gallon (18.9 L) liquid

Shelf Life

1 year when properly stored

Storage

Store and transport in unopened containers at 60 to 80° F (16 to 27° C) in clean, dry conditions. Do not allow the liquid component to freeze.

Features

- Lightweight
- Shrinkage compensated
- Polymer modified
- Low permeability
- Excellent freeze/thaw resistance
- Coefficient of thermal expansion similar to concrete

Benefits

- Fast, easy overhead repairs
- Minimizes shrinkage and stresses on the bond line
- Enhanced adhesion
- Provides protection against carbon dioxide and chloride intrusion
- Durable repairs in cold temperatures
- Reduces failures caused by thermal movement

Where to Use

APPLICATION

- Structural concrete repairs
- Applications that require high levels of resistance to chlorides and carbon-dioxide
- Parking garages
- Columns and beams
- High-rise buildings

LOCATION

- Vertical and overhead surfaces
- Interior or exterior

SUBSTRATE

- Concrete

How to Apply

Concrete

1. Concrete substrate must be structurally sound. Loose or unsound concrete should be removed.
2. Saw cut the edges of the repair locations to a depth of at least 3/8" (10 mm) to avoid feather-edging and to provide a square edge. Break out the complete repair area to a minimum depth of 3/8" (10 mm) up to the sawn edge.
3. Clean the surface by removing any dust, unsound or contaminated material, oil, paint, greases, and corrosion deposits.
4. Where breaking out is not required, roughen the surface and remove any laitance by mechanical means or high-pressure water wash. Remove oil and grease deposits by steam cleaning, detergent scrubbing, or degreasing.
5. To ensure optimum repair results, assess the effectiveness of decontamination by a pull-off test.



Technical Data

Composition

HB2 Repair Mortar is a proprietary blend of cement, graded aggregate, shrinkage-compensating agents, additives, and latex.

Test Data

The following results were obtained with a liquid / powder ratio of 3.7 quarts per 45 lb (3.5 L per 20.5 kg) bag.

PROPERTY	RESULTS	TEST METHODS
Fresh wet density , lb/ft ³ (kg/m ³)	105 (1,682)	ASTM C 138
Working time , min, at 72° F (22° C), 50% relative humidity	45	
Set time , hrs, at 72° F (22° C), 50% relative humidity		ASTM C 191
Initial	3	
Final	4	
Compressive strength , psi (MPa), 2" (51 mm) cubes		ASTM C 109
1 day	2,300 (15.9)	
7 days	4,500 (31.0)	
28 days	5,800 (40.0)	
Compressive strength , psi (MPa), 3 by 6" (76 by 152 mm) cylinders, at 28 days	5,000 (34.5)	ASTM C 39
Flexural strength , psi (MPa) at 28 days	1,000 (6.9)	ASTM C 348
Slant shear bond strength , psi (MPa)		ASTM C 882, modified ¹
7 days	2,100 (14.5)	
28 days	2,700 (18.6)	
Splitting tensile strength , psi (MPa)		ASTM C 496
7 days	300 (2.1)	
28 days	590 (4.1)	
Elastic modulus , psi (GPa)	2.0 x 10 ⁶ (13.8)	ASTM C 469
Coefficient of thermal expansion ² , 1" (25 mm) prisms, in/in/° F (cm/cm/° C)	4.5 x 10 ⁻⁶ (8.1 x 10 ⁻⁶)	CRD C 39
Drying shrinkage , μstrain, at 28 days	350	ASTM C 157
Freeze/thaw resistance , % RDM ³ , at 300 cycles	100	ASTM C 666
Rapid chloride permeability , coulombs	941 (very low)	ASTM C 1202

All application and performance values are typical for the material, but may vary with test methods, conditions, and configurations.

¹No bonding agent scrubbed into prepared surface.

²Portland cement concrete, typical range is 4.0 – 8.0 x 10⁻⁶ in/in/° F (7.2 – 14.4 x 10⁻⁶ cm/cm/° C), according to American Concrete Institute.

³Relative dynamic modulus

REINFORCING STEEL

1. Remove all oxidation and scale from the exposed reinforcing steel in accordance with ICRI Technical Guideline No. 03730 "Guide for Surface Preparation for the Repair of Deteriorated Concrete Resulting from Reinforcing Steel Corrosion."
2. For additional protection from future corrosion, coat the prepared reinforcing steel with Zincrich Rebar Primer or install Corr-Stops® CM.

Mixing

1. Ensure that HB2 Repair Mortar is thoroughly mixed; a forced action mixer is essential. Do not use free-fall mixers.
2. For the occasional 1 bag mix, using a suitably sized container and an appropriate paddle and variable-speed (400 – 500 rpm) heavy-duty drill is acceptable. Do not mix partial bags. Always mix the material in a clean container.
3. For normal applications, place 3 quarts (2.8 L) of MBT® Polymer Liquid into the clean mixer for each complete 45 lb (20.5 kg) bag of HB2 Repair Mortar. The powder should always be added to the liquid.
4. Mix 3 – 5 minutes until fully homogeneous. Avoid overmixing.
5. Depending on the ambient temperature and the desired consistency, additional MBT® Polymer Liquid may be added, but the maximum liquid content should not exceed 1 gallon (3.8 L) per 45 lb (20.5 kg) bag of HB2 Repair Mortar.

Application

1. Substrate should be saturated surface-dry (SSD) with no standing water.
2. Using a stiff brush, scrub a thin coat of the mixed material thoroughly into the surface to ensure sufficient bonding.
3. Before bond coat dries, thoroughly compact the mortar onto the substrate and around the exposed reinforcement.
4. HB2 Repair Mortar can be applied in single lifts up to 3" (76 mm) in thickness on vertical surfaces and up to 1-1/2" (38 mm) in thickness on overhead surfaces (without the use of form work).
5. Depending on the actual configuration of the repair area and the volume of exposed reinforcing steel, applications can be made in either single or multiple lifts. If multiple lifts are used, lightly rake the surface after initial set and before applying subsequent lifts.
6. If the material sags during application, completely remove HB2 Repair Mortar. Properly reprime the substrate and reapply the mortar at a reduced thickness.
7. Finish HB2 Repair Mortar by striking off with a straight edge and close with a steel trowel. Wooden or plastic floats or sponges may also be used to achieve the desired surface texture. Do not overwork the completed surface.

Curing

1. Proper curing is extremely important. For peak performance of the repair, cure immediately after finishing in accordance with good concrete practices (refer to ACI 308).
2. An ASTM C 309-compliant curing compound may be used in place of moist curing. Apply the curing compound when the surface cannot be marred by the application process.

Clean Up

Remove HB2 Repair Mortar from tools, equipment, and mixers with clean water immediately after use. Cured material can only be removed mechanically. Clean hands and skin immediately with soap and water or industrial hand cleaner.

For Best Performance

- Do not mix partial bags.
- Exposure to heavy rainfall before the final set may result in surface scour.
- In cold conditions down to 40° F (4° C), maintain MBT® Polymer Liquid at 80° F (26° C) to accelerate strength development. Adopt normal precautions for working with cementitious materials in the winter. Do not apply if the temperature is expected to fall below 40° F (4° C) within 24 hours of application. For cold-weather applications, consider using HBA Repair Mortar (see Form No. 1018991).
- At ambient temperatures above 80° F (26° C), store the materials in the shade. Cool MBT® Polymer Liquid to 60° F (16° C) before using.
- Make certain the most current versions of product data sheet and MSDS are being used; call Customer Service (1-800-433-9517) to verify the most current version.
- Proper application is the responsibility of the user. Field visits by BASF personnel are for the purpose of making technical recommendations only and not for supervising or providing quality control on the jobsite.

Health and Safety

HB2 REPAIR MORTAR

Caution

HB2 Repair Mortar contains crystalline silica, and Portland cement.

Risks

Product is alkaline on contact with water and may cause injury to skin or eyes. Ingestion or inhalation of dust may cause irritation. Contains free respirable quartz, which has been listed as a suspected human carcinogen by NTP and IARC. Repeated or prolonged overexposure to free respirable quartz may cause silicosis or other serious and delayed lung injury.

Precautions

KEEP OUT OF THE REACH OF CHILDREN. Prevent contact with skin and eyes. Prevent inhalation of dust. DO NOT take internally. Use only with adequate ventilation. Use impervious gloves, eye protection and if the TLV is exceeded or used in a poorly ventilated area, use NIOSH/MSHA approved respiratory protection in accordance with applicable federal, state and local regulations.

First Aid

In case of eye contact, flush thoroughly with water for at least 15 minutes. SEEK IMMEDIATE MEDICAL ATTENTION. In case of skin contact, wash affected areas with soap and water. If irritation persists, SEEK MEDICAL ATTENTION. Remove and wash contaminated clothing. If inhalation causes physical discomfort, remove to fresh air. If discomfort persists or any breathing difficulty occurs or if swallowed, SEEK IMMEDIATE MEDICAL ATTENTION.

Refer to Material Safety Data Sheet (MSDS) for further information.

Proposition 65

This product contains material listed by the state of California as known to cause cancer, birth defects, or other reproductive harm.

VOC Content

0 lbs/gal or 0 g/L

**For medical emergencies only,
call ChemTrec (1-800-424-9300).**

BASF Building Systems

889 Valley Park Drive
Shakopee, MN, 55379

www.BASFBUILDINGSYSTEMS.COM

Customer Service 800-433-9517

Technical Service 800-243-6739

LIMITED WARRANTY NOTICE: Every reasonable effort is made to apply BASF exacting standards both in the manufacture of our products and in the information which we issue concerning these products and their use. We warrant our products to be of good quality and will replace or, at our election, refund the purchase price of any products proved defective. Satisfactory results depend not only upon quality products, but also upon many factors beyond our control. Therefore, except for such replacement or refund, BASF MAKES NO WARRANTY OR GUARANTEE, EXPRESS OR IMPLIED, INCLUDING WARRANTIES OF FITNESS FOR A PARTICULAR PURPOSE OR MERCHANTABILITY, RESPECTING ITS PRODUCTS, and BASF shall have no other liability with respect thereto. Any claim regarding product defect must be received in writing within one (1) year from the date of shipment. No claim will be considered without such written notice or after the specified time interval. User shall determine the suitability of the products for the intended use and assume all risks and liability in connection therewith. Any authorized change in the printed recommendations concerning the use of our products must bear the signature of the BASF Technical Manager.

This information and all further technical advice are based on BASF's present knowledge and experience. However, BASF assumes no liability for providing such information and advice including the extent to which such information and advice may relate to existing third party intellectual property rights, especially patent rights. In particular, BASF disclaims all CONDITIONS AND WARRANTIES, WHETHER EXPRESS OR IMPLIED, INCLUDING THE IMPLIED WARRANTIES OF FITNESS FOR A PARTICULAR PURPOSE OR MERCHANTABILITY. BASF SHALL NOT BE RESPONSIBLE FOR CONSEQUENTIAL, INDIRECT OR INCIDENTAL DAMAGES (INCLUDING LOSS OF PROFITS) OF ANY KIND. BASF reserves the right to make any changes according to technological progress or further developments. It is the customer's responsibility and obligation to carefully inspect and test any incoming goods. Performance of the product(s) described herein should be verified by testing and carried out only by qualified experts. It is the sole responsibility of the customer to carry out and arrange for any such testing. Reference to trade names used by other companies is neither a recommendation, nor an endorsement of any product and does not imply that similar products could not be used.

For professional use only. Not for sale to or use by the general public.

Form No. 1018990 8/06
Printed on recycled paper including 10% post-consumer fiber.

© 2006 BASF
Printed in U.S.A.



The Chemical Company

PRODUCT DATA

3 03 01 00 Maintenance of Concrete

SET® 45 AND SET® 45 HW

Chemical-action repair mortar

Description

Set® 45 is a one-component magnesium phosphate-based patching and repair mortar. This concrete repair and anchoring material sets in approximately 15 minutes and takes rubber-tire traffic in 45 minutes. It comes in two formulations: Set® 45 Regular for ambient temperatures below 85° F (29° C) and Set® 45 Hot Weather for ambient temperatures ranging from 85 to 100° F (29 to 38° C).

Yield

A 50 lb (22.7 kg) bag of mixed with the required amount of water produces a volume of approximately 0.39 ft³ (0.011 m³); 60% extension using 1/2" (13 mm) rounded, sound aggregate produces approximately 0.58 ft³ (0.016 m³).

Packaging

50 lb (22.7 kg) multi-wall bags

Color

Dries to a natural gray color

Shelf Life

1 year when properly stored

Storage

Store in unopened containers in a clean, dry area between 45 and 90° F (7 and 32° C).

Features

- Single component
- Reaches 2,000 psi compressive strength in 1 hour
- Wide temperature use range
- Superior bonding
- Very low drying shrinkage
- Resistant to freeze/thaw cycles and deicing chemicals
- Only air curing required
- Thermal expansion and contraction similar to Portland cement concrete
- Sulfate resistant

Benefits

- Just add water and mix
- Rapidly returns repairs to service
- From below freezing to hot weather exposures
- Bonds to concrete and masonry without a bonding agent
- Improved bond to surrounding concrete
- Usable in most environments
- Fast, simple curing process
- More permanent repairs
- Stable where conventional mortars degrade

Where to Use

APPLICATION

- Heavy industrial repairs
- Dowel bar replacement
- Concrete pavement joint repairs
- Full-depth structural repairs
- Setting of expansion device nosings
- Bridge deck and highway overlays
- Anchoring iron or steel bridge and balcony railings
- Commercial freezer rooms
- Truck docks
- Parking decks and ramps
- Airport runway-light installations

LOCATION

- Horizontal and formed vertical or overhead surfaces
- Indoor and outdoor applications

How to Apply

Surface Preparation

1. A sound substrate is essential for good repairs. Flush the area with clean water to remove all dust.
2. Any surface carbonation in the repair area will inhibit chemical bonding. Apply a pH indicator to the prepared surface to test for carbonation.
3. Air blast with oil-free compressed air to remove all water before placing Set® 45.



Technical Data

Composition

Set® 45 is a magnesium-phosphate patching and repair mortar.

Test Data

PROPERTY	RESULTS				TEST METHODS
Typical Compressive Strengths*, psi (MPa)					ASTM C 109, modified
	Plain Concrete 72° F (22° C)	Set® 45 Regular 72° F (22° C)	Set® 45 Regular 36° F (2° C)	Set® 45 HW 95° F (35° C)	
1 hour	—	2,000 (13.8)	—	—	
3 hour	—	5,000 (34.5)	—	3,000 (20.7)	
6 hour	—	5,000 (34.5)	1,200 (8.3)	5,000 (34.5)	
1 day	500 (3.5)	6,000 (41.4)	5,000 (34.5)	6,000 (41.4)	
3 day	1,900 (13.1)	7,000 (48.3)	7,000 (48.3)	7,000 (48.3)	
28 day	4,000 (27.6)	8,500 (58.6)	8,500 (58.6)	8,500 (55.2)	
NOTE: Only Set® 45 Regular formula, tested at 72° F (22° C), obtains 2,000 psi (13.8 MPa) compressive strength in 1 hour.					
Modulus of Elasticity, psi (MPa)					ASTM C 469
		7 days	28 days		
Set® 45 Regular		4.18 x 10 ⁶ (2.88 x 10 ⁴)	4.55 x 10 ⁶ (3.14 x 10 ⁴)		
Set® 45 Hot Weather		4.90 x 10 ⁶ (3.38 x 10 ⁴)	5.25 x 10 ⁶ (3.62 x 10 ⁴)		
Freeze/thaw durability test, % RDM, 300 cycles, for Set® 45 and Set 45® HW					ASTM C 666, Procedure A (modified**)
			80		
Scaling resistance to deicing chemicals, Set® 45 and Set 45® HW					ASTM C 672
5 cycles			0		
25 cycles			0		
50 cycles			1.5 (slight scaling)		
Sulfate resistance					ASTM C 1012
Set® 45 length change after 52 weeks, %			0.09		
Type V cement mortar after 52 weeks, %			0.20		
Typical setting times, min, for Set® 45 at 72° F (22° C), and Set® 45 Hot Weather at 95° F (35° C)					Gilmore ASTM C 266, modified
Initial set			9 – 15		
Final set			10 – 20		
Coefficient of thermal expansion,***					CRD-C 39
both Set® 45 Regular and Set® 45 Hot Weather coefficients			7.15 x 10 ⁻⁶ /° F (12.8 x 10 ⁻⁶ /° C)		
Flexural Strength, psi (MPa), 3 by 4 by 16" (75 by 100 by 406 mm) prisms, 1 day strength,					ASTM C 78, modified
Set® 45 mortar			550 (3.8)		
Set® 45 mortar with 3/8" (9 mm) pea gravel			600 (4.2)		
Set® 45 mortar with 3/8" (9 mm) crushed angular noncalcareous hard aggregate			650 (4.5)		

* All tests were performed with neat material (no aggregate)

**Method discontinues test when 300 cycles or an RDM of 60% is reached.

***Determined using 1 by 1 by 11" (25 mm by 25 mm by 279 mm) bars. Test was run with neat mixes (no aggregate).
 Extended mixes (with aggregate) produce lower coefficients of thermal expansion.

Test results are averages obtained under laboratory conditions. Expect reasonable variations.

Mixing

1. Set® 45 must be mixed, placed, and finished within 10 minutes in normal temperatures (72° F [22° C]). Only mix quantities that can be placed in 10 minutes or less.
2. Do not deviate from the following sequence; it is important for reducing mixing time and producing a consistent mix. Use a minimum 1/2" slow-speed drill and mixing paddle or an appropriately sized mortar mixer. Do not mix by hand.
3. Pour clean (potable) water into mixer. Water content is critical. Use a maximum of 4 pts (1.9 L) of water per 50 lb (22.7 kg) bag of Set® 45. Do not deviate from the recommended water content.
4. Add the powder to the water and mix for approximately 1 – 1-1/2 minutes.
5. Use neat material for patches from 1/2 – 2" (6 – 51 mm) in depth or width. For deeper patches, extend a 50 lb (22.7 kg) bag of Set® 45 HW by adding up to 30 lbs (13.6 kg) of properly graded, dust-free, hard, rounded aggregate or noncalcareous crushed angular aggregate, not exceeding 1/2" (6 mm) in accordance with ASTM C 33, #8. If aggregate is damp, reduce water content accordingly. Special procedures must be followed when angular aggregate is used. Contact your local BASF representative for more information. (Do not use calcareous aggregate made from soft limestone. Test aggregate for fizzing with 10% HCL).

Application

1. Immediately place the mixture onto the properly prepared substrate. Work the material firmly into the bottom and sides of the patch to ensure good bond.
2. Level the Set® 45 and screed to the elevation of the existing concrete. Minimal finishing is required. Match the existing concrete texture.

Curing

No curing is required, but protect from rain immediately after placing. Liquid-membrane curing compounds or plastic sheeting may be used to protect the early surface from precipitation, but never wet cure Set® 45.

For Best Performance

- Color variations are not indicators of abnormal product performance.
- Regular Set® 45 will not freeze at temperatures above -20° F (-29° C) when appropriate precautions are taken.
- Do not add sand, fine aggregate, or Portland cement to Set® 45.
- Do not use Set® 45 for patches less than 1/2" (13 mm) deep. For deep patches, use Set® 45 Hot Weather formula extended with aggregate, regardless of the temperature. Consult your BASF representative for further instructions.
- Do not use limestone aggregate.
- Water content is critical. Do not deviate from the recommended water content printed on the bag.
- Precondition these materials to approximately 70° F (21° C) for 24 hours before using.
- Protect repairs from direct sunlight, wind, and other conditions that could cause rapid drying of material.
- When mixing or placing Set® 45 in a closed area, provide adequate ventilation.
- Do not use Set® 45 as a precision nonshrink grout.
- Never featheredge Set® 45; for best results, always sawcut the edges of a patch.
- Prevent any moisture loss during the first 3 hours after placement. Protect Set® 45 with plastic sheeting or a curing compound in rapid-evaporation conditions.
- Do not wet cure.
- Do not place Set® 45 on a hot (90° F [32° C]), dry substrate.

- When using Set® 45 in contact with galvanized steel or aluminum, consult your local BASF sales representative.
- Make certain the most current versions of product data sheet and MSDS are being used; call Customer Service (1-800-433-9517) to verify the most current versions.
- Proper application is the responsibility of the user. Field visits by BASF personnel are for the purpose of making technical recommendations only and not for supervising or providing quality control on the jobsite.

Health and Safety

SET® 45

WARNING!

Contains silica, crystalline quartz, fly ash, magnesium oxide, phosphoric acid, monoammonium salt, iron oxide, silica, amorphous, aluminum oxide, sulfur trioxide.

Risks

Product is alkaline on contact with water and may cause injury to skin or eyes. Ingestion or inhalation of dust may cause irritation. Contains small amount of free respirable quartz which has been listed as a suspected human carcinogen by NTP and IARC. Repeated or prolonged overexposure to free respirable quartz may cause silicosis or other serious and delayed lung injury.

Precautions

Avoid contact with skin, eyes and clothing. Prevent inhalation of dust. Wash thoroughly after handling. Keep container closed when not in use. DO NOT take internally. Use only with adequate ventilation. Use impervious gloves, eye protection and if the TLV is exceeded or used in a poorly ventilated area, use NIOSH/MSHA approved respiratory protection in accordance with applicable Federal, state and local regulations.

First Aid

In case of eye contact, flush thoroughly with water for at least 15 minutes. In case of skin contact, wash affected areas with soap and water. If irritation persists, SEEK MEDICAL ATTENTION. Remove and wash contaminated clothing. If inhalation causes physical discomfort, remove to fresh air. If discomfort persists or any breathing difficulty occurs or if swallowed, SEEK IMMEDIATE MEDICAL ATTENTION.

Waste Disposal Method

This product when discarded or disposed of is not listed as a hazardous waste in federal regulations. Dispose of in a landfill in accordance with local regulations.

For additional information on personal protective equipment, first aid, and emergency procedures, refer to the product Material Safety Data Sheet (MSDS) on the job site or contact the company at the address or phone numbers given below.

Proposition 65

This product contains material listed by the State of California as known to cause cancer, birth defects or other reproductive harm.

VOC Content

0 g/L or 0 lbs/gal less water and exempt solvents.

**For medical emergencies only,
call ChemTrec (1-800-424-9300).**

BASF Construction Chemicals, LLC – Building Systems

889 Valley Park Drive
Shakopee, MN, 55379

www.BuildingSystems.BASF.com

Customer Service 800-433-9517
Technical Service 800-243-6739



LIMITED WARRANTY NOTICE: Every reasonable effort is made to apply BASF exacting standards both in the manufacture of our products and in the information which we issue concerning these products and their use. We warrant our products to be of good quality and will replace or, at our election, refund the purchase price of any products proved defective. Satisfactory results depend not only upon quality products, but also upon many factors beyond our control. Therefore, except for such replacement or refund, BASF MAKES NO WARRANTY OR GUARANTEE, EXPRESS OR IMPLIED, INCLUDING WARRANTIES OF FITNESS FOR A PARTICULAR PURPOSE OR MERCHANTABILITY, RESPECTING ITS PRODUCTS, and BASF shall have no other liability with respect thereto. Any claim regarding product defect must be received in writing within one (1) year from the date of shipment. No claim will be considered without such written notice or after the specified time interval. User shall determine the suitability of the products for the intended use and assume all risks and liability in connection therewith. Any authorized change in the printed recommendations concerning the use of our products must bear the signature of the BASF Technical Manager.

This information and all further technical advice are based on BASF's present knowledge and experience. However, BASF assumes no liability for providing such information and advice including the extent to which such information and advice may relate to existing third party intellectual property rights, especially patent rights. In particular, BASF disclaims all CONDITIONS AND WARRANTIES, WHETHER EXPRESS OR IMPLIED, INCLUDING THE IMPLIED WARRANTIES OF FITNESS FOR A PARTICULAR PURPOSE OR MERCHANTABILITY. BASF SHALL NOT BE RESPONSIBLE FOR CONSEQUENTIAL, INDIRECT OR INCIDENTAL DAMAGES INCLUDING LOSS OF PROFITS OF ANY KIND. BASF reserves the right to make any changes according to technological progress or further developments. It is the customer's responsibility and obligation to carefully inspect and test any incoming goods. Performance of the products described herein should be verified by testing and carried out only by qualified experts. It is the sole responsibility of the customer to carry out and arrange for any such testing. Reference to trade names used by other companies is neither a recommendation, nor an endorsement of any product and does not imply that similar products could not be used.

Form No. 1019335 8/07

Printed on recycled paper including 10% post-consumer fiber.

© 2007 BASF
Printed in U.S.A.

For professional use only. Not for sale to or use by the general public.

APPENDIX B: REPAIR MATERIAL AND SHEAR KEY GROUT VOLUME REQUIRED FOR EACH TEST

Test	Specimen Size (in)	Volume of Material for 1 Specimen (in ³)	Total Volume of Material (ft ³)	Number of Specimens	Number of Grout Materials	Total Volume of Material (in ³)	Total Volume of Material (ft ³)
Flow test		15	0.00867	1	1	15	0.00867
Air Content		10	0.00578	3	1	30	0.01734
Compressive Strength	2 x 2	8	0.004624	18	1	144	0.083232
Slant Shear Bond Strength	3 x 6	42.39	0.02450142	3	1	127.17	0.07350426
Length Change	1 x 12	12	0.006936	6	1	72	0.041616
Elastic Modulus	3 x 6	42.39	0.02450142	3	1	127.17	0.07350426
Fatigue			0				0
Freeze/thaw	3 x 4 x 16	192	0.110976	3	1	576	0.332928
Rapid Chloride Permeability	4 x 6	75.36	0.04	3	1	226.08	0.13067424
Sorptivity	4 x 6	75.36	0.04355808	2	1	150.72	0.08711616
Air Content of hardened concrete	4 x 6	75.36	0.04355808	1	1	75.36	0.04355808
Restrained Ring Test				3	1		2.1
							2.992143

APPENDIX C: COMPRESSIVE STRENGTH OF REPAIR MATERIALS AND SHEAR KEY GROUTS

Table C-1 SikaTop 123 Plus

Age	Load	Compressive Strength (psi)	Age	Load	Compressive Strength (psi)	Age	Load	Compressive Strength (psi)
1 day	13,000	3250	7 days	23,000	5750	28 days	27,900	6975
	18,500	4625		20,000	5000		27,100	6775
	6,000	1500		23,000	5750		24,500	6125
	15,500	3875		20,100	5025		26,300	6575
	13,500	3375		13,500	3375		27,200	6800
	14,000	3500		17,500	4375		26,000	6500
	AVG	3500		AVG	5381.25		AVG	6725
	STDEV	270.03		STDEV	425.92		STDEV	189.57
	COV	7.72		COV	7.91		COV	2.82

Table C-2 SikaRepair SHA

Age	Load	Compressive Strength (psi)	Age	Load	Compressive Strength (psi)	Age	Load	Compressive Strength (psi)
1 day	7,000	1750	7 days	16,500	4125	28 day	22,700	5675
	9,800	2450		15,750	3937.5		26,200	6550
	10,500	2625		15,000	3750		25,600	6400
	9,500	2375		13,800	3450		24,100	6025
	11,000	2750		17,200	4300		25,500	6375
	9,800	2450		17,350	4337.5		22,000	5500
	AVG	2530		AVG	4090		AVG	6205
	STDEV	153.50		STDEV	342.57		STDEV	427.42
	COV	6.07		COV	8.38		COV	6.89

Table C-3 Conpatch VO

Age	Load	Compressive Strength (psi)	Age	Load	Compressive Strength (psi)	Age	Load	Compressive Strength (psi)
1 day	15,500	3875	7 days	24,500	6125	28 day	41,000	10250
	20,800	5200		25,000	6250		41,000	10250
	18,900	4725		24,000	6000		42,200	10550
	16,300	4075		25,000	6250		39,500	9875
	19,900	4975		25,000	6250		37,000	9250
	20,200	5050		24,000	6000		37,500	9375
	AVG	4805		AVG	6146		AVG	9925
	STDEV	442.79		STDEV	122.90		STDEV	522.02
	COV	9.22		COV	2.00		COV	5.26

Table C-4 HB2 Mortar Repair

Age	Load	Compressive Strength (psi)	Age	Load	Compressive Strength (psi)	Age	Load	Compressive Strength (psi)
1 day	9,500	2375	7 days	18,650	4663	28 day	26,500	6625
	11,500	2875		19,200	4800		27,000	6750
	10,850	2713		19,900	4975		25,800	6450
	9,250	2313		18,500	4625		25,850	6463
	10,200	2550		18,000	4500		25,000	6250
	11,600	2900		20,100	5025		27,250	6813
	AVG	2534		AVG	4766		AVG	6538
	STDEV	263.66		STDEV	158.57		STDEV	239.14
	COV	10.40		COV	3.33		COV	3.66

Table C-5 SET 45

Age	Load	Compressive Strength (psi)	Age	Load	Compressive Strength (psi)	Age	Load	Compressive Strength (psi)
1 day	17,000	4250	7 days	23,000	5750	28 days	27,900	6975
	19,200	4800		20,000	5000		27,500	6875
	16,200	4050		23,000	5750		24,500	6125
	18,200	4550		20,100	5025		26,300	6575
	16,000	4000		13,500	3375		26,850	6712.5
	13,100	3275		17,500	4375		27,450	6862.5
	AVG	4330		AVG	5381		AVG	6688
	STDEV	340.22		STDEV	425.92		STDEV	381.61
	COV	7.86		COV	7.91		COV	5.71

Table C-6 Type I Cement Grout

Age	Load	Compressive Strength (psi)	Age	Load	Compressive Strength (psi)	Age	Load	Compressive Strength (psi)
1 day	11,600	2900	7 days	13,500	3375	28 days	18,250	4563
	10,300	2575		14,200	3550		18,000	4500
	10,600	2650		13,900	3475		17,850	4463
	8,600	2150		13,700	3425		18,000	4500
	9,000	2250		13,600	3400		17,900	4475
	8,500	2125		13,600	3400		17,800	4450
	AVG	2442		AVG	3450		AVG	4500
	STDEV	314.11		STDEV	64.71		STDEV	40.05
	COV	12.86		COV	1.88		COV	0.89

Table C-7 Masonry Cement Grout

Age	Load	Compressive Strength (psi)	Age	Load	Compressive Strength (psi)	Age	Load	Compressive Strength (psi)
1 day	11,600	2900	7 days	13,500	3375	28 days	18,250	4563
	10,300	2575		14,200	3550		18,000	4500
	10,600	2650		13,900	3475		17,850	4463
	8,600	2150		13,700	3425		18,000	4500
	9,000	2250		13,600	3400		17,900	4475
	8,500	2125		13,600	3400		17,800	4450
	Avg	2442		Avg	3450		Avg	4500
SD	314.11	SD	64.71	SD	40.05			
COV	12.86	COV	1.88	COV	0.89			

APPENDIX D: SLANT SHEAR BOND STRENGTH

Table D-1 SikaTop 123 Plus

Sample #	Load	Slant Shear Strength 1 day (psi)	Mode of Failure	Sample #	Load	Slant Shear Strength 7 day (psi)	Mode of Failure
1	14600	1033	shear	1	18000	1274	compressive
2	14000	991	shear	2	18800	1331	compressive
3	14000	991	compressive	3	18200	1288	shear
	AVG	1005			AVG	1297	
	STDEV	20.02			STDEV	24.06	
	COV	1.99			COV	1.85	

Table D-2 SikaRepair SHA

Sample #	Load	Slant Shear Strength 1 day (psi)	Mode of Failure	Sample #	Load	Slant Shear Strength 7 day (psi)	Mode of Failure
1	11900	842	shear	1	16500	1168	shear
2	13000	920	compressive	2	15900	1125	shear
3	12200	863	shear	3	17000	1203	shear
	AVG	875			AVG	1165	
	STDEV	32.86			STDEV	31.83	
	COV	3.75			COV	2.73	

Table D-3 Conpatch VO

Sample #	Load	Slant Shear Strength 1 day (psi)	Mode of Failure	Sample #	Load	Slant Shear Strength 7 day (psi)	Mode of Failure
1	15100	1069	compressive	1	19300	1366	shear
2	15100	1069	compressive	2	18900	1338	compressive
3	15000	1062	shear	3	19250	1362	compressive
	AVG	1066			AVG	1355	
	STDEV	3.34			STDEV	12.59	
	COV	0.31			COV	0.93	

Table D-4 HB2 Mortar Repair

Sample #	Load	Slant Shear Strength 1 day (psi)	Mode of Failure	Sample #	Load	Slant Shear Strength 7 day (psi)	Mode of Failure
1	4500	366	shear	1	12800	1041	compressive
2	4200	341	compressive	2	14500	1179	compressive
3	3700	301	compressive	3	15000	1220	compressive
	AVG	336			AVG	1146	
	STDEV	26.83			STDEV	76.56	
	COV	7.98			COV	6.68	

Table D-5 SET 45

Sample #	Load	Slant Shear Strength 7 day (psi)	Mode of Failure	Sample #	Load	Slant Shear Strength 7 day (psi)	Mode of Failure
1	19200	1561	shear	1	23200	1886	compressive
2	18000	1463	shear	2	23300	1894	shear
3	18600	1512	compressive	3	23600	1919	shear
	AVG	1512			AVG	1900	
	STDEV	39.83			STDEV	13.82	
	COV	2.63			COV	0.73	

Table D-6 Type I Cement Grout

Sample #	Load	Slant Shear Strength 7 day (psi)	Mode of Failure	Sample #	Load	Slant Shear Strength 7 day (psi)	Mode of Failure
1	13000	1057	compressive	1	17250	1402	compressive
2	12000	976	shear	2	17500	1423	compressive
3	13500	1098	compressive	3	17000	1382	compressive
	AVG	1043			AVG	1402	
	STDEV	50.70			STDEV	16.60	
	COV	4.86			COV	1.18	

Table D-7 Masonry Cement Grout

Sample #	Load	Slant Shear Strength 7 day (psi)	Mode of Failure	Sample #	Load	Slant Shear Strength 7 day (psi)	Mode of Failure
1	11000	894	compressive	1	14500	1179	shear
2	11500	935	compressive	2	13800	1122	compressive
3	11600	943	compressive	3	14000	1138	compressive
	AVG	924			AVG	1146	
	STDEV	21.34			STDEV	23.93	
	COV	2.31			COV	2.09	

APPENDIX E: FREE SHRINKAGE DATA FOR REPAIR MORTAR AND SHEAR KEY GROUTS

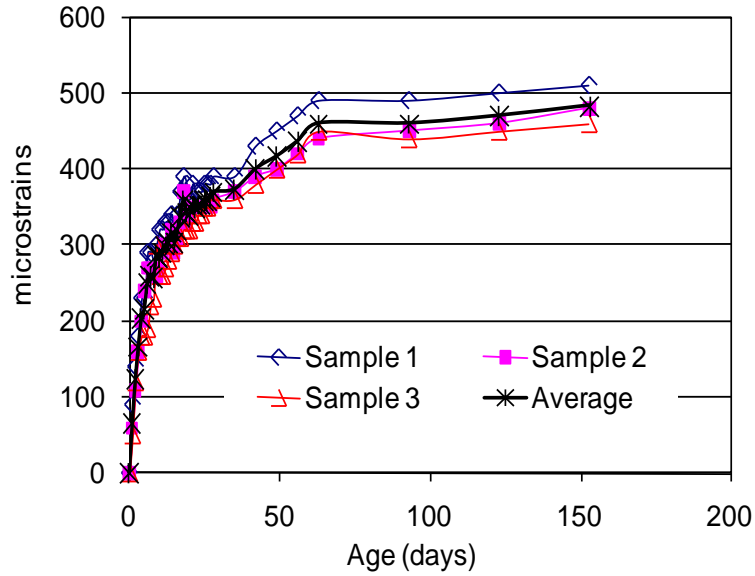


Figure E-1. Development of free shrinkage in Sika Top®123 PLUS in 100 % RH

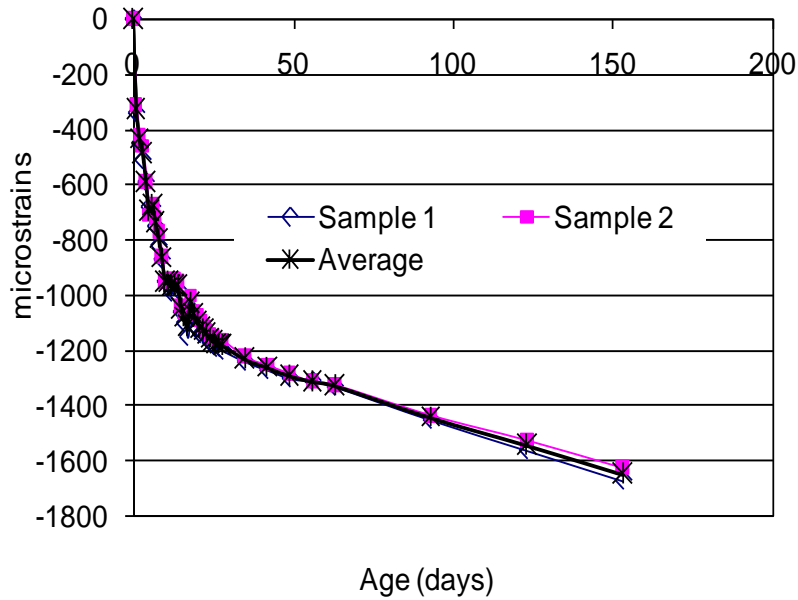


Figure E-2. Development of free shrinkage in Sika Top®123 PLUS in 50 % RH

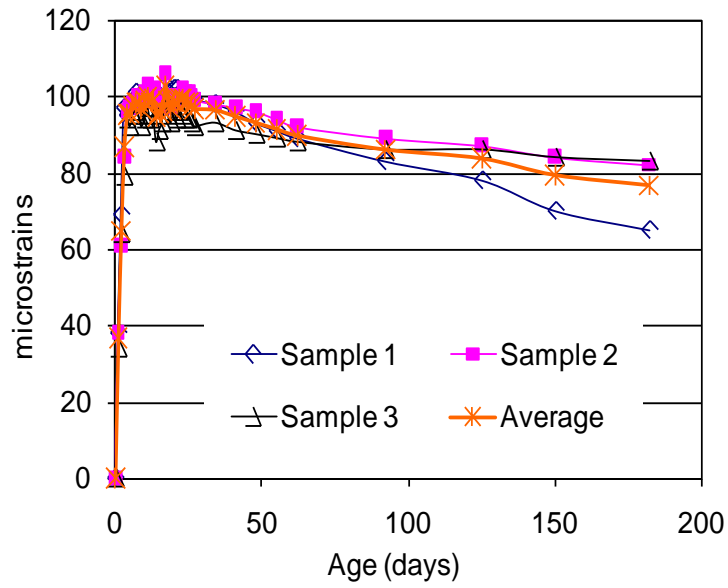


Figure E-3. Development of free shrinkage in Sika Repair[®] SHA in 100 % RH

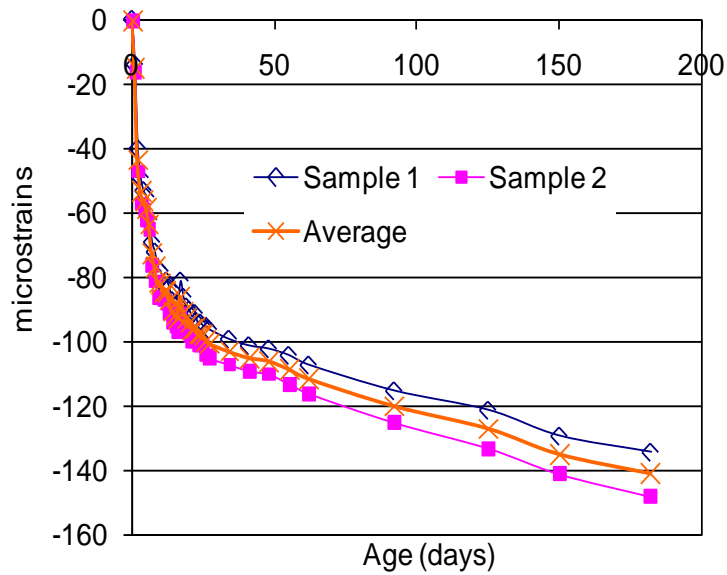


Figure E-4. Development of free shrinkage in Sika Repair[®] SHA in 50 % RH

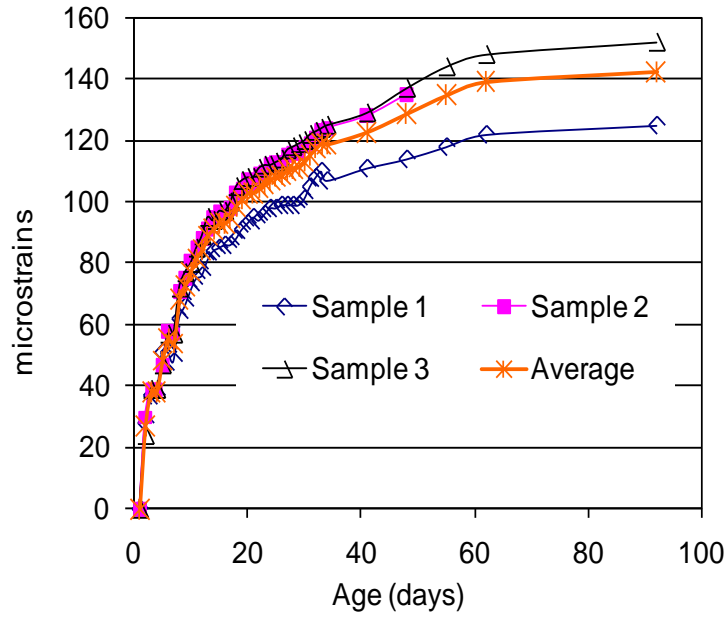


Figure E-5. Development of free shrinkage in HB2 Repair Mortar in 100 % RH

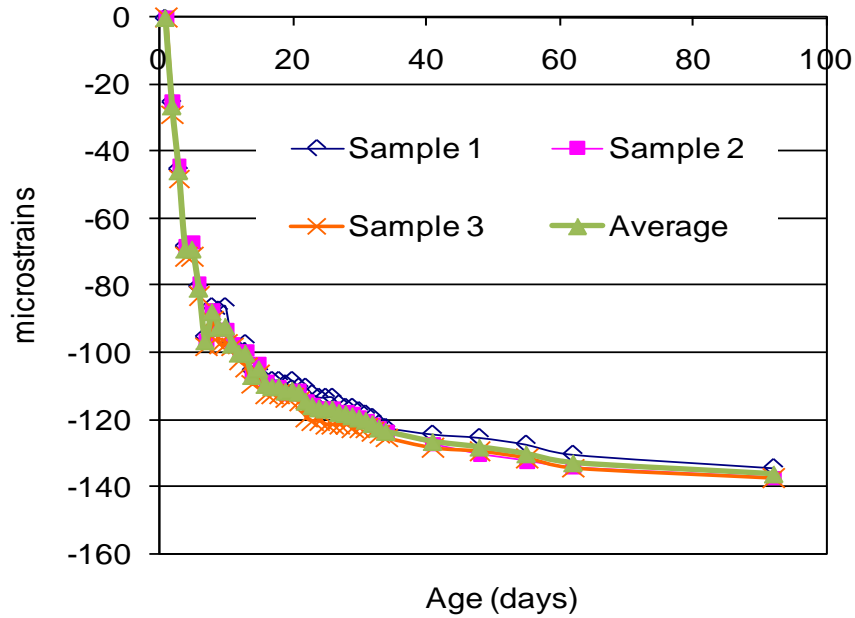


Figure E-6. Development of free shrinkage in HB2 Repair Mortar in 50 % RH

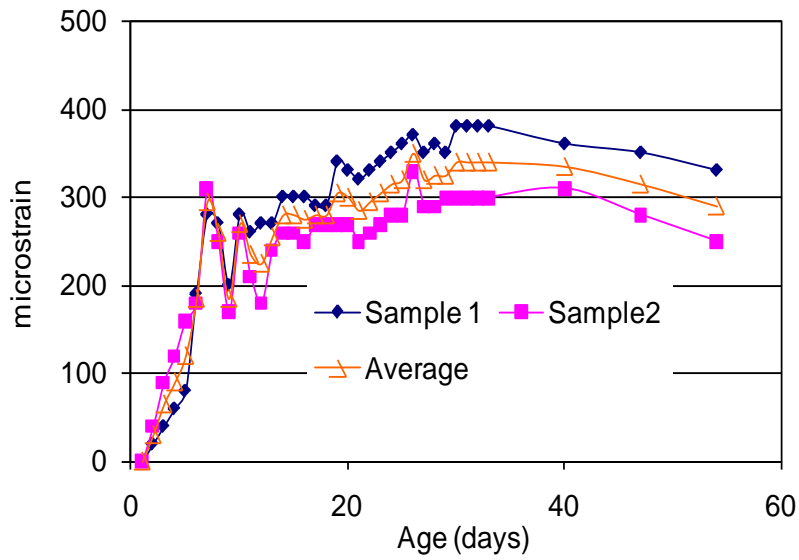


Figure E-7. Development of free shrinkage in Conpatch VO in 100 % RH

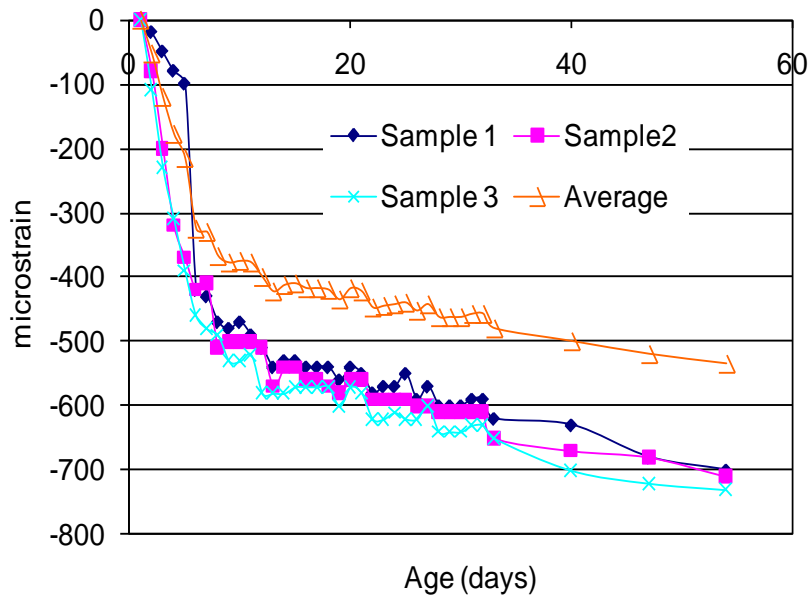


Figure E-8. Development of free shrinkage in Conpatch VO in 50 % RH

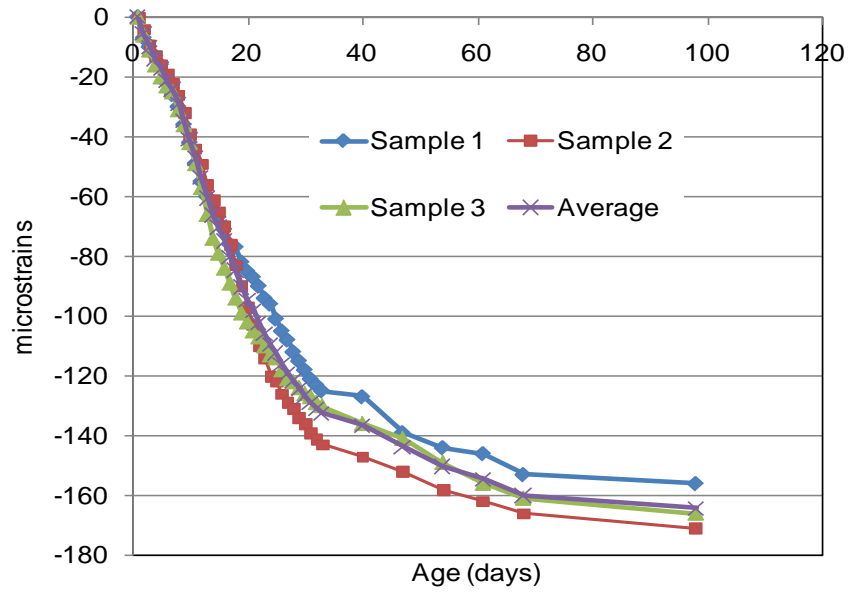


Figure E-9. Development of free shrinkage in SET 45 in 100 % RH

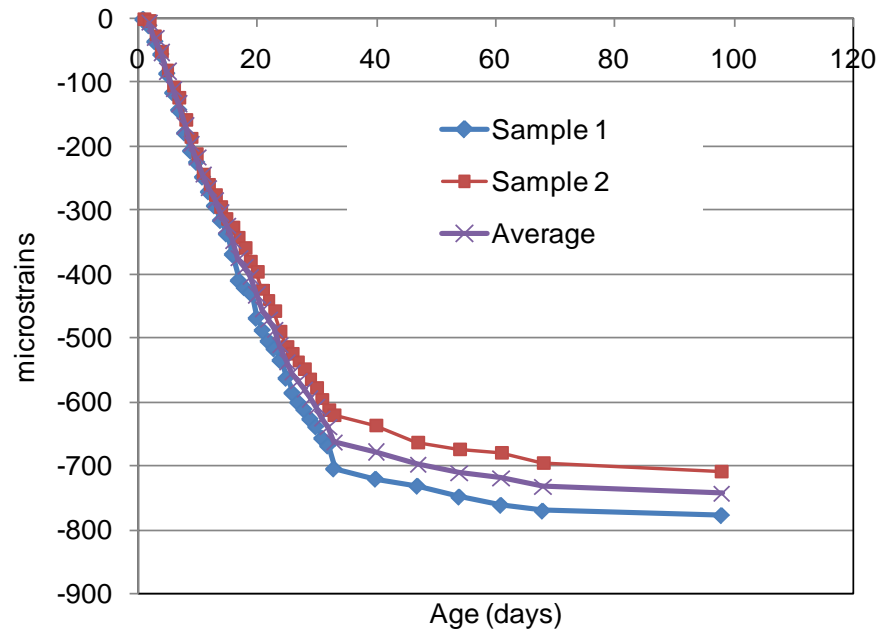


Figure E-10. Development of free shrinkage in SET 45 in 50 % RH

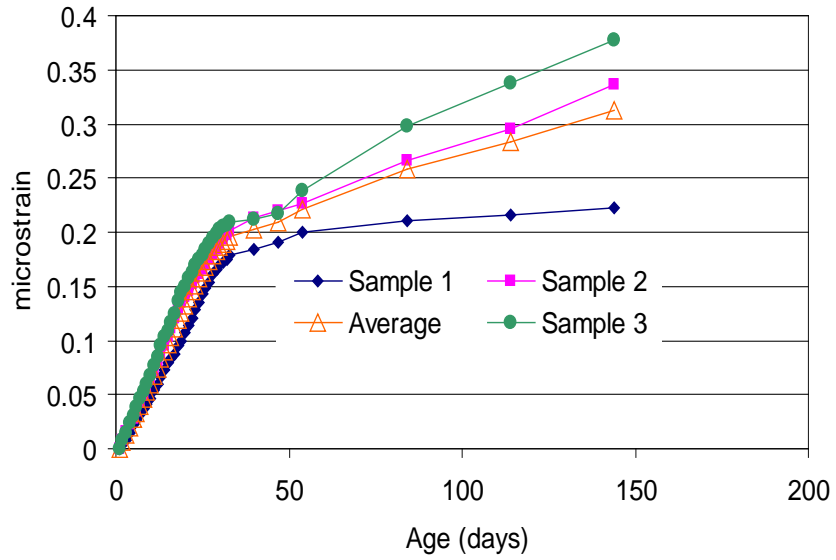


Figure E-11. Development of free shrinkage in Type I Cement Grout in 100 % RH

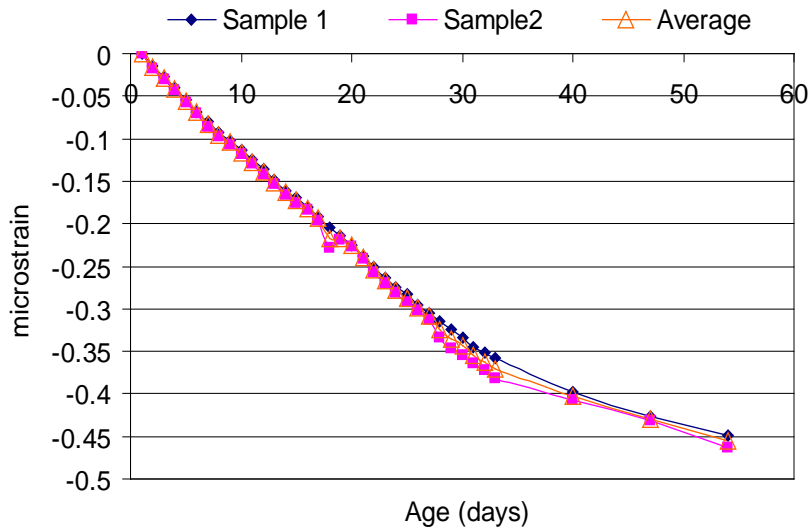


Figure E-12. Development of free shrinkage in Type I Cement Grout in 50 % RH

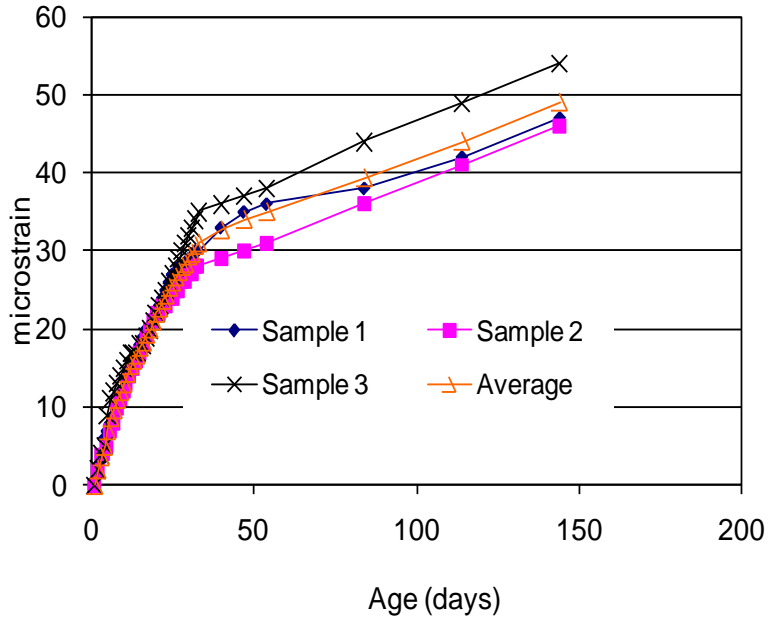


Figure E-13. Development of free shrinkage in Masonry Cement Grout in 100 % RH

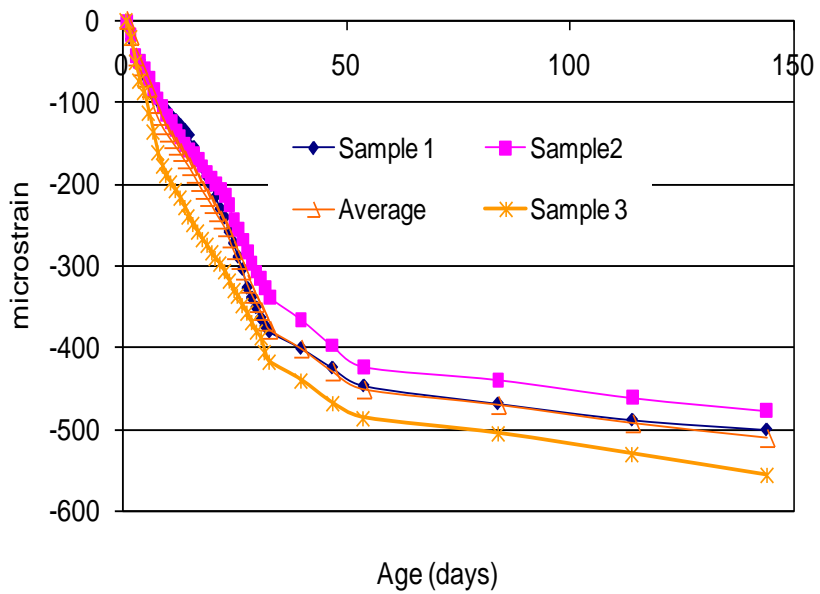


Figure E-14. Development of free shrinkage in Masonry Cement Grout in 50 % RH

APPENDIX F: RESISTANCE TO FREEZING AND THAWING

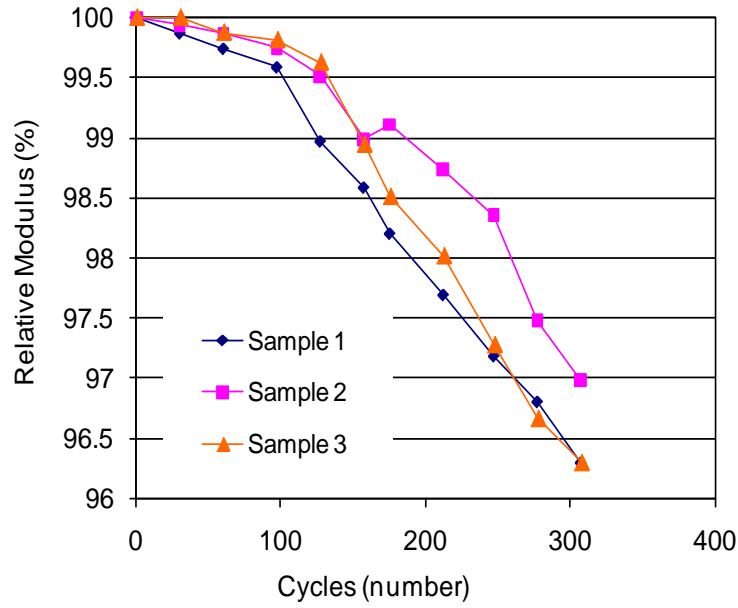


Figure F-1. Relative Dynamic Modulus of Sika Top®123 PLUS over 300 cycles

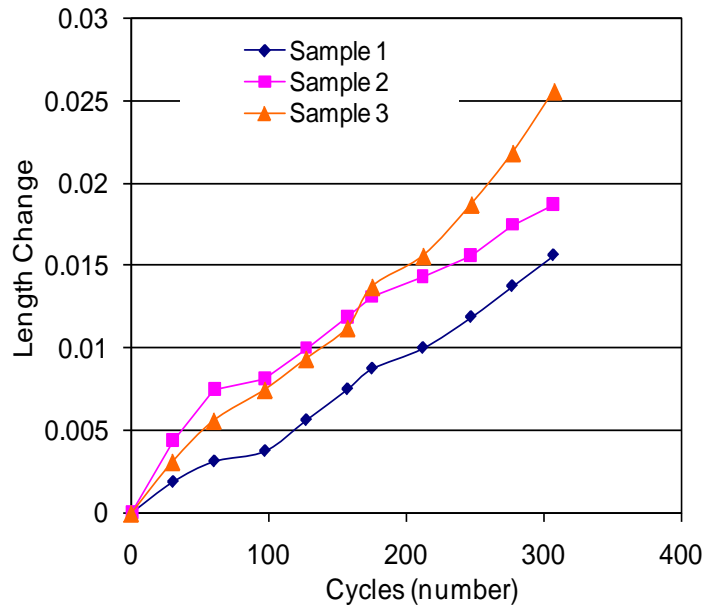


Figure F-2. Length Change in Sika Top®123 PLUS over 300 cycles

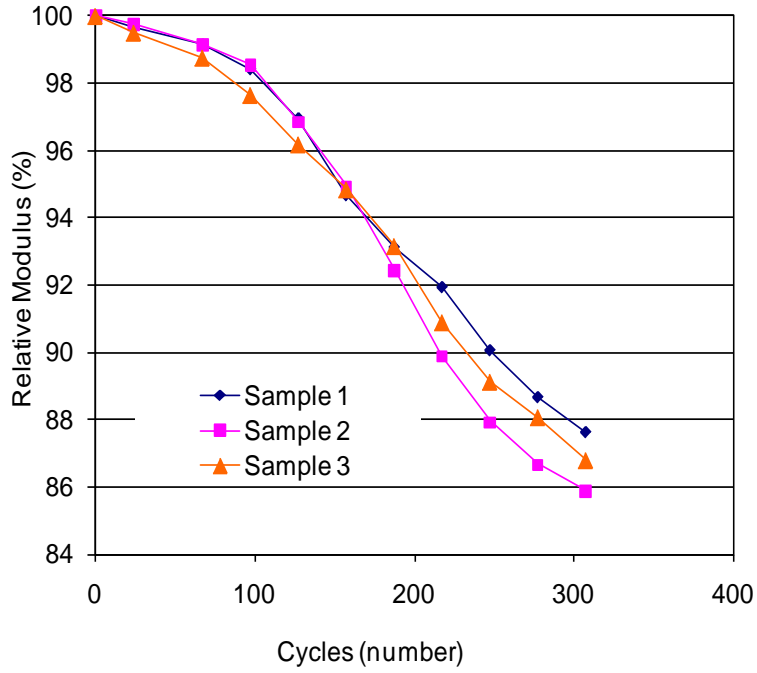


Figure F-3. Relative Dynamic Modulus of Sika Repair[®] SHA over 300 cycles

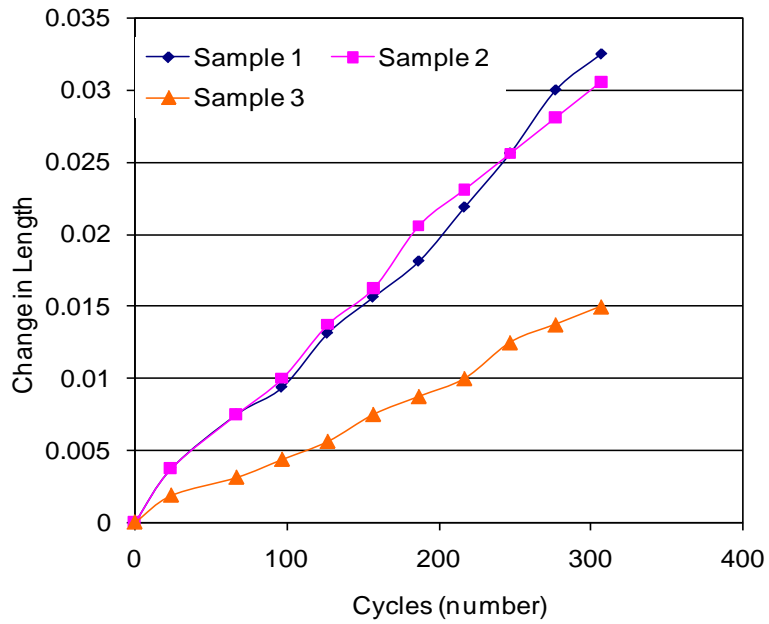


Figure F-4. Length Change in Sika Repair[®] SHA over 300 cycles

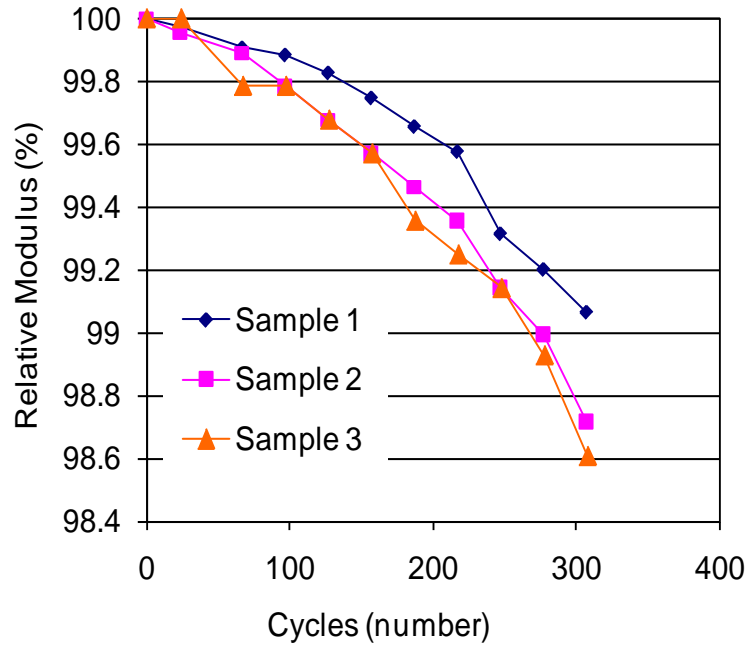


Figure F-5. Relative Dynamic Modulus of Conpatch VO over 300 Cycles

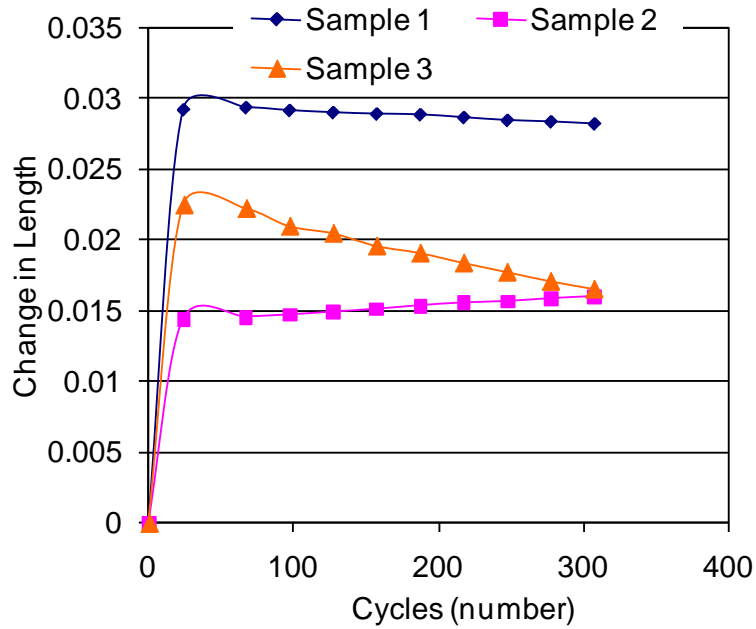


Figure F-6. Length Change in Conpatch VO over 300 cycles

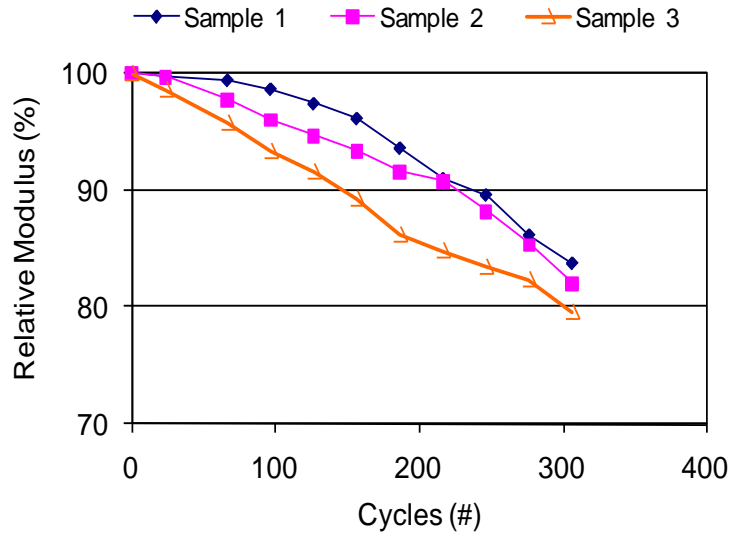


Figure F-7. Development of free shrinkage in SET 45 in 100 % RH

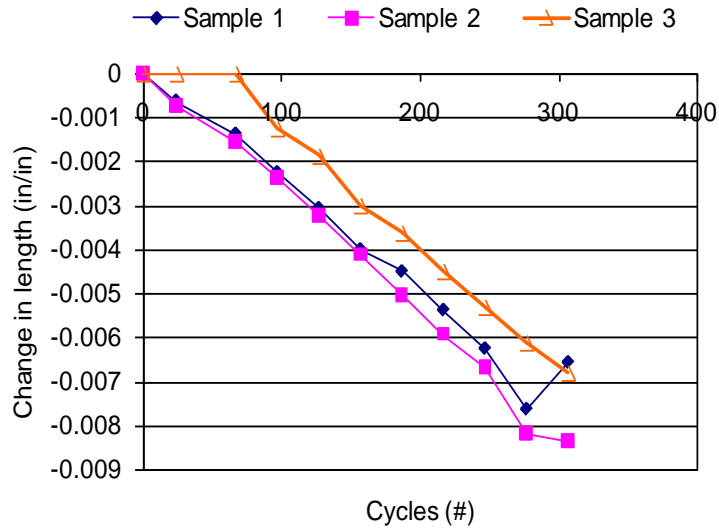


Figure F-8. Development of free shrinkage in SET 45 in 50 % RH

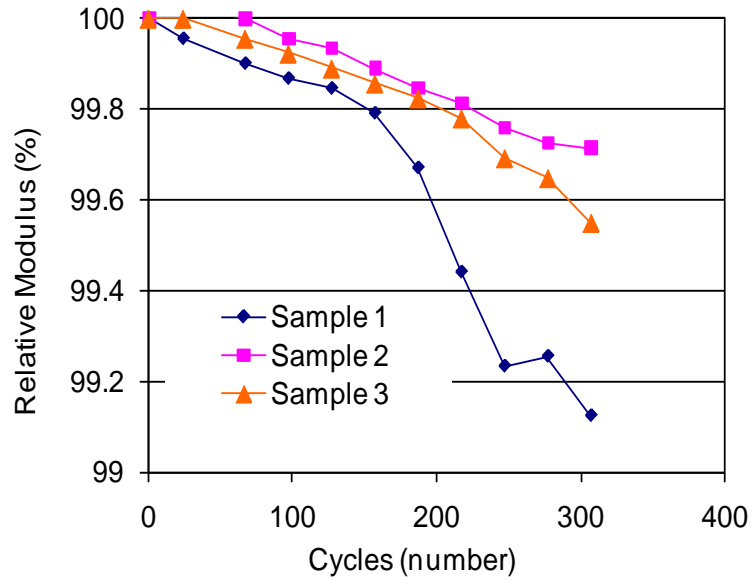


Figure F-9. Development of free shrinkage in Type I Cement Grout in 100 % RH

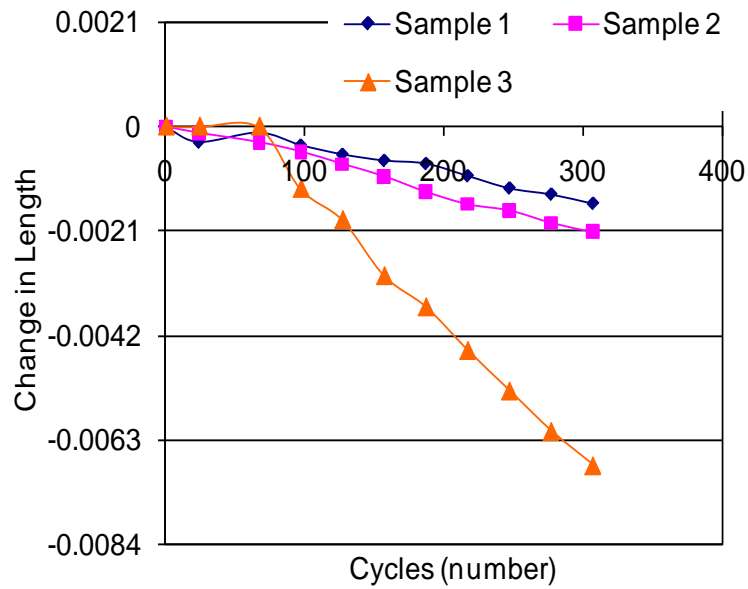


Figure F-10. Development of free shrinkage in Type I Cement Grout in 50 % RH

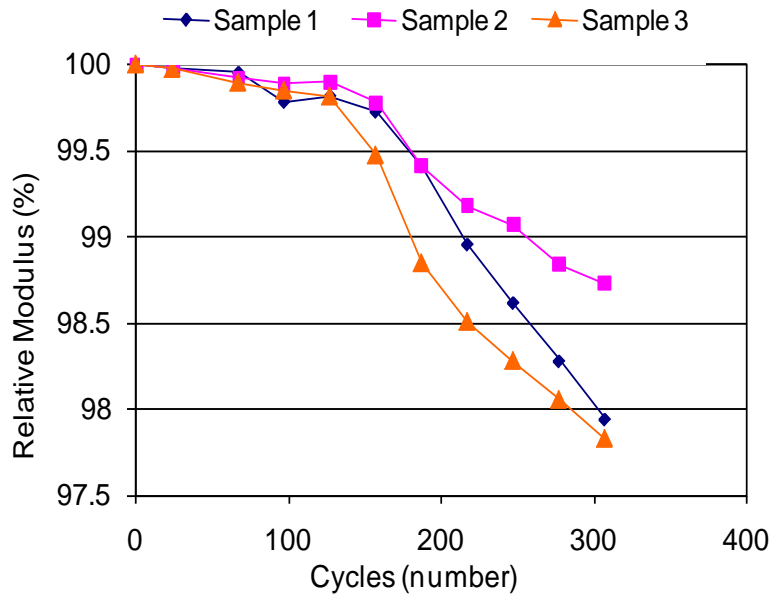


Figure F-11. Development of free shrinkage in Masonry Cement Grout in 100 % RH

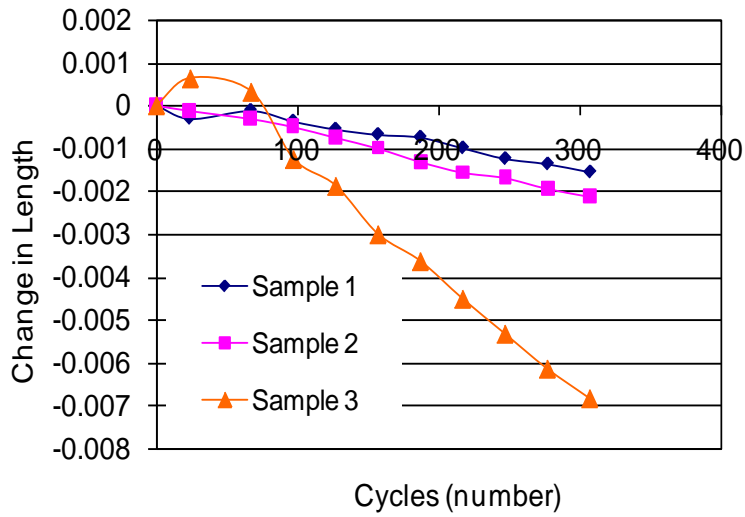


Figure F-12. Development of free shrinkage in Masonry Cement Grout in 50 % RH



Figure F-13. Photograph of Sika Top 123 PLUS at the End of 300 Cycles of Freezing and Thawing



Figure F-14. Photograph of Sika Repair SHA at the End of 300 Cycles of Freezing and Thawing



Figure F-15. Photograph of Conpatch VO at the End of 300 Cycles of Freezing and Thawing



Figure F-16. Photograph of HB2 Repair Mortar Sample Cast for F/T Testing

APPENDIX G: AIR CONTENT OF REPAIR MATERIALS AND SHEAR KEY GROUTS

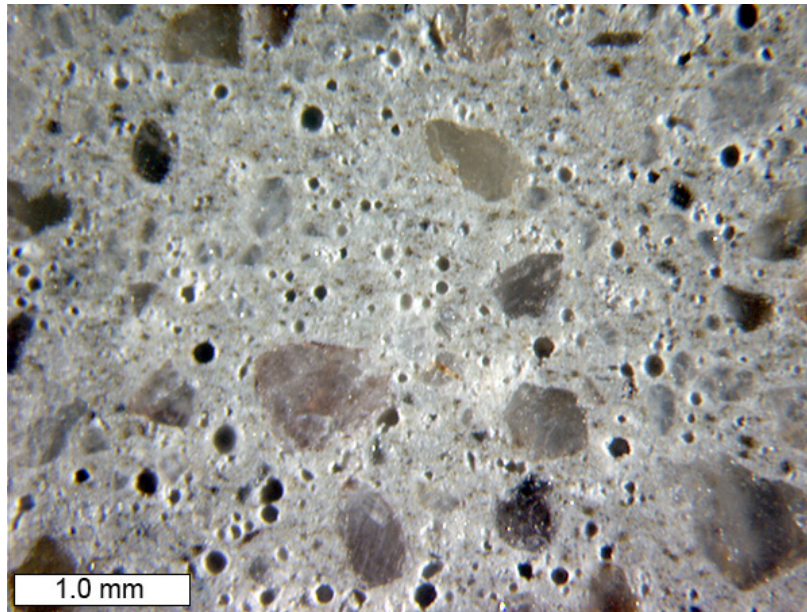


Figure G-1. Stereo Image of Sika Top 123 PLUS Mortar

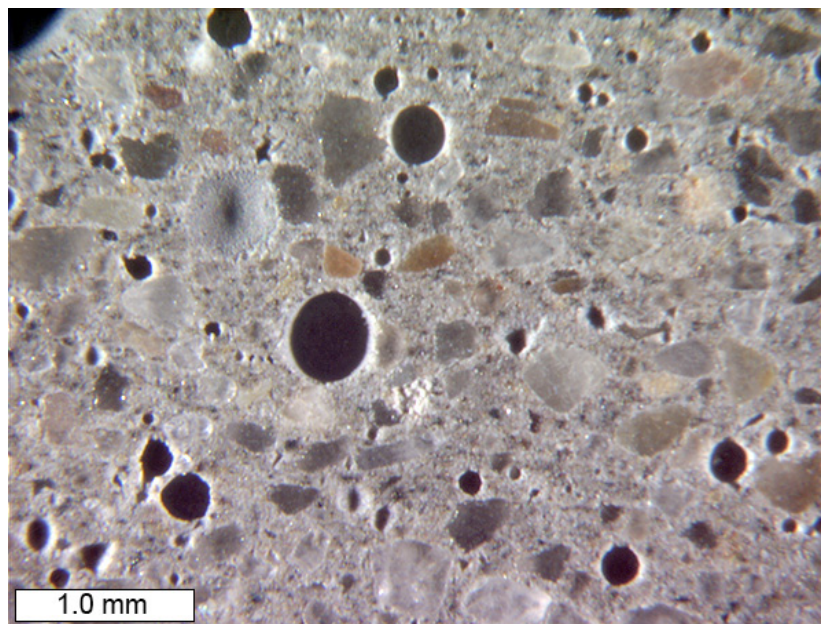


Figure G-2. Stereo Image of Sika Repair SHA Mortar

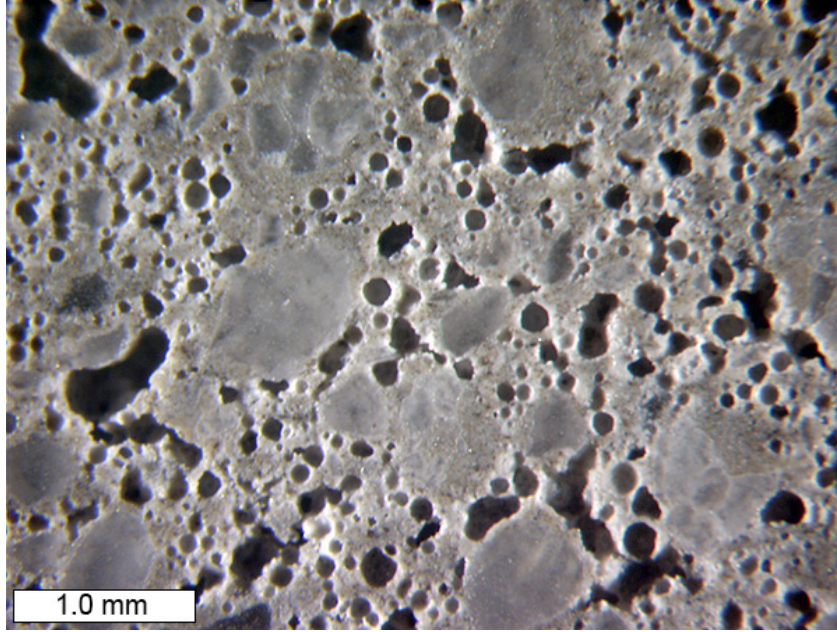


Figure G-3. Stereo Image of HB2 Repair Mortar

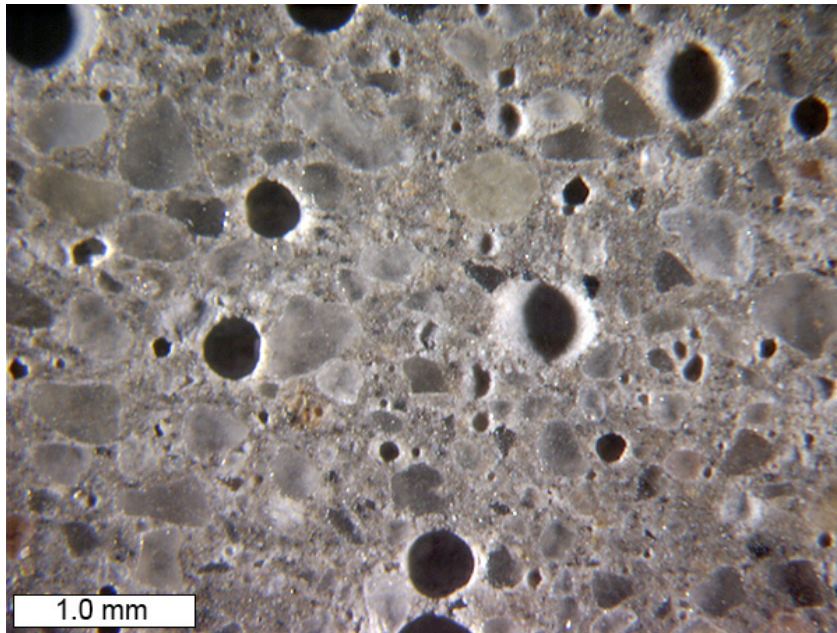


Figure G-4. Stereo Image of Conpatch VO Mortar

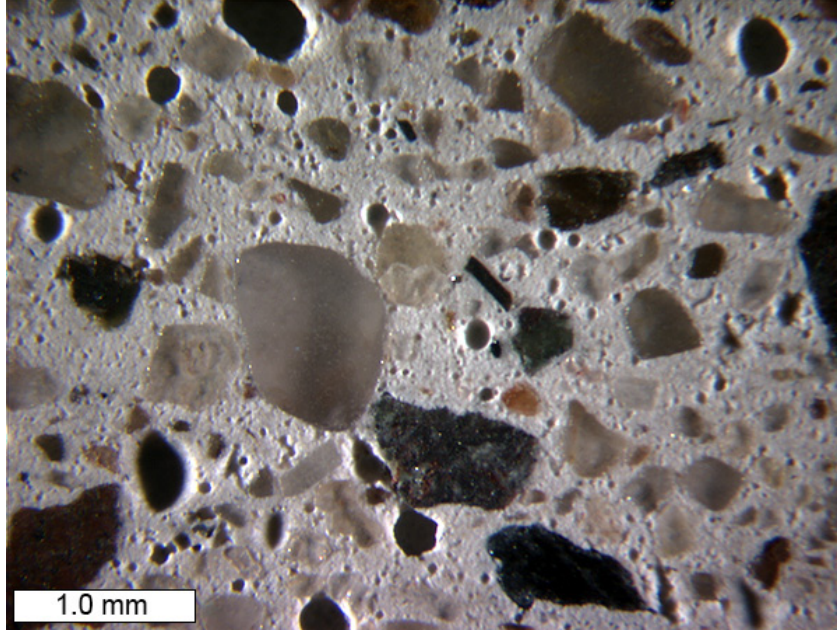


Figure G-5. Stereo Image of Type I Cement Shear Key Grout

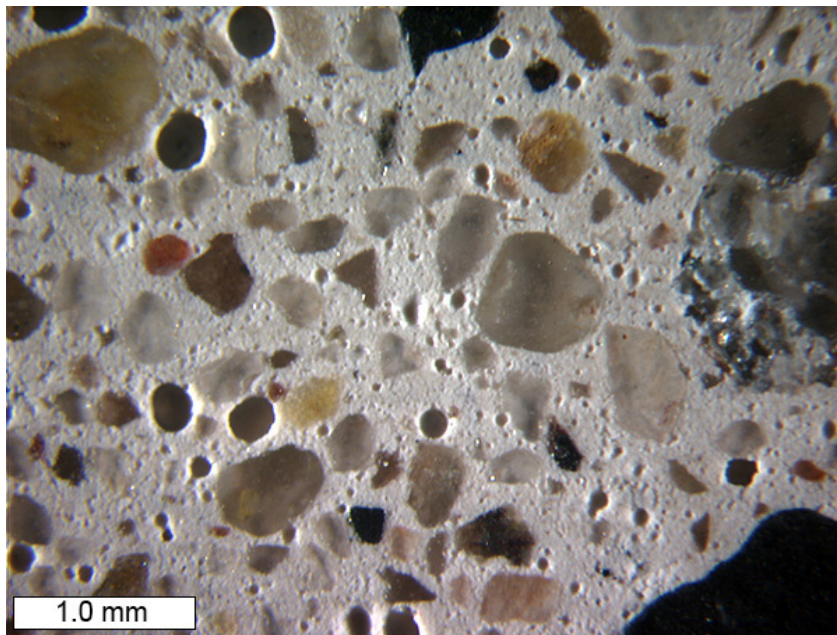


Figure G-6. Stereo Image of Masonry Cement Shear key Grout

APPENDIX H: COEFFICIENT OF THERMAL EXPANSION

Table H-1. CTE analysis for Repair Mortar and Shear key Grouts

Material	CTE for Sample 1 (mm/mm/°C)	Age (days)	CTE for Sample 2 (mm/mm/°C)	Age (days)	Average CTE (mm/mm/°C)	SD	COV
Substrate Concrete	1.32E-05	28	13.24E-6	30	1.32E-05	2.11E-08	0.16
Sika Top 123 PLUS	18.88E-6	7	18.88E-6	11	1.89E-05	0.00E+00	0.00
Sika Repair SHA	15.34E-6	7	14.26E-6	9	1.48E-05	7.59E-07	5.13
HB2 Repair Mortar	11.78E-6	7	9.98E-06	11	1.09E-05	1.27E-06	11.71
Conpatch VO	13.58E-6	7	13.74E-6	9	1.37E-05	1.08E-07	0.79
SET 45	12.59E-6	28	12.38E-6	28	1.25E-05	1.43E-07	1.15
Type I Cement Grout	10.78E-6	28	9.87E-6	28	1.03E-05	6.44E-07	6.24
Masonry Cement Grout	9.41E-6	28	9.73E-6	28	9.57E-06	2.28E-07	2.38

APPENDIX I: SORPTIVITY

Table I-1 Sorptivity Analysis of Repair Mortar and Shear Key Grouts

Material	Initial Rate of Absorption (mm*s ^{-1/2})	Regression Coefficient	Secondary Rate of Absorption (mm*s ^{-1/2})	Regression Coefficient	Average Initial Rate of Absorption (mm*s ^{-1/2})	Average Secondary Rate of Absorption (mm*s ^{-1/2})	COV of Initial Rate of Absorption	COV Secondary Rate of Absorption
Sika Top 123 PLUS	7.00E-6	0.9882	6.00E-7	0.97	5.50E-06	8.00E-07	38.57	35.36
	4.00E-6	0.9903	1.00E-6	0.99				
Sika Repair SHA	4.00E-6	0.9728	7.00E-6	0.9846	3.00E-06	5.00E-06	47.14	56.57
	2.00E-6	0.9717	3.00E-6	0.9921				
HB2 Repair Mortar	3.00E-7	0.5495	8.00E-7	0.98	6.00E-07	8.00E-07	70.71	0.00
	9.00E-7	0.8405	8.00E-7	0.98				
Conpatch VO	7.00E-6	0.9756	2.00E-6	0.9943	7.50E-06	3.00E-06	9.43	47.14
	8.00E-6	0.9815	4.00E-6	0.989				
SET 45	30.00E-6	0.976	5.00E-6	0.9849	3.00E-05	3.00E-06	0.00	94.28
	30.00E-6	0.9893	1.00E-6	0.9905				
Type I Cement Grout	40.00E-6	0.984	7.00E-6	0.9944	2.50E-05	8.00E-06	84.85	17.68
	10.00E-6	0.9915	9.00E-6	0.9905				
Masonry Cement Grout	30.00E-6	0.976	5.00E-6	0.9849	3.00E-05	3.00E-06	0.00	94.28
	30.00E-6	0.9893	1.00E-6	0.9905				

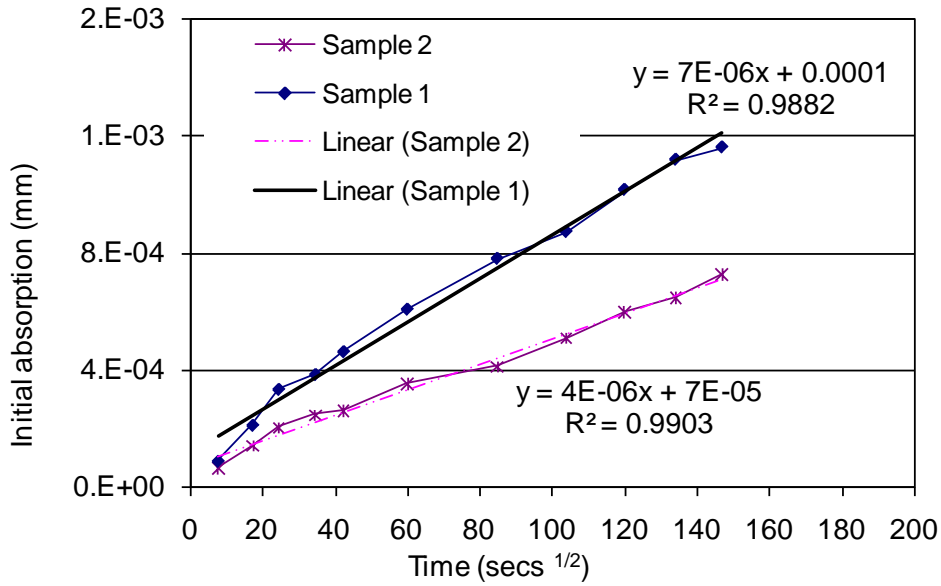


Figure I-1. Initial Absorption Curves for Sika Top 123 PLUS

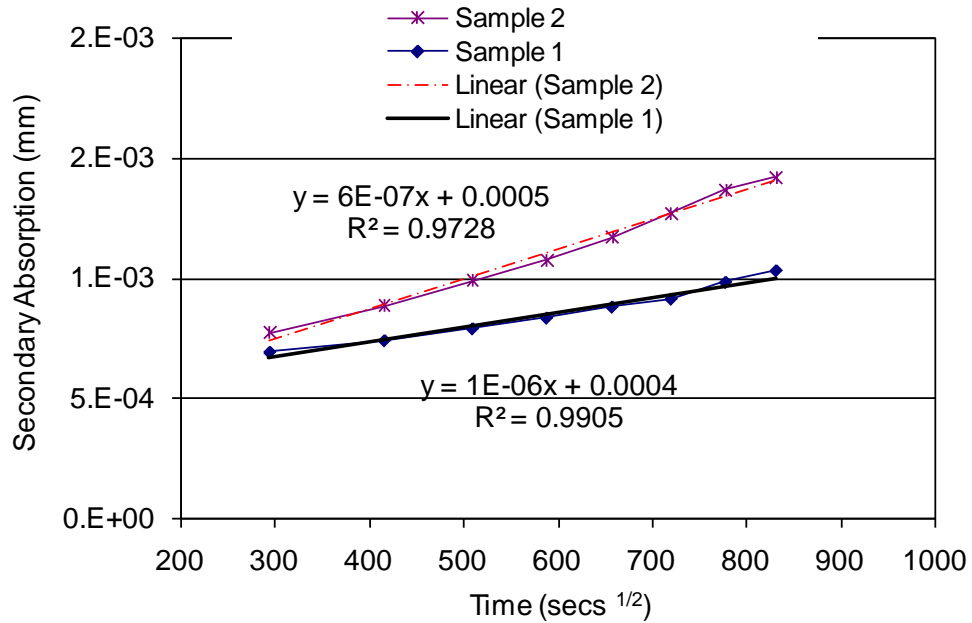


Figure I-2. Secondary Absorption Curves for Sika Top 123 PLUS

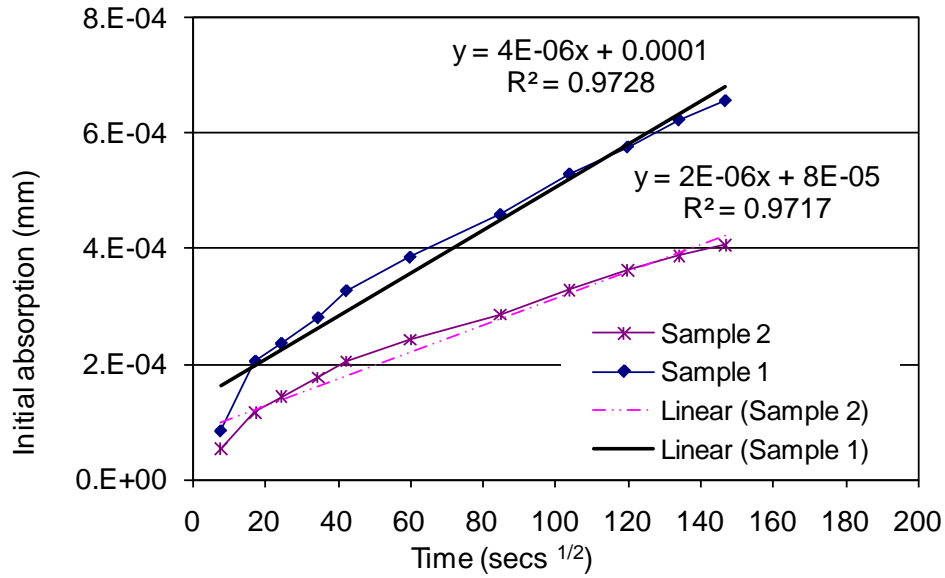


Figure I-3. Initial Absorption Curves for Sika Repair SHA

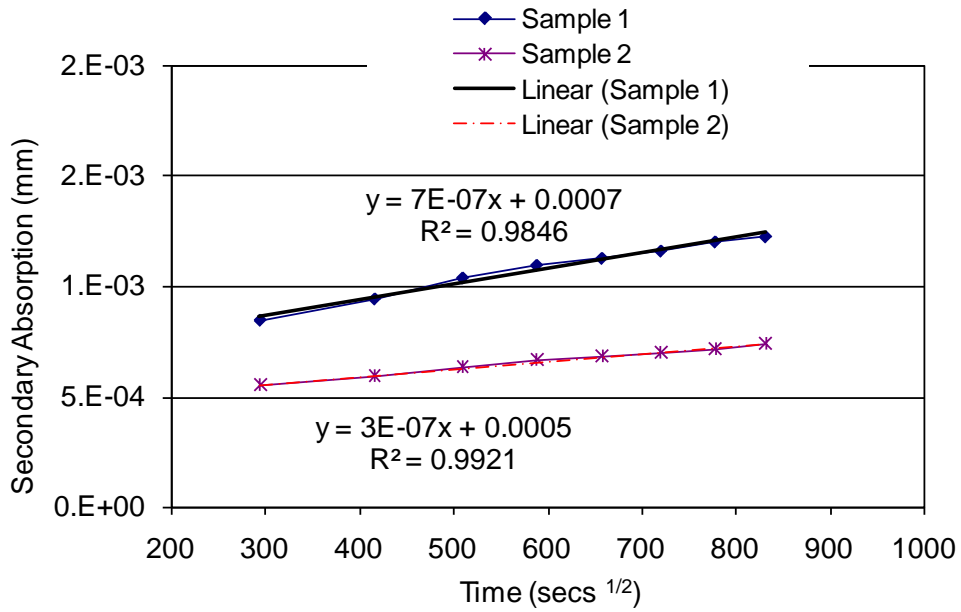


Figure I-4. Secondary Absorption Curves for Sika Repair SHA

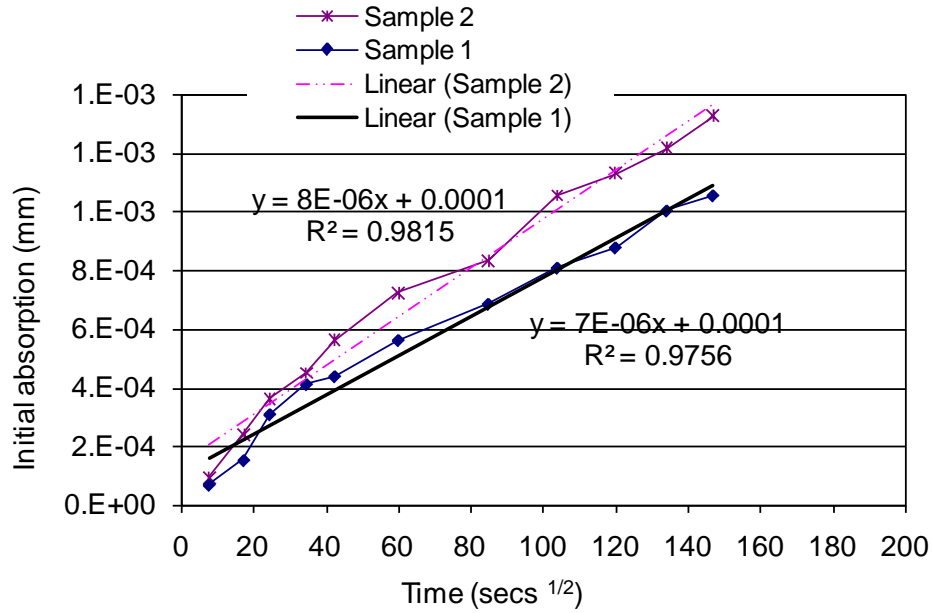


Figure I-5. Initial Absorption Curves for Conpatch VO

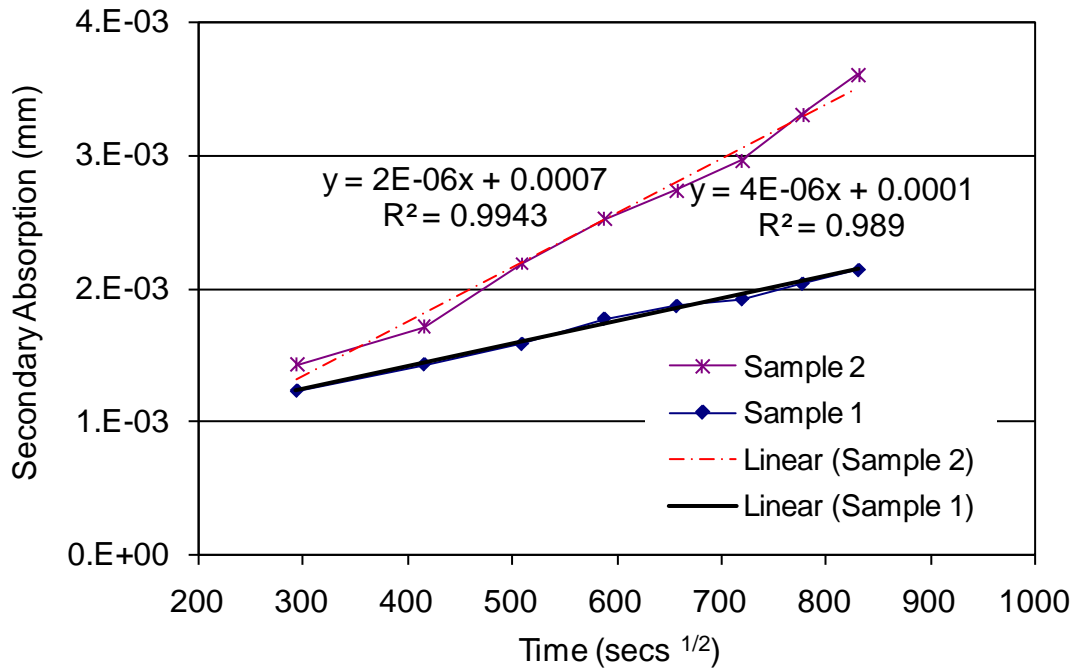


Figure I-6. Secondary Absorption Curves for Conpatch VO

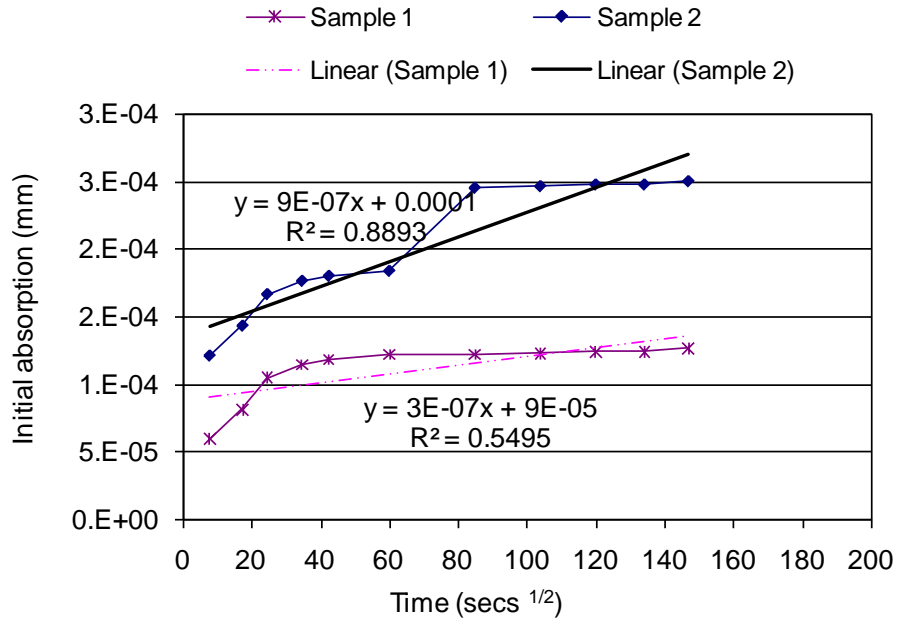


Figure I-7. Initial Absorption Curves for HB2 Repair Mortar

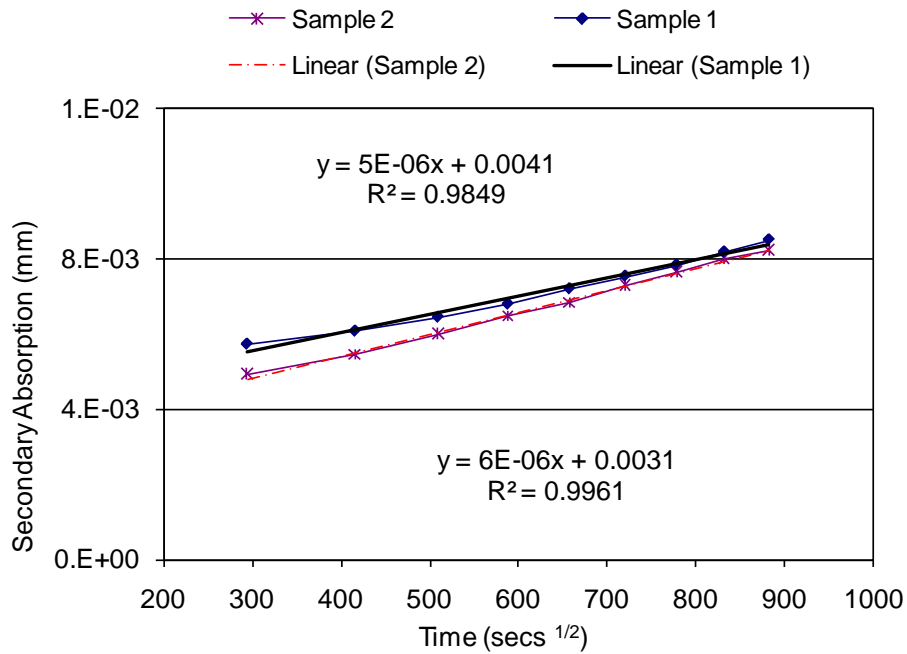


Figure I-8. Secondary Absorption Curves for HB2 Repair Mortar

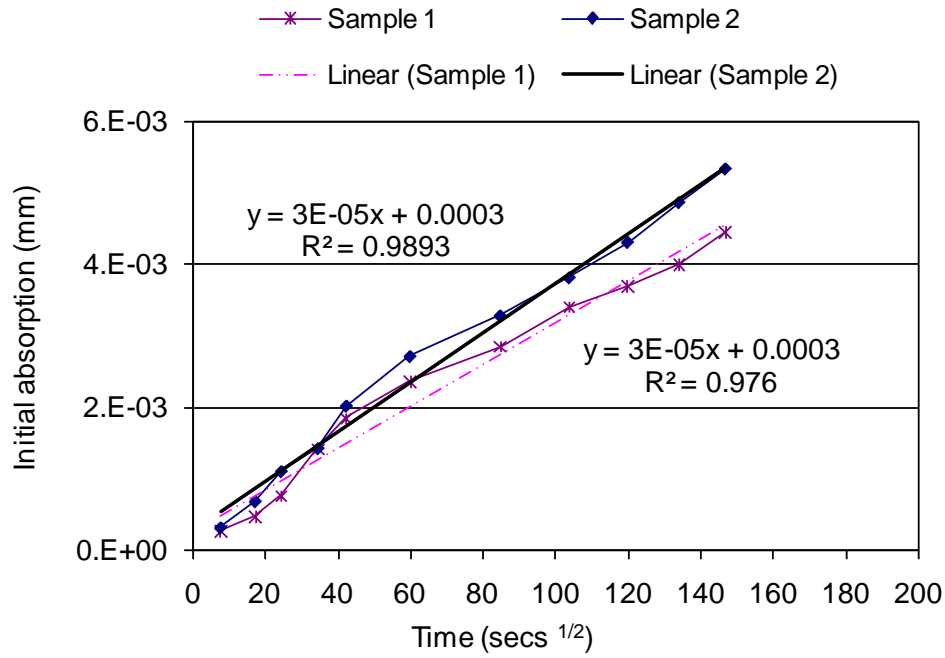


Figure I-9. Initial Absorption Curves for SET 45

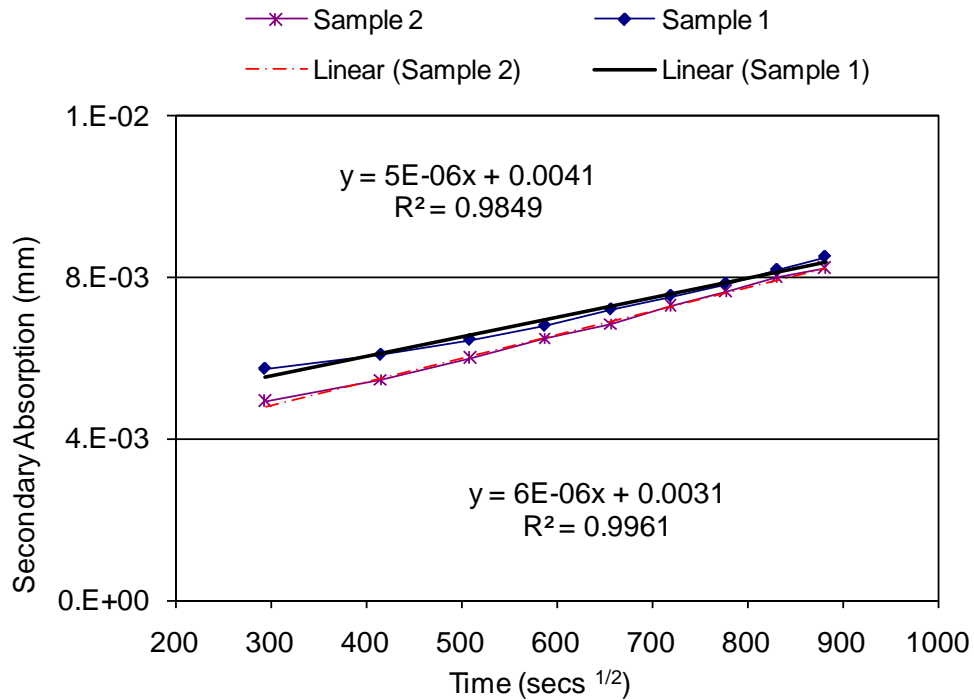


Figure I-10. Secondary Absorption Curves for SET 45

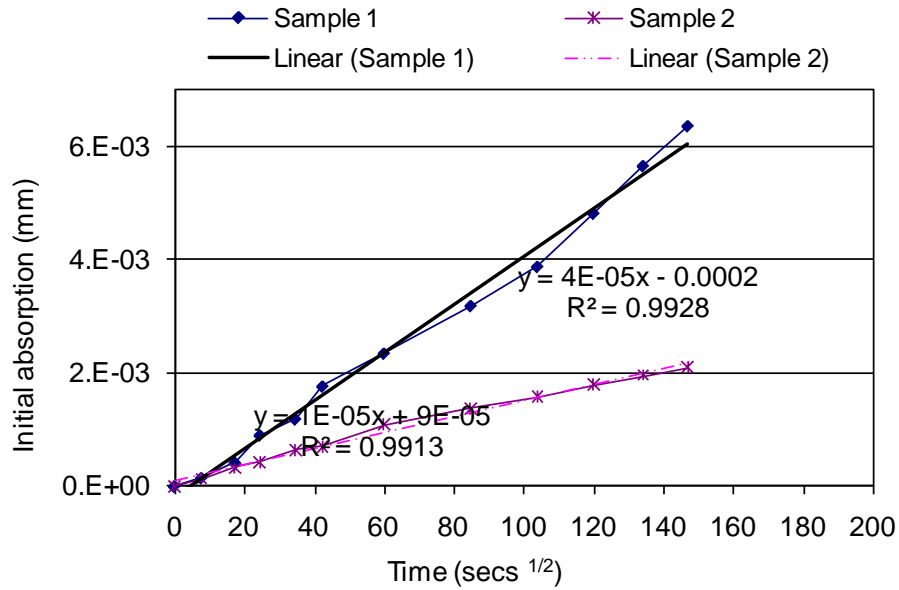


Figure I-11. Initial Absorption Curves for Type I Cement Grout

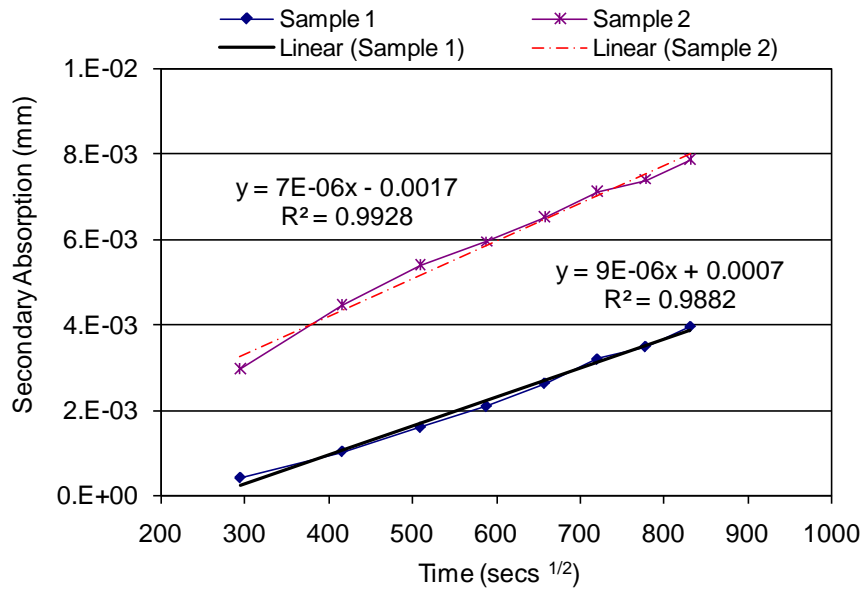


Figure I-12. Secondary Absorption Curves for Type I Cement Grout

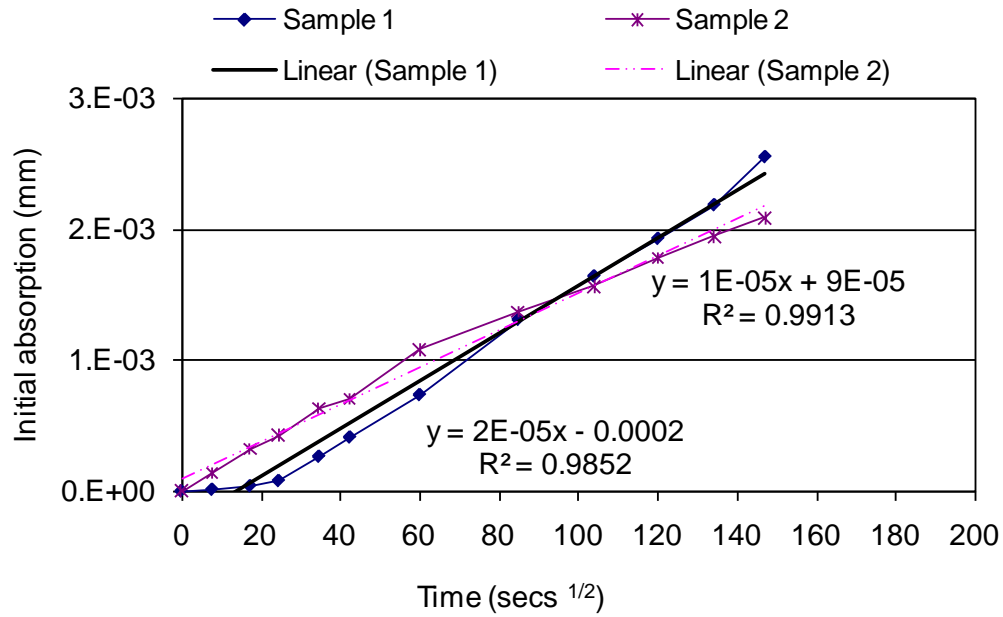


Figure I-15. Initial Absorption Curves for Mortar Cement Grout

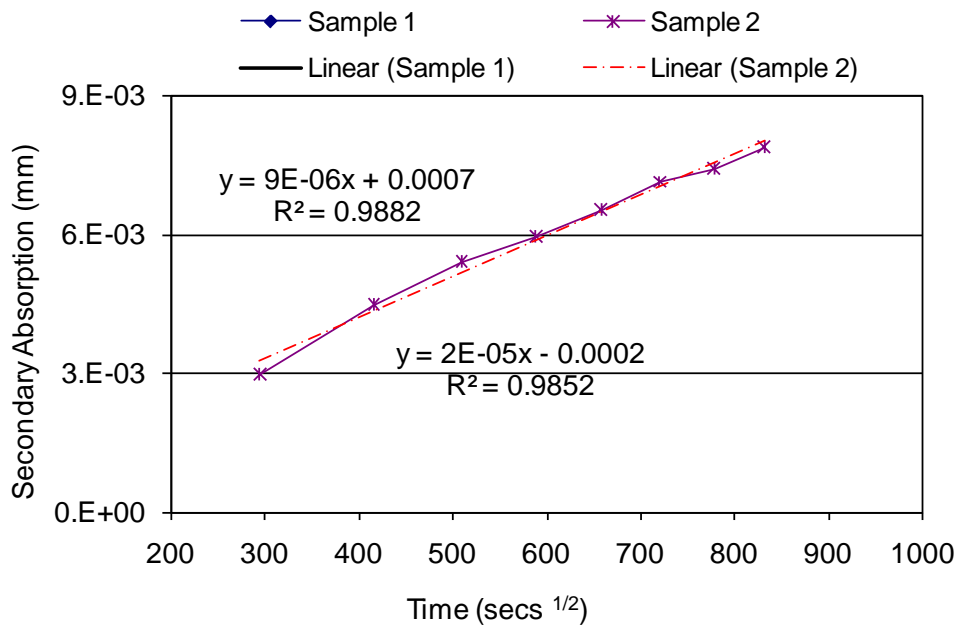


Figure I-16. Secondary Absorption Curves for Mortar Cement Grout

APPENDIX J: RATIONAL TRANSVERSE POSTTENSION DESIGN

TABLE J-1 Averaged Transverse Moment, N-m/m (in-lb/in)

Row No.	Shear key location m (in.)	End Diaphragm Moment Averaged within 1.91m (75 in.)						Intermediate Diaphragm Moment Averaged within 3.81 m (150 in.)						Midspan Diaphragm Moment Averaged within 3.81 m (150 in.)					
		Loads						Loads						Loads					
		Deck (a)	Barrier (b)	1 truck (c)	1 lane (d)	2 trucks (e)	2 lanes (f)	Deck (g)	Barrier (h)	1 truck (i)	1 lane (j)	2 trucks (k)	2 lanes (l)	Deck (m)	Barrier (n)	1 truck (o)	1 lane (p)	2 trucks (q)	2 lanes (r)
1	0.95 (37.5)	-730 (-164)	-2982 (-670)	-2728 (-613)	-547 (-123)	-1838 (-413)	-263 (-59)	2283 (513)	-2332 (-524)	8669 (1948)	2532 (569)	7432 (1670)	2078 (467)	3039 (683)	-2554 (-574)	10992 (2470)	3244 (729)	9372 (2106)	2657 (597)
2	1.94 (76.5)	779 (175)	-2439 (-548)	739 (166)	863 (194)	988 (222)	828 (186)	3974 (893)	-4303 (-967)	10805 (2428)	3872 (870)	9919 (2229)	3453 (776)	5224 (1174)	-5006 (-1125)	14098 (3168)	4873 (1095)	13087 (2941)	4406 (990)
3	2.93 (115.5)	1460 (328)	-2194 (-493)	1833 (412)	1095 (246)	2390 (537)	1077 (242)	5002 (1124)	-5304 (-1192)	13025 (2927)	3484 (783)	14374 (3230)	3698 (831)	6501 (1461)	-6439 (-1447)	16105 (3619)	4388 (986)	18165 (4082)	4810 (1081)
4	3.92 (154.5)	1606 (371)	-2140 (-481)	1384 (311)	360 (81)	2768 (622)	721 (162)	5345 (1201)	-5611 (-1261)	5994 (1347)	1571 (353)	11988 (2694)	3142 (706)	6920 (1555)	-6906 (-1552)	7939 (1784)	2145 (482)	15878 (3568)	4294 (965)
5	4.91 (193.5)	1460 (328)	-2194 (-493)	552 (124)	-18 (-4)	2390 (537)	1077 (242)	5002 (1124)	-5304 (-1192)	1348 (303)	209 (47)	14374 (3230)	3698 (831)	6501 (1461)	-6439 (-1447)	2060 (463)	423 (95)	18165 (4082)	4810 (1081)
6	5.91 (232.5)	779 (175)	-2439 (-548)	249 (56)	-36 (-8)	988 (222)	828 (186)	3974 (893)	-4303 (-967)	-886 (-199)	-414 (-93)	9919 (2229)	3453 (776)	5224 (1174)	-5006 (-1125)	-1010 (-227)	-467 (-105)	13087 (2941)	4406 (990)
7	6.9 (271.5)	-730 (-164)	-2982 (-670)	890 (200)	285 (64)	-1838 (-413)	-263 (-59)	2283 (513)	-2332 (-524)	-1237 (-278)	-454 (-102)	7432 (1670)	2078 (467)	3039 (683)	-2554 (-574)	-1620 (-364)	-587 (-132)	9372 (2106)	2657 (597)

Note: Negative (-) moments develop tension on top of the deck

Highlighted cells contain the critical moments for AASHTO LRFD (15) Service I combination

Design of Transverse Posttension Force

The design calculations for transverse posttension are included in detail. The sign convention in these calculations is: tension negative (-) and compression positive (+). Additionally, using the common moment sign convention negative moment develops tension at the top.

Step 1: First Stage Posttension (before Cast-in-Place Deck Placement)

Cast-in-place concrete deck weight is applied as a dead load to the analysis model with stiffness properties of RVE without a deck.

Step 1.1: Moments at End Diaphragm

Maximum averaged negative moment = -730 N-m/m (-164 lb-in/in) (Table J-1: row 1, column a)

Maximum nominal negative moment (M_1) = $-730 \text{ (N-m/m)} \times 1.9 \text{ m} = -1.387 \text{ kN-m}$ (-1.0 ft-kips)

Maximum averaged positive moment = 1606 N-m/m (371 lb-in/in) (Table J-1: row 4, column a)

Maximum nominal positive moment (M_2) = $1606 \text{ (N-m/m)} \times 1.9 \text{ m} = 3.051 \text{ kN-m}$ (2.3 ft-kips)

Step 1.2: Stresses at End Diaphragm

Moment of inertia (I) = $1.708 \times 10^{10} \text{ mm}^4$ (Table J-2: row 2, column a)

Neutral axis depth (y) = 343 mm (Table J-2: row 3, column a)

Stress at the top fiber due to M_1

$$f_{1,top} = \frac{M_1 y}{I} = \frac{-1.387 \text{ (kN-m)} \times 343 \text{ (mm)}}{1.708 \times 10^{10} \text{ (mm}^4\text{)}} = -2.8 \times 10^{-2} \text{ MPa} \text{ } (-4.1 \times 10^{-3} \text{ ksi})$$

Stress at the bottom fiber due to M_1

$$f_{1,bot} = 2.8 \times 10^{-2} \text{ MPa} \text{ } (4.1 \times 10^{-3} \text{ ksi})$$

Stress at the top fiber due to M_2

$$f_{2,top} = \frac{M_2 y}{I} = \frac{3.051 \text{ (kN-m)} \times 343 \text{ (mm)}}{1.708 \times 10^{10} \text{ (mm}^4\text{)}} = 6.1 \times 10^{-2} \text{ MPa} \text{ } (8.9 \times 10^{-3} \text{ ksi})$$

Stress at the bottom fiber due to M_2

$$f_{2,bot} = -6.1 \times 10^{-2} \text{ MPa} \text{ } (-8.9 \times 10^{-3} \text{ ksi})$$

Step 1.3: Moment at Intermediate Diaphragm

Maximum averaged positive moment = 5345 N-m/m (1201 lb-in/in) (Table J-1: row 4, column g)

Maximum nominal positive moment (M) = 5345 (N-m/m) × 3.81 m = 20.365 kN-m (15.0 ft-kips)

Step 1.4: Stresses at Intermediate Diaphragm

Moment of inertia (I) = 9.557 × 10⁹ mm⁴ (Table J-2: row 2, column b)

Neutral axis depth (y) = 343 mm (Table J-2: row 3, column b)

Stress at the top fiber due to M

$$f_{top} = \frac{My}{I} = \frac{20.365 (kN - m) \times 343 (mm)}{9.557 \times 10^9 (mm^4)} = 7.309 \times 10^{-1} MPa (1.06 \times 10^{-1} ksi)$$

Stress at the bottom fiber due to M

$$f_{bot} = -7.309 \times 10^{-1} MPa (-1.06 \times 10^{-1} ksi)$$

Step 1.5: Moment at Mid Diaphragm

Maximum averaged positive moment = 6920 N-m/m (1555 lb-in/in) (Table J-1: row 4, column m)

Maximum nominal positive moment (M) = 6920 (N-m/m) × 3.81 m = 26.365 kN-m (19.4 ft-kips)

Step 1.6: Stresses at Mid Diaphragm

Moment of inertia (I) = 9.557 × 10⁹ mm⁴ (Table J-2: row 2, column b)

Neutral axis depth (y) = 343 mm (Table J-2: row 3, column a)

Stress at the top fiber due to M

$$f_{top} = \frac{My}{I} = \frac{26.365 (kN - m) \times 343 (mm)}{9.557 \times 10^9 (mm^4)} = 9.462 \times 10^{-1} MPa (1.37 \times 10^{-1} ksi)$$

Stress at the bottom fiber due to M

$$f_{bot} = -9.462 \times 10^{-1} MPa (-1.37 \times 10^{-1} ksi)$$

Step 1.7: Required Posttension Force before 6-in. Cast-in-Place Concrete Deck Placement

AASHTO LRFD (I5) Service I limit state is implemented. Posttension force is calculated based on no tension criterion. It is assumed that the posttension stress is uniformly distributed across the diaphragm cross-section.

The posttension force required at the end diaphragm is determined using the maximum tensile stress calculated in step 1.2. Posttension force is calculated multiplying the tensile stress (step 1.2) and the intermediate diaphragm cross-section area (Table J-2: row 1, column a).

$$\begin{aligned} \text{Post Tension Force Required} &= 6.1 \times 10^{-2} MPa \times 4.356 \times 10^5 (mm^2) \\ &= 26.6 kN \cong \mathbf{30 kN (6.8 kips)} \end{aligned}$$

The posttension force required at the intermediate diaphragm is determined using the maximum tensile stress calculated in step 1.4. Posttension force is calculated multiplying the tensile stress (step 1.4) and the end diaphragm cross-section area (Table J-2: row 1, column b).

$$\begin{aligned} \text{Post Tension Force Required} &= 7.309 \times 10^{-1} \text{MPa} \times 2.442 \times 10^5 (\text{mm}^2) \\ &= 178.5 \text{ kN} \cong \mathbf{180 \text{ kN} (40.5 \text{ kips})} \end{aligned}$$

The posttension force required at the midspan diaphragm is determined using the maximum tensile stress calculated in step 1.6. Posttension force is calculated multiplying the tensile stress (step 1.6) and the midspan diaphragm cross-section area (Table J-2: row 1, column b).

$$\begin{aligned} \text{Post Tension Force Required} &= 9.462 \times 10^{-1} \text{MPa} \times 2.442 \times 10^5 (\text{mm}^2) \\ &= 231.1 \text{ kN} \cong \mathbf{232 \text{ kN} (52 \text{ kips})} \end{aligned}$$

Step 2: Second Stage Posttension (after Cast-in-Place Deck Placement)

Barrier and HL-93 (lane and HS-20 truck) load are applied to the analysis model with stiffness properties of RVE with deck. Truck and lane loads are positioned considering one and two-loaded lanes.

AASHTO LRFD (I5) service I limit state is considered. Multiple presence factors of 1.2 and 1.0 for one and two-lane cases are included in the calculations. The dynamic allowance factor of 1.75 for deck joints is considered.

Step 2.1: Moments at End Diaphragm

The maximum service I nominal negative moment is a result of applying barrier load and single-lane truck and lane loads (Table J-1: row 1, column b, c, d)

The averaged moment due to

barrier load = -2982 N-m/m (-670 lb-in/in) (Table J-1: row 1, column b)

single truck load = -2728 N-m/m (-613 lb-in/in) (Table J-1: row 1, column c)

single lane load = -547 N-m/m (-123 lb-in/in) (Table J-1: row 1, column d).

The nominal moment due to

barrier load = -2982 (N-m/m) \times 1.9 m = -5.666 kN-m (-4.2 ft-kips)

single truck load = -2728 (N-m/m) \times 1.2 \times 1.75 \times 1.9 m = -10.885 kN-m (-8.0 ft-kips)

single lane load = -547 (N-m/m) \times 1.2 \times 1.9 m = -1.247 kN-m (-0.92 ft-kips).

The maximum service I nominal negative moment

$$M_1 = -5.666 - 1.0 [10.885 + 1.247] = -17.8 \text{ kN} - \text{m} (-13.12 \text{ ft-k})$$

The maximum service I nominal positive moment is a result of applying truck and lane loads on to both lanes of the structure in conjunction with the barrier load (Table J-1: row 3, column b, e, f)

The averaged moment due to

barrier load = -2194 N-m/m (-493 lb-in/in) (Table J-1: row 3, column b)

two-truck load = 2390 N-m/m (537 lb-in/in) (Table J-1: row 3, column e)

two-lane load = 1077 N-m/m (242 lb-in/in) (Table J-1: row 3, column f).

The nominal moment due to

barrier load = $-2194 \text{ (N-m/m)} \times 1.9 \text{ m} = -4.169 \text{ kN-m} (-3.1 \text{ ft-kips})$

single truck load = $2390 \text{ (N-m/m)} \times 1.0 \times 1.75 \times 1.9 \text{ m} = 7.947 \text{ kN-m} (5.86 \text{ ft-kips})$

single lane load = $1077 \text{ (N-m/m)} \times 1.0 \times 1.9 \text{ m} = 2.046 \text{ kN-m} (1.5 \text{ ft-kips})$.

The maximum service I nominal positive moment

$$M_2 = -4.169 + 1.0 [7.947 + 2.046] = 5.824 \text{ kN-m} (4.3 \text{ ft-k})$$

Step 2.2: Stresses at End Diaphragm

Moment of inertia (I) = $3.114 \times 10^{10} \text{ mm}^4$ (Table J-2: row 5, column a)

Neutral axis depth (y_i) = 419 mm (Table J-2: row 6)

Stress at the top fiber due to M_1

$$f_{1,top} = \frac{M_1 y}{I} = \frac{-17.8 \text{ (kN-m)} \times 419 \text{ (mm)}}{3.114 \times 10^{10} \text{ (mm}^4\text{)}} \\ = -2.4 \times 10^{-1} \text{ MPa} (-3.4 \times 10^{-2} \text{ ksi})$$

Stress at the bottom fiber due to M_1

$$f_{1,bot} = 2.4 \times 10^{-1} \text{ MPa} (3.4 \times 10^{-2} \text{ ksi})$$

Stress at the top fiber due to M_2

$$f_{2,top} = \frac{M_2 y}{I} = \frac{5.824 \text{ (kN-m)} \times 419 \text{ (mm)}}{3.114 \times 10^{10} \text{ (mm}^4\text{)}} = 7.8 \times 10^{-2} \text{ MPa} (1.14 \times 10^{-2} \text{ ksi})$$

Stress at the bottom fiber due to M_2

$$f_{2,bot} = -7.8 \times 10^{-2} \text{ MPa} (-1.14 \times 10^{-2} \text{ ksi})$$

Step 2.3: Moments at Intermediate Diaphragm

The maximum service I nominal negative moment is a result of applying barrier load and single-lane truck and lane loads (Table J-1: row 6, column h, i, j).

The averaged moment due to

barrier load = $-4303 \text{ N-m/m} (-967 \text{ lb-in/in})$ (Table J-1: row 6, column h)

single truck load = $-886 \text{ N-m/m} (-199 \text{ lb-in/in})$ (Table J-1: row 6, column i)

single lane load = $-414 \text{ N-m/m} (-93 \text{ lb-in/in})$ (Table J-1: row 6, column j).

The nominal moment due to

barrier load = $-4303 \text{ (N-m/m)} \times 3.81 \text{ m} = -16.4 \text{ kN-m} (-12.1 \text{ ft-kips})$

single truck load = $-886 \text{ (N-m/m)} \times 1.2 \times 1.75 \times 3.81 \text{ m} = -7.1 \text{ kN-m} (-5.2 \text{ ft-kips})$

single lane load = $-414 \text{ (N-m/m)} \times 1.2 \times 3.81 \text{ m} = -1.9 \text{ kN-m} (-1.4 \text{ ft-kips})$.

The maximum service I nominal negative moment

$$M_1 = -16.4 - 1.0 [7.1 + 1.9] = -25.4 \text{ kN-m} (-18.73 \text{ ft-k})$$

The maximum service I nominal positive moment is a result of applying barrier load and single-lane truck and lane loads (Table J-1: row 3, column h, i, j).

The averaged moment due to

barrier load = $-5304 \text{ N-m/m} (-1192 \text{ lb-in/in})$ (Table J-1: row 3, column h)

single truck load = 13025 N-m/m (2927 lb-in/in) (Table J-1: row 3, column i)
 single lane load = 3484 N-m/m (783 lb-in/in) (Table J-1: row 3, column j).

The nominal moment due to

barrier load = $-5304 \text{ (N-m/m)} \times 3.81 \text{ m} = -20.21 \text{ kN-m} (-15.0 \text{ ft-kips})$

single truck load = $13025 \text{ (N-m/m)} \times 1.2 \times 1.75 \times 3.81 \text{ m} = 104.2 \text{ kN-m} (76.8 \text{ ft-kips})$

single lane load = $3484 \text{ (N-m/m)} \times 1.2 \times 3.81 \text{ m} = 16.0 \text{ kN-m} (11.74 \text{ ft-kips})$.

The maximum service I nominal positive moment

$$M_2 = -20.21 + 1.0 [104.2 + 16] = 100 \text{ kN-m} (73.7 \text{ ft-k})$$

Step 2.4: Stresses at Intermediate Diaphragm

Moment of inertia (I) = $1.746 \times 10^{10} \text{ mm}^4$ (Table J-2: row 5, column b)

Neutral axis depth (y_i) = 419 mm (Table J-2: row 6)

Stress at the top fiber due to M_1

$$f_{1,top} = \frac{M_1 y}{I} = \frac{-25.4 \text{ (kN-m)} \times 419 \text{ (mm)}}{1.746 \times 10^{10} \text{ (mm}^4\text{)}} = -6.1 \times 10^{-1} \text{ MPa} (-8.8 \times 10^{-2} \text{ ksi})$$

Stress at the bottom fiber due to M_1

$$f_{1,bot} = 6.1 \times 10^{-1} \text{ MPa} (8.8 \times 10^{-2} \text{ ksi})$$

Stress at the top fiber due to M_2

$$f_{2,top} = \frac{M_2 y}{I} = \frac{100 \text{ (kN-m)} \times 419 \text{ (mm)}}{1.746 \times 10^{10} \text{ (mm}^4\text{)}} = 2.4 \text{ MPa} (3.5 \times 10^{-1} \text{ ksi})$$

Stress at the bottom fiber due to M_2

$$f_{2,bot} = -2.4 \text{ MPa} (-3.5 \times 10^{-1} \text{ ksi})$$

Step 2.5: Moments at Midspan Diaphragm

The maximum service I nominal negative moment is a result of applying barrier load and single-lane truck and lane loads (Table J-1: row 6, column n, o, p).

The averaged moment due to

barrier load = $-5006 \text{ N-m/m} (-1125 \text{ lb-in/in})$ (Table J-1: row 6, column n)

single truck load = $-1010 \text{ N-m/m} (-227 \text{ lb-in/in})$ (Table J-1: row 6, column o)

single lane load = $-467 \text{ N-m/m} (-105 \text{ lb-in/in})$ (Table J-1: row 6, column p).

The nominal moment due to

barrier load = $-5006 \text{ (N-m/m)} \times 3.81 \text{ m} = -19.1 \text{ kN-m} (-14.1 \text{ ft-kips})$

single truck load = $-1010 \text{ (N-m/m)} \times 1.2 \times 1.75 \times 3.81 \text{ m} = -8.1 \text{ kN-m} (-6.0 \text{ ft-kips})$

single lane load = $-467 \text{ (N-m/m)} \times 1.2 \times 3.81 \text{ m} = -2.1 \text{ kN-m} (-1.6 \text{ ft-kips})$.

The maximum service I nominal negative moment

$$M_1 = -19.1 - 1.0 [8.1 + 2.1] = -29.3 \text{ kN-m} (-21.6 \text{ ft-k})$$

The maximum service I nominal positive moment is a result of applying barrier load and single-lane truck and lane loads (Table J-1: row 3, column n, o, p).

The averaged moment due to

barrier load = -6439 N-m/m (-1447 lb-in/in) (Table J-1: row 3, column n)
 single truck load = 16105 N-m/m (3619 lb-in/in) (Table J-1: row 3, column 0)
 single lane load = 4388 N-m/m (986 lb-in/in) (Table J-1: row 3, column p).

The nominal moment due to

barrier load = -6439 (N-m/m) × 3.81 m = -24.53 kN-m (-18.1 ft-kips)
 single truck load = 16105 (N-m/m) × 1.2 × 1.75 × 3.81 m = 129.0 kN-m (95.0 ft-kips)
 single lane load = 4388 (N-m/m) × 1.2 × 3.81 m = 20.1 kN-m (14.8 ft-kips).

The maximum service I nominal positive moment

$$M_2 = -24.53 + 1.0 [129 + 20.1] = 124.6 \text{ kN} - \text{m} \text{ (91.8 ft-k)}$$

Step 2.6: Stresses at Midspan Diaphragm

Moment of inertia (I) = $1.746 \times 10^{10} \text{ mm}^4$ (Table J-2: row 5, column b)
 Neutral axis depth (y_t) = 419 mm (Table J-2: row 6)

Stress at the top fiber due to M_1

$$f_{1,top} = \frac{M_1 y}{I} = \frac{-29.3 \text{ (kN} - \text{m)} \times 419 \text{ (mm)}}{1.746 \times 10^{10} \text{ (mm}^4\text{)}} \\ = -7.0 \times 10^{-1} \text{ MPa} \text{ (-1.0} \times 10^{-1} \text{ ksi)}$$

Stress at the bottom fiber due to M_1

$$f_{1,bot} = 7.0 \times 10^{-1} \text{ MPa} \text{ (1.0} \times 10^{-1} \text{ ksi)}$$

Stress at the top fiber due to M_2

$$f_{2,top} = \frac{M_2 y}{I} = \frac{124.6 \text{ (kN} - \text{m)} \times 419 \text{ (mm)}}{1.746 \times 10^{10} \text{ (mm}^4\text{)}} = 3.0 \text{ MPa} \text{ (4.3} \times 10^{-1} \text{ ksi)}$$

Stress at the bottom fiber due to M_2

$$f_{1,bot} = -3.0 \text{ MPa} \text{ (-4.3} \times 10^{-1} \text{ ksi)}$$

Step 2.7: Required Posttension Force after 6-in. Cast-in-Place Concrete Deck Placement

The posttension force required at end diaphragm is calculated in order to suppress the maximum tensile stress developed at the top or bottom fiber due to applied loads. The maximum tensile stress is calculated in step 2.2 as 0.24 MPa. Resultant posttension force is eccentric to the neutral axis of the deck-beam composite section and develops a moment as shown in Table J-2: row 6.

Other variables used in the calculations are defined in Table J-2.

for $f_{top} > 0$

$$\text{Post Tension Force} \geq \frac{f_{top}}{\left(\frac{1}{A} - \frac{(y_2 - y_1)}{2I} y_t\right)} = \frac{2.4 \times 10^{-1} \text{ (MPa)}}{\left(\frac{1}{5.321 \times 10^5 \text{ (mm}^2\text{)}} - \frac{(241 - 89) \text{ (mm)} \times 419 \text{ (mm)}}{2 \times 3.114 \times 10^{10} \text{ (mm}^4\text{)}}\right)} \\ \text{Post Tension Force} \geq \mathbf{281 \text{ kN}} \text{ (63 kips)}$$

With the level of applied posttension, grout close to the beam bottom fiber is subjected to the highest level of compression. It is required to check if the grout capacity is adequate to carry the level of stress exerted by the posttension force.

$$f_{bot} (P = 281 \text{ kN}) = \frac{P}{A} + \frac{P(y_2 - y_1)y_t}{2I} = \frac{281 \text{ (kN)}}{5.321 \times 10^5 (\text{mm}^2)} + \frac{281 \text{ (kN)} \times (241 - 89) (\text{mm}) \times 419 (\text{mm})}{2 \times 3.114 \times 10^{10} (\text{mm}^4)}$$

$$f_{bot} (P = 281 \text{ kN}) = 815 \text{ kPa} \ll \text{grout compressive strength}$$

The posttension required at intermediate diaphragm is calculated to suppress the tensile stresses calculated in step 2.4.

The maximum tensile stress at the top fiber = $6.1 \times 10^{-1} \text{ MPa}$

The maximum tensile stress at the bottom fiber = 2.4 MPa

for $f_{top} > 0$

$$\text{Post Tension Force} \geq \frac{f_{top}}{\left(\frac{1}{A} - \frac{(y_2 - y_1)y_t}{2I}\right)} = \frac{6.1 \times 10^{-1} (\text{MPa})}{\left(\frac{1}{2.983 \times 10^5 (\text{mm}^2)} - \frac{(241 - 89) (\text{mm}) \times 419 (\text{mm})}{2 \times 1.746 \times 10^{10} (\text{mm}^4)}\right)}$$

$$\text{Post Tension Force} \geq 400 \text{ kN (90 kips)}$$

for $f_{bot} > 0$

$$\text{Post Tension Force} \geq \frac{f_{bot}}{\left(\frac{1}{A} + \frac{(y_2 - y_1)y_t}{2I}\right)} = \frac{2.4 (\text{MPa})}{\left(\frac{1}{2.983 \times 10^5 (\text{mm}^2)} + \frac{(241 - 89) (\text{mm}) \times 419 (\text{mm})}{2 \times 1.746 \times 10^{10} (\text{mm}^4)}\right)}$$

$$\text{Post Tension Force} \geq \mathbf{464 \text{ kN (105 kips)}}$$

Under service conditions, stress in grout is in a safe range, much smaller than the compressive strength.

The posttension required at midspan diaphragm is calculated to suppress the tensile stresses calculated in step 2.6.

The maximum tensile stress at the top fiber = $7.0 \times 10^{-1} \text{ MPa}$

The maximum tensile stress at the bottom fiber = 3.0 MPa

for $f_{top} > 0$

$$\text{Post Tension Force} \geq \frac{f_{top}}{\left(\frac{1}{A} - \frac{(y_2 - y_1)y_t}{2I}\right)} = \frac{7 \times 10^{-1} (\text{MPa})}{\left(\frac{1}{2.983 \times 10^5 (\text{mm}^2)} - \frac{(241 - 89) (\text{mm}) \times 419 (\text{mm})}{2 \times 1.746 \times 10^{10} (\text{mm}^4)}\right)}$$

$$\text{Post Tension Force} \geq 458 \text{ kN (103 kips)}$$

for $f_{bot} > 0$

$$\text{Post Tension Force} \geq \frac{f_{bot}}{\left(\frac{1}{A} + \frac{(y_2 - y_1)y_t}{2I}\right)} = \frac{3.0 (\text{MPa})}{\left(\frac{1}{2.983 \times 10^5 (\text{mm}^2)} + \frac{(241 - 89) (\text{mm}) \times 419 (\text{mm})}{2 \times 1.746 \times 10^{10} (\text{mm}^4)}\right)}$$

$$\text{Post Tension Force} \geq \mathbf{580 \text{ kN (130 kips)}}$$

Under service conditions, stress in grout is in a safe range, much smaller than the compressive strength.

The transverse posttension force requirements calculated in step 1.7 and 2.7 are summarized in Table J-3.

Table J-2 Geometric Parameters of Diaphragms and Transverse Posttension Locations along the Beam Height

Transverse Posttension Locations along Beam Height		
Diaphragm Cross-Section without Deck		
	End Diaphragm (a)	Intermediate and Midspan Diaphragms (b)
1. Cross-Section Area (A) mm ²	4.356×10^5	2.442×10^5
2. Moment of Inertia (I) mm ⁴	1.708×10^{10}	9.557×10^9
3. Neutral Axis Depth (y) mm	343	343
Diaphragm Cross-Section with Deck		
4. Cross-Section Area (A) mm ²	5.321×10^5	2.983×10^5
5. Moment of Inertia (I) mm ⁴	3.114×10^{10}	1.746×10^{10}
6. Miscellaneous Parameters		

TABLE J-3 Posttension Force Requirement for the Sample Bridge

	Posttension Force at Diaphragm, kN (kips)		
	End Diaphragm	Intermediate Diaphragm	Middle Diaphragm
Before deck placement	30 (7)	180 (41)	232 (52)
After deck placement	281 (63)	464 (105)	580 (130)
Total	311 (70)	644 (146)	812 (182)